Forecasts of Two-Field Inflation

Godfrey Leung

The University of Nottingham

UNITED KINGDOM · CHINA · MALAYSIA

Thesis submitted to the University of Nottingham
for the degree of Doctor of Philosophy, August 2014

“Most people say that it is the intellect which makes a great scientist. They are wrong: it is character.”

– Albert Einstein

”Research is what I’m doing when I don’t know what I’m doing.”

– Wernher von Braun

“Physics is like sex: sure, it may give some practical results, but that’s not why we do it.”

– Richard Feymann

“All science is either physics or stamp collecting.”

– Ernest Rutherford

Supervisor: Prof. Edmund J.Copeland

Examiners: Prof. Andrew Liddle
Dr. Adam Moss

Abstract

Inflation is currently the most promising paradigm of the Early Universe. The simple paradigm involves a single canonical scalar field minimally coupled to gravity slowly rolling down a potential.

In this thesis, we discuss an extension to the simple paradigm, multifield inflation, in which inflation is driven by more than one scalar field. Unlike in the single field paradigm, isocurvature perturbations could be non-vanishing and source curvature perturbation on superhorizon scales.

Analytic model predictions during the slow-roll regime in some classes of multifield inflation models have been worked out in the literature. However, curvature perturbation may continue to evolve after slow-roll as isocurvature perturbations are not necessarily exhausted when inflation ends. In this thesis, by using the δN formalism, we investigate the effects of perturbative reheating on the curvature perturbation and related observables in multifield models. By considering various two-field models, we demonstrate that the subsequent (p)reheating evolution is significant and must be taken into account even for perturbative reheating. How the model predictions evolve during reheating is a model dependent question, implying that models of multifield inflation cannot be compared to observations directly without specifying how reheating takes place.

We also discuss a different class of two-field models, conformal inflation, which is locally scale invariant. Universal behaviour emerges as a critical phenomenon near the enhanced $SO(1,1)$ or shift symmetry point, leading to model independent predictions. Going beyond the original model proposed by Kallosh and Linde, we show that this universal behaviour extends to more generalised models involving higher order

derivatives for slow-roll potential driven inflation.

Acknowledgements

I would like to express my deepest gratitude to my supervisor Ed Copeland for his support and guidance, especially his encouragement and inspiring ideas. Special thanks to my collaborator Chris Byrnes, with whom it has been a pleasure to work with. I would also like to thank my undergraduate supervisor Ian Lawrie, for his enlightening lectures and inspiring me to pursue a research career in theoretical physics. I am also fortunate enough to work and have some lively discussions with many people such as Misao Sasaki, Ming-chung Chu, Antonio Padilla, Ewan Tarrant, David Seery, David Stefanyszyn, Thorsten Battefeld, Paul Saffin, David Mulryne and Jonathan White.

Thanks to Ian, Ewan, Sophie (especially for organising particle nights), David, Bradley and other members of the Astro and Particle theory groups at the University of Nottingham for producing a friendly working environment.

I would also like to thanks Prof Andrew Liddle and Dr Adam Moss for being my thesis examiners. Reviewing a PhD thesis is never an easy task, and I am grateful for their thoughtful and detailed comments and feedbacks to this work.

Finally, to my family, especially my parents who show empathy and support my ”selfish” decision to pursue a research career in science, leaving them behind for the past few years.

This work was funded by the University of Nottingham.

List of Publications

I hereby declare that the work contained within this thesis is entirely my own work, unless stated otherwise. This thesis contains material from the following papers:

1. Leung G., Tarrant E.R., Byrnes C.T., and Copeland E.J., "Reheating, Multifield Inflation and the Fate of the Primordial Observables," *JCAP* **1209** (2012) 008

2. Leung G., Tarrant E.R., Byrnes C.T., and Copeland E.J., "Influence of Reheating on the Trispectrum and its Scale Dependence," *JCAP* **1308** (2013) 006

3. Leung G., Stefanyszyn D., "Universality Classes in Conformal Inflation," (to appear)

I did most of the analytical analysis in the first two papers, whereas the numerical code used in the two papers was originally written by E.R.Tarrant. I later modified the code to compute third order δN coefficients for analysis in the second paper.

Material in paper 1 and 2 are presented in Chapter 4 and 5 respectively. Paper 3 is discussed in Chapter 6.

Units and Notations

Frequently used symbols and their definitions:

Symbol	Definition
$\mathcal{L}$	Lagrangian density
$M_{\rm p}$	Reduced Planck mass, defined as $1/8\pi G$
a	scale factor
φ	Inflaton
H	Hubble parameter, defined as $\dot{a}/a$
ρ	Energy density
P	Pressure density
N	number of e-folds of expansion, $N \equiv \int H dt$
W, V	Scalar Potential
S	action
$\mathcal{R}$	Comoving curvature perturbation
$T_{\mu\nu}$	Stress-Energy Momentum tensor
α	Running of the spectral index $n_{\rm s}$
ζ	Curvature perturbation on uniform-density hypersurface
$n_{\rm s}$	Scalar spectral index
$n_{\rm T}$	Tensor spectral index
X	canonical kinetic term, $X \equiv -\frac{1}{2} g^{\mu\nu}\partial_\mu\varphi\partial_\nu\varphi$
r	tensor-to-scalar ratio
A_ζ	amplitude of power spectrum of ζ
P_ζ	Power spectrum of ζ
B_ζ	Bispectrum of ζ
T_ζ	Trispectrum of ζ
$f_{\rm NL}$	Non-linear parameter of Bispectrum
$g_{\rm NL}, \tau_{\rm NL}$	Non-linear parameters of Trispectrum
$n_{f_{\rm NL}}$	Spectral index of $f_{\rm NL}$
$n_{\tau_{\rm NL}}$	Spectral index of $\tau_{\rm NL}$

In this thesis, we use the metric signature $\eta_{\mu\nu} = \mathrm{diag}(-,+,+,+)$. Throughout the whole thesis, we adapt the natural units where $\hbar = c = 1$ unless stated otherwise. Spacetime indices are raised by the metric $g^{\mu\nu}$ and Einstein summation are implicitly assumed. The stress-energy momentum tensor $T_{\mu\nu}$ is defined as $T_{\mu\nu} \equiv -\frac{2}{\sqrt{-g}}\frac{\delta S_{\mathrm{m}}}{\delta g^{\mu\nu}}$, where S_{m} is the matter action.

$\Box$ is the d'Alembert operator, defined as $\Box \equiv g^{\mu\nu}\nabla_\mu\nabla_\nu$. Symmetriser and anti-symmetriser are defined as $U_{(\mu_1\mu_2\ldots\mu_n)} \equiv \frac{1}{n!}\delta_{\mu_1\mu_2\ldots\mu_n}\delta^{\nu_1\nu_2\ldots\nu_n}U_{\nu_1\nu_2\ldots\nu_n}$ and $U_{[\mu_1\mu_2\ldots\mu_n]} \equiv \frac{1}{n!}\varepsilon_{\mu_1\mu_2\ldots\mu_n}\varepsilon^{\nu_1\nu_2\ldots\nu_n}U_{\nu_1\nu_2\ldots\nu_n}$, where $\varepsilon_{\mu_1\mu_2\ldots\mu_n}$ is the Levi-Civita symbol.

Greek indices $\mu, \nu, \ldots$ correspond to spacetime indices, whereas Roman indices $I, J, \ldots$ correspond to field indices. Overline denotes background homogeneous and isotropic quantities. Variables with subscript $*$ correspond to values evaluated at horizon-exit. Dot $\dot{}$ denotes differentiation with respect to cosmic time t, whereas prime $'$ denotes differentiation with respect to conformal time η. Unless stated otherwise, subscripts φ and χ denote partial differentiations with respect to φ and χ respectively.

Contents

Forecasts of Two-Field Inflation

Chapter 1

Introduction

Since the beginning of human civilisation, understanding the origin of our Universe has always been the core of most studies, including science, philosophy and religion. However, it was the beginning of the twentieth century that Cosmology started to be incorporated in a mathematical and scientific framework. Tracing back to Einstein's formulation of general relativity in 1915, a mathematically consistent model describing our Universe was first constructed. The discovery of Hubble's law and the Cosmic Microwave Background (CMB) then confirmed the Big Bang theory, suggesting our Universe has been expanding since its birth.

Later the discovery of Cosmic Microwave Background (CMB) Anisotropies by COBE [1] in 1992, which later confirmed by WMAP [2] in 2003, enabled us to start to address some very fundamental questions such as the origin of structure formation in our Universe and to understand our Universe at the very early stage. The observed nearly scale-invariant CMB spectrum strongly favours the theory of inflation.

I, a universe of atoms, an atom in the universe. - Richard Feynman

Inflation, an era of a dramatic expansion of spacetime, is currently the most promising paradigm of the Early Universe. It typically occurs at an energy scale that is far beyond the reach of any possible particle physics experiments on Earth. As a result, inflation acts as an excellent probe to physics beyond the Standard Model. Despite the success and enormous advances in the field in recent years, inflation remains a phenomenological model with many open questions to be addressed. In particular, we still do not

know what the true underlying particle physics model for inflation is. Motivated by particle physics, various modifications to the simple inflationary paradigm have been considered since it was first formulated.

In this thesis we discuss a simple extension to the original paradigm, multifield inflation. We focus on the observational aspects of a simple representative class, models involving two scalar fields. This thesis is organised as follows: in Chapter 1, we first briefly describe the standard Big Bang picture and its shortcomings which eventually led to the introduction of cosmic inflation. The simplest slow-roll single field inflation paradigm is later introduced in the chapter.

In Chapter 2, we start by introducing cosmology perturbation theory and gauge-invariant quantities, the curvature perturbation ζ in particular. Then we discuss the statistical properties of ζ and how they could be quantified. A simpler alternative to the cosmological perturbation theory, the separate universe picture and the consequent δN formalism, are then introduced later in the chapter. Using the δN formalism, we show that ζ is conserved on superhorizon scales in the absence of isocurvature perturbations.

In Chapter 3, we introduce the 'in-in' formalism and δN formulae that are used to compute ζ and the related observables. We discuss the inflationary model predictions of the primordial observables, particularly focussing on the statistics of ζ, up to the level of four-point statistics. We start with the simplest single-field model with a canonical kinetic term. We then introduce the multifield models and discuss how the models are different to the simple single-field paradigm. Model predictions of canonical multifield models are later given in terms of the δN coefficients in the chapter.

In Chapter 4, by considering various two-field models, we discuss how perturbative reheating could change the model predictions evaluated during the slow-roll regime, at the level of power and bispectra, if isocurvature perturbations persist after inflation ends. In Chapter 5, we extend the discussion to non-linear parameters of the trispectrum and their scale dependences. We also discuss the effects of perturbative reheating on various consistency relations between observables in some classes of multifield models.

In Chapter 6, we discuss a new class of two-field inflation models which is locally scale invariant, known as conformal inflation. We start by introducing the original

model first proposed by Kallosh and Linde [3] and discussing its universal behaviour near the enhanced $SO(1,1)$ symmetry point. We then discuss how one can go beyond the original paradigm and show the universal behaviour of the original model extends to more general models. Finally, we summarise, conclude and give future directions on how the field of inflationary cosmology may be pursued in Chapter 7.

1.1 Friedmann Universe, Standard Big Bang Cosmology

In today's modern Cosmology, it is assumed that our Universe is homogeneous and isotropic on large scales. This is known as the **Copernican principle**. Under this assumption, our Universe is described by a Friedmann-Robertson-Walker (FRW) metric at the background level

$$\begin{aligned} \mathrm{d}s^2 &= -\mathrm{d}t^2 + a^2(t)\tilde{g}_{ij}(\mathrm{d}x^i\mathrm{d}x^j) \\ &= -\mathrm{d}t^2 + a^2(t)\left[\frac{\mathrm{d}x^2}{1-Kx^2} + x^2(\mathrm{d}\theta^2 + \sin^2\theta\mathrm{d}\phi_{\mathrm{c}}^2)\right] \end{aligned} \tag{1.1}$$

in Cartesian and radial coordinates. Here $a(t)$ is the scale factor and K takes value of $\{-1, 0, +1\}$, representing negative, flat and positive intrinsic spatial curvature respectively.

The Copernican Cosmological principle is well tested through today's observations. In particular, CMB experiments and Large Scale Structure (LSS) surveys give strong evidence that our Universe is homogeneous and isotropic, starting from scales taken to be typically around $100\mathrm{Mpc}$ [4, 5, 6]. [1]

Assuming the constituents of our Universe can be well described by a perfect fluid with a 4-velocity u^μ, the general form of the energy-momentum tensor $\bar{T}^\mu_\nu$ is

$$\bar{T}^\mu_\nu = (\bar{P} + \bar{\rho})u^\mu u_\nu + \bar{P}\delta^\mu_\nu\,, \tag{1.2}$$

[1] Controversially, there has been a claim by Clowes et.al. against the Cosmological principle, arguing from the observation of a potential massive structure of size much larger than $100\mathrm{Mpc}$, the Huge Large Quasar Group [7].

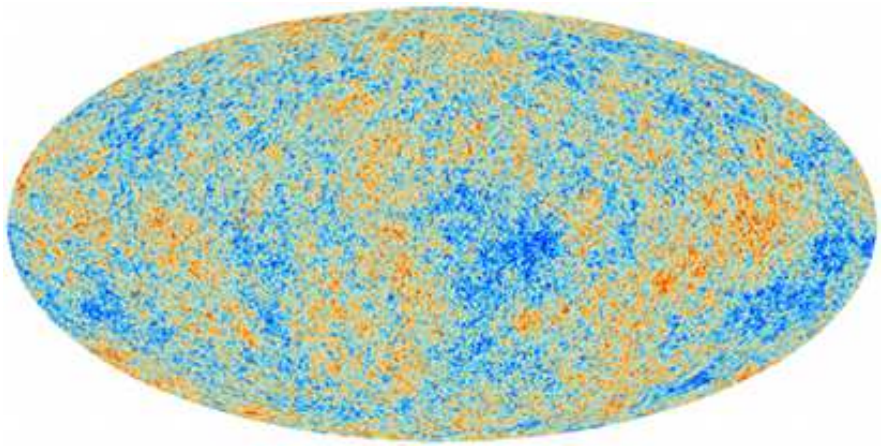

Figure 1.1: Full sky CMB map measured by Planck, showing our Universe is isotropic on large scales, with an amplitude of temperature fluctuations of order $\delta T/T \approx 10^{-5}$. Note the dipole asymmetry due to our relative motion to the CMB has been removed. Credit: ESA and the Planck Collaboration [8]

where $\bar{P}$ and $\bar{\rho}$ are the isotropic pressure and energy density of the cosmic fluid, and $g_{\mu\nu}u^\mu u^\nu = -1$. The Bianchi identity or the conservation of the stress energy-momentum tensor then leads to the continuity equation

$$\dot{\bar{\rho}} = -3H(\bar{\rho} + \bar{P})\,. \tag{1.3}$$

Here H is the Hubble parameter, defined as $H \equiv \dot{a}/a$. Now consider Einstein's General Relativity with the background field equation $\bar{G}_{\mu\nu} + \Lambda g_{\mu\nu} = 8\pi G\bar{T}_{\mu\nu}$, where $G_{\mu\nu}$ is the Einstein tensor and G is the Newton's constant. Λ is the cosmological constant, which is present as a constant in the theory of Einstein gravity. For a cosmic fluid with the stress-energy tensor Eq. (1.2) in a FRW background, the time-time component of the Einstein equation results in the well-known **Friedmann equation** (for a detailed derivation of the Friedmann Equation from GR, see [9] for example)

$$H^2 = \frac{\bar{\rho}}{3M_{\rm p}^2} - \frac{K}{a^2} + \frac{\Lambda}{3}\,. \tag{1.4}$$

K again is the flatness parameter, corresponding to the closed ($K = 1$), open ($K = -1$) and flat ($K = 0$) universes. Overline denotes the averaged background quantities. $M_{\rm p}$ is the reduced Planck mass, defined as $M_{\rm p}^2 \equiv 1/8\pi G$. Although Λ may contribute to the dark energy (DE) that explains the observed late-time acceleration of our Universe [10], naive estimates from the vacuum energy of quantum field theory gener-

ically predicts its value many orders of magnitude larger than the observed DE value and therefore leads to the well-known cosmological constant problem in cosmology today. For a review on the cosmological constant problem, see [11, 12]. In this thesis however, we will focus on the Early Universe when the DE contribution is assumed to be small and negligible. We therefore take $\Lambda = 0$ in the following.

Together with the continuity equation Eq. (1.3), we then end up with a system of equations

$$\begin{aligned} H^2 &= \frac{\bar{\rho}}{3M_{\rm p}^2} - \frac{K}{a^2} \\ \dot{H} + H^2 &= -\frac{\bar{\rho} + 3\bar{P}}{6M_{\rm p}^2} \,. \end{aligned} \tag{1.5}$$

The second equation is commonly known as the **Friedmann acceleration equation** or **Raychaudhuri Equation**. Finally to close the system of equations we also need to know the relation between the pressure P and the energy density ρ of the cosmic fluid. For an adiabatic fluid where P is a unique function of ρ, i.e. $P(\rho)$, we can define an equation of state ω where $P = \omega\rho$. For instance, a radiation fluid gives $\omega = 1/3$ and a matter fluid gives $\omega = 0$. Given the equation of state ω and together with Eqs. (1.5), we can then solve for $a(t)$ and find the background dynamics of the Universe. For example, we find $a \propto t^{1/2}$ and $a \propto t^{2/3}$ in radiation-dominated and matter-dominated universes respectively.

It is also useful to define a new dimensionless quantity Ω, known as the density parameter

$$\Omega - 1 \equiv \frac{K}{a^2 H^2} \,. \tag{1.6}$$

In Einstein gravity, with the use of the Friedmann equation Eq. (1.4), the density parameter becomes

$$\Omega(t) = \frac{\bar{\rho}(t)}{\rho_{\rm crit}(t)} \,, \tag{1.7}$$

where $\rho_{\rm crit}$ is the critical energy density defined by $3H^2M_{\rm p}^2$, or the energy density for a spatially flat Universe $(K = 0)$. From Eq. (1.6) we can see Ω is a measure of the

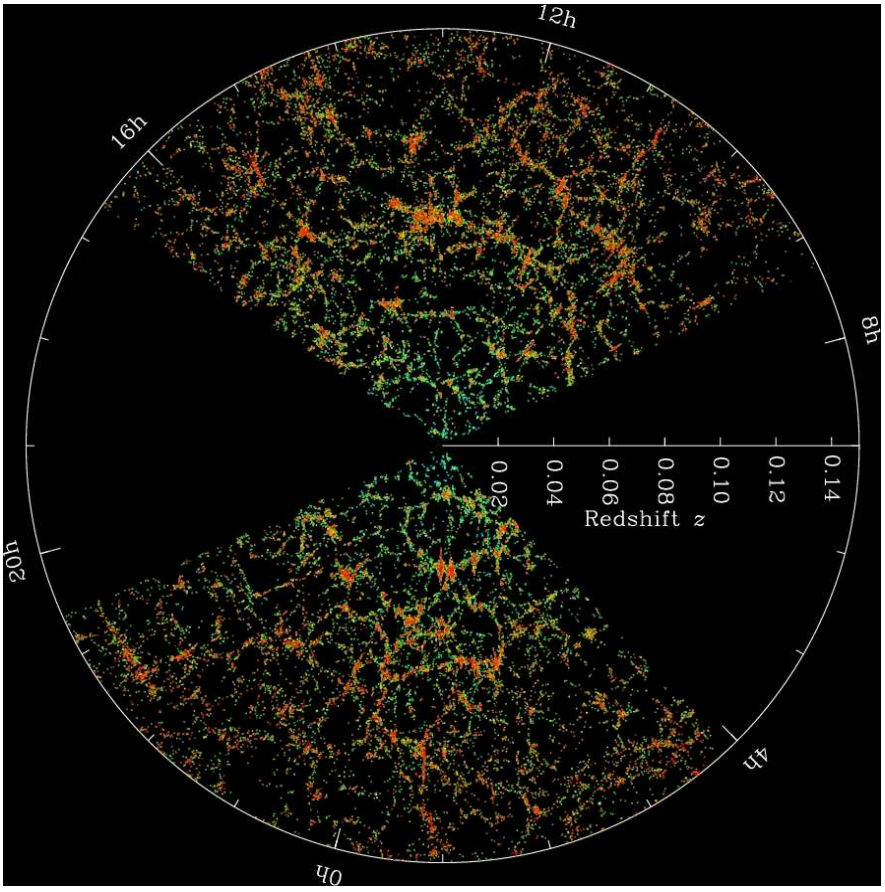

Figure 1.2: 3-dimensional map of galaxy distribution in our Universe in the Sloan Digital Sky Survey. Credit: M. Blanton and the Sloan Digital Sky Survey

instrinsic spatial curvature of the background geometry in units of H^2, independent of the theory of gravity.

Eqs. (1.5) form the basis for the development of the **Hot Big Bang model**. According to the Hot Big Bang model, our Universe originated from an extremely dense and hot state and is expanding. The greatest successes of the hot Big Bang model are the prediction of the existence of the CMB and the theory of Big Bang nucleosynthesis that explains the origin of chemical elements in our Universe. The standard model of cosmology, the Λ**CDM model**, is a parametrisation of the Big Bang model which suggests our Universe is made up of normal baryonic matter and Standard Model particles, some form of unknown, invisible non-relativistic matter named as Cold Dark Matter (CDM) and a cosmological constant Λ that gives rise to late-time acceleration. The background geometry is a flat one, where $K = 0$.

1.2 Problems of Standard Big Bang Cosmology

However, despite the success of the standard Big Bang picture, there are problems associated with it. First of all, it is obvious that our Universe is not completely homogeneous. There are small inhomogeneities on top of the background on small scales that can be seen in the CMB and in large scale structures such as galaxies and cosmic voids. One of the quests of modern cosmology is to explain the origin of primordial perturbations that seed structure formation in our Universe. While the standard Big Bang picture successfully describes the background history of our Universe, it does not tell us how and why the initial conditions of our Universe, including these small perturbations, are set.

On the other hand, there are fine-tuned initial conditions problems at the background level, conventionally given in terms of the flatness and horizon problems [2]. There is also the relic problem, which is related to formation of topological defects during spontaneous symmetry breaking in the early Universe. These relics can be long-lived and dominate our Universe, thus completely change the cosmic evolution. All these problems will be explained in detail in the following.

Flatness Problem

In simple words, the flatness problem corresponds to the question why our Universe remains flat to such a high precision today. It was first elucidated by Dicke and Peebles [14]. This can be easily seen from the definition of the density parameter Ω Eq. (1.6). From Eq. (1.6) and the definition of the Hubble parameter H, we can see

$$\Omega - 1 \equiv \frac{K}{a^2 H^2} = \frac{K}{\dot{a}^2}\,. \tag{1.8}$$

Thus during any era of attractive gravity such that $(\ddot{a} < 0)$, Ω is always driven away from 1 and the solution $\Omega = 1$ is unstable. For example, in Einstein gravity, using the Friedmann equation Eq. (1.4), one can easily find that in a matter-dominated Universe

[2] Recently Carroll has argued against this conventional picture, suggesting that the initial conditions problems should been formulated in terms of the measure on the space of cosmological trajectories instead, see [13].

$|\Omega - 1| \propto t^{2/3}$ and in a radiation-dominated Universe $|\Omega - 1| \propto t$. Therefore unless the Universe is exactly flat where $K = 0$, given a small deviation from a flat Universe to begin with, i.e. $1 - \Omega(t_i) = \epsilon$ where ϵ is small, one would always end up in a closed or open Universe where Ω deviates significantly from 1. Current observations however suggest Ω_0, the density parameter today, cannot deviate more than a few percent from unity. For example, measurements of CMB anisotropies suggest

$$-0.09 < \Omega_K \equiv 1 - \Omega_0 < 0.001 \qquad \text{at} \qquad 95\%\text{C.L.} \tag{1.9}$$

in recent combined Planck + WP + highL data [15], perfectly consistent with $K = 0$. [3]

As a result, in a ΛCDM Universe, to be consistent with the current observed constraint on $|\Omega_0 - 1|$, we would need very fine-tuned initial conditions to start with. For example taking t_i to be the epoch of Big Bang nucleosynthesis (BBN), around 1MeV, we would need

$$|\Omega(t_i) - 1| \leq 10^{-16}\,. \tag{1.10}$$

Such fine-tuned initial condition seems extremely unlikely. For any generic initial values for Ω apart from 1, we would always find ourselves with a closed Universe that recollapses very quickly or an open Universe that is too young to be consistent with observations. An explanation is needed for why Ω either identically equals or remains close to unity in our Universe. This is the conventional picture of the flatness problem, which implicitly assumes a measure that is uniform in Ω_K. Recently it was argued by Carroll and Tam that the problem does not exist but arises simply because of the use of an incorrect measure [17].

Horizon Problem

Consider the comoving horizon $(aH)^{-1}$ which characterises the fraction of comoving space that is in casual contact. It is usually of the same order of the effective comoving particle horizon which is the maximum distance light can travel since the Big Bang.

[3] It was argued recently that the observed large scale CMB anomalies in Planck favours a marginally open Universe [16].

For attractive gravity, the scale factor grows as $a \propto t^n$, where $0 < n < 1$ in both radiation or matter-dominated eras. Physical wavelengths λ thus grow as $a\lambda \propto t^n$, whereas the Hubble radius evolves as $H^{-1} \propto t$. Going back in time, the physical wavelength is therefore much smaller than the Hubble radius at early times.

Current observations of the CMB find that the whole observable Universe is in thermal equilibrium, suggesting that our Universe is very homogeneous and isotropic everywhere, to one part in 10^{-5} at the time of decoupling. Yet as we see, the comoving scales entering the horizon today should have been far outside the horizon at decoupling. Contradicting the observations, we therefore should instead expect the CMB to be much more anisotropic, with many casually disconnected regions establishing thermal equilibrium independently at different temperatures.

More precisely, let us consider the particle horizon, defined as

$$D_H(t) = a(t)d_H(t) = \int_{t_i}^{t} \mathrm{d}t'/a(t')\,, \tag{1.11}$$

where d_H corresponds to the comoving particle horizon. The particle horizon $D_H(t)$ gives the size of any casually connected region at time t. Comparing the comoving particle horizon at decoupling $t_{\rm dec}$ to that of today t_0, we find

$$\frac{d_H(t_{\rm dec})}{d_H(t_0)} \approx \left(\frac{t_{\rm dec}}{t_0}\right)^{1/3} \approx 10^{-2}\,. \tag{1.12}$$

This ratio implies that the comoving horizon at the surface of last-scattering corresponds to an angle of order 1° in today's CMB sky. Given that there is no way for casually disconnected regions to establish thermal equilibrium with each other, the near-isotropy of today's CMB sky suggests again we need very fine-tuned and special initial conditions. This is the **horizon problem**, first suggested by Misner [18].

Relics Problem

In models beyond the Standard Model of particle physics, our Universe may go through several epochs of phase transitions during which spontaneous symmetry breaking happens. During these phase transitions, it is typical that massive objects like magnetic

monopoles [19] will be produced as relics. These relics, if massive compared to H, are non-relativistic and contribute to the total matter energy density $\rho_{\rm m}$. But from the continuity equation Eq. (1.3) we can see that the relativistic radiation energy density ρ_γ decreases more rapidly compared to $\rho_{\rm m}$ as the universe expands. Thus a small amount of $\rho_{\rm m}$ from the relics in the Early Universe could dominate very quickly and lead to an early matter-dominated era and rapid closure of the Universe, if the relics are sufficiently stable.

1.3 Inflation, a Solution to Hot Big Bang Problems

Inflation, proposed by a number of independent authors including Alan Guth in the 1980s [20, 21], offers an explanation to the conventional flatness and horizon problems and provides the seed of structure formation in the Early Universe. It is now the most promising paradigm of the Early Universe.

By definition, inflation is an era of rapid expansion of spacetime, during which the scale factor accelerates

$$\ddot{a} > 0\,. \tag{1.13}$$

The condition of inflation can be written as

$$\frac{\mathrm{d}}{\mathrm{d}t}\frac{H^{-1}}{a} < 0 \quad \text{or} \quad -\frac{\dot{H}}{H^2} < 1\,. \tag{1.14}$$

This is the era when the Hubble parameter varies slowly as compared to the Hubble timescale. Taking H to be approximately constant over many Hubble times, we then have $a \propto e^{Ht}$, corresponding to a quasi-de Sitter Universe with an exponential expansion of spacetime.

Assuming Einstein gravity, we can rewrite Eq. (1.14) in terms of a condition for ρ and P of the cosmic fluid

$$\overline{\rho} + 3\overline{P} < 0\,. \tag{1.15}$$

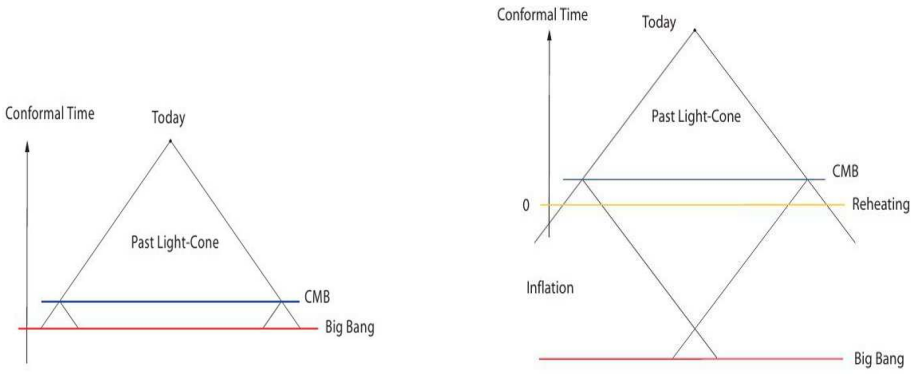

Figure 1.3: Conformal diagram of a Hot Big Bang universe with and without an inflationary phase. Inflation extends the conformal time η to negative values. The end of inflation creates an 'apparent' Big Bang at $\eta = 0$. Yet there is no singularity at $\eta = 0$ and the light cones intersect at an earlier time. Credit: Daniel Baumann

Since the energy density $\overline{\rho}$ is always assumed to be positive, inflation only happens when the pressure $\overline{P}$ becomes negative.

The conventional flatness and horizon problems are solved by inflation if the observable Universe is well within the horizon before inflation begins. From the definition of the density parameter Eq. (1.8), since inflation is an era where $(\ddot{a} > 0)$, inflation always drives Ω towards 1 even if our Universe is not flat $(K \neq 0)$ to begin with. For the horizon problem, since our observable Universe is within the horizon H^{-1} at the start of inflation, regions which look as if separated by distances larger than the horizon today are indeed within the horizon and in casual contact to begin with. This justifies the observed isotropy in the CMB. This is illustrated in Fig. 1.3. These conventional arguments are however controversial. It was argued by Penrose that inflation does not solve the horizon problem, or the initial conditions problems in the Early Universe, since the onset of inflation requires extremely fine-tuned initial conditions [22].

For the relics problem, things are less controversial. Consider relics formed before inflation, by the continuity equation Eq. (1.3), we can see that $\rho_{\rm relic} \propto a^{-3}$ for non-relativistic relics. Since the scale factor a increases by many orders of magnitude during inflation, the energy density of relics is effectively diluted away, giving negligible contribution to the Early Universe dynamics. Or in the physical picture, the distance between any relics formed before are stretched well beyond the horizon during inflation and therefore the number density of relics becomes negligible in the observable Universe.

Besides solving the problems of the standard Big Bang picture, inflation also offers an explanation to the origin of the seeds of structure formation. Because of quantum mechanics, there are vacuum fluctuations associated with the inflaton field. During inflation, these quantum fluctuations are stretched outside the horizon and become classical. These perturbations are then converted to primordial density perturbations during a phase called (p)reheating [4] and lead to the subsequent structure formation as they later re-enter the horizon.

The original model proposed by Alan Guth, now named the 'old inflation', involves a scalar field tunnelling through a metastable vacuum state to the true vacuum [20]. However this model was later replaced by 'new inflation', as it was found that the model does not reheat properly: the Universe would expand too rapidly for bubble collisions to occur if inflation lasts long enough to solve the initial conditions problems.

The simplest viable 'new inflation' model assumes the Universe is dominated by a single homogeneous scalar field with a standard canonical kinetic term, slowly rolling down a flat potential [23]. This is standard slow-roll inflation. The action is given by

$$S = \int \mathrm{d}^4x\sqrt{-g}\left[\frac{M_\mathrm{p}^2 R}{2} - \frac{1}{2}\partial_\mu\varphi\partial^\mu\varphi - V(\varphi)\right], \tag{1.16}$$

with the scalar field φ obeying the Klein-Gordon field equation in an expanding background

$$\ddot{\varphi} + 3H\dot{\varphi} + V_\varphi = 0\,, \tag{1.17}$$

where V_φ is the derivative of the potential V with respect to φ. With the Universe dominated by the scalar field, the Friedmann equation then reads as

$$3H^2 = V(\varphi) + \frac{1}{2}\dot{\varphi}^2\,. \tag{1.18}$$

The instantaneous slow-roll parameters at time t are defined as

$$\epsilon_H \equiv -\frac{\dot{H}}{H^2}\,,\ \eta_H \equiv -\frac{1}{2}\frac{\dot{\epsilon}_H}{H\epsilon_H}\,, \tag{1.19}$$

[4] To be explained in detail in Chapter 4.

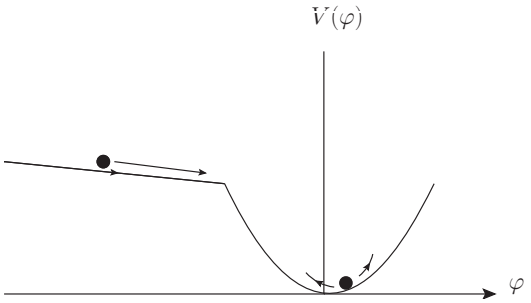

Figure 1.4: Slow-roll Inflation: a scalar field rolling down a flat potential.

or in terms of the potential as [24]

$$\epsilon_V \equiv \frac{M_{\rm p}^2}{2}\left(\frac{V_\varphi}{V}\right)^2 \,,\ \eta_V \equiv M_{\rm p}^2\frac{V_{\varphi\varphi}}{V}\,. \tag{1.20}$$

To realise slow-roll inflation, we require these slow-roll parameters to be smaller than $O(1)$. This corresponds to when the kinetic energy $\dot{\varphi}^2$ is subdominant compared to the potential energy V and φ is slowly rolling. In the simple canonical slow-roll models discussed above, these slow-roll parameters are related by

$$\epsilon_H \to \epsilon_V \,,\ \eta_H \to \eta_V - 2\epsilon_V \tag{1.21}$$

in the slow-roll limit. Assuming slow-roll, matching the energy-momentum tensor $T^{\mu\nu}$ with that of a perfect fluid, the scalar field then behaves approximately as a fluid with $\overline{\rho}(\varphi) \approx -\overline{P}(\varphi)$

$$\begin{aligned}\overline{\rho}(\varphi) &= \frac{1}{2}\dot{\varphi}^2 + V \approx V\,,\\ \overline{P}(\varphi) &= \frac{1}{2}\dot{\varphi}^2 - V \approx -V\,,\end{aligned} \tag{1.22}$$

which satisfies the conditions for inflation Eq. (1.15). The amount of inflation is quantified by the number of e-folds N, defined by

$$N = \ln(a_{\rm e}/a_*) = \int_{t_*}^{t_{\rm e}} H{\rm d}t\,. \tag{1.23}$$

Here subscript $*$ denotes the epoch when the pivot scale under consideration leaves the horizon and subscript e denotes the epoch of the end of inflation.

To solve the horizon problem, at least $N = 60$ e-folds of observable inflation is needed for the pivot CMB scale $k_* = 0.002\mathrm{Mpc}^{-1}$ with the assumption that the usual post-inflationary history follows. This follows from the relation

$$1 = \frac{a_* H_*}{a_{\rm ent} H_{\rm ent}} = e^{-N} \frac{a_{\rm e} H_*}{a_{\rm reh} H_{\rm reh}} \frac{a_{\rm reh} H_{\rm reh}}{a_{\rm eq} H_{\rm eq}} \frac{a_{\rm eq} H_{\rm eq}}{a_{\rm ent} H_{\rm ent}} \,, \tag{1.24}$$

where subscripts 'eq' and 'reh' correspond to the epoch of matter-radiation equality and the reheating epoch, whereas subscript 'ent' corresponds to the epoch when the pivot scale re-enters the horizon. This gives an estimate of the number of e-folds of observable inflation for the pivot scale k_* [25]

$$N_{\rm obs} = 56 - \frac{2}{3} \ln \frac{10^{16} GeV}{\rho_*^{1/4}} - \frac{1}{3} \ln \frac{10^9 GeV}{T_R} \,, \tag{1.25}$$

assuming each change in the isotropic pressure P to be instantaneous. Here T_R is the reheating temperature. For reasonable choices of ρ_* and T_R, we get an estimate bound on the observable inflation $N_{\rm obs}$, where $70 > N_{\rm obs} > 50$. [5].

This is however only the background picture. There is also small inhomogeneities arise on top of the background because of quantum fluctuations, which later seeds structure formation in our Universe. To understand how these small in inhomogeneities arise, we need to study perturbations about the inflationary background, which will be discussed in the following chapters.

[5] More extreme values are in principle possible, see [26].

Chapter 2

Cosmological Perturbation Theory

In this chapter we first briefly introduce cosmological perturbation theory [27, 28, 29] at linear order. We then introduce the concept of gauge-invariant quantities and discuss how they can be constructed. In particular, we discuss the curvature perturbation ζ, which is a measure of the density perturbation and quantifies the scalar fluctuations in the universe.

In Section 2.3, we discuss statistical properties of a stochastic field and discuss how they can be quantified by various parameters. Without loss of generality, we focus on ζ as an example and introduce various primordial cosmological parameters which can be related to the statistical properties of CMB anisotropies.

Finally in Section 2.4 we discuss the separate universe approximation [30, 31, 32] and explain the alternative δN formalism [33, 34] which has been proved to be very useful in Early Universe applications. We also show that ζ is conserved on superhorizon scales in the adiabatic limit.

2.1 Cosmological Perturbation Theory

The basic idea of cosmological/relativistic perturbation theory is straightforward: given a theory of gravity, we perform Taylor expansions and perturb the metric $g_{\mu\nu}$ and the stress-energy tensor of the cosmic fluid $T^{\mu\nu}$ to appropriate orders about certain backgrounds, relate the perturbations and solve for the dynamics of these perturbations

using the coupled system of field equations derived in the gravity theory. For simplicity, we consider only linear perturbations about FRW universes and the theory of gravity below is GR.

The most generic form of a perturbed FRW metric up to first order is

$$\begin{aligned} ds^2 = & \quad (\bar{g}_{\mu\nu} + \delta g_{\mu\nu}) \mathrm{d}x^\mu \mathrm{d}x^\nu \\ = & \quad -a^2(\eta) \left\{ (1+2\psi) \mathrm{d}\eta^2 - 2B_i dx^i \mathrm{d}\eta - [(1-2\phi)\delta_{ij} + 2E_{ij}] \, \mathrm{d}x^i \mathrm{d}x^j \right\} \end{aligned} \tag{2.1}$$

where the quantities ψ, ϕ, B_i and E_{ij} are all functions of η and x^i. E_{ij} is a symmetric, trace-free tensor. Here we have introduced the conformal time η, which is related to the cosmic time t in Eq. (1.1) by $\mathrm{d}t = a\mathrm{d}\eta$. We can use η to define a conformal Hubble parameter $\mathcal{H} \equiv a'/a$, where prime denotes differentiation with respect to η. Note that ψ and ϕ are scalar functions but not Lorentz scalars. It is also convenient to decompose B_i and E_{ij} into scalar, vector and tensor parts

$$\begin{aligned} B_i &\equiv \partial_i B + B_i^T \,, \\ E_{ij} &\equiv \partial_i \partial_j E + \partial_{(i} E_{j)}^T + h_{ij} \,, \end{aligned} \tag{2.2}$$

where E_i^T, B_i^T are divergence-free and h_{ij} is symmetric, trace-free and divergence-free.

At linear order, scalar, vector and tensor perturbations are decoupled from each other and therefore it is convenient to study them independently. It is not the case at higher orders in general though, for instance see [35].

The components of stress-energy tensor for a perfect fluid, up to first-order, are given by

$$\begin{aligned} T_0^0 &= -(\bar{\rho} + \delta\rho) \,, \\ T_0^i &= q^i \,, \\ T_j^i &= (\overline{P} + \delta P)\delta^{ij} + \Pi^{ij} \,. \end{aligned} \tag{2.3}$$

Here $T_\nu^\mu \equiv T^{\mu\sigma} g_{\sigma\nu}$ and overline denotes the background averaged quantities, whereas $\delta\rho(\eta, x^i)$ and $\delta P(\eta, x^i)$ are linear perturbations of energy density and pressure. Π^{ij} is

the trace-free anisotropic stress, which is already of linear order. This can be seen from the fact that the background geometry in a Friedmann Universe is homogeneous and isotropic. Defining the perculiar velocity of the fluid as $v^i \equiv dx^i/d\eta$, one can show that the 3-momentum density perturbation q_i is related to v_i through

$$q_i = (\bar{\rho} + \bar{P})(B_i + v_i) \tag{2.4}$$

to linear order. We can also decompose q_i into scalar and vector parts, i.e $q_i = \partial_i \delta q + q_i^T$ and similarly for v_i as previously described. Focussing on the scalar part of the 3-momentum, we therefore have $\delta q = (\bar{\rho} + \bar{P})(B + v)$.

After perturbing all quantities to linear order, we then work out how the perturbations evolve by solving the perturbed Einstein equation

$$\delta G_{\mu\nu} = 8\pi G \delta T_{\mu\nu} - \Lambda \delta g_{\mu\nu} \, . \tag{2.5}$$

Restricting ourselves to the early Universe where Λ is negligible, the perturbed Einstein equation then reads as $\delta G_{\mu\nu} = 8\pi G \delta T_{\mu\nu}$.

2.2 Gauge Invariant Quantities

Because of differomorphism invariance in GR, there are gauge degrees of freedom in the theory. Under a coordinate transformation $x^\mu \to x^\mu + \xi^\mu$ where $x^\mu = (\eta, x^i)$ and $\xi^\mu = (T, L^i)$, any perturbation of a given tensorial quantity $\delta y^{\alpha_1,\alpha_2\ldots}_{\beta_1,\beta_2,\ldots}$ transforms as Lie derivatives

$$\delta y^{\alpha_1,\alpha_2\ldots}_{\beta_1,\beta_2,\ldots} \to \delta y^{\alpha_1,\alpha_2\ldots}_{\beta_1,\beta_2,\ldots} - (\mathcal{L}_\xi y)^{\alpha_1,\alpha_2\ldots}_{\beta_1,\beta_2,\ldots} \tag{2.6}$$

where the Lie derivative is given by

$$\begin{aligned}(\mathcal{L}_\xi y)^{\alpha_1,\alpha_2\ldots}_{\beta_1,\beta_2,\ldots} = \quad & \xi^\sigma(\nabla_\sigma y^{\alpha_1,\alpha_2\ldots}_{\beta_1,\beta_2,\ldots}) \\ & -(\nabla_\sigma \xi^{\alpha_1}) y^{\sigma,\alpha_2\ldots}_{\beta_1,\beta_2,\ldots} - (\nabla_\sigma \xi^{\alpha_2}) y^{\alpha_1,\sigma,\ldots}_{\beta_1,\beta_2,\ldots} - \ldots \\ & +(\nabla_{\beta_1} \xi^\sigma) y^{\alpha_1,\alpha_2\ldots}_{\sigma,\beta_2,\ldots} + (\nabla_{\beta_2} \xi^\sigma) y^{\alpha_1,\alpha_2,\ldots}_{\beta_1,\sigma,\ldots} + \ldots \end{aligned} \tag{2.7}$$

The perturbations we discussed previously in the last section are therefore not gauge-invariant, i.e. they depend upon the coordinate we choose. For example, the gravitational potential ψ transforms as $\psi \to \psi - T' - \mathcal{H}T$.

By considering how the perturbations of different quantities transform, one can combine them together to form gauge-invariant quantities. Combining the four scalar perturbations in the metric we can construct the so-called **Bardeen variables** [27]

$$\begin{aligned} \Psi_{\rm B} &\equiv \psi + \mathcal{H}(B - E') + B' - E'' \,, \\ \Phi_{\rm B} &\equiv \phi - \mathcal{H}(B - E') \,. \end{aligned} \tag{2.8}$$

Any physical observables should be independent of the choice of coordinate system and can be constructed from gauge-invariant quantities. For instance, the curvature perturbation ζ that we will introduce shortly, is constructed to be gauge-invariant by definition.

2.2.1 Curvature Perturbation, ζ

A very useful gauge-invariant quantity is the **comoving curvature perturbation** $\mathcal{R}$. This is the intrinsic curvature perturbation on comoving or constant η hypersurfaces, i.e. hypersurfaces orthogonal to worldlines that are comoving with the cosmic fluid where $q^i = 0$ [29, 36, 37]

$$\mathcal{R} \equiv -\phi + \mathcal{H}(B + v) \,, \tag{2.9}$$

or in terms of the 3-momentum δq

$$\mathcal{R} \equiv -\phi + \frac{\mathcal{H}}{\bar{\rho} + \bar{P}} \delta q \,. \tag{2.10}$$

Another commonly used gauge-invariant quantity is ζ, **the curvature perturbation on uniform energy density hypersurfaces**. It is defined as [38, 39]

$$\zeta \equiv -\phi + \frac{\mathcal{H}}{\bar{\rho}'} \delta\rho \,. \tag{2.11}$$

In the flat gauge where $\phi = 0$, it is related to the density constrast $\delta\rho/\rho$ for an adiabatic fluid. The two quantities $\mathcal{R}$ and ζ are related by

$$\zeta = \mathcal{R} + \frac{\mathcal{H}}{\bar{\rho}'}\delta\rho_{\rm com}\,, \tag{2.12}$$

where $\rho_{\rm com}$ is the comoving density perturbation defined as $\delta\rho_{\rm com} \equiv \delta\rho - 3\mathcal{H}\delta q$. In the case of slow-roll inflation, the difference vanishes and ζ and $\mathcal{R}$ coincide on superhorizon scale as $\delta\rho_{\rm com} \to 0$. In the following we will therefore refer to the curvature perturbation as ζ unless stated otherwise. ζ quantifies the scalar fluctuations in the universe and can be related to the amplitude of the primordial fluctuations we see in the CMB and the density constrast in the large-scale structure.

An important property of the curvature perturbation ζ is the fact that it is conserved on superhorizon scales for an adiabatic fluid for which its pressure P is a unique function of its energy density ρ, i.e. $P = P(\rho)$, as we will show later in Section 2.4 using the separate universe approximation.

Although ζ is gauge-invariant, it was found recently by White et al. that ζ is frame-dependent if isocurvature perturbations (to be introduced in Chapter 3) exist, i.e. ζ evaluated in the Jordan frame is in general different to that evaluated in the Einstein frame [40, 41]. [1]

2.3 Primordial Cosmological Observables

Just as with any physical measurements, the gauge-invariant cosmological perturbations we have discussed earlier in general have random statistical disturbations even at a fixed instant of time. They act as statistical ensembles. It is therefore the statistical properties of these distributions we could like to measure and compare with theoretical model predictions.

In this section we will briefly discuss the essential mathematics concerning the statistics of a stochastic field. Focussing on the curvature perturbation ζ, we will illustrate how we construct observables related to the statistical properties of the perturbations

[1] Recently it has been argued by Postma and Volponi that this can be resolved if ζ is defined purely in terms of dimensionless and gauge-invariant quantities [42].

of interest.

2.3.1 Two-Point Statistics

Consider a random field $f(\mathbf{x})$ with zero mean $\langle f(\mathbf{x})\rangle = 0$ where

$$\langle f(\mathbf{x})\rangle = \int \mathcal{D}f \Pr[f] f(\mathbf{x})\,, \tag{2.13}$$

where the integral means the functional integral over all field configurations. Here $\Pr[f]$ denotes the probability of realising the field configuration $f(x)$. The two-point correlation function of this random field is given by

$$\langle f(\mathbf{x})f(\mathbf{y})\rangle = \int \mathcal{D}f \Pr[f] f(\mathbf{x})f(\mathbf{y})\,. \tag{2.14}$$

If this field $f(\mathbf{x})$ is also statistically homogeneous and isotropic, then the two-point function depends only on the distance between **x** and **y**

$$\langle f(\mathbf{x})f(\mathbf{y})\rangle \propto F(|\mathbf{x}-\mathbf{y}|)\,. \tag{2.15}$$

In Fourier space, this gives a δ-function in the correlation function

$$\langle f(\mathbf{k})f^*(\mathbf{k}')\rangle = \frac{2\pi^2}{k^3} P_f(k)\delta(\mathbf{k}-\mathbf{k}')\,, \tag{2.16}$$

where $k = |\mathbf{k}|$. Here the normalisation factor $2\pi^2/k^3$ is introduced such that P_f is defined as the dimensionless power spectrum given $f(\mathbf{k})$ is dimensionless.

Now consider the curvature perturbation ζ as an example. As mentioned, for the two-point function, we can define a dimensionless power spectrum $P_\zeta(k)$ as in Eq. (2.16)

$$\langle \zeta(\mathbf{k})\zeta^*(\mathbf{k}')\rangle = \frac{2\pi^2}{k^3} P_\zeta(k)\delta(\mathbf{k}-\mathbf{k}')\,. \tag{2.17}$$

For an exact scale-invariant spectrum, the amplitude of P_ζ is constant and independent of k. However, in general ζ depends on scale k and so does P_ζ. We will see that however inflation generically predicts a nearly scale-invariant spectrum in the next chapter. In that case, at leading order, it is convenient to parameterise the scale dependence of

the power spectrum P_ζ by **the tilt or the spectral index** $n_\mathrm{s} - 1$, defined by

$$n_\mathrm{s} - 1 \equiv \frac{\mathrm{d}\ln P_\zeta(k)}{\mathrm{d}\ln k}\,. \tag{2.18}$$

In the most general case, n_s may also depend on k, which can be quantified by **the running** α, defined in a similar fashion

$$\alpha \equiv \frac{\mathrm{d}n_\mathrm{s}}{\mathrm{d}\ln k}\,. \tag{2.19}$$

Note that P_ζ, n_s and α depend on the pivot scale k_* we choose. For all-sky CMB observations, the pivot scale is usually set to be $k_* = 0.002\mathrm{Mpc}^{-1}$. [2] Eqs. (2.18)-(2.19) correspond to parametrising the power spectrum $P_\zeta(k)$ as

$$P_\zeta(k) = A_\zeta \left(\frac{k}{k_*}\right)^{n_\mathrm{s}-1+\frac{\alpha}{2}\ln(k/k_*)}\,. \tag{2.20}$$

Here A_ζ denotes the amplitude of the power spectrum P_ζ. Observations of the CMB from the Planck satellite mission suggests $A_\zeta \sim 2\times 10^{-9}$, $n_s = 0.9603 \pm 0.0073$ at 95% C.L. (Planck + WP data), with negligible running [44].

Similar to the scalar mode, tensor modes or primordial gravitational waves are also excited during inflation via vacuum excition. We can also define a dimensionless power spectrum for the tensor perturbation h_{ij} as $\int \mathrm{d}\ln k P_h \equiv \langle h_{ij}h^{ij}\rangle$, and similarly a corresponding tensor tilt n_T.

$$P_h(k) = A_h \left(\frac{k}{k_*}\right)^{n_\mathrm{T}}\,. \tag{2.21}$$

The primordial tensor perturbation is usually quantified by **the tensor-to-scalar ratio** r, defined as

$$r \equiv A_h/A_\zeta\,, \tag{2.22}$$

which is the ratio between the amplitudes of the tensor and scalar power spectra. The current constraint given by the Planck + WP + high-l CMB ACT and SPT data is

[2] For discussion on the choice of pivot scale, see [43].

$r < 0.11$ at 95% C.L. for the same pivot scale $k_* = 0.002\mathrm{Mpc}^{-1}$ [44]. Recently, however, there is a claim of discovery of $r \sim 0.2$ by BICEP2 [45], which appears to be in tension with the Planck results. Questions about foregrounds substraction in BICEP2 data have been raised [46]. This will be resolved when the full Planck polarisation data are released in late 2014.

For purely Gaussian fluctuations, all statistical information is contained in the two-point correlation function. In simple single-field models, we will see in the next chapter that ζ is indeed Gaussian to a very good approximation. Higher order correlation functions are negligible and observationally irrelevant in single-field models. The above parameters are enough to describe the primordial fluctuations we see on the CMB. However, for inflation models with multiple fields, this may not be true in general and higher order correlation functions could become important.

2.3.2 Primordial Non-Gaussianity

Primordial non-Gaussianity is the measure of deviation from a perfect Gaussian fluctuation for the curvature perturbation ζ. By definition, for any pure Gaussian fluctuations f, all the statistical information is contained via the two-point statistics $\langle f(x)f(y)\rangle$. Any higher-order correlation functions like $\langle f(x)f(y)f(z)\rangle$ are either zero for odd numbers of f or functions of the two-point correlation function for even numbers. At leading order, non-Guassianity is quantified in terms of the bi- and trispectrum, which are defined respectively in Fourier space by

$$\langle \zeta_{\mathbf{k}_1}\, \zeta_{\mathbf{k}_2}\, \zeta_{\mathbf{k}_3}\rangle \equiv (2\pi)^3\delta^3(\mathbf{k_1}+\mathbf{k_2}+\mathbf{k_3})B_\zeta(k_1,k_2,k_3)\,, \tag{2.23}$$

$$\langle \zeta_{\mathbf{k}_1}\, \zeta_{\mathbf{k}_2}\, \zeta_{\mathbf{k}_3}\, \zeta_{\mathbf{k}_4}\rangle \equiv (2\pi)^3\delta^3(\mathbf{k_1}+\mathbf{k_2}+\mathbf{k_3}+\mathbf{k_4})T_\zeta(k_1,k_2,k_3,k_4,k_{12},k_{13})\,, \tag{2.24}$$

where $k_{ij} \equiv |\mathbf{k}_i+\mathbf{k}_j|$. Again the delta functions come from the assumption of statistical homogeneity and isotropy. The level of non–gaussianity is quantified by the amplitudes of these higher-order correlation functions, which are conventionally parametrised by

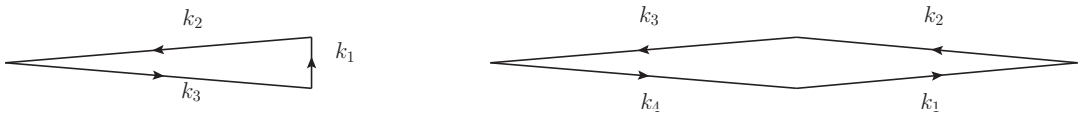

Figure 2.1: Local non-Gaussianity peaks in the the squeezed limit for $f_{\rm NL}$, and in the collapsed limit for $\tau_{\rm NL}$

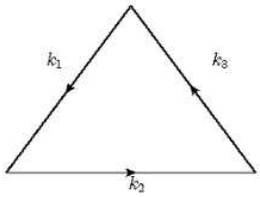

Figure 2.2: Equilateral non-Gaussianity peaks in the equilateral limit for $f_{\rm NL}$

the dimensionless non-linear parameters $f_{\rm NL}$ [47], $\tau_{\rm NL}$ and $g_{\rm NL}$ [48, 49]

$$B_\zeta(k_1,k_2,k_3) = \frac{6}{5} f_{\rm NL}\left[P_\zeta(k_1)P_\zeta(k_2) + 2\,\text{perms}\right]\,, \tag{2.25}$$

$$T_\zeta(k_1,k_2,k_3,k_4,k_{12},k_{13}) = \tau_{\rm NL}\left[P_\zeta(k_{12})P_\zeta(k_1)P_\zeta(k_3) + 11\,\text{perms}\right] + \frac{54}{25} g_{\rm NL}\left[P_\zeta(k_1)P_\zeta(k_2)P_\zeta(k_3) + 3\,\text{perms}\right] \tag{2.26}$$

where $\rm perms$ denotes permutations over k_i. In general these non-linear parameters $f_{\rm NL}$, $\tau_{\rm NL}$ and $g_{\rm NL}$ are functions of wavevectors $\mathbf{k}_i$ and thus are shape dependent. A particular type of non-Gaussianity is that of the form

$$\zeta = \zeta_G + (3/5) f_{\rm NL}(\zeta_G^2 - \langle\zeta_G^2\rangle) + (9/24) g_{\rm NL}\zeta_G^3\,, \tag{2.27}$$

where ζ_G is the Gaussian part. This is known as a **local type of non-Gaussianity**. In the local shape, $\langle\zeta\zeta\zeta\rangle$ peaks in the squeezed limit for $f_{\rm NL}$ ($k_1 \to 0$), and $\langle\zeta\zeta\zeta\zeta\rangle$ peaks in the collapsed limit for $\tau_{\rm NL}$ ($k_1 + k_2 \to 0$), see Fig. 2.1. Recalling that the skewness of a probability distribution g is defined as $S_g \equiv \langle g^3\rangle \,/\, \langle g^2\rangle^{3/2}$, we can see that $f_{\rm NL}$ is an estimator of the skewness of the statistics of ζ. Similarly, $g_{\rm NL}$ gives an estimate of the kurtosis.

Another type which is often considered is the **equilateral non-Gaussianity**. As the name suggests, the equilateral type peaks in the limit where all the external momenta are equal, i.e. $k_1 = k_2 = k_3$. This shape is usually enhanced by non-linear interactions at horizon-crossing. In this thesis, we will focus only on the local and equilateral

shapes of non-Gaussianity. For a complete review on the topic of non-Gaussianity, see [50].

No convincing evidence of primordial non-Gaussianity has so far been observed. Current constraints from Planck data on $f_{\rm NL}$ are: $f_{\rm NL}^{\rm local} = 2.7 \pm 5.8$ at 68% C.L. for the local shape, $f_{\rm NL}^{\rm eq} = -42 \pm 75$ at 68% C.L. for the equilateral shape [51]. Less tight constraints come from large scale structure measurements, where $-37 < f_{\rm NL}^{\rm local} < 25$ from measurements of galaxy clustering and the integrated Sachs-Wolfe effect [52] and recently $-49 < f_{\rm NL}^{\rm local} < 31$ from measurements of the clustering of 800,000 photometric quasars [53], all at 95% C.L. [3]. For the local trispectrum, Planck data gives $\tau_{\rm NL}/10^3 < 2.8$ at 95% C.L. [51], whereas the constraints on $g_{\rm NL}$ have yet been worked out, though there has been discussion on the implications of the Planck bispectrum constraints for the trispectrum [55]. On the other hand, WMAP 9–year data gives the following constraint: $-5.5 < g_{\rm NL}/10^5 < -1.1$ at 68% C.L. [56], with Regan et al. finding a compatible constraint $-6.4 < g_{\rm NL}/10^5 < -1.8$ at 68% C.L. [57]. Similar constraints for $g_{\rm NL}$ were also found in [52, 53] using large scale structure measurements.

Scale Dependent Non-Gaussianity

Like the power spectrum, it is natural that the non-linearity parameters are scale dependent [58, 59, 60, 61], quantified by their spectral indices. For instance, the spectral indices of $f_{\rm NL}$ and $\tau_{\rm NL}$, denoted by $n_{f_{\rm NL}}$ and $n_{\tau_{\rm NL}}$, are defined by

$$n_{f_{\rm NL}} \equiv \frac{{\rm d}\ln|f_{\rm NL}|}{{\rm d}\ln k}\,, \tag{2.28}$$

$$n_{\tau_{\rm NL}} \equiv \frac{{\rm d}\ln|\tau_{\rm NL}|}{{\rm d}\ln k}\,, \tag{2.29}$$

where k marks the length of any one side of the n-gon, provided that all sides are scaled in the same proportion [60]. Examples of models where $n_{f_{\rm NL}}$ and $n_{\tau_{\rm NL}}$ can be observably large, i.e. $O(0.1)$, are the curvaton model with quartic self-interaction

[3] Recently there has been a claim of a detection of local $f_{\rm NL}$ from quasar measurements in the Sloan Digital Sky Survey [54].

terms [62, 63] [4] and Modulated Reheating [60].

Forecasts have been made to assess our ability to detect the spectral indices of the non–linear parameters. For $n_{f_{\rm NL}}$, Planck could reach a $1-\sigma$ sensitivity of $\sigma_{n_{f_{\rm NL}}} \sim 0.1$ given $f_{\rm NL} = 50$ [65]. By measurements of the CMB μ-distortion in a CMB experiment such as PIXIE, $n_{f_{\rm NL}}$ and $n_{\tau_{\rm NL}}$ could also be measured to an accurancy of the order of $O(0.3)$ and $O(0.6)$ respectively for $f_{\rm NL} = 20$ and $\tau_{\rm NL} = 5000$, and similarly in large-scale surveys such as Euclid [66].[5]

2.4 Separate Universe Picture

An alternative approach to the cosmological perturbation theory discussed earlier is the **separate universe approximation** [30, 31, 32], if we are interested only in perturbations on superhorizon scales. It is a powerful tool for studying perturbations in the Early Universe. The separate universe picture refers to the behaviour of the Universe after smoothing on a specified scale k much larger than the horizon. The underlying assumption is that spatial derivatives are negligible compared to time derivatives.

The separate universe approximation is also related to the **gradient expansion approximation** [67]. In the gradient expansion scheme, the full non-linear field equations are written in terms of a small gradient expansion parameter $\epsilon \equiv k/aH$ [6] and the limit $\epsilon \to 0$ corresponds to an unperturbed FRW universe. That is, the metric of any local region can be written as an unperturbed FRW metric in an appropriate set of coordinates

$$ds^2 = -\mathrm{d}t^2 + a^2(t)_{\rm local}\delta_{ij}\mathrm{d}x^i\mathrm{d}x^j \,. \tag{2.30}$$

During inflation, the gradient terms quickly drop out after horizon exit as aH grows exponentially, justifying ϵ being a small parameter. At zeroth order $O(\epsilon^0)$, we can see

[4] Note if the BICEP2 result is verified such that $r \sim 0.1$, then pure curvaton models will be ruled out [64].

[5] Their definition of $n_{\tau_{\rm NL}}$ differs from the one used here, in the fact that in their case, $n_{\tau_{\rm NL}} \neq \mathrm{d}\ln|\tau_{\rm NL}|/(\mathrm{d}\ln k)$. The two definitions are related when the four k vectors form a square by $2n^{\rm theirs}_{\tau_{\rm NL}} = n^{\rm ours}_{\tau_{\rm NL}}$, in which case we have to double their forecasted error bars when comparing to our definition of $n_{\tau_{\rm NL}}$.

[6] Do not confuse this with the slow-roll parameter ϵ_H that was defined previously in Eq. (1.19).

that the full non-linear field equations have the same forms as those at the background level. This suggests we can treat the whole Universe as an ensemble of independent FRW universes, which only differ by initial conditions that are sourced by quantum fluctuations. This simplifies the analysis of superhorizon perturbation evolution [31, 34, 37, 38, 68, 69] and leads to the famous δN formalism, which will be explained in detail in the following section.

2.5 The δN Formalism

One consequence of the separate universe approximation is the δN formalism, which will be used extensively in this thesis. The formalism can be understood as follows: Consider a foliation of spacetime $\Sigma(t)$, where $\Sigma(t)$ is the spacelike hypersurface at time t. Let n^μ be the unit vector normal to $\Sigma(t)$. Define the rate of change of n^μ as θ

$$\theta \equiv \nabla_\mu n^\mu \,. \tag{2.31}$$

The volume expansion rate along some worldlines is

$$\tilde{N} \equiv \int \frac{\theta}{3} \mathrm{d}\tau \,, \tag{2.32}$$

where τ is the proper time. This is defined purely geometrically. It is convenient to write the full perturbed metric in the ADM form [70]

$$\mathrm{d}s^2 = -\mathcal{N}^2 \mathrm{d}t^2 + \gamma_{ij}(\mathrm{d}x^i + \beta^i \mathrm{d}t)(\mathrm{d}x^j + \beta^j \mathrm{d}t) \,, \tag{2.33}$$

where $\mathcal{N}$ and β^i are the lapse and shift functions, and γ_{ij} is the spatial 3-metric. Without loss of generality, we choose the foliation of spacetime $\Sigma(t)$ as $x^0 = t = \mathrm{const.}$ The unit vector n^μ normal to $\Sigma(t)$ is then

$$n^\mu = \left(\frac{1}{\mathcal{N}}, -\frac{\beta^i}{\mathcal{N}} \right) \,. \tag{2.34}$$

We then define $\tilde{\zeta}$ by rewriting the spatial part of the metric in the form

$$\gamma_{ij} = \tilde{a}^2(\mathbf{x},t)\tilde{\gamma}_{ij}(\mathbf{x}) \text{ with } \tilde{a}(\mathbf{x},t) \equiv a(t)e^{\tilde{\zeta}(\mathbf{x},t)}, \quad \tilde{\gamma}_{ij}(\mathbf{x}) \equiv (Ie^h)_{ij}\,. \tag{2.35}$$

Here $a(t)$ is the homogeneous background scale factor after smoothing. Here $\tilde{\gamma}$ has unit determinant and the matrix h is traceless. We can see this corresponds to $\tilde{\zeta} = \ln(\tilde{a}/a) = \delta(\ln\tilde{a})$. Note that we have not assumed $\tilde{\zeta}$ to be small here. From the separate universe approximation we know the metric can be written as an unperturbed FRW metric locally, we can thus deduce β^i is of order $O(\epsilon)$, $g\tilde{a}\tilde{m}m a_{ij}$ and h_{ij} must be time-independent, whereas $\tilde{\zeta}$ must vanish locally because $\tilde{a}(\mathbf{x},t)$ is the locally defined scale factor. The volume expansion Eq. (2.32) as seen by a comoving observer between t_1 and t_2 is thus

$$\tilde{N} = \int_{t_1}^{t_2} \frac{\theta}{3}\mathrm{d}\tau = \int_{t_1}^{t_2} \frac{\theta}{3}\mathcal{N}\mathrm{d}t = \int_{t_1}^{t_2} \left(\frac{\dot{a}}{a} + \dot{\tilde{\zeta}}\right)\mathrm{d}t\,, \tag{2.36}$$

which equals the corresponding number of e-folds of expansion between t_1 and t_2 defined by $H_{\rm local}$

$$N(t_2,t_1;\mathbf{x}) = \ln\left[\frac{a(t_2)}{a(t_1)}\right] + \tilde{\zeta}(t_2,\mathbf{x}) - \tilde{\zeta}(t_1,\mathbf{x})\,. \tag{2.37}$$

Choosing the initial hypersurface to be flat ($\zeta = 0$) and the final one to be the uniform density ($\delta\rho = 0$), we immediately arrive at the result [67]

$$\tilde{\zeta}(t_2,\mathbf{x})|_\rho = N(t_2,t_1;\mathbf{x}) - \ln\left[\frac{a(t_2)}{a(t_1)}\right] = \delta N(t_1,t_2;\mathbf{x})\,. \tag{2.38}$$

Recall that on uniform-density slicing, $\zeta = \tilde{\zeta}$ and thus we have $\zeta = \delta N$. This is the well-known δN **formalism** [33, 34], which states that the curvature perturbation ζ is equal to the difference in the number of e-folds expansion between an initial flat hypersurface and a final uniform-density hypersurface, i.e. $\zeta(\mathbf{x},t) = \delta N(\mathbf{x},t)$. This formalism holds as long as the Universe can be locally approximated by a FRW universe. This is an important result and we will use this in most of the analysis that follows.

2.5.1 Conservation of ζ

In Section 2.2.1, we have stated that the curvature perturbation ζ is conserved on superhorizon scales. We will now show this by using the gradient expansion in the following, first done by Lyth et al. [67].

In comoving coordinates, the 4-velocity of the comoving fluid is

$$\begin{aligned} u^\mu &= \left(\frac{1}{\mathcal{N}}, 0\right) + O(\epsilon^2) \\ u_\mu &= \left(-\mathcal{N}, \frac{\beta^i}{\mathcal{N}}\right) + O(\epsilon^2)\,. \end{aligned} \tag{2.39}$$

To leading order in the gradient expansion parameter ϵ, the expansion rate of u^μ is equal to that of n^μ. Recall the definition of the energy-momentum tensor for a perfect fluid Eq. (1.2), on uniform-density slicings, the continuity equation $u_\mu \nabla_\nu T^{\mu\nu} = 0$ then reads as

$$\begin{aligned} \dot{\rho}(t) \quad &= -3\frac{\dot{\tilde{a}}(\mathbf{x},t)}{\tilde{a}(\mathbf{x},t)}\left[\rho(t) + P(\mathbf{x},t)\right] + O(\epsilon^2) \\ &= -3\left[\frac{\dot{a}}{a} + \dot{\tilde{\zeta}}\right]\left[\rho(t) + P(\mathbf{x},t)\right] + O(\epsilon^2) \end{aligned} \tag{2.40}$$

to leading order in the gradient expansion. For an adiabatic fluid where $P = P(\rho)$, the spatial dependence of P also vanishes and thus from Eq. (2.40) we can deduce $\dot{\tilde{\zeta}}$ is independent of the position. Without loss of generality, we can choose the background scale factor $a(t)$ such that $\dot{\tilde{\zeta}}$ vanishes. However we also know that on uniform-density slicings, the curvature perturbation is given by $\tilde{\zeta}$. As a result, we conclude that the curvature perturbation ζ is conserved on superhorizon scale beyond linear order regardless of the theory of gravity in the adiabatic limit as long as the continuity equation holds. For all single-field models where slow-roll solution is an attractor in phase space, the perturbations are purely adiabatic and ζ is conserved on superhorizon scales. In multifield models however, as we will see in Chapter 3, entropic or isocurvature perturbations exist and $\delta P_{\rm nad} \neq 0$ [7] in general. ζ is no longer conserved and it is important to follow the superhorizon evolution of ζ when comparing with observations. **In fact ζ is only conserved on superhorizon scales when these entropic perturbations van-**

[7] Define later.

ish, first demonstrated by Rigopoulos and Shellard [71]. This was later generalised to non-canonical multifield models minimally coupled to gravity with at most first derivatives by Christopherson and Malik [72], and recently to higher-derivative models that preserve second-order field equations by Naruko and Sasaki [73] and Gao [74].

Chapter 3

Predictions from Slow-roll Inflation

In this chapter we discuss the observational predictions of the standard canonical slow-roll inflation paradigm, including single and multiple field models. In particular, we focus on canonical models minimally coupled to gravity.

We start by introducing the 'in-in' formalism and the δN formulae which are commonly used to compute cosmological correlation functions of ζ in Sections 3.1 and 3.2. In Section 3.3 we discuss the model predictions of simplest single-field models, compute the correlation functions of ζ and the corresponding primordial observables. In particular, we reproduce the famous Maldacena result [75], a no-go theorem for primordial non-Gaussianity in simplest single-field inflation.

Then in Section 3.4, we introduce the multifield inflation models and discuss the main difference between single and multifield models, which is the existence of entropic perturbations. We give the multifield model predictions in terms of the δN coefficients in Section 3.4.2. Finally we end this chapter by discussing the technical difficulties in computing the δN coefficients in general.

3.1 In-In Formalism

Before discussing inflationary model predictions, we first introduce the operator formalism used in computing correlation functions in cosmology, namely the **'in-in' formalism or the 'closed time path (CPT)' formalism** [76, 77]. This formalism is simi-

lar to canonical quantisation in QFT, except for the fact that we are now computing on a closed time path. Unlike in QFT in which we compute the S-matrix, the transition amplitude between asymptotic 'in' and 'out' states, in the 'in-in' formalism we are interested in correlation functions evaluated at a fixed instant of time given some initial conditions.

In this formalism, the correlation function of some operator $\hat{Q}$ evaluated at time t is given by

$$\left\langle \hat{Q}(t) \right\rangle = \left\langle \Omega \middle| \hat{T}^{\dagger} \exp\left(i \int_{t_0}^{t} \hat{H}_{\rm int}(t') \mathrm{d}t' \right) \hat{Q}(t) \hat{T} \exp\left(-i \int_{t_0}^{t} \hat{H}_{\rm int}(\tilde{t}') \mathrm{d}\tilde{t}' \right) \middle| \Omega \right\rangle \quad (3.1)$$

in the interaction picture, where the full Hamiltonian is split into two parts: a free part H_0 and an interaction part $H_{\rm int}$, i.e. $\hat{H} = \hat{H}_0 + \hat{H}_{\rm int}$. Here $\hat{T}$, $\hat{T}^{\dagger}$ are the time and anti-time ordering operators, and $|\Omega\rangle$ is the interacting theory vacuum at t_0. One then expands the evolution operator, $\exp(-i \int H_{\rm int} \mathrm{d}t')$, in Eq. (3.1) to compute the correlation functions of interest to leading order as in perturbation theory.

For instance, take $\hat{Q} = (\hat{\delta\varphi})^3$, by Taylor expanding the exponentials in Eq. (3.1), we find the 3-point function of a scalar field perturbation $\delta\varphi$ in Fourier space at time t is given by

$$\langle \delta\varphi_{\mathbf{k_1}}(t) \delta\varphi_{\mathbf{k_2}}(t) \delta\varphi_{\mathbf{k_3}}(t) \rangle = -i \int_{t_0}^{t} \langle \delta\varphi_{\mathbf{k_1}}(t) \delta\varphi_{\mathbf{k_2}}(t) \delta\varphi_{\mathbf{k_3}}(t) H_{\rm int}(t') \rangle \, \mathrm{d}t' + \mathrm{c.c}\,. \quad (3.2)$$

to leading order. Here c.c stands for the complex conjugate.

3.2 Separate Universe Approach, δN Formulae

An alternative formalism for calculating correlation functions of ζ on superhorizon scales is the δN formalism discussed in Section 2.5. It follows that in a FRW universe dominated by M canonical slow-roll scalar fields φ^I at horizon-exit t_*, the difference in the number of e-folds of expansion between different superhorizon patches can be

accounted for by perturbations of the scalar fields at horizon-exit $\delta\varphi^I_*$ [69] [1]

$$\zeta(\mathbf{x},t) = \delta N(\mathbf{x},t) = \sum_I N_I \delta\varphi^I_* + \frac{1}{2}\sum_{IJ} N_{IJ}\delta\varphi^I_*\delta\varphi^J_* + ... \tag{3.3}$$

from perturbative Taylor expansion. Again N is defined as the total number of e-folds of expansion from an initial flat hypersurface at horizon-exit t_* to a final uniform-density hypersurface at time t. Here I, J are the field labels, whereas N_I, N_{IJ}, etc are the δN coefficients defined as partial derivatives with respect to the scalar fields, e.g. $N_I \equiv \partial N/\partial\varphi^I$. This was later generalised to models with a curved field space metric, where the kinetic terms are non-canonical, by Saffin [78] and Elliston et.al. [79]. It should be stressed that we only require slow-roll at horizon exit, but not the entire evolution.

From Eq. (3.3), we can then relate the correlation functions of ζ, $\langle\zeta\zeta...\zeta\rangle$, to that of the field perturbations $\left\langle\delta\varphi^{I_1}\delta\varphi^{I_2}...\delta\varphi^{I_n}\right\rangle$ at horizon-exit. For instance, to leading order, the 3-point function $\langle\zeta\zeta\zeta\rangle$ at time t is given by

$$\begin{aligned}\langle\zeta(\mathbf{k}_1,t)\zeta(\mathbf{k}_2,t)\zeta(\mathbf{k}_3,t)\rangle &= \sum_{IJK} N_I N_J N_K \left\langle\delta\varphi^I(\mathbf{k}_1,t_*)\delta\varphi^J(\mathbf{k}_2,t_*)\delta\varphi^K(\mathbf{k}_3,t_*)\right\rangle \\ &+\frac{1}{2}\sum_{IJKL} N_I N_J N_{KL}\left\langle\delta\varphi^I(\mathbf{k}_1,t_*)\delta\varphi^J(\mathbf{k}_2,t_*)[\delta\varphi^K\star\delta\varphi^L](\mathbf{k}_3,t_*)\right\rangle + \text{perms} + ...\end{aligned} \tag{3.4}$$

where $\star$ denotes the convolution product over momentum $\mathbf{k}_3$

$$[\delta\varphi^K\star\delta\varphi^L](\mathbf{k}_3,t_*) \equiv \int\frac{\mathrm{d}^3q}{(2\pi)^3}\delta\varphi^K(\mathbf{q},t_*)\delta\varphi^L(\mathbf{q}-\mathbf{k}_3,t_*) \tag{3.5}$$

and perm denotes permutation over $\mathbf{k}_i$ for the second term on the RHS. The corresponding ζ-related primordial observables such as $f_{\rm NL}$ can then be deduced once the the correlation functions of $\delta\varphi$ at horizon-exit are known. For single-field models, Eq. (3.3) simply corresponds to the gauge transformation from the flat to the uniform-density gauge.

[1] The slow-roll approximation allows us to write the field velocities $\dot\varphi^I$ as a function of all the scalar fields φ^J, i.e. $\dot\varphi^I(\varphi^J)$. Thus explicit $\dot\varphi^I$ dependence drops out.

3.3 Single-Field Inflation

We start with predictions of the simplest single-field inflation models with the action Eq. (1.16). [2] We assume there exists some regions in the potential V that are flat enough for inflation to proceed, where $\epsilon_V, \eta_V \ll O(1)$. It is convenient to first rewrite the action in the ADM form, i.e. substituting the ADM metric Eq. (2.33) into Eq. (1.16)

$$S = \frac{1}{2}\int \mathrm{d}^4x\sqrt{h}\left[\mathcal{N}R^{(3)}M_{\rm p}^2 - 2\mathcal{N}V + \mathcal{N}^{-1}(E_{ij}E^{ij} - E^2)M_{\rm p}^2 \right. \\ \left. + \mathcal{N}^{-1}(\dot{\varphi} - \beta^i\partial_i\varphi)^2 - \mathcal{N}\gamma^{ij}\partial_i\varphi\partial_j\varphi\right] . \tag{3.6}$$

Here $R^{(3)}$ is the Ricci-scalar built from the spatial metric γ_{ij} and E_{ij} is defined as

$$E_{ij} \equiv \frac{1}{2}(\dot{h}_{ij} - \nabla_i\beta_j - \nabla_j\beta_i) \tag{3.7}$$

and E is the trace of E_{ij}. ∇_i denotes the covariant derivative with respect to the 3-metric γ_{ij}.

To evaluate the predictions of single-field inflation, we consider perturbations about a de Sitter background and work in the spatially-flat gauge where $\gamma_{ij} = a^2\delta_{ij}$. To quantise the inflaton field, we first split the inflaton φ into a homogeneous slow-varying background field $\overline{\varphi}(t)$ and a small perturbation $\delta\varphi(\mathbf{x}, t)$

$$\varphi(\mathbf{x}, t) = \overline{\varphi}(t) + \delta\varphi(\mathbf{x}, t) . \tag{3.8}$$

We also perturb the lapse and shift functions to linear order in scalar perturbations

$$\mathcal{N} = 1 + \lambda_1 , \quad \beta_i = \partial_i\beta . \tag{3.9}$$

The background equations of motion are the Klein-Gordon and Hamilton-Jacobi equations

$$\ddot{\overline{\varphi}} + 3H\dot{\overline{\varphi}} + V_\varphi = 0 \\ 2M_{\rm p}^2\dot{H} = -\dot{\overline{\varphi}}^2 . \tag{3.10}$$

[2] Similar analysis using the covariant perturbation scheme [80] was done for single-field models with curved field space metric by Elliston et.al. [79].

By perturbing the full action Eq. (3.6) to quadratic order in perturbations, we get

$$\begin{aligned} S^{(2)} = \quad & \frac{1}{2}\int \mathrm{d}^4x a^3 \left[\lambda_1\left(-6M_\mathrm{p}^2H^2\lambda_1 + \lambda_1\dot{\overline{\varphi}}^2 - 2\dot{\overline{\varphi}}\dot{\delta\varphi} - 2V_\varphi\delta\varphi\right)\right. \\ & \left. -\frac{2}{a^2}\partial^2\beta\left(2M_\mathrm{p}^2H\lambda_1 - \dot{\overline{\varphi}}\delta\varphi\right) + \dot{\delta\varphi}^2 - \frac{1}{a^2}\partial_i\delta\varphi\partial^i\delta\varphi - V_{\varphi\varphi}\delta\varphi^2\right] \end{aligned} \tag{3.11}$$

upon integration by parts. Note that $\mathcal{N}$ and β_i act as Lagrange multipliers and are not dynamical. Their equations of motion correspond to momentum and Hamiltonian constraints

$$\begin{aligned} & \nabla_j\left[\frac{1}{\mathcal{N}}(E_i^j - E\delta_i^j)\right] = \frac{1}{\mathcal{N}}(\dot{\varphi} - \beta^j\partial_j\varphi)\partial_i\varphi\,, \\ & -2V - \mathcal{N}^{-2}(E_{ij}E^{ij} - E^2)M_\mathrm{p}^2 - \mathcal{N}^{-2}(\dot{\varphi} - \beta^i\partial_i\varphi)^2 - \gamma^{ij}\partial_i\varphi\partial_j\varphi = 0\,, \end{aligned} \tag{3.12}$$

which to leading order gives

$$\begin{aligned} & 2M_\mathrm{p}^2H\lambda_1 = \dot{\overline{\varphi}}\delta\varphi \\ & \lambda_1(\dot{\overline{\varphi}}^2 - 6H^2M_\mathrm{p}^2) - \dot{\overline{\varphi}}\dot{\delta\varphi} - V_\varphi\delta\varphi - 2M_\mathrm{p}^2\frac{H}{a^2}\partial^2\beta = 0\,. \end{aligned} \tag{3.13}$$

Substituting the solutions of λ_1 and β back into Eq. (3.11), we finally arrive at

$$S^{(2)} = \frac{1}{2}\int \mathrm{d}^4x a^3\left[(\dot{\delta\varphi})^2 - \frac{1}{a^2}(\partial\delta\varphi)^2 + \mathcal{M}(\delta\varphi)^2\right]\,, \tag{3.14}$$

where we have used the background equations Eq. (3.10). Here the effective mass $\mathcal{M}$ is given by

$$\mathcal{M} \equiv V_{\varphi\varphi} - \frac{1}{M_\mathrm{p}^2a^3}\frac{\mathrm{d}}{\mathrm{d}t}\left(\frac{a^3\dot{\overline{\varphi}}^2}{H}\right)\,. \tag{3.15}$$

Eq. (3.14) then yields the field equation for the field perturbations $\delta\varphi$ in Fourier space

$$\ddot{\delta\varphi} + 3H\dot{\delta\varphi} + \left(\frac{k}{a}\right)^2\delta\varphi + V_{\varphi\varphi}\delta\varphi - \frac{1}{M_\mathrm{p}^2a^3}\frac{\mathrm{d}}{\mathrm{d}t}\left(\frac{a^3\dot{\overline{\varphi}}^2}{H}\right)\delta\varphi = 0\,. \tag{3.16}$$

Writing Eq. (3.16) in terms of a conformal scalar field $v \equiv a\delta\varphi$ and conformal time η,

we then have

$$\left[\frac{\partial^2}{\partial\eta^2} + k^2 - \frac{z''}{z}\right] v_k(\eta, k) = 0\,, \tag{3.17}$$

where $z \equiv a\dot{\overline{\varphi}}/H$. This is the Mukhanov-Sasaki equation and v_k is known as the Mukhanov-Sasaki variable [81, 82]. From here onwards we will drop the overline for the background homogeneous field $\overline{\varphi}$. The effective mass term z''/z can be expressed in terms of slow-roll parameters [83, 84, 85]

$$\frac{z''}{z} = 2(aH)^2\left[1 - \frac{1}{2}\epsilon_H - \frac{3}{2}\eta_H + \frac{1}{2}\epsilon_H\eta_H + \frac{1}{2}\eta_H^2 + \frac{1}{2}\epsilon_H^2 - \frac{1}{2H}\dot{\eta}_H\right]. \tag{3.18}$$

During slow-roll inflation, these slow-roll parameters are slowly varying in time and thus we can neglect their time dependence at leading order, which gives

$$\eta \approx -\frac{1}{(1-\epsilon_H)aH}\,, \tag{3.19}$$

where η runs from $-\infty$ to 0. Thus Eq. (3.18) becomes

$$\frac{z''}{z} = \frac{\nu_{\rm R}^2 - 1/4}{\eta^2}\,,\ \ \nu_{\rm R} \approx \frac{3}{2} + \epsilon_H - \eta_H\,. \tag{3.20}$$

The general solution to Eq. (3.17) can then be expressed as a linear combination of Hankel functions

$$v_k \approx \sqrt{\frac{\pi}{4k}}(\sqrt{-k\eta})\exp\left[i(1+2\nu_R)\frac{\pi}{4}\right]\left[c_1 H^{(1)}_{\nu_{\rm R}}(-k\eta) + c_2 H^{(2)}_{\nu_{\rm R}}(-k\eta)\right]. \tag{3.21}$$

Note that $\nu_R = 3/2$ is the de Sitter limit. Here c_1 and c_2 are some constants.

Canonical Quantization

We would like to canonically quantise the conformal scalar field v. From the Mukhanov-Sasaki Equation (3.17), we can see that this is equivalent to quantisation of a 'free' scalar field with time-dependent mass $m^2 = z''/z$. As in standard canonical quantisa-

tion, we define the conjugate momentum to v as

$$\pi_v \equiv \frac{\partial \mathcal{L}}{\partial \dot{v}} = \dot{v}\,, \tag{3.22}$$

and promote v_k and π_v to operators which satisfy the following equal-time commutation relations

$$[\hat{v}(\mathbf{x},\eta), \hat{\pi}_v(\mathbf{x}',\eta)] = i\delta^{(3)}(\mathbf{x}-\mathbf{x}') \tag{3.23}$$

and are zero otherwise. We can write $\hat{v}(\mathbf{x},\eta)$ in terms of annihilation and creation operators

$$\hat{v}(\mathbf{x},\eta) = \int \frac{\mathrm{d}^3\mathbf{k}}{(2\pi)^{3/2}} \left[\hat{a}(\mathbf{k})u_k(\eta)e^{i\mathbf{k}\cdot\mathbf{x}} + \hat{a}^\dagger(\mathbf{k})u_k^*(\eta)e^{-i\mathbf{k}\cdot\mathbf{x}}\right]\,. \tag{3.24}$$

Here u_k is the mode function satisfying the same Mukhanov-Sasaki equation Eq. (3.17). From Eq. (3.23), one can show that $\hat{a}$ and $\hat{a}^\dagger$ satisfy the following commutation relation

$$[\hat{a}(\mathbf{k}), \hat{a}^\dagger(\mathbf{k}')] = \delta^{(3)}(\mathbf{k}-\mathbf{k}')\,. \tag{3.25}$$

To solve for u_k, we apply appropriate asymptotic boundary conditions to the solution Eq. (3.21).

At early times when $k^2 \gg \ddot{a}/a$ and the short-wavelength limit applies, we can approximate the FRW background as Minkowski. Choosing the vacuum to be the Minkowski vacuum where $\hat{a}(\mathbf{k})|0\rangle = 0$, the solution becomes

$$u_k(\eta) \to \frac{e^{-ik\eta}}{\sqrt{2k}} \tag{3.26}$$

in the asymptotic limit ($k\eta \to -\infty$). $|0\rangle$ is known as the **Bunch-Davies vacuum** [86]. This corresponds to choosing $c_1 = 1$ and $c_2 = 0$ in the general solution Eq. (3.21).

Well after the mode exits the horizon, where $k\eta \to 0$, the solution then asymptotes to

$$\begin{aligned} u_k(\eta) \quad &= \sqrt{\frac{\pi}{4k}}(\sqrt{-k\eta}) \exp\left[i(1+2\nu_R)\frac{\pi}{4}\right] H^{(1)}_{\nu_R}(-k\eta) \\ &\to -\frac{i\exp(-ik\eta)}{\eta\sqrt{2k^3}}\,. \end{aligned} \tag{3.27}$$

From Eq. (3.19), we can see this corresponds to a growing solution with $u_k \propto a$. The two-point correlation function for v_k, given by its quantum expectation value, is therefore

$$\begin{aligned}\langle \hat{v}_k(\eta)\hat{v}_{k'}(\eta)\rangle = & \quad |u_k(\eta)|^2 \left\langle 0 \right| \left[\hat{a}_k, \hat{a}^\dagger_{k'}\right] \left| 0 \right\rangle \\ = & \quad |u_k(\eta)|^2 \delta^{(3)}(\mathbf{k}-\mathbf{k}') = \left(\frac{a^2 H_*^2}{2k^3}\right)(-k\eta)^{3-2\nu_R}\,\delta^{(3)}(\mathbf{k}-\mathbf{k}')\,.\end{aligned} \tag{3.28}$$

Here H_* is the Hubble parameter evaluated at horizon-exit for the mode $\mathbf{k}$.

Scalar Spectrum

With the solution to the mode function u_k, we can now compute the power spectrum for the inflaton fluctuation $\delta\varphi$. Transferring back to the inflaton fluctuation $\delta\varphi$, we can thus see the modes quickly become constant a few e-folds after horizon exit. As in the convention, we assume this happens at the epoch of horizon exit. [3] The corresponding dimensionless power spectrum is therefore

$$P_{\delta\varphi}(k) \equiv \frac{k^3}{2\pi^2}\left|\frac{u_k}{a}\right|^2 = \left(\frac{H_*}{2\pi}\right)^2 (-k\eta)^{3-2\nu_R}\,. \tag{3.29}$$

Using the definition of the curvature perturbation ζ Eq. (2.11) and the fact that ζ is conserved on superhorizon scales in the slow-roll single-field model, we can then compute the power spectrum

$$P_\zeta(k) = \left(\frac{H}{\dot{\varphi}}\right)^2_* P_{\delta\varphi}(k)\,, \tag{3.30}$$

using the fact that $\delta\rho/\dot{\rho} \approx \delta\varphi/\dot{\varphi}$ to leading order in slow-roll. Since the Hubble parameter H is slowly varying during inflation, the spectrum induced by inflation is generically very close to scale-invariant. This can be seen from the spectral index n_s. Differentiating $\ln P_\zeta$ with respect to $\ln k$, we find [24]

$$n_\mathrm{s} - 1 \approx 3 - 2\nu_R = 2(\eta_V)_* - 6(\epsilon_V)_*\,. \tag{3.31}$$

[3] For discussions on the associated error with this assumption, see [87].

Here the subscript $*$ denotes the slow-roll parameters are evaluated at horizon exit. Since during slow-roll inflation we generically have $(\epsilon_V)_*, |(\eta_V)_*| \ll O(1)$, inflation predicts an almost scale invariant spectrum with small red tilt ($n_{\rm s} < 1$) for chaotic inflation where $V \propto \varphi^n$.

One can go further to study the running of the spectral index α in Eq.(2.19) as well. It is not difficult to see from Eq. (3.31) that α is second-order in slow-roll as $n_{\rm s}$ is first-order. Precisely, we have

$$\alpha = 16(\epsilon_V\eta_V)_* - 24(\epsilon_V)_*^2 - 2(\xi_V)_*^2 \tag{3.32}$$

where $\xi_V \equiv M_{\rm p}^4 \frac{V_\varphi V_{\varphi\varphi\varphi}}{V^2}$.

Tensor Spectrum

Tensor perturbations are also excited during inflation just as scalar perturbations. Again we work in the flat gauge and consider a FRW metric with tensor perturbation of the form

$$\mathrm{d}s^2 = a^2(\eta)\left[-\mathrm{d}\eta^2 + (\delta_{ij} + h_{ij})\mathrm{d}x^i\mathrm{d}x^j\right] , \tag{3.33}$$

where h_{ij} is divergence and trace-free, obeying $h^{ij}_{,j} = h^i_i = 0$. By perturbing the action to second-order in h_{ij}, one finds

$$S_h^{(2)} = -\frac{M_{\rm p}^2}{8}\int \mathrm{d}^4x a h^{ij}\left[\ddot{h}_{ij} + 3Hh_{ij} - \partial^2 h_{ij}\right] \tag{3.34}$$

and the tensor perturbation h_{ij} satisfies an equation of motion similar to that of $\delta\varphi$ Eq. (3.16) in the massless limit

$$\ddot{h_{ij}} + 3H\dot{h}_{ij} + \frac{k^2}{a^2}h_{ij} = 0\,. \tag{3.35}$$

Decomposing h_{ij} into a scalar amplitude h and polarisation tensors $e_{ij}^{(+,\mathrm{x})}$ and promoting h_{ij} to operators, we can write

$$\hat{h}_{ij}(\mathbf{x},\eta) = \int \frac{\mathrm{d}^3\mathbf{k}}{(2\pi)^{3/2}} \sum_{s=+,\mathrm{x}} \frac{M_\mathrm{p}}{2} \left[\hat{a}(\mathbf{k}) e_{ij}^s h_k^s(\eta) e^{i\mathbf{k}\cdot\mathbf{x}} + c.c.\right] \tag{3.36}$$

in Fourier space in terms of annihilation and creation operators. Here $s = +, \mathrm{x}$ denotes the two polarisation states of the tensor mode. The polarisation tensors $e_{ij}^{(+,\mathrm{x})}$ satisfy the transverse and traceless condition

$$\sum_i k_i e_{ij} = 0\,, \tag{3.37}$$

$$\sum_{ij} e_{ij}^{*s} e_{ij}^{s'} = 2\delta_{ss'}\,, \tag{3.38}$$

$$\sum_{ijl} \varepsilon_{ilk} e_{ij}^{*s} e_{jl}^{s'} = -\sum_{ijl} \varepsilon_{ilk} e_{ij}^{*s} e_{jl}^{s'} = 2\frac{k_k}{|\mathbf{k}|}(1-\delta_{ss'})\,. \tag{3.39}$$

Now we define $\tilde{h}_k^s \equiv a M_\mathrm{p} h_k^s/2$. It is not difficult to see $\tilde{h}_k^s$ satisfies the same Mukhanov-Sasaki equation with $z \to a$

$$\tilde{h}_k^{s\prime\prime} + \left(k^2 - \frac{a''}{a}\right)\tilde{h}_k^s = 0\,. \tag{3.40}$$

The solution to this equation of motion is the same as in the scalar case with $\nu_\mathrm{R} \to \nu_\mathrm{T} = 3/2 + \epsilon_H$. Defining a dimensionless tensor spectrum $P_h(k)$ as

$$\left\langle h_{ij}(\mathbf{k}) h^{ij}(\mathbf{k}')\right\rangle = 2(2\pi)^3 \frac{2\pi^2}{k^3} P_h(k) \delta^{(3)}(\mathbf{k}-\mathbf{k}')\,, \tag{3.41}$$

where the additional factor of 2 comes from the two polarisations of gravitational waves, we therefore have

$$P_h(k) = \frac{8}{M_\mathrm{p}^2}\left(\frac{H_*}{2\pi}\right)^2 (-k\eta)^{3-2\nu_T}\,, \tag{3.42}$$

with the tensor tilt n_T and tensor-to-scalar ratio r given by

$$n_\mathrm{T} = -2(\epsilon_V)_*\,,\ r = 16(\epsilon_V)_*\,. \tag{3.43}$$

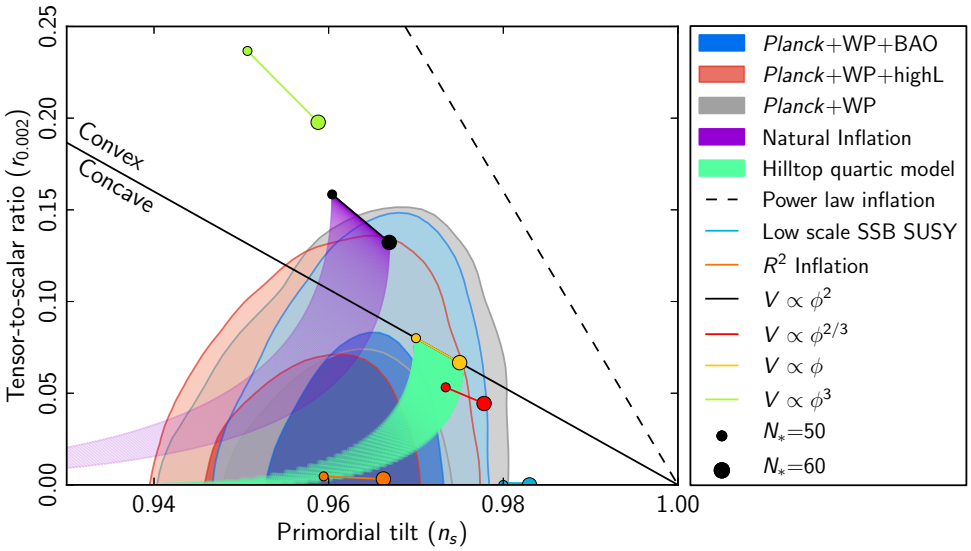

Figure 3.1: Theoretical predictions of $(n_{\rm s}, r)$ for various canonical single-field inflation models and comparison with the current observational constraints. Credit: ESA and the Planck collaboration [44].

Theoretical predictions of $n_{\rm s}$ and r from various canonical simple single-field inflation models are summarised in Fig. 3.1. Models such as power-law inflation and $V \propto \varphi^4$ are now already ruled out by current data from Planck, while $V \propto \varphi^2$ is under tension. Though the recent BICEP2 discovery of primordial gravitational waves, if verified, will bring the φ^2 model back in agreement with observations.

Non-Gaussianity, No-go Theorem for Simplest Single-Field Models

Besides the scalar and tensor power spectra P_ζ and P_h, statistics beyond the two-point functions as quantified by non-Gaussianity may also be detected in precision CMB experiments. To work out the level of non-Gaussianity in the single-field model, we expand the action Eq. (3.6) to cubic order

$$\begin{aligned} S^{(3)} \quad &= \frac{1}{2}\int \mathrm{d}^4x a^3 \left\{ -\frac{1}{3}V_{\varphi\varphi\varphi}(\delta\varphi)^3 - \lambda_1 V_{\varphi\varphi}(\delta\varphi)^2 + 6H^2\lambda_1^3 M_{\rm p}^2 - \lambda_1^3\dot{\varphi}^2 + 2\lambda_1^2\dot{\varphi}\dot{\delta\varphi} \right. \\ &\quad -a^{-4}\lambda_1\left[\partial_i\partial_j\beta\partial^i\partial^j\beta - (\partial^2\beta)^2\right]M_{\rm p}^2 + 4H^2\lambda_1^2 a^{-2}(\partial^2\beta)M_{\rm p}^2 - \lambda_1(\dot{\delta\varphi})^2 \\ &\quad \left. -a^{-2}\lambda_1(\partial\delta\varphi)^2 - 2\dot{\delta\varphi}\beta^i\partial_i\delta\varphi + 2\lambda_1\dot{\varphi}\beta^i\partial_i\delta\varphi \right\} , \end{aligned} \tag{3.44}$$

Note that we only need to expand N and β^i to first order as the second-order terms in N and β^i are multiplied by the momentum and Hamiltonian constraints at first order.

Again λ_1 and β can be eliminated using the constraints Eqs. (3.13). Now we collect the leading slow-roll order pieces in Eq. (3.44). Note that λ_1 and β are of order $O(\dot{\varphi}/H)$ to leading order in slow-roll. Eq. (3.44) then reduces to

$$S^{(3)} \supseteq \int \mathrm{d}^4x \left\{ -\frac{a^3}{4HM_{\mathrm{p}}^2}\dot{\varphi}\delta\varphi(\dot{\delta\varphi})^2 - \frac{a}{4HM_{\mathrm{p}}^2}\dot{\varphi}\delta\varphi(\partial\delta\varphi)^2 + \frac{a^3}{2HM_{\mathrm{p}}^2}\dot{\varphi}\dot{\delta\varphi}\delta^{ij}\partial_j\partial^{-2}(\dot{\delta\varphi})\partial_i(\delta\varphi) \right\} , \tag{3.45}$$

This gives the cubic interaction Hamiltonian H_{int} to leading order in slow-roll. To compute the 3-point correlation function for $\delta\varphi$, we apply the 'in-in' formalism discussed in Section 3.1. Recall that to leading order, the 3-point correlation function for $\delta\varphi$ is given by Eq. (3.2). Substituting the cubic order terms Eq. (3.45) into the interaction Hamiltonian H_{int}, we can then work out the 3-point function to leading order in slow-roll. For details of the calculations, see [75, 88].

As an example, we compute the contribution coming from the first term in Eq. (3.45)

$$\int \mathrm{d}^4x \left\{ -\frac{a^3}{4HM_{\mathrm{p}}^2}\dot{\varphi}\delta\varphi(\dot{\delta\varphi})^2 \right\} . \tag{3.46}$$

Written in conformal time, the corresponding contribution is then

$$\begin{aligned} \langle\delta\varphi(\mathbf{x}_1,\tau)\delta\varphi(\mathbf{x}_2,\tau)\delta\varphi(\mathbf{x}_3,\tau)\rangle \quad \subseteq & \int \mathrm{d}^3y\mathrm{d}\eta \left\{ -\frac{a}{4M_{\mathrm{p}}H^2}\varphi'(\eta)\,\langle\delta\varphi(\mathbf{x}_1,\tau)\delta\varphi(\mathbf{y},\eta)\rangle \right. \\ & (\langle\delta\varphi(\mathbf{x}_2,\tau)\delta\varphi(\mathbf{y},\eta)\rangle)'\,(\langle\delta\varphi(\mathbf{x}_3,\tau)\delta\varphi(\mathbf{y},\eta)\rangle)' \\ & \left. +\mathrm{perm} + \mathrm{c.c} \right\} , \end{aligned} \tag{3.47}$$

which in momentum space gives

$$\begin{aligned} &\langle\delta\varphi(\mathbf{k}_1,\tau)\delta\varphi(\mathbf{k}_2,\tau)\delta\varphi(\mathbf{k}_3,\tau)\rangle \\ &\qquad \subseteq -i(2\pi)^3\delta^{(3)}(\sum_i \mathbf{k}_i)\frac{H_*^3}{4}\frac{\dot{\varphi}_*}{\prod_i 2k_i^3}\left[\sum_{\mathrm{perm}}\left(-\frac{k_2^2k_3^2}{k_t} - \frac{k_1k_2^2k_3^2}{k_t^2}\right)\right] , \end{aligned} \tag{3.48}$$

where we have Wick rotated on to the positive imaginary axis to perform the integral. Here again perm stands for permutation over $\mathbf{k}_i$ or $\mathbf{x}_i$. k_t denotes the sum of the magnitudes of $\mathbf{k}_i$, i.e. $k_t = k_1 + k_2 + k_3$.

Together with the two remaining terms, we find the 3-point function for the field perturbations $\delta\varphi$ [88]

$$\langle\delta\varphi(\mathbf{k}_1)\delta\varphi(\mathbf{k}_2)\delta\varphi(\mathbf{k}_3)\rangle = (2\pi)^3\delta^{(3)}(\sum_i k_i)\frac{4\pi^4}{\prod_i k_i^3}\left(\frac{H_*^2}{4\pi^2}\right)^2\mathcal{A}(k_1,k_2,k_3)\,, \quad (3.49)$$

where

$$\mathcal{A}(k_1,k_2,k_3) \equiv \frac{\dot\varphi_*}{4H_*}\left[-3\frac{k_2^2k_3^2}{k_t} - \frac{k_2^2k_3^2}{k_t^2}(k_1+2k_3) + \frac{1}{2}k_1^3 - k_1k_2^2 + \text{perm}\right]. \quad (3.50)$$

Translating this into the 3-point function of the curvature perturbation ζ by appropriate gauge transformation using Eq. (3.3)

$$\begin{aligned}\langle\zeta(\mathbf{k}_1)\zeta(\mathbf{k}_2)\zeta(\mathbf{k}_3)\rangle = &-\frac{H_*^3}{\dot\varphi_*^3}\langle\delta\varphi(\mathbf{k}_1)\delta\varphi(\mathbf{k}_2)\delta\varphi(\mathbf{k}_3)\rangle_* \\ &+ \frac{1}{2(\epsilon_V)_*}\left(\frac{1}{4}-\frac{\eta_V}{4\epsilon_V}\right)_*\langle\delta\varphi(\mathbf{k}_1)\delta\varphi(\mathbf{k}_2)[\delta\varphi\star\delta\varphi](\mathbf{k}_3)\rangle_* + \text{perm}\,. \quad (3.51)\end{aligned}$$

Combining Eqs. (3.49) and (3.51), we finally arrive at Maldacena's famous result for the corresponding non-linear parameter $f_{\rm NL}$ in single-field inflation [75]

$$f_{\rm NL} \approx \frac{5}{12}\left[\frac{2\ddot\varphi_*}{\dot\varphi_* H_*} + \left(\frac{\dot\varphi_*}{H_*}\right)^2(2+f(k))\right] = \frac{5}{12}(1-n_{\rm s}+f(k)n_{\rm T})\,, \quad (3.52)$$

where $f(k)$ is some function of k lying in the range $0 < f < 5/6$, peaking at the equilateral limit and vanishing in the squeezed limit. Eq. (3.52) gives the single-field consistency relation $f_{\rm NL}^{\rm local} = 5(1-n_{\rm s})/12$.

From Eq. (3.52) we can see the non-linear parameter $f_{\rm NL}$ is of order of $O(\epsilon_H)$. For an ideal CMB experiment, we can only distangle the primordial signals from contributions due to non-linear evolution of GR if the primordial signals give $|f_{\rm NL}| \sim O(5)$ [89]. The level of non-Gaussianity is therefore negligible in CMB observations for the simplest single-field model, independent of the shape. This is the famous **No-Go Theorem** for non-Gaussianity in the simplest single-field inflation, first derived by Maldacena in 2006 [75]. As in the literature, we refer to a large Gaussianity when any of the non-linear model parameters $f_{\rm NL}$, $\tau_{\rm NL}$ or $g_{\rm NL}$ is large, particularly $|f_{\rm NL}| > O(5)$. Any detection of primordial non-Gaussianity of order $O(5)$ will rule out the simplest single-

field inflation paradigm. As discussed in Chapter 2, no convincing evidence of a large primordial non-Gaussianity is observed so far today.

3.4 Multifield Inflation Models

Absence of evidence is not the evidence of absence. - Carl Sagan

So far we have only considered the simplest model of inflation, which involves one minimally coupled single scalar field with a canonical kinetic term. Although this simple paradigm is consistent with current observations, it is often regarded as a phenomenological model only as we are yet to connect the inflation model with particle physics theory. Particularly, the field (or fields) that plays the role of the inflaton is still unknown. It is therefore natural to go beyond this simplest picture and consider more complicated models that are still consistent with observations but may have richer phenomenology.

Everything should be made as simple as possible, but not simpler. - Albert Einstein

For example, particle physics motivated models can give rise to models with non-canonical kinetic terms such as DBI-inflation [90] and models with features in the inflaton potential [91, 92, 93, 94, 95]. Besides, unified theories like GUT and string theory generically give rise to multiple scalar fields instead of one. Mechanisms that make one of the scalar fields light often apply to other scalar fields as well. Thus it is natural during inflation that there are additional light scalar fields as well [96, 97]. Instead of the single-field paradigm, a multiple field model should be considered as a result. This is **multifield inflation**, the main focus of this thesis. Examples of multifield inflation models are assisted inflation [98] and N-flation [99].

The general multifield action with at most first-order derivatives we will consider is

$$S = \int \mathrm{d}^4x\sqrt{-g}\left[f(\varphi^I)\frac{R}{2} - S_{IJ}(\varphi^I)\frac{1}{2}g^{\mu\nu}\partial_\mu\varphi^I\partial_\nu\varphi^J - W(\varphi^I)\right], \tag{3.53}$$

where f is the non-minimal coupling to gravity, S_{IJ} is the Kahler metric and W is the scalar potential. Here all f, S_{IJ} and W are functions of all of the scalar fields φ^I.

3.4.1 Difference Between Single and Multifield Models: Entropic Perturbations

A crucial difference between single-field and multifield models is the presence of **entropic perturbations or isocurvature perturbations**. With the existence of isocurvature modes, the slow-roll solution is no longer an attractor, leading to non-vanishing non-adiabatic pressure perturbations and thus possible superhorizon evolution of ζ. To see this, recall that under the separate universe approximation, ζ follows the evolution equation Eq. (2.40) on uniform-density slicings. In this gauge, the pressure perturbation is non-vanishing only if the non-adiabatic pressure perturbation $\delta P_{\rm nad}$, defined by $\delta P_{\rm nad} \equiv \delta P - (\dot{P}/\dot{\rho})\delta\rho$, is non-zero. The adiabatic regime corresponds to $\delta P_{\rm nad} = 0$. The evolution equation for ζ can be written in terms of $\delta P_{\rm nad}$

$$\dot{\zeta} \approx -\frac{H}{\overline{\rho} + \overline{P}} \delta P_{\rm nad} \tag{3.54}$$

to first order. In multifield models with M canonical scalar fields, $\delta P_{nad} \neq 0$ on superhorizon scales in general. This can be seen by redefining the M scalar fields φ^I into an adiabatic direction σ, i.e. a direction parallel to the classical field trajectory, and corresponding $M-1$ orthogonal directions s^I [100]

$$\begin{aligned} \sigma &\equiv \int \hat{\sigma}_I \delta\varphi^I \mathrm{d}t \,, \\ s^I &\equiv \sum_J \hat{s}_{IJ} \varphi^J \,, \end{aligned} \tag{3.55}$$

where $\hat{\sigma}_I \equiv \dot{\varphi}^I / \sqrt{\sum_J (\dot{\varphi}^J)^2}$ and $\sum_I \hat{s}_{IJ}\hat{\sigma}_I = 0$. We also assume all the s^I to be orthogonal to each other. We then decompose the field perturbations $\delta\varphi^I$ in terms of an adiabatic perturbation $\delta\sigma$ and entropic perturbations δs^I

$$\delta\sigma = \sum_I \hat{\sigma}_I \delta\varphi^I \tag{3.56}$$

$$\delta s^I = \hat{s}_{IJ} \delta\varphi^J \,. \tag{3.57}$$

The adiabatic field σ follows the Klein-Gordon equation as in the case of a single-field

$$\ddot{\sigma} + 3H\dot{\sigma} + W_\sigma = 0\,. \tag{3.58}$$

Here W_σ denotes the partial derivative of W with respect to σ. By expressing the stress-energy tensor $T^{\mu\nu}$ in the form of a perfect fluid, the pressure and momentum perturbations in the uniform-density gauge are

$$\begin{aligned}\delta P &= \sum_I \left[\dot{\varphi}^I(\dot{\delta\varphi}^I - \dot{\varphi}^I\Psi) - W_I\delta\varphi^I\right] = -2W_\sigma\delta\sigma + 2\delta_s W\,,\\ \delta q &= -\sum_I \dot{\varphi}^I\delta\varphi^I = -\dot{\sigma}\delta\sigma\,,\end{aligned} \tag{3.59}$$

where we have defined $\delta_s W \equiv \sum_I W_I\delta\varphi^I - W_\sigma\delta\sigma$. The non-adiabatic pressure perturbation is then given by

$$\delta P_{\rm nad} = -\frac{2W_\sigma}{3H\dot{\sigma}}\delta\rho_{\rm com} - 2\delta_s W\,. \tag{3.60}$$

Since the comoving density perturbation $\delta\rho_{\rm com}$ follows the Poisson equation $(k^2/a^2)\phi = -4\pi G\delta\rho_{\rm com}$ from the time-time component of the Einstein equation, the first term in Eq. (3.60) vanishes on superhorizon scales. However, the second term in Eq. (3.60) need not be small in general and can source $\delta P_{\rm nad}$ on superhorizon scales. As $\delta\sigma$ denotes the perturbation along the classical field trajectory, which is the adiabatic perturbation, $\delta_s W$ is a measure of the entropic perturbations. Note that $\delta_s W$ vanishes for the case of a single field. Therefore we conclude that **entropic perturbations δs^I act as source terms for the adiabatic mode and lead to superhorizon evolution of ζ, which is a main feature of multifield models**.

3.4.2 Multifield Predictions for Primordial Observables

Now we consider the predictions from multifield models. In particular, we consider the case where all the fields are minimally coupled with canonical kinetic terms. Using the δN formalism Eq. (3.3), we can express the primordial observables related to ζ defined earlier in Section 2.3 in terms of the δN coefficients in the case of slow-roll

scalar field inflation. In general, **the δN coefficients depend on the initial conditions at horizon-exit and so do the model predictions**.

Following a similar approach as adopted in Section 3.3 for the canonical single field, we can work out the correlation functions for the field perturbations $\delta\varphi^I$ given by [101] (for general multifield model with a non-flat field space metric, see [80])

$$\left\langle \delta\varphi^I(\mathbf{k}_1,t_*)\delta\varphi^J(\mathbf{k}_2,t_*)\right\rangle = \left(\frac{H_*}{2\pi}\right)^2 \delta^{IJ}\delta^{(3)}(\mathbf{k}_1-\mathbf{k}_2)\,, \tag{3.61}$$

$$\left\langle \delta\varphi^I(\mathbf{k}_1,t_*)\delta\varphi^J(\mathbf{k}_2,t_*)\delta\varphi^K(\mathbf{k}_3,t_*)\right\rangle = (2\pi)^3\delta^{(3)}(\sum_i \mathbf{k}_i)\frac{4\pi^4}{\prod_i k_i^3}\left(\frac{H_*^2}{4\pi^2}\right)^2 \mathcal{A}^{IJK}\,, \tag{3.62}$$

to leading order. Here $\mathcal{A}^{IJK}$ is a function of the external momenta k_i, defined as

$$\mathcal{A}^{IJK}(k_1,k_2,k_3) \equiv \frac{\dot\varphi_*^I}{4H_*}\delta^{JK}\left[-3\frac{k_2^2k_3^2}{k_t} - \frac{k_2^2k_3^2}{k_t^2}\,(k_1+2k_3) + \frac{1}{2}k_1^3 - k_1k_2^2 + \text{perm}\right]. \tag{3.63}$$

Power Spectrum

For the two-point statistics of ζ, at leading order, the δN formalism gives [102]

$$A_\zeta = \sum_I N_I^2 P_*\,, \tag{3.64}$$

$$n_\text{s} - 1 = -2(\epsilon_H)_* + \frac{2}{H_*}\frac{\sum_{IJ}\dot\varphi_*^J N_{IJ}N_I}{\sum_K N_K^2}\,, \tag{3.65}$$

$$r = \frac{8}{\sum_I N_I^2}\,. \tag{3.66}$$

for the power spectrum P_ζ, the spectral index $n_\text{s}-1$ and the tensor-to-scalar ratio r. Here P_* is the power spectrum for the scalar field perturbations $\langle\delta\varphi(\mathbf{k},t_*)\delta\varphi(\mathbf{k}',t_*)\rangle$ at horizon-exit. To derive the expression for n_s Eq. (3.65), we have used the slow-roll approximation to replace $d/d\ln k$ with the field derivatives

$$\frac{\mathrm{d}}{\mathrm{d}\ln k} \approx \dot\varphi_*^I\frac{\mathrm{d}t}{\mathrm{d}\ln k}\frac{\partial}{\partial\varphi_*^I}\,, \tag{3.67}$$

where the field index I is summed over. Here the subscript $*$ corresponds to quantities evaluated at horizon-exit for the pivot scale k_* under consideration, i.e. when $k_* = aH_*$.

For the running of the spectral index α, using again Eq.(3.67), Eq. (2.19) can be written as

$$\alpha = -4(\epsilon_H)_*^2 + \frac{2\ddot{H}_*}{H_*^3} - \frac{2\dot{H}_*}{H_*^3}\frac{\sum_{IJ}\dot{\varphi}_*^J N_{IJ}N_I}{\sum_K N_K^2} + \frac{2}{H_*^2}\left[\frac{\sum_{IJ}\ddot{\varphi}_*^J N_{IJ}N_I}{\sum_K N_K^2} + \sum_{IJK}\dot{\varphi}_*^J\dot{\varphi}_*^K\left(\frac{N_{IJK}N_I + N_{IJ}N_{IK}}{\sum_L N_L^2} - \frac{2N_{IJ}N_I\sum_M N_M N_{MK}}{\left(\sum_L N_L^2\right)^2}\right)\right], \quad (3.68)$$

which is second-order in slow-roll in general.

Non-linear Parameters

We can also express the non–linear parameters in terms of the δN coefficients similarly by considering higher order terms in the δN expansion. In terms of the expansion Eq. (3.3), we can separate out two different contributions to higher order correlation functions: the instrinsic non-gaussianity of the field perturbations such as $\langle\delta\varphi\delta\varphi\delta\varphi\rangle$ and higher-order derivatives of N. It is convenient to parametrise the non-linear parameters into shape dependent and independent parts as in [103, 104], for instance $f_{\rm NL} = f_{\rm NL}^{(3)} + f_{\rm NL}^{(4)}$, which are defined as

$$f_{\rm NL}^{(3)} \equiv \frac{5}{6}\frac{\sum_{IJK}A^{IJK}N_I N_J N_K}{(\sum_L N_L^2)^2\sum_i k_i^3}\,, \quad f_{\rm NL}^{(4)} \equiv \frac{5}{6}\frac{\sum_{IJ}N_{IJ}N_I N_J}{(\sum_K N_K^2)^2}\,. \quad (3.69)$$

For canonical models, the non–linear parameters defined in Eq. (2.25)-(2.26) are dominated by their shape-independent parts, which under the δN formalism are expressed as [48, 69]

$$f_{\rm NL}^{(4)} = \frac{5}{6}\frac{\sum_{IJ}N_{IJ}N_I N_J}{(\sum_K N_K^2)^2}\,, \quad (3.70)$$

$$\tau_{\rm NL} = \frac{\sum_{IJK}N_{IJ}N_{JK}N_K N_I}{(\sum_L N_L^2)^3}\,, \quad (3.71)$$

$$g_{\rm NL} = \frac{25}{54}\frac{\sum_{IJK}N_{IJK}N_I N_J N_K}{(\sum_L N_L^2)^3}\,. \quad (3.72)$$

Unlike the simplest single-field model, local non-Gaussianity can be enhanced in canonical multifield models subject to appropriate initial conditions even during slow-roll, with $|f_{\rm NL}^{\rm local}| > O(5)$, if some of the second order δN coefficients N_{IJ} are large. It has been shown that this typically requires the fields to start near some extreme points of the potential at horizon exit [105, 106]. A necessary condition for realising a large non-Gaussianity in the case of canonical two-field models with separable potentials is a hierachy between the horizon crossing field velocities, which was found using a heatmap analysis by Byrnes et al. and Elliston et al. [102, 107].

Scale Dependence of Non-linear Parameters

The spectral indices $n_{f_{\rm NL}}$ and $n_{\tau_{\rm NL}}$ of the shape-independent parts are given by [60, 108]

$$n_{f_{\rm NL}} = -2[n_{\rm s} - 1 + 2(\epsilon_H)_*] + \frac{5}{6f_{\rm NL}}\left(\frac{1}{H_*}\right)\left[\frac{\sum_{IJK} N_{IJK}N_I N_J(\dot\varphi_K)_*}{(\sum_L N_L^2)^2} + 2\frac{\sum_{IJK} N_{IJ}N_{IK}N_J(\dot\varphi_K)_*}{(\sum_L N_L^2)^2}\right], \quad (3.73)$$

$$n_{\tau_{\rm NL}} = -3[n_{\rm s} - 1 + 2(\epsilon_H)_*] + \frac{2}{\tau_{\rm NL}}\left(\frac{1}{H_*}\right)\left[\frac{\sum_{IJKL} N_{IJL}N_{IK}N_J N_K(\dot\varphi_L)_*}{(\sum_M N_M^2)^3} + \frac{\sum_{IJKL} N_{IJ}N_{IK}N_{JL}N_K(\dot\varphi_L)_*}{(\sum_M N_M^2)^3}\right], \quad (3.74)$$

which are given in terms of third-order derivatives of N. These can be further simplified using $dN/dt_* = -H_*$ and the slow–roll field equations. In particular, the δN coefficients can be related to the partial derivatives of the potential by

$$\sum_I N_I W_{I*} = W_*\,, \quad (3.75)$$

$$\sum_I N_{IJ} W_{I*} = W_{J*} - \sum_I N_I W_{IJ*}\,, \quad (3.76)$$

$$\sum_I N_{IJK} W_{I*} = W_{JK*} - \sum_I N_{IJ}W_{IK*} - \sum_I N_{IK}W_{IJ*} - \sum_I N_I W_{IJK*}\,, \quad (3.77)$$

where Eqs. (3.76)-(3.77) are derived by differentiating Eq. (3.75) with respect to φ^I_*. Here subscripts I, J, K denote partial differentiation with respect to the scalar fields. W_{I*} can be replaced by $\dot{\varphi}^I_*$ using the slow–roll field equations $3H\dot{\varphi}^I_* \approx -W_{I*}$. Using these, we can work out alternative expressions for $n_{\rm s}$ and α [96, 109]

$$n_{\rm s} - 1 = -2(\epsilon_H)_* - \frac{2}{\sum_K N_K^2} + \frac{1}{3H_*^2}\frac{2\sum_{IJ} N_I N_J (W_{IJ})_*}{\sum_K N_K^2}\,, \tag{3.78}$$

$$\begin{aligned}\alpha = &-\sum_{IJ}\left(\frac{2W_I W_J W_{IJ}}{W^3}\right)_* + \sum_I \left(\frac{2W_I^2}{W^4}\right)_* + \sum_{IJK}\left(\frac{4}{W}\right)_*\left(\frac{W - N_I N_J W_{IJ}}{N_K^2}\right)_*^2 \\ &+ \sum_{IJKL}\left(\frac{2N_I N_J N_K W_{IJK}}{N_L^2}\right)_* + \sum_{IJKL}\left(\frac{4}{W}\right)_*\left[\frac{(W_K - N_I W_{IK})(N_J W_{Jk})}{N_L^2}\right]_*\,,\end{aligned} \tag{3.79}$$

for canonical models.

Following a similar approach here, we extend it to the case of $n_{f_{\rm NL}}$ and $n_{\tau_{\rm NL}}$, allowing us to rewrite them in terms of only first and second order derivatives of N as follows [110]

$$\begin{aligned}n_{f_{\rm NL}} = &-2[n_{\rm s} - 1 + 2(\epsilon_H)_*] - \frac{10}{6f_{\rm NL}}\left(\frac{1}{\sum_L N_L^2}\right)^2 \\ &+ \frac{5}{6f_{\rm NL}}\sum_{IJK}\left[\frac{4(\eta_{IK})_* N_{IJ} N_J N_K + (\eta_{IJ})_* N_I N_J + (W_{IJK}/W)_* N_I N_J N_K}{(\sum_L N_L^2)^2}\right]\,,\end{aligned} \tag{3.80}$$

$$\begin{aligned}n_{\tau_{\rm NL}} = &-3[n_{\rm s} - 1 + 2(\epsilon_H)_*] - \frac{2}{\tau_{\rm NL}}\left(\frac{1}{\sum_M N_M^2}\right)^3 + \frac{2}{\tau_{\rm NL}}\sum_{IJKL}\left[\frac{2(\eta_{JL})_* N_{IJ} N_{IK} N_L N_K}{(\sum_M N_M^2)^3}\right. \\ &\left. + \frac{(\eta_{IJ})_* N_I N_J + (\eta_{IJ})_* N_{JL} N_{IK} N_L N_K + (W_{IJL}/W)_* N_{IK} N_J N_K N_L}{(\sum_M N_M^2)^3}\right]\,.\end{aligned} \tag{3.81}$$

Here $\eta_{IJ} \equiv W_{IJ}/W$. Eqs. (3.80)-(3.81) are two useful results. Whilst Eqs. (3.80)-(3.81) are equivalent to Eqs. (3.73)-(3.74), they possess significant computational advantages over the former since they involve lower order δN derivatives which are rel-

atively easier to evaluate in general compared to higher order ones. From Eqs. (3.80)-(3.81), we can also see the error bars on the scale dependence of the non-linear parameters $f_{\rm NL}$ and $\tau_{\rm NL}$ are approximately inversely proportional to their fiducial values [65].

δN expressions for the primordial observables also exist for generalised multifield models with non-minimal couplings and non-canonical kinetic terms, see [111].

An Example: Two Field Canonical Models

In the following, we consider a simple subclass of multifield models, the minimally coupled two-field model with canonical kinetic terms. This class of model is described by the following action

$$S = \int \mathrm{d}^4x\sqrt{-g}\left[M_{\rm p}^2\frac{R}{2} - \frac{1}{2}g^{\mu\nu}\partial_\mu\varphi\partial_\nu\varphi - \frac{1}{2}g^{\mu\nu}\partial_\mu\chi\partial_\nu\chi - W(\varphi,\chi)\right], \quad (3.82)$$

where $W(\varphi,\chi)$ is the scalar potential which is a function of both scalar fields. The standard slow roll parameters in the two-field case are defined as

$$\begin{aligned} \epsilon_\varphi &= \frac{M_{\rm p}^2}{2}\left(\frac{W_\varphi}{W}\right)^2, \quad \epsilon_\chi = \frac{M_{\rm p}^2}{2}\left(\frac{W_\chi}{W}\right)^2, \quad \epsilon = \epsilon_\varphi + \epsilon_\chi\,, \\ \eta_{\varphi\varphi} &= M_{\rm p}^2\frac{W_{\varphi\varphi}}{W}, \quad \eta_{\varphi\chi} = M_{\rm p}^2\frac{W_{\varphi\chi}}{W}, \quad \eta_{\chi\chi} = M_{\rm p}^2\frac{W_{\chi\chi}}{W}, \end{aligned} \quad (3.83)$$

where subscripts denote differentiations with respect to the fields φ and χ respectively. Here we assume these slow-roll parameters are much smaller than $O(1)$ during inflation [4].

The background dynamics of the scalar fields are again governed by the Klein-Gordon equation

$$\ddot{\varphi} + 3H\dot{\varphi} + W_\varphi = 0 \quad (3.84)$$

$$\ddot{\chi} + 3H\dot{\chi} + W_\chi = 0 \quad (3.85)$$

where the first terms in both equations can be neglected during slow-roll inflation. The fields then evolve monotonically and we can therefore write the number of e-folds N

[4] For discussion and alternative definitions for slow-roll parameters in multifield models, see [112]

from the horizon exit t_* to time t_e as

$$N = \int_{t_*}^{t_e} H\mathrm{d}t \approx \frac{1}{M_{\rm p}^2}\int_{\varphi_e}^{\varphi_*}\frac{W}{W_\varphi}\mathrm{d}\varphi = \frac{1}{M_{\rm p}^2}\int_{\chi_e}^{\chi_*}\frac{W}{W_\chi}\mathrm{d}\chi \tag{3.86}$$

by using the slow-roll equations. We can then compute the δN coefficients by differentiating Eq. (3.86). For instance, the first order δN coefficient N_φ is given by

$$N_\varphi = \frac{1}{M_{\rm p}^2}\left(\frac{W}{W_\varphi}\right)_* - \frac{1}{M_{\rm p}^2}\left(\frac{W}{W_\varphi}\right)_e\left(\frac{\partial\varphi_e}{\partial\varphi_*}\right)_H + \frac{1}{M_{\rm p}^2}\int_e^*\left(\frac{\partial\chi}{\partial\varphi_*}\right)\frac{\partial}{\partial\chi}\left(\frac{W}{W_\varphi}\right)\mathrm{d}\varphi\,, \tag{3.87}$$

where $\frac{\partial\varphi_e}{\partial\varphi_*}$ is evaluated on final uniform hypersurfaces, denoted by subscript H.

Technical Difficulties in Computing δN Coefficients

In Section 3.4.2, we have given the canonical multifield model predictions in terms of the δN coefficients. Given the potential W and initial conditions at horizon-exit, by solving the Klein-Gordon field equations subject to the Friedmann equation, we can then evaluate the corresponding δN coefficients and make our specific model predictions. However, the coupled field equations are difficult to solve analytically in general even for two fields in the slow-roll limit and it is not always possible to obtain analytic expressions for the δN coefficients. In fact, analytic expressions only exist for potentials of separable form, where $W = U(\varphi) + V(\chi)$ or $W = U(\varphi)V(\chi)$, see Appendix A.

Another important condition required in deriving analytic expressions for the δN coefficients is the slow-roll approximation. Most analysis to date for multifield models is done in the slow-roll regime. This only gives the correct predictions for models where the adiabatic regime is reached by the end of inflation. In general, however, entropic perturbations may persist after inflation ends. As a result, the curvature perturbation ζ could continue to evolve beyond the slow-roll regime. In order to properly compare with observations, we should follow the evolution of the curvature perturbation ζ until the Universe reaches the adiabatic regime. Any post-inflationary evolution, particularly (p)reheating, may alter the multifield model predictions derived in the slow-roll

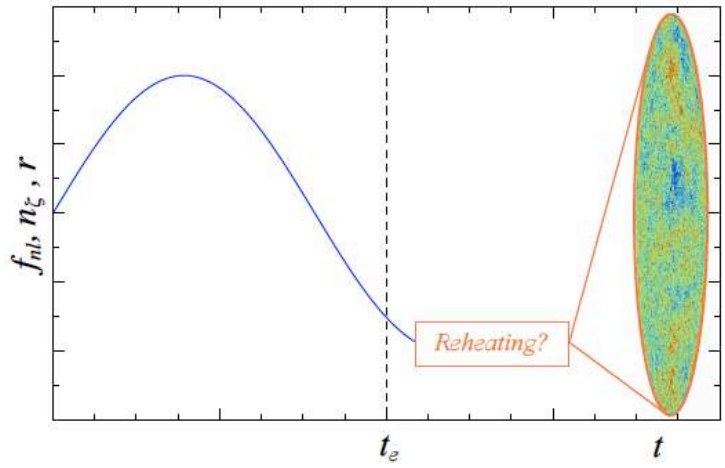

Figure 3.2: To compare with observations, model predictions should be evaluated at the time of measurements or until the Universe reaches the adiabatic regime, which might happen after inflation ends. Credit: Ewan Tarrant

regime. This is illustrated in Fig. 3.2.

It is important to study how sensitive ζ and the related primordial observables are to the subsequent post-inflationary evolution in multifield models in as generic a setup as feasible in order to compare with observations and put constraints on the models.

While we require the slow-roll approximation for deriving analytic expressions, it should be emphasised that the δN formulae given in Section 3.4.2 for model predictions only require slow-roll at horizon exit and are valid beyond the slow-roll regime. We can apply these formulae to the post-inflationary regime and study the evolution of ζ and the primordial observables by numerically solving the field equations. Considering a wide range of canonical multifield models, we will see in the following chapters that even in the simplest perturbative reheating setup, post-inflationary evolution does change the multifield model predictions and should be taken into account before comparing with observations in general.

Chapter 4

The Influence of Reheating on the Power and Bispectra

As we have previously argued, to compare with observations, post-inflationary evolution needs to be taken into account in multifield inflation unless the adiabatic limit is reached during slow-roll. In this chapter, we illustrate this and the influence of reheating on multifield model predictions. Particularly we address questions like whether (p)reheating could significantly change the multifield model predictions evaluated under the slow-roll approximation and induce any generic model-independent features.

In Section 4.1, we first give a brief review of the elementary theory of perturbative reheating and discuss the limitations of the setup. We then discuss the evolution of primordial observables, at the level of the power spectrum P_ζ in Section 4.2 and bispectrum B_ζ in Section 4.3, both during and after a period of perturbative reheating in various canonical two-field models. We compare the end of reheating predictions with the slow-roll predictions evaluated at the end of inflation, illustrating the importance of taking reheating into account. We also compare the qualitative behaviour between quadratic and quartic potentials in Section 4.4, and separable and non-separable potentials in Section 4.5.

4.1 Elementary Theory of Reheating

As discussed earlier in Section 1.3, inflation effectively dilutes the energy density of any cosmic fluids except that of the inflaton field. We can see this from the continuity equation Eq. (1.3), which suggests $\rho_{\rm m} \propto a^{-3}$ and $\rho_\gamma \propto a^{-4}$. Thus after an almost exponential expansion of spacetime during which a changes by many orders of magnitude, the energy density of any cosmic fluids is effectively driven to zero except that of the inflaton field.

After inflation ends, the Universe therefore ends up in a non-thermal state with effective zero temperature [1] except in the case of warm inflation where there is a continuous production of radiation [113].

To recover the standard Big Bang scenario in subsequent evolution, the fluctuations and the energy locked in the inflaton field must be somehow converted to other fields including the Standard Model (SM) particles we observe today. Such a process is called **(p)reheating**. This is an important epoch and must be accounted for in realistic inflation model building from particle physics theory. For reviews of the theory of (p)reheating, see [114, 115].

In this thesis we will consider the simple model of **perturbative reheating** in slow-roll canonical models. This is based on perturbative decays of the inflaton field, first developed by Dolgov and Linde [116] and Abbot et al. [117]. We will explain the model setup in the following.

Let us consider the single-field case first. Recall that in canonical single-field inflation, the dynamics of the inflaton field φ are governed by the Klein-Gordon equation

$$\ddot{\varphi} + 3H\dot{\varphi} + W_\varphi = 0\,. \tag{4.1}$$

During slow-roll, the first term in Eq. (4.1) is negligible and φ simply flows along the gradient of the potential. After slow-roll ends, φ approaches the minimum of the potential and starts oscillating about it. This is the oscillating regime.

To study perturbative reheating, we are interested in these classical oscillations of the

[1] There is a Hawking temperature associated with the horizon, but is very much subdominant compared to the energy density of the inflaton field.

homogeneous background φ field. Take the quadratic potential $W(\varphi) = \frac{1}{2}m^2\varphi^2$ as an example. After a few oscillations, the amplitude of the oscillations become sub-Planckian and the inflaton φ approaches the aymptotic solution [118, 119]

$$\begin{aligned}\varphi(t) &= \Phi(t)\cdot\sin(mt)\\ \Phi(t) &= \frac{M_{\rm p}}{\sqrt{3\pi}mt} \sim \frac{M_{\rm p}}{2\pi\sqrt{3\pi}N_{\rm osc}}\,,\end{aligned} \tag{4.2}$$

where $\Phi(t)$ is the amplitude of the oscillations and $N_{\rm osc}$ is the number of oscillations since the end of inflation. This corresponds to rapid sinusoidal oscillations with slowly decaying amplitude. Averaging over several oscillations, one finds that $a \propto t^{2/3}$ and φ behaves as in the same way as that of non-relativistic particles of mass m. Hence coherent oscillations of the homogeneous φ field correspond to a matter fluid with an effective equation of state $\omega = 0$. For a quartic potential $W(\varphi) = \frac{1}{4}\tilde{\lambda}\varphi^4$, the corresponding asymptotic solution for φ is [120]

$$\begin{aligned}\varphi(\eta) &= \Phi(\eta){\rm cn}\left(\frac{w_\varphi\eta}{c}, \frac{1}{\sqrt{2}}\right)\,,\\ \Phi(\eta) &= \sqrt{\frac{3}{2\pi}}M_{\rm p}\frac{c}{w_\varphi\eta}\end{aligned} \tag{4.3}$$

in conformal time η. Here c is a numerical constant given by $c \approx 0.85$, w_φ is the effective frequency of oscillation where $w_\varphi = c\sqrt{\tilde{\lambda}}a\Phi$ and cn is the elliptic function. To a good approximation, the solution Eq. (4.3) can be written as $\varphi(\eta) = \Phi\sin(c\sqrt{\tilde{\lambda}}a\Phi\eta)$. Again averaging over several oscillations, we can see coherent oscillations of φ mimic a relativistic fluid with an effective equation of state $\omega = 1/3$.

So far we have not taken particle production into account due to interactions between φ and other particles. In general, φ may decay into bosons $\chi_{\rm b}$ and fermions $\psi_{\rm f}$ due to terms in the interaction Lagrangian $\mathcal{L}_{\rm int}$ such as

$$\mathcal{L}_{\rm int} \supseteq -h\bar{\psi}_{\rm f}\psi_{\rm f}\varphi - \left(b\varphi + \frac{1}{2}g^2\varphi^2\right)\chi_{\rm b}^2 \tag{4.4}$$

where h, g are dimensionless coupling constants and b is a coupling constant of mass dimension one. Now we consider the effect of particle production due to these interaction terms in the case of the quadratic potential. As discussed earlier, a homogeneous

scalar field oscillating about a quadratic minimum with frequency $w_\varphi = m$ can be interpreted as a collection of φ particles with zero momenta. Based on this interpretation, the effects of particle production can be incorporated into the field equation Eq. (4.1) by means of a polarisation operator [121]

$$\ddot{\varphi} + 3H\dot{\varphi} + \left(m^2 + \Pi(k_0)\right)\varphi = 0\,. \tag{4.5}$$

Here, $\Pi(k_0)$ is the flat-space polarisation operator for the field φ at four–momentum $k = (k_0, 0, 0, 0) = (w_\varphi, 0, 0, 0)$. The real part of $\Pi(k_0)$ gives only a small correction to m^2, but when k_0 is larger than either the mass of χ_b or ψ_f, i.e. $k_0 \geq \min\{2m_{\chi_\mathrm{b}}, 2m_{\psi_\mathrm{f}}\}$, $\Pi(k_0)$ acquires an imaginary part $\mathrm{Im}\,\Pi$. We work in the limit where $m^2 \gg \max\{H^2, \mathrm{Im}\,\Pi\}$, which are usually satisfied after inflation ends. This is the condition for rapid oscillations. Neglecting the time–dependence of $\mathrm{Im}\,\Pi$ and using $H \approx 2/3t$, the approximate solution to Eq. (4.5) is

$$\varphi(t) \approx \frac{M_\mathrm{p}}{\sqrt{3\pi}mt}\exp\left(-\frac{1}{2}\frac{\mathrm{Im}\Pi}{m}t\right)\sin(mt)\,. \tag{4.6}$$

From unitarity relations, it follows that $\mathrm{Im}\,\Pi = m\Gamma$ [122], where Γ is the total decay rate of φ particles, i.e. $\Gamma = \Gamma_{\varphi\to\chi_\mathrm{b}\chi_\mathrm{b}} + \Gamma_{\varphi\to\psi_\mathrm{f}\psi_\mathrm{f}}$. Eq. (4.6) implies that the amplitude of the φ oscillations decays as $\varphi(t) \sim a^{-3/2}\exp(-\frac{1}{2}\Gamma t)$. The decay rate Γ can be computed using perturbation theory in quantum field theory. For interaction terms given in Eq. (4.4), decay rates for the corresponding decay channels are given by [122]

$$\Gamma_{\varphi\to\chi_\mathrm{b}\chi_\mathrm{b}} = \frac{b^2}{8\pi m} + \frac{g^2\Phi^2}{8\pi m}\,,\ \Gamma_{\varphi\to\psi_\mathrm{f}\psi_\mathrm{f}} = \frac{h^2 m}{8\pi}\,. \tag{4.7}$$

For a phenomenological prescription, one can add an extra friction term $\Gamma_\varphi\dot{\varphi}$ to the classical equation of motion of the field φ instead of the polarisation operator during the rapid oscillations regime [123]

$$\ddot{\varphi} + (3H + \Gamma)\dot{\varphi} + W_\varphi = 0\,. \tag{4.8}$$

The rapid oscillations condition now reads as $m \gg \max\{H, \Gamma\}$. Multiplying through

by $\dot{\varphi}$ it is intuitive to rewrite Eq. (4.8) in terms of the energy density of the φ field, ρ_φ

$$\dot{\rho}_\varphi + 3H\dot{\varphi}^2 + \Gamma\dot{\varphi}^2 = 0\,. \tag{4.9}$$

Now, since the oscillation of φ is approximately sinusoidally, $\dot{\varphi}^2$ can be replaced by its average over a single oscillation cycle, i.e. $\langle\dot{\varphi}^2\rangle_{\rm cycle} = \rho_\varphi$. This can be seen by multiplying Eq. (4.8) by φ. In the rapid oscillations regime, this reduces to

$$\frac{\mathrm{d}}{\mathrm{d}t}\left(\varphi\dot{\varphi}\right) - \dot{\varphi}^2 + \varphi W_\varphi \approx 0\,. \tag{4.10}$$

Averging over a single cycle, the first term vanishes and thus we can deduce $\langle\dot{\varphi}^2\rangle \approx \langle\varphi W_\varphi\rangle$. If the decay products of the oscillating φ field are very light relative to φ itself, we can model them as a (single) relativistic radiation fluid with energy density ρ_γ

$$\dot{\rho}_\gamma + 4H\rho_\gamma = \Gamma\rho_\varphi = \Gamma\dot{\varphi}^2\,, \tag{4.11}$$

$$H^2 = \frac{1}{3M_{\rm p}^2}\left(\rho_\varphi + \rho_\gamma\right)\,. \tag{4.12}$$

Here Eq. (4.11) follows from energy conservation. Similar analysis can be applied for the quartic potential $\frac{1}{4}\tilde{\lambda}\varphi^4$, except now φ behaves as an effective relativistic fluid with $\rho_\varphi \propto a^{-4}$ and now we have $\langle\dot{\varphi}^2\rangle_{\rm cycle} = 4\rho_\varphi/3$. Also the mass m is replaced by the effective oscillation frequency $w_\varphi = c\sqrt{\tilde{\lambda}}\Phi$. Together Eqs. (4.9), (4.11) and (4.12) give the phenomenological description of the simple perturbative reheating of the Universe.

When $\Gamma > H$, the energy density of the φ field decays exponentially as $\rho_\varphi \propto \exp(-\Gamma t)$. This justisfies the interpretation of treating the oscillating φ field as a coherent wave of decaying φ particles. ρ_φ quickly becomes subdominant compared to that of the decay products ρ_γ and reheating is said to be completed. The density of the Universe at this moment is

$$\rho(t_c) \simeq 3H^2(t_c)M_{\rm p}^2 = 3\Gamma^2 M_{\rm p}^2\,. \tag{4.13}$$

If the decay products interact with each other strongly enough, then thermal equilibrium is quickly established and may be maintained at a temperature $T_{\rm R}$. Treating this

ultrarelativistic gas of particles with Bose–Einstein statistics, the energy density of the Universe in thermal equilibrium is then

$$\rho(T_{\rm R}) \simeq \left(\frac{\pi^2}{30}\right) g_* T_{\rm R}^4 \,, \tag{4.14}$$

where the factor $g_*(T_{\rm R}) \sim 10^2 - 10^3$ depends on the number of ultrarelativistic degrees of freedom. Comparing Eqs. (4.13) and (4.14) we arrive at

$$T_{\rm R} \sim 0.1 \sqrt{\Gamma M_{\rm p}} \,. \tag{4.15}$$

Here we have assumed perfect energy transfer from inflaton to the effective radiation fluid (ignoring damping due to expansion of the Universe). If there is significant production of non-relativistic matter not in the form of radiation, $T_{\rm R}$ decreases as H is modified.

In order not to spoil the success of Big Bang nucleosynthesis (BBN), the inflaton decay products should be quickly thermalised through scatterings, annihilations, pair creation and further decays, such that the Universe is completely radiation dominated before the BBN epoch. This constrains the reheating temperature to be $T_{\rm R} \gtrsim 5\,\text{MeV}$ [124, 125], which in turn implies $\Gamma \gtrsim 4 \times 10^{-40} M_{\rm p}$. There is also an upper bound on $T_{\rm R}$ set by the energy scale of inflation, where $T_{\rm R} \leq 10^{16} GeV$. A stronger bound $T_{\rm R} \leq 10^{6-8} GeV$ can also be found, which comes from the overproduction of gravitinos if one considers supersymmetric models [126, 127, 128].

It is straightforward to extend the perturbative reheating setup to canonical multifield models given that the fields are weakly coupled. To do so, we simply consider multiple copies of the φ field discussed above for fields that undergo rapid sinusodial oscillations. The main difference between the single-field and multifield paradigm is that the fields are coupled via the potential in multifield models except the case of sum-separable potentials. This modifies the effective masses of the fields and thus modulates the decay rates. For weak couplings, we expect the modulation to be small and thus can be safely neglected.

Discussion on the Validity of Perturbative Reheating

In this section, we would like to comment on the validity and limitions of the perturbative reheating setup. Firstly and most importantly, it should be emphasised that the simple phenomenological equations are only valid when the fields are rapidly oscillating about some minima: the 'particle creation' term, $\Gamma\dot{\varphi}$, should not be present beyond the rapid oscillation regime.

Furthermore, in reality, the transition from inflation to a hot Big Bang Universe could happen via very different mechanisms than the perturbative reheating setup discussed earlier. In particular, parametric resonance effects may be significant under certain regimes, particularly early in the oscillating regime when the oscillation amplitude is large. To a first approximation, the inflaton φ acts as a classical external force acting on the quantum fields $\chi_{\rm b}$ and $\psi_{\rm f}$ to which it couples. Since φ is time-dependent, the effective masses of χ_b and ψ_f could change rapidly if the bare masses are small, leading to non-adiabatic excitations. This process is known as **preheating** [118, 119, 129].

Despite various limitations, the elementary theory of reheating is appealing due to its simplicity and its ability to be very successful in describing the reheating process in certain regimes. Whilst reheating may well be more complex than the simple perturbative model we consider, it is a useful scheme for determining how sensitive the primordial observables may be to reheating, and to check whether any general trends exist across different models. For example, one might naviely speculate that any large non–Gaussianity is generically damped to zero after reheating, as is often (but not always [130]) the case during inflation if the isocurvature mode decays during slow roll [131, 132]. This is not the case however even in the simple perturbative reheating setup [110, 133, 134, 135].

4.2 Two-Point Statistics After Reheating

In this section, we illustrate the influence of reheating in multifield models at the level of the power spectrum. We focus on the simple class of two-field models discussed in Section 3.4.2. In particular, we consider several different two-field models where min-

ima exist in either the direction of one or both fields. The results were first presented in [133].

We model perturbative reheating as discussed in the last section by the following field equations

$$\begin{aligned}
&\ddot{\varphi} + (3H + \Gamma_\varphi)\dot{\varphi} + W_\varphi = 0 \\
&\ddot{\chi} + (3H + \Gamma_\chi)\dot{\chi} + W_\chi = 0 \\
&\dot{\rho}_\gamma + 4H\rho_\gamma = \Gamma_\varphi \dot{\varphi}^2 + \Gamma_\chi \dot{\chi}^2 \\
&H^2 = \frac{1}{3M_{\rm p}^2}\left(\frac{1}{2}\dot{\chi}^2 + \frac{1}{2}\dot{\varphi}^2 + W + \rho_\gamma\right) ,
\end{aligned} \tag{4.16}$$

where Γ_χ and Γ_φ are the decay rates for the χ and φ fields respectively, which only turn on during the rapid oscillation regime. For simplicity, we take the decay rates to be constants. There is a lower bound on Γ_χ and Γ_φ from BBN as discussed earlier, given by $\Gamma_\varphi, \Gamma_\chi \gtrsim 4 \times 10^{-40} M_{\rm p}$. We ensure that this bound is always satisfied. For such weak decay rates, reheating would proceed incredibly slowly if the process were entirely perturbative. In reality however, as alluded to above, the universe is unlikely to be reheated via a mechanism that can be described completely by standard perturbation theory, and so we interpret the bound rather loosely. The upper bound due to overproduction of gravitinos can be evaded by considering non-supersymmetric models. Where applicable, we also give the value of the Hubble rate at the start of reheating H_r so a direct comparison between the expansion and decay rate can be made.

To compute ζ and the primordial observables we apply the δN formalism. The corresponding δN coefficients are computed numerically using the central finite difference method. Here we choose to switch on the decay rates when the corresponding fields first pass through their respective minima which they oscillate about. We denote this epoch as the start of reheating. For the two minima case, there are two such epochs, which we denote as $N_{\varphi=0}$ and $N_{\chi=0}$. While these choices of reheating hypersurfaces are arbitrary, the main qualitative results are very much independent of how the reheating hypersurfaces are defined (see Appendix B). Details of the numerical recipe used are summarised in Appendix B.

The reader should be reminded that model predictions in multifield inflation depends

on the initial conditions set at horizon-crossing in general. Since we are interested in the evolution of statistics beyond the power spectrum as well, we focus on models and regions of parameter space where some of the second order δN coefficients N_{IJ} and the magnitude of the non-linear parameter $|f_{\rm NL}|$ can become large (at least momentarily) here.

Models with One Minimum

The first model we considered is the 'runaway' type quadratic times exponential potential

$$W(\varphi, \chi) = W_0 \chi^2 e^{-\lambda\varphi^2/M_{\rm p}^2} \,. \tag{4.17}$$

Here W_0 sets the energy scale of the potential and is of mass dimension two. Whilst its value sets the scale of inflation and determines the amplitude of the primordial power spectrum and hence is constrained, it does not affect the statistics of ζ and so we leave W_0 as a free parameter. Inflation happens when χ is of super-Planckian field values and the exponential factor is very much suppressed, i.e. $\lambda\varphi^2/M_{\rm p}^2 \ll 1$. In what follows, we identify χ as the inflaton and φ as the subdominant field which sources the isocurvature perturbations. This potential was first introduced by [102] in the context of primordial non-Gaussianity, and has made frequent appearances in the literature since then, for instance in [105, 106, 132, 136, 137, 138]. Without any minimum for a corresponding oscillating phase, the φ field is not directly involved in the reheating phase and so we set $\Gamma_\varphi = 0$ at all times.

This model does not contain a 'focussing' region in the potential where neighbouring trajectories in the bundle may converge such that non-adiabatic perturbations vanish. Hence, ζ and its statistics will continue to evolve after inflation has ended. The adiabatic regime is only possible with reheating. The switching on of the decay terms at the reheating surface sources the radiation density. As the χ field oscillates about its minimum, its kinetic energy is transferred to the radiation fluid, resulting in bursts of particle production. As radiation fills the universe, Hubble damping slows the motion of φ to a crawl and as we approach $\Omega_\gamma \sim 1$, it asymptotes to a constant:

$\varphi(t \to \infty) \approx \text{const}$. Herein is the fundamental difference in the motion of φ when $\Gamma_\chi \neq 0$ compared to $\Gamma_\chi = 0$: as radiation comes to dominate, trajectories in the bundle cease to evolve. The bundle does not degenerate to a caustic as would be the case if the trajectories were naturally focussed by a region of the potential, but nonetheless this freezing of the φ field guarantees that ζ becomes conserved. This does not happen in the $\Gamma_\chi = 0$ limit where the trajectories continue to diverge in the φ direction, always sourcing ζ.

Evolution of the δN Coefficients

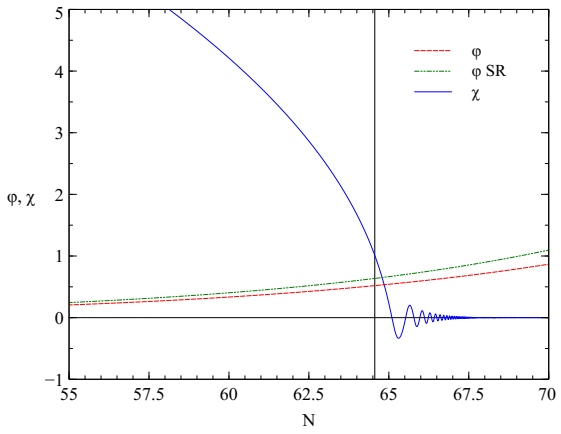

Figure 4.1: Potential: $W(\varphi, \chi) = W_0 \chi^2 e^{-\lambda\varphi^2/M_\mathrm{p}^2}$. The evolution of the background fields (in Planck units) without reheating for model parameters $\lambda = 0.05$, $\varphi_* = 10^{-3} M_\mathrm{p}$ and $\chi_* = 16.0 M_\mathrm{p}$. The solid vertical (black) line denotes the end of inflation, N_e.

Before showing the influence of reheating on the two-point statistics of ζ, it is useful to inspect the evolution of the subdominant φ field and the δN coefficients in this model first. In the slow-roll regime, the solution to the Klein-Gordon equation for φ and the corresponding slow-roll parameter $\eta_{\varphi\varphi}$ are given by

$$\varphi = \varphi_* e^{2\lambda N}\,, \qquad \eta_{\varphi\varphi} = 2\lambda\left[2\lambda\varphi_*^2 e^{4\lambda N}/M_\mathrm{p}^2 - 1\right]\,. \tag{4.18}$$

Eq. (4.18) shows that φ will continue to increase exponentially with the number of e-folds N. We expect this solution to break down beyond slow-roll, but remains a good approximation as long as $|\eta_{\varphi\varphi}| < 1$. In Fig. 4.1 we compare this solution with the exact numerical solution without reheating, showing the slow-roll solution indeed remains a

good approximation for φ for the first few e-folds after inflation ends ($\epsilon_H = 1$).

For the δN coefficients, N_χ remains practically constant, $N_\chi M_{\rm p} \approx (1/\sqrt{2\epsilon_\chi})_*$, throughout the entire inflationary and post–inflationary phase except momentarily during the χ oscillations, regardless of the decay rate Γ_χ. It acquires this value as the fields leave the horizon. This is shown in Fig. 4.2. This can be explained in the following.

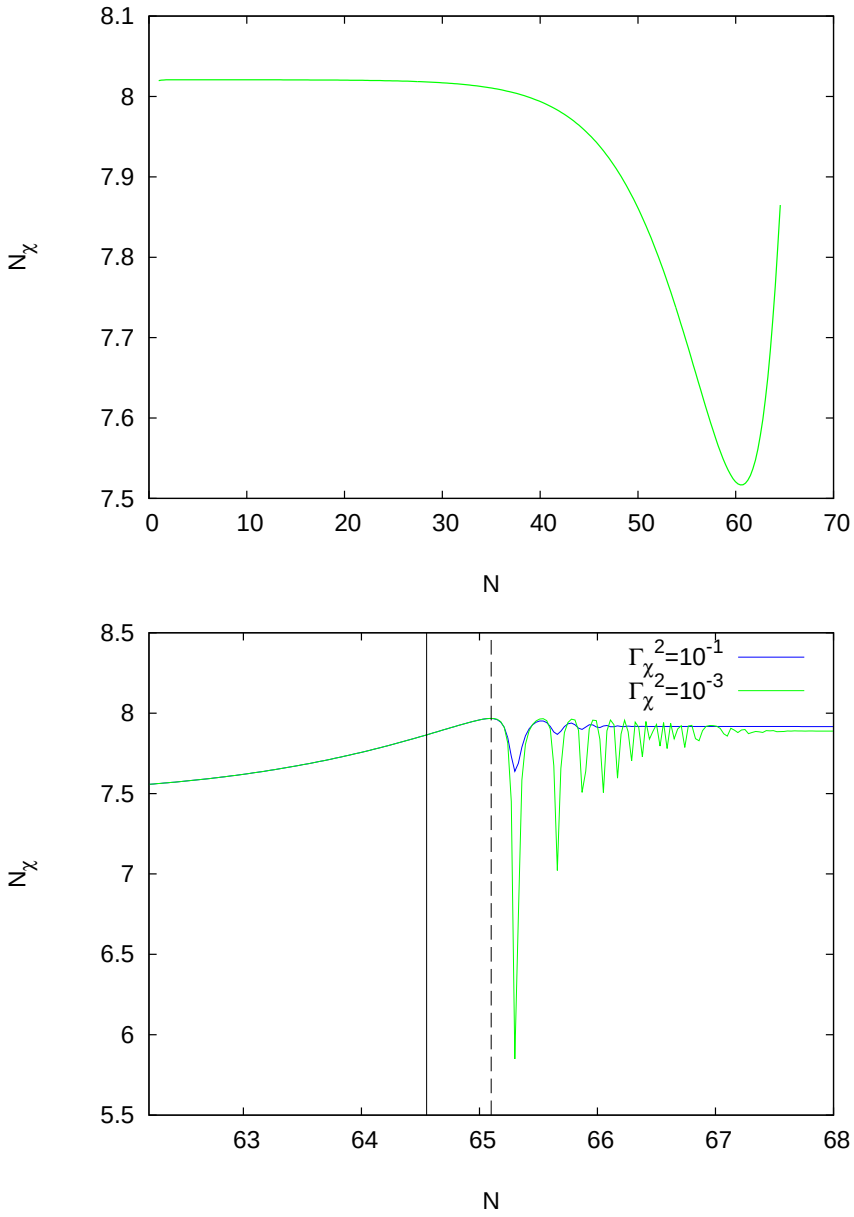

Figure 4.2: Potential: $W(\varphi, \chi) = W_0 \chi^2 e^{-\lambda\varphi^2/M_{\rm P}^2}$. The evolution of the first order δN coefficient N_χ in unit of $M_{\rm P}^{-1}$ for the model parameters $\lambda = 0.06$, $\varphi_* = 10^{-3} M_{\rm P}$ and $\chi_* = 16.0 M_{\rm P}$. The top panel shows the slow-roll inflationary evolution from horizon-exit, whereas the bottom panel shows the reheating evolution with two different decay rates Γ_χ. The decay rates are given in unit of $\sqrt{W_0}$. The solid vertical (black) line denotes the end of inflation, $N_{\rm e}$, and the dashed vertical (black) line denotes the start of reheating, $N_{\chi=0}$ where χ first crosses $\chi = 0$. The Hubble rate at the start of reheating is $H_r \approx \sqrt{7 \times 10^{-2} W_0}$.

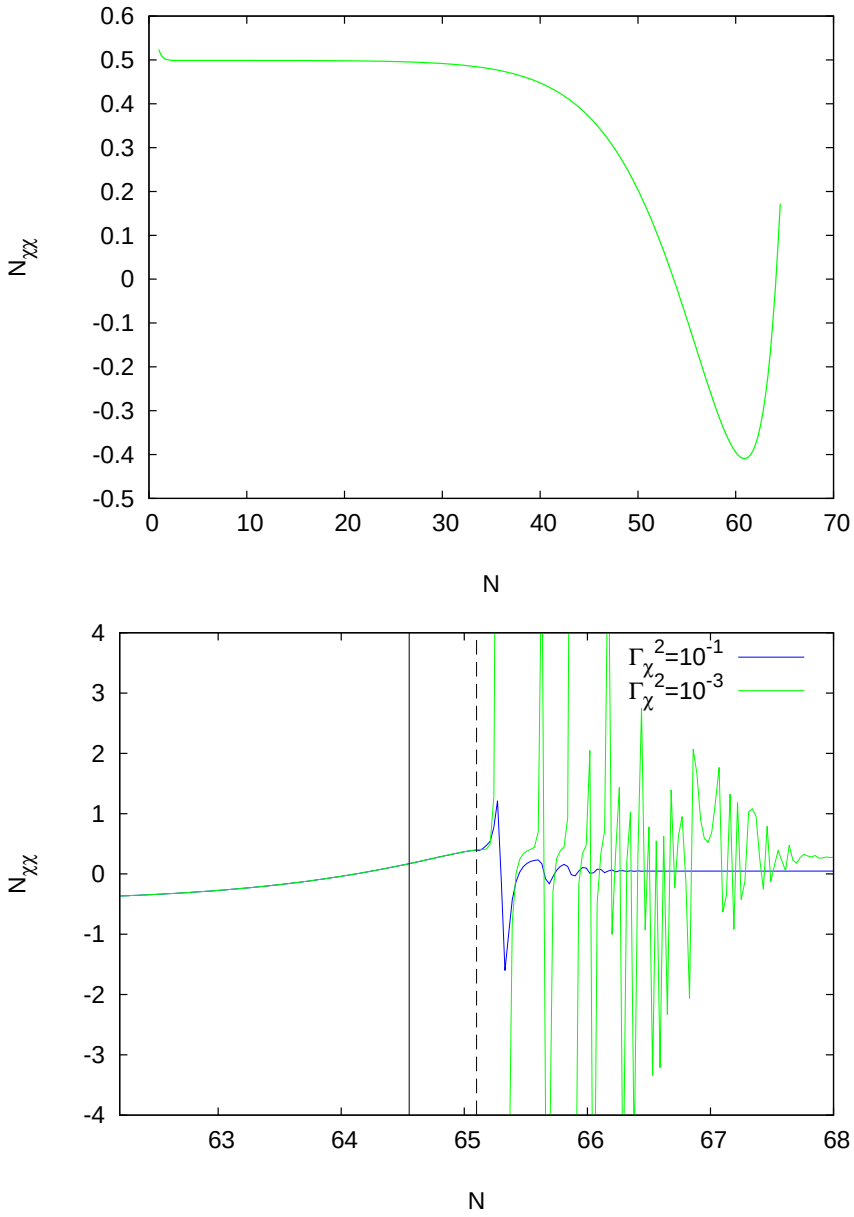

Figure 4.3: Potential: $W(\varphi,\chi) = W_0\chi^2 e^{-\lambda\varphi^2/M_{\rm p}^2}$. The evolution of the second order δN coefficient $N_{\chi\chi}$ in unit of $M_{\rm p}^{-2}$ for the model parameters $\lambda = 0.06$, $\varphi_* = 10^{-3}M_{\rm p}$ and $\chi_* = 16.0M_{\rm p}$. The top panel shows the slow-roll inflationary evolution from horizon-exit, whereas the bottom panel shows the reheating evolution with two different decay rates Γ_χ. The decay rates are given in unit of $\sqrt{W_0}$. The solid vertical (black) line denotes the end of inflation, $N_{\rm e}$, and the dashed vertical (black) line denotes the start of reheating, $N_{\chi=0}$ where χ first crosses $\chi = 0$. The Hubble rate at the start of reheating is $H_r \approx \sqrt{7\times10^{-2}W_0}$.

Given H is monotonic in time, we first rewrite the number of e-folds N from an initial flat hypersurface at t_* to a final uniform-density hypersurface at t_c as

$$N \equiv \int_{t_*}^{t_c} H\mathrm{d}t = \int_{H_*}^{H_c}\left(\frac{H}{\dot{H}}\right)\mathrm{d}H\,. \tag{4.19}$$

Taking the derivative with respect to χ_* as in the δN formalism we find

$$N_\chi = \left(\frac{H}{\dot{H}}\right)_* \left(\frac{\partial H}{\partial \chi}\right)_* + \int_{H_*}^{H_c} \frac{\partial}{\partial \chi_*} \left(\frac{1}{\dot{H}}\right)_H H \mathrm{d}H \,, \tag{4.20}$$

where the derivative inside the integral is computed by holding H constant. The derivative at the boundary c vanishes, since by definition the final hypersurface at t_c corresponds to one of uniform-density and thus constant H from the Friedmann equation. Using the fact that the fields are in slow-roll at horizon exit, the first term on the RHS of Eq. (4.20) reduces to $(1/M_\mathrm{p}\sqrt{2\epsilon_\chi})_*$ if $|\dot{\chi}_*| \gg |\dot{\varphi}_*|$. Then, to explain why N_χ remains constant at this value requires arguing that the integral term in Eq. (4.20) is negligible, i.e., after perturbing χ_*, surfaces of constant $\dot{H}$ must coincide with surfaces of constant H. This is indeed the case if a hierarchy of kinetic energies exists between the fields at horizon crossing, i.e., $|\dot{\chi}_*| \gg |\dot{\varphi}_*|$. Since the kinetic terms are canonical, the fields follow the gradient of the potential, and as they are in slow-roll at horizon exit, this hierarchy implies $|W_\chi|_* \gg |W_\varphi|_*$. If this is the case, the dependence of $\dot{H}$ on χ_* is rapidly washed out, and the two–dimensional bundle in the χ direction (holding φ_* fixed) degenerates to a caustic. We have found that the condition $|W_\chi|_* \gg |W_\varphi|_*$ is sufficient to guarantee that the integrand of Eq. (4.20) is always small from horizon crossing until oscillations of χ begin.

During the oscillatory phase, the integrand oscillates about zero with an amplitude that decays with the Hubble expansion, and when integrated over many oscillations, the net result is a negligible correction to N_χ. This is shown in Fig. 4.4. By the same argument, differentiating Eq. (4.20) with respect to χ_* again, we deduce $N_{\chi\chi}$ remains roughly constant at $N_{\chi\chi} M_\mathrm{p}^2 \approx 1 - (\eta_{\chi\chi}/2\epsilon_\chi)_*$, which, for this particular potential is independent of λ and the field values at horizon crossing, $N_{\chi\chi} \approx 0.5 M_\mathrm{p}^{-2}$.

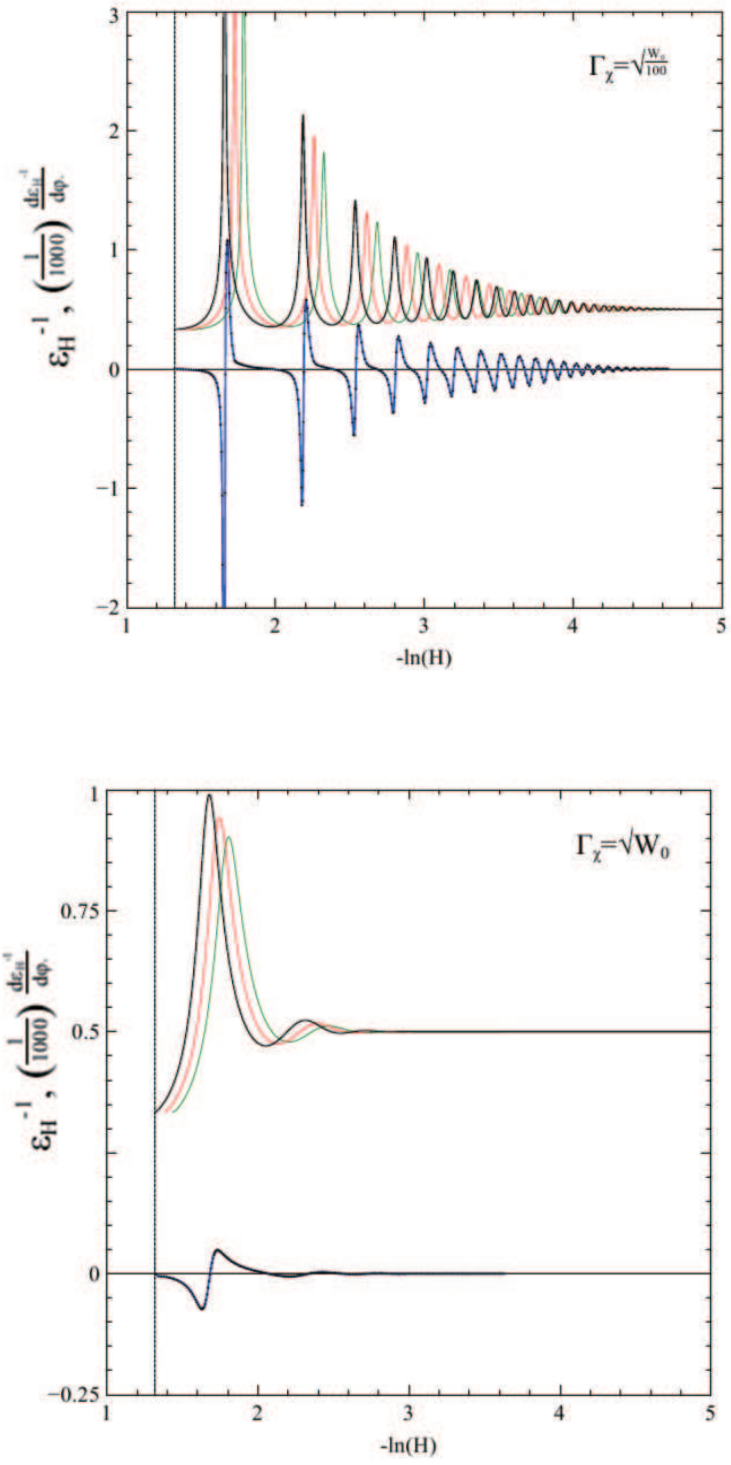

Figure 4.4: Potential: $W(\varphi,\chi) = W_0\chi^2 e^{-\lambda\varphi^2/M_{\rm P}^2}$. The evolution of $(\epsilon_H)^{-1}$ as a function of $-\ln H$ (here H defined in unit of $W_0/M_{\rm P}$), denoted by the solid black line, for two different Γ_χ: $\Gamma_\chi = \sqrt{W_0/100}$ (*top panel*) and $\Gamma_\chi = \sqrt{W_0}$ (*bottom panel*). As H decreases in time, ϵ_H evolves to greater values of $\ln H$ and the limit of the $x-$axis represents the completion of reheating. Here we also plot the evolution of ϵ_H^{-1} for slightly different initial condition φ_*, denoted by the solid green and red lines. We see that the effect of varying φ_* is to introduce a relative phase into the oscillations of ϵ_H. In both panels, the vertical dashed line represents the value of $\ln H$ at the start of reheating. The thick blue line shows the derivative of ϵ_H^{-1} with respect to φ_* while holding H constant, scaled by a factor of 10^{-3}. The model parameters here are $\lambda = 0.05$, $\varphi_* = 10^{-3}M_{\rm P}$ and $\chi_* = 16.0M_{\rm P}$.

Things are different for the other δN coefficients N_φ and $N_{\varphi\varphi}$ however. Unlike N_χ, N_φ continues to evolve after horizon-exit. It settles down to constant value only in the adiabatic limit after φ becomes frozen and reheating ends. The evolution of N_φ and $N_{\varphi\varphi}$ for $\lambda = 0.05$ is shown in Figs. 4.5 and 4.6, from which we see $|N_{\varphi\varphi}|$ and $|N_\varphi|$ asymptote to smaller values as the decay rate Γ_χ increases and the reheating phase becomes longer. One should also note that $N_{\varphi\varphi} \gg N_{\chi\chi}$ here.

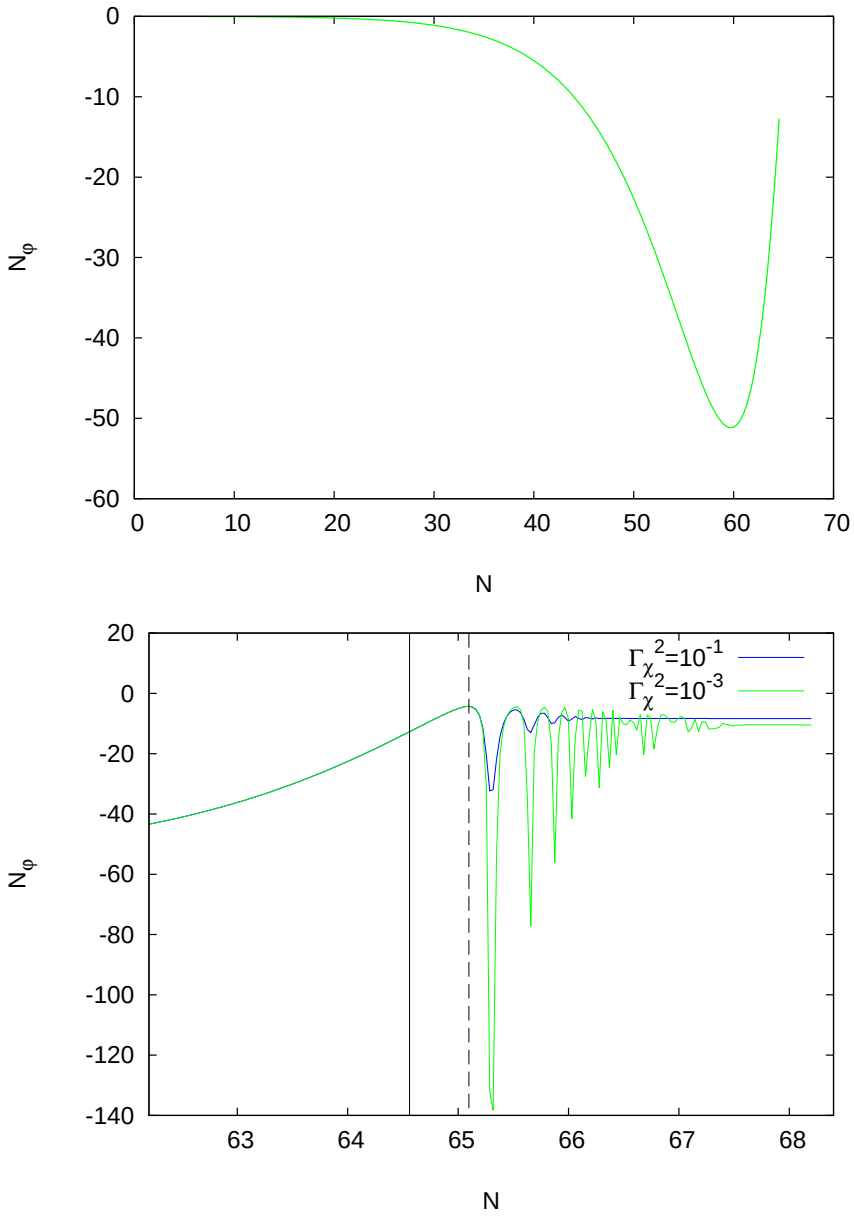

Figure 4.5: Potential: $W(\varphi,\chi) = W_0\chi^2 e^{-\lambda\varphi^2/M_{\rm p}^2}$. The evolution of the first order δN coefficient N_φ in unit of $M_{\rm p}^{-1}$. The top panel shows the slow-roll inflationary evolution from horizon-exit, whereas the bottom panel shows the reheating evolution for two decay rates Γ_χ. The model parameters $\lambda = 0.05$, $\varphi_* = 10^{-3}M_{\rm p}$ and $\chi_* = 16.0M_{\rm p}$. Here the Γ_χ is given in unit of $\sqrt{W_0}$. The solid vertical (black) line denotes the end of inflation, $N_{\rm e}$, and the dashed vertical (black) line denotes the start of reheating, $N_{\chi=0}$ where χ first crosses $\chi = 0$. The Hubble rate at the start of reheating is $H_r \approx \sqrt{7\times10^{-2}W_0}$.

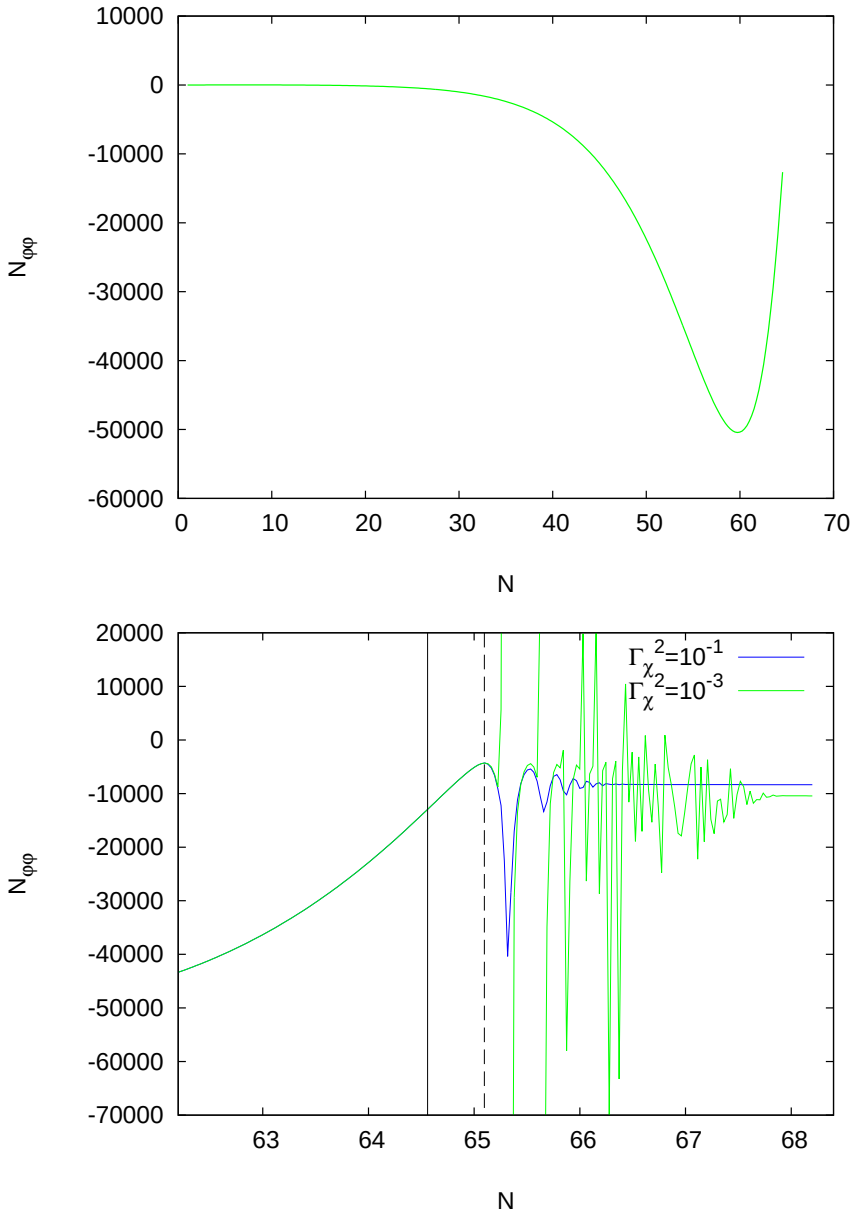

Figure 4.6: Potential: $W(\varphi,\chi) = W_0\chi^2 e^{-\lambda\varphi^2/M_{\rm p}^2}$. The evolution of the second order δN coefficient $N_{\varphi\varphi}$ in unit of $M_{\rm p}^{-2}$. The top panel shows the slow-roll inflationary evolution from horizon-exit, whereas the bottom panel shows the reheating evolution for two decay rates Γ_χ. The model parameters $\lambda = 0.05$, $\varphi_* = 10^{-3}M_{\rm p}$ and $\chi_* = 16.0M_{\rm p}$. Here the Γ_χ is given in unit of $\sqrt{W_0}$. The solid vertical (black) line denotes the end of inflation, $N_{\rm e}$, and the dashed vertical (black) line denotes the start of reheating, $N_{\chi=0}$ where χ first crosses $\chi = 0$. The Hubble rate at the start of reheating is $H_r \approx \sqrt{7\times 10^{-2}W_0}$.

Scaling Relations Between δN Coefficients

Furthermore, the following approximate scaling relations exist between the δN coefficients throughout the entire inflationary and post–inflationary evolution

$$N_{\varphi\varphi} \approx \frac{N_\varphi}{\varphi_*}, \tag{4.21}$$

$$N_{\varphi\chi} \approx 4\lambda N_\varphi N_\chi \approx \frac{4\lambda}{(\sqrt{2\epsilon_\chi})_*}\frac{N_\varphi}{M_{\rm p}}. \tag{4.22}$$

The scaling relation between $N_{\varphi\varphi}$ and N_φ was first derived in [106] by considering a first order Taylor expansion about a 'ridge', situated at $\varphi = 0$, of a generic potential.

Assuming the slow-roll conditions, the same analysis applies to the model we study here as long as the potential remains well approximated by $W \approx W_0\chi^2(1-\lambda\varphi^2)$, i.e., higher order terms in $\lambda\varphi^2$ remain small. This requires $\varphi \ll \mathcal{O}(\lambda^{-1/2}M_{\rm p})$. In this regime, φ grows exponentially with H as the bundle of trajectories rolls off the ridge: $\varphi = \varphi_* e^{\tilde{\alpha}(H_*^2-H^2)}$, $\tilde{\alpha} = 3\lambda/2W_0$. A short calculation reveals

$$N_\varphi \approx -3\beta H^2\varphi_*\left(\frac{\varphi}{\varphi_*}\right)^2, \tag{4.23}$$

where β is some model–dependent constant. We refer the reader to [106] where the complete derivation is presented. Taking $\frac{\partial}{\partial\varphi_*}$ (on the final hypersurface of constant H) on both sides of Eq. (4.23) gives Eq. (4.21) as long as $(\partial H/\partial\varphi)_* \approx 0$. Similarly, taking the derivative with respect to χ_* and using the φ slow-roll solution Eq. (4.18) gives Eq. (4.22).

We show evolution of the N_φ, $N_{\varphi\varphi}$ and $N_{\varphi\chi}$ derivatives before and *after* inflation for a particular decay rate Γ_χ in Fig. 4.7, which clearly illustrates the scaling behaviour captured in Eqs. (4.21) and (4.22). Remarkably, not only does this scaling behaviour holds after inflation has ended, but it also holds during reheating.

The derivation of these scaling relations as sketched above relies on a number of approximations, including slow-roll. The subdominant field φ always remains slowly rolling where $3H\dot{\varphi} \gg \ddot{\varphi}$, however χ does not necessarily. χ not being slow-roll does not seem to violate Eqs. (4.21) and (4.22), suggesting that validity of these relations are more reliant on φ being a linear function of φ_*, and that φ grows exponentially

as the bundle slides off the ridge. As mentioned above, these conditions will break down when $\varphi \sim \mathcal{O}(\lambda^{-1/2} M_{\rm p})$. Then, using $\varphi \sim \lambda^{-1/2} M_{\rm p}$ in Eq. (4.18) we may very roughly estimate how many e–folds we expect the scaling relations to remain valid for $N \sim \frac{1}{2\lambda} \ln\left(\lambda^{-1/2} M_{\rm p}/\varphi_*\right)$. For example, for $\lambda = 0.05$ and $\varphi_* = 10^{-3} M_{\rm p}$ we have $N \sim 85$.

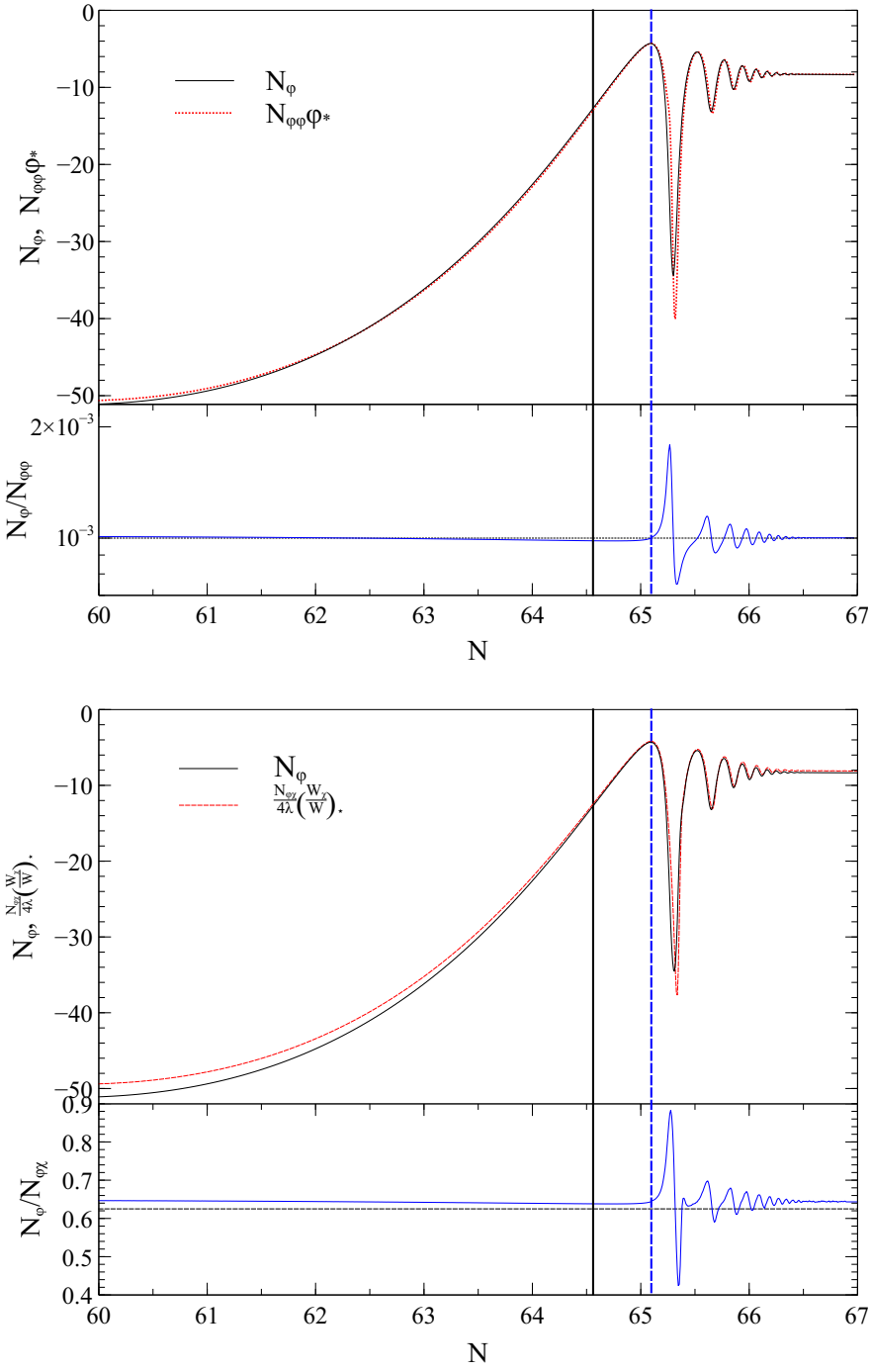

Figure 4.7: Potential: $W(\varphi,\chi) = W_0\chi^2 e^{-\lambda\varphi^2/M_{\rm p}^2}$. Numerical verification of the scaling relations Eqs. (4.21) and (4.22). *Top panel*: Evolution of the derivatives $N_{\varphi\varphi}$ and N_φ (in Planckian units). The horizontal dashed line in the lower panel represents the value of φ_*, the constant of proportionality between $N_{\varphi\varphi}$ and N_φ. *Bottom panel*: Evolution of the derivatives $N_{\varphi\chi}$ and N_φ (in unit of $M_{\rm p}$). The horizontal dashed line in the lower panel represents the value $\frac{1}{4\lambda}(W_\chi/W)_* = \frac{1}{4\lambda}(2\epsilon_\chi)_*^{1/2}$, the constant of proportionality between $N_{\varphi\chi}$ and N_φ. We show evolution of the derivatives for the last few e–folds of inflation, up until ζ has become conserved at the completion of reheating. We see small departures from scaling at the start of reheating as χ oscillates about its minimum, but as χ settles down, the scaling behaviour is quickly recovered. In both panels, the parameters used are: $\lambda = 0.05$, $\varphi_* = 10^{-3}M_{\rm p}$, $\chi_* = 16.0M_{\rm p}$ and $\Gamma_\chi = \sqrt{10^{-1}W_0}$. The solid vertical (black) line denotes the end of inflation, $N_{\rm e}$, and the dashed vertical (blue) line denotes the start of reheating, $N_{\chi=0}$. The Hubble rate at the start of reheating is $H_r \approx \sqrt{7\times10^{-2}W_0}$.

Amplitude of the Power Spectrum, A_ζ

Now we consider how sensitive two-point statistics of ζ, including the tensor–to–scalar ratio r and spectral index n_s, are to the reheating phase in this model. The post-inflationary evolution of the amplitude of the power spectrum A_ζ is illustrated in Fig. 4.8. As expected, we see A_ζ continues to evolve after inflation ends since isocurvature perturbations persist. In the adiabatic limit after reheating ends, ζ becomes conserved and A_ζ asymptotes to a constant value. The final asymptotic value is larger for smaller the decay rate Γ_χ and longer the reheating phase. As mentioned earlier, P_* and thus A_ζ depend on the energy scale W_0. By tuning W_0 for different Γ_χ, we can always match A_ζ with the normalisation of CMB measurements in WMAP and Planck where $A_\zeta \sim 10^{-9}$ [44].

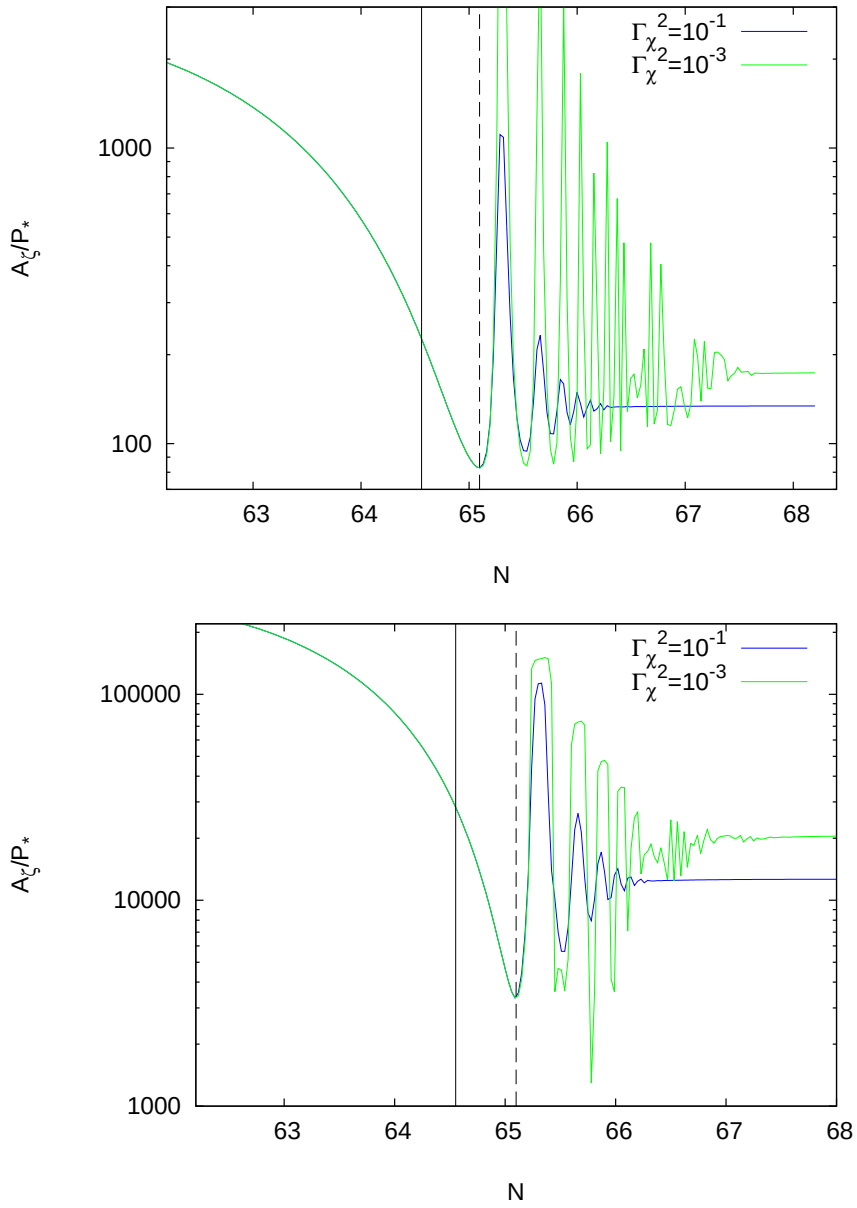

Figure 4.8: Potential: $W(\chi,\varphi) = W_0\chi^2 e^{-\lambda\varphi^2/M_{\rm p}^2}$, with $\varphi_* = 10^{-3}M_{\rm p}$, $\chi_* = 16M_{\rm p}$. The evolution of A_ζ/P_* (in unit of $M_{\rm p}^{-2}$) for two different decay rates Γ_χ. Here $\lambda = 0.05$ (*top panel*) and $\lambda = 0.06$ (*bottom panel*). Γ_χ is given in unit of $\sqrt{W_0}$. The solid vertical (black) line denotes the end of inflation, $N_{\rm e}$, and the dashed vertical (black) line denotes the start of reheating, $N_{\chi=0}$ where reheating starts. The Hubble rate at the start of reheating is $H_r \approx \sqrt{7\times10^{-2}W_0}$.

Spectral Index $n_{\rm s}$ and Tensor-to-Scalar Ratio r

Similarly, the tensor–to–scale ratio r and spectral index $n_{\rm s}$ evolve during reheating and are different to the values evaluated at the end of inflation in general. Yet they do not depend on the energy scale W_0 and thus cannot be tuned to match observations for

any decay rate Γ_χ. The evolution of r and n_s during reheating in this model for two different decay rates Γ_χ are shown in Figs. 4.9 to 4.12. Notice that Figs. 4.9 and 4.10 are simply the inverse of Fig. 4.8 as $(8/r)M_\mathrm{p}^{-2} = A_\zeta/P_*$. From the plots, we see the final value of r is bounded from above and remains very much negligible with $r < O(0.1)$, although the final asymptotic value does depend on Γ_χ.

This can be understood as follow: Recall from Eq. (3.66), in multifield models, $r = 8/M_\mathrm{p}^2(\sum_I N_I^2)$. Because of the hierarchy in magnitude between the scalar field kinetic energies $\dot{\varphi}_*^2$ and $\dot{\chi}_*^2$ at horizon exit and φ remains subdominant, N_χ is approximately constant, i.e. $N_\chi \approx (1/M_\mathrm{p}\sqrt{2\epsilon_\chi})_*$. For the region of parameter space of interest, as Γ_χ is decreased from infinity, the time taken for reheating to complete is increased and φ freezes out later, increasing the magnitude of N_φ as shown in Fig. 4.5. Hence, the smaller the decay rate, the more suppressed the tensor–to–scalar ratio, and the following bound exists:

$$r \leq \frac{8}{M_\mathrm{p}^2}\frac{1}{N_{0,\varphi_*}^2 + g_*^2}\,. \tag{4.24}$$

Here $g_* \equiv (1/M_\mathrm{p}\sqrt{2\epsilon_\chi})_*$ and N_{0,φ_*} is defined as the value of N_φ at the start of reheating.

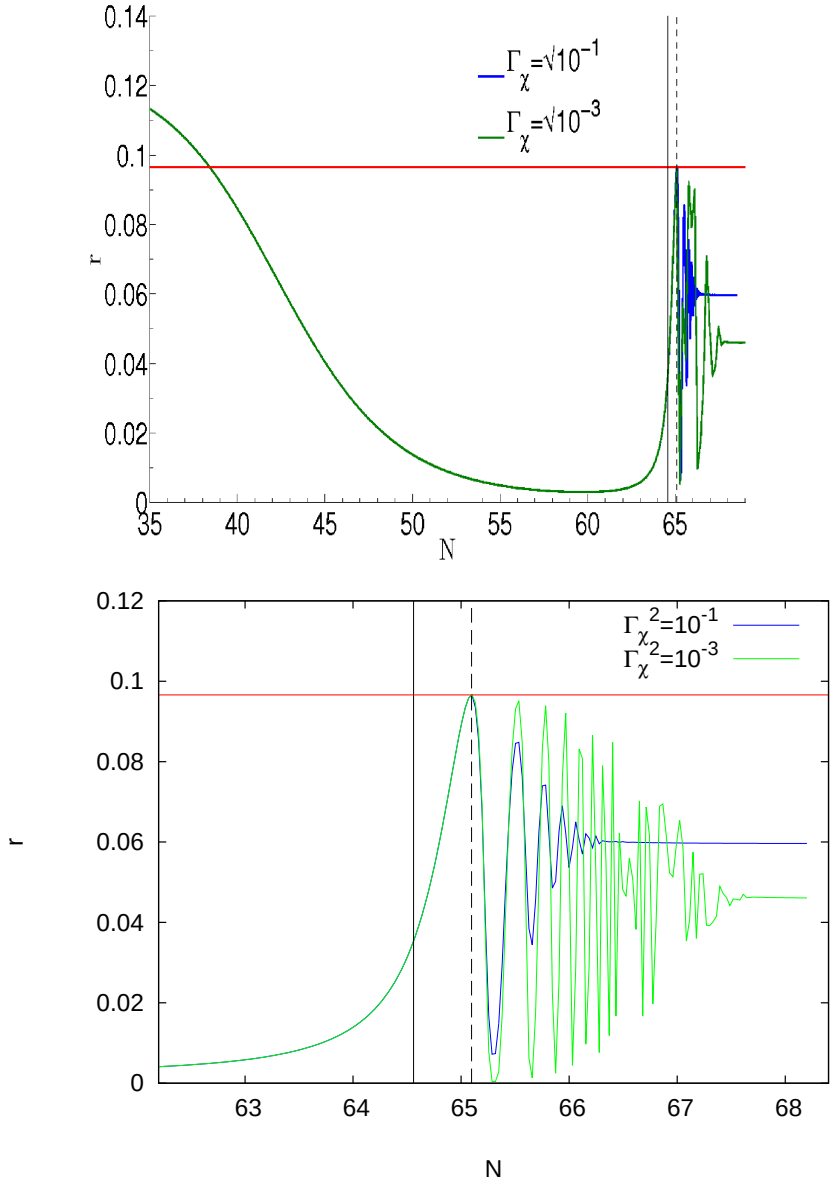

Figure 4.9: Potential: $W(\varphi, \chi) = W_0 \chi^2 e^{-\lambda\varphi^2/M_{\rm P}^2}$. Evolution of r for two different decay rates Γ_χ, with $\lambda = 0.05$. The parameters used are: $\varphi_* = 10^{-3} M_{\rm p}$, $\chi_* = 16.0 M_{\rm p}$, and Γ_χ is given in unit of $\sqrt{W_0}$. The solid vertical (black) line denotes the end of inflation, $N_{\rm e}$, and the dashed vertical (black) line denotes the start of reheating, $N_{\chi=0}$. The horizontal solid (red) line shows the upper bound of the final asymptotic value of r as in Eq. (4.24). The Hubble rate at the start of reheating is $H_r \approx \sqrt{7 \times 10^{-2} W_0}$. The top panel shows the whole evolution from $N \sim 30$ since horizon-exit, whereas the bottom panel shows the reheating evolution.

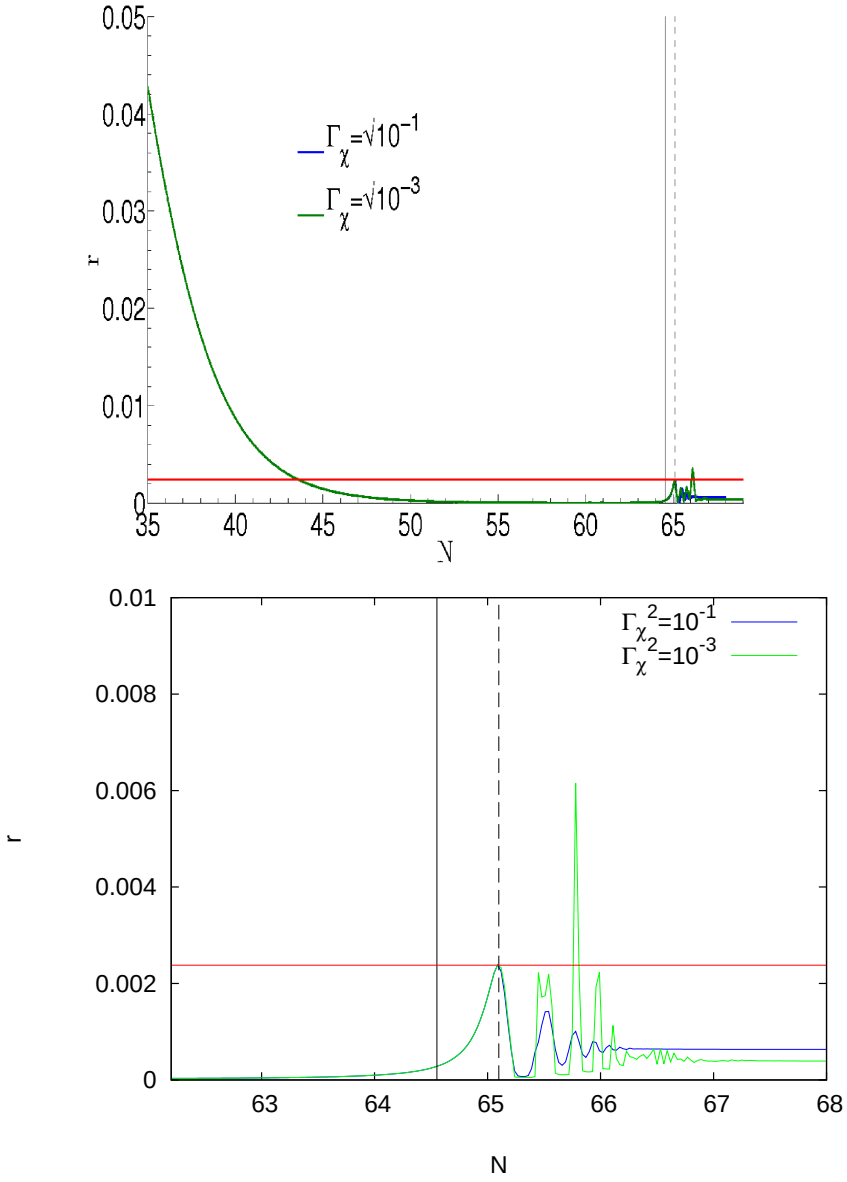

Figure 4.10: Potential: $W(\varphi,\chi) = W_0\chi^2 e^{-\lambda\varphi^2/M_{\rm P}^2}$. Evolution of r for two different decay rates Γ_χ, with $\lambda = 0.06$. The parameters used are: $\varphi_* = 10^{-3}M_{\rm P}$, $\chi_* = 16.0M_{\rm P}$, and Γ_χ is given in unit of $\sqrt{W_0}$. The solid vertical (black) line denotes the end of inflation, $N_{\rm e}$, and the dashed vertical (black) line denotes the start of reheating, $N_{\chi=0}$. The horizontal solid (red) line shows the upper bound of the final asymptotic value of r as in Eq. (4.24). The Hubble rate at the start of reheating is $H_r \approx \sqrt{7\times10^{-2}W_0}$. The top panel shows the whole evolution from $N \sim 30$ since horizon-exit, whereas the bottom panel shows the reheating evolution.

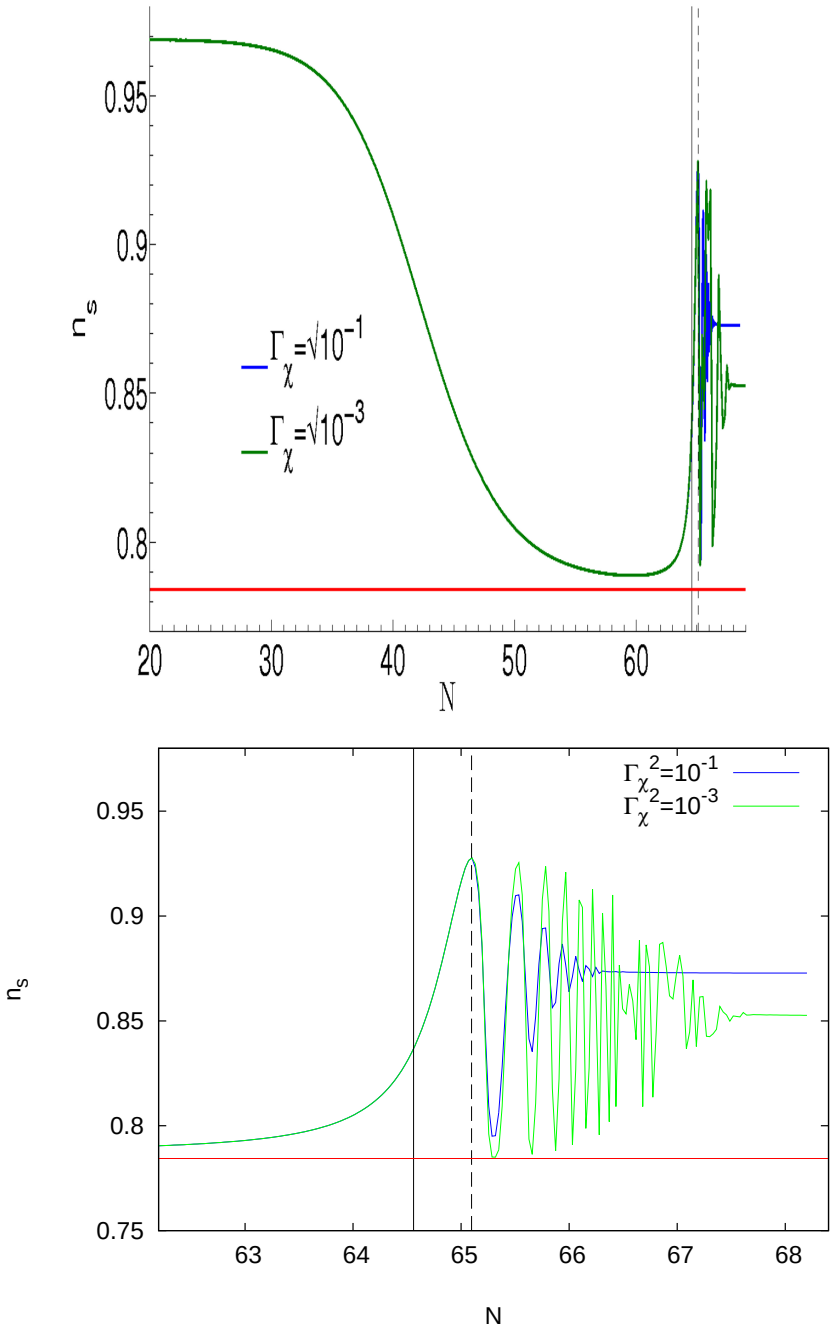

Figure 4.11: Potential: $W(\varphi,\chi) = W_0\chi^2 e^{-\lambda\varphi^2/M_{\rm p}^2}$. Evolution of $n_{\rm s}$ during for two decay rates, with $\lambda = 0.05$. The parameters used are: $\varphi_* = 10^{-3}M_{\rm p}$, $\chi_* = 16.0M_{\rm p}$, and the decay rates are given in unit of $\sqrt{W_0}$. The solid vertical (black) line denotes the end of inflation, $N_{\rm e}$, and the dashed vertical (black) line denotes the start of reheating, $N_{\chi=0}$. The horizontal solid (red) line shows the lowest bound of $n_{\rm s}$ as in Eq. (4.26). The Hubble rate at the start of reheating is $H_r \approx \sqrt{7\times10^{-2}W_0}$. The top panel shows the whole evolution from $N \sim 30$ since horizon-exit, whereas the bottom panel shows the reheating evolution.

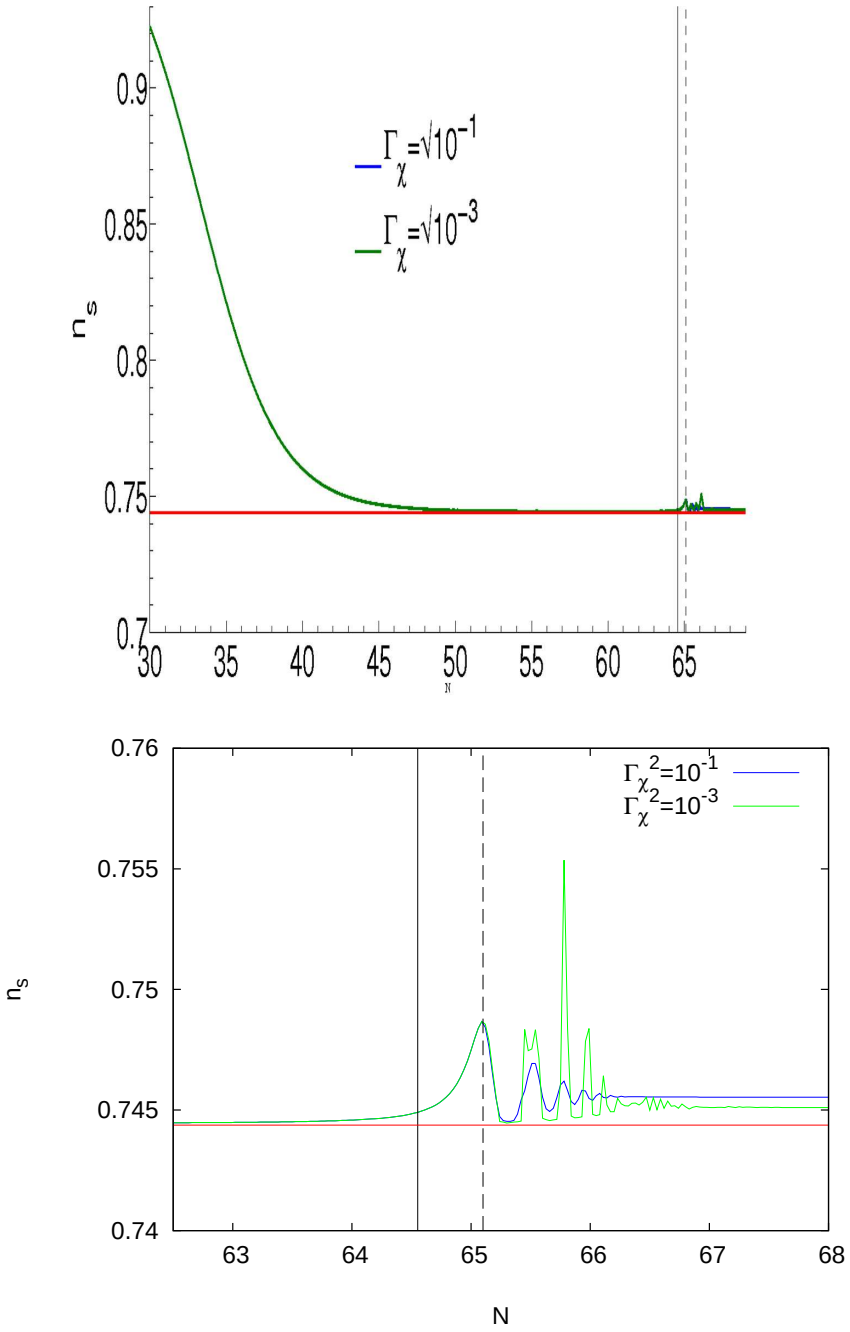

Figure 4.12: Potential: $W(\varphi, \chi) = W_0 \chi^2 e^{-\lambda\varphi^2/M_{\rm P}^2}$. Evolution of $n_{\rm s}$ during for two decay rates, with $\lambda = 0.06$. The parameters used are: $\varphi_* = 10^{-3} M_{\rm P}$, $\chi_* = 16.0 M_{\rm P}$, and the decay rates are given in unit of $\sqrt{W_0}$. The solid vertical (black) line denotes the end of inflation, $N_{\rm e}$, and the dashed vertical (black) line denotes the start of reheating, $N_{\chi=0}$. The horizontal solid (red) line shows the lowest bound of $n_{\rm s}$ as in Eq. (4.26). The Hubble rate at the start of reheating is $H_r \approx \sqrt{7 \times 10^{-2} W_0}$. The top panel shows the whole evolution from $N \sim 30$ since horizon-exit, whereas the bottom panel shows the reheating evolution.

A similar bound also exists for the spectral index. To see this, it is useful to consider the alternative expression of $n_{\rm s}$ Eq. (3.78) that involves only the first-order δN coefficients.

In this quadratic times exponential model, the slow-roll parameters η_{IJ} at horizon-exit are given by

$$(\eta_{\varphi\varphi})_* \approx -2\lambda M_{\rm p}^2\,,\ (\eta_{\varphi\chi})_* \approx -4\lambda M_{\rm p}^2 \left(\frac{\varphi}{\chi}\right)_*\,,\ (\eta_{\chi\chi})_* \approx M_{\rm p}^2 \left(\frac{2}{\chi^2}\right)_*\,. \tag{4.25}$$

As discussed earlier, for inflation to proceed, we typically have $\lambda\varphi^2/M_{\rm p}^2 \ll 1$. For sufficient observable inflation where $N_{\rm obs} > 50$, we also need $\chi_* \sim 15M_{\rm p}$. Therefore we can deduce $|(\eta_{\varphi\varphi})_*| \gg |(\eta_{\varphi\chi})_*|, |(\eta_{\varphi\varphi})_*|$ for $\varphi_* < O(1)$. As a result, the third term in the expression Eq. (3.78) is dominated by the $(\eta_{\varphi\varphi})_*$ term, as long as N_φ is not too small compared to N_χ. Given the magnitude of N_φ is monotonically increasing in time after the start of reheating, from Eq. (3.78) we can see the spectral index $n_{\rm s}$ is bounded from below if $(\eta_{\varphi\varphi})_*$ is negative

$$n_{\rm s} - 1 \approx -2(\epsilon_H)_* - \frac{1}{M_{\rm p}^2}\frac{2}{N_\varphi^2 + g_*^2} + \frac{2N_\varphi^2(\eta_{\varphi\varphi})_*}{N_\varphi^2 + g_*^2} \geq -(2\epsilon_H)_* - 4\lambda\,. \tag{4.26}$$

In addition, we see both r and $n_{\rm s}$ are very insensitive to Γ_χ and thus reheating for $\lambda = 0.06$, whereas they are much more sensitive for $\lambda = 0.05$. This dramatic change in behaviour for a small shift in λ can be explained from Eqs. (3.66) and (4.26) as $N_\varphi \gg N_\chi$ in the former case ($\lambda = 0.06$), but N_φ and N_χ are of the same order of magnitude in the latter case ($\lambda = 0.05$).

Models with Two Minima

In the last section, we have discussed the influence of reheating on the two-point statistics in two-field models where there exists a minimum in only one of the field directions. Next we consider two-field models where both fields are directly involved in reheating. An example we consider is the effective two-field description of axion N-flation. Note that in this model 'the start of reheating' can no longer be denoted by a single time instant, but rather two epoch $N_{\varphi=0}$ and $N_{\chi=0}$ corresponding to the times when the decay rates Γ_χ and Γ_φ are switched on [2].

[2]Note that unlike the single minimum case, the two 'start of reheating' surfaces $N_{\chi=0}$ and $N_{\varphi=0}$ are not identical for the same model parameters and initial conditions, but depend also on the decay rates Γ_χ and Γ_φ

Assisted inflation [98] may be realised via a collection of string axions. In this scenario, known as N–flation [99], the many axion fields *cooperatively* source inflation even if their potentials are individually too steep. The collective potential is comprised of a sum of N_f uncoupled axions φ_i:

$$W(\varphi) = \sum_{i=1}^{N_f} \Lambda_i^4 \left[1 - \cos\left(\frac{2\pi}{f_i}\varphi_i\right)\right] . \tag{4.27}$$

With only a single field present, this model is more commonly known as natural inflation [139]. Each axion is fully described by its decay constant f_i and its potential energy scale Λ_i^4. The standard arguments show that we should expect $f_i \sim 10^{16}\mathrm{GeV}$. The mass of each field in vacuum satisfies $m^2_{\varphi(i)} = 4\pi^2\Lambda_i^4/f_i^2$. Due to the shift symmetry $\varphi_i \to \varphi_i + 2\pi f_i$, we can without loss of generality set the initial conditions $\varphi_{*(i)} \in [0,\ f_i]$.

Follow from [106], supposing that the initial conditions are chosen so that only a single axion populates this hilltop region. This field sources the non–Gaussianity, whilst the remaining $N_f - 1$ axions, which begin far away from the hilltop, dominate over the energy density of the Universe. By expanding about the minimum of the remaining $N_f - 1$ fields, these axions may be replaced by a single effective field χ with a quadratic potential. With $f_i = f$ for all axions, the effective two–field potential then reads:

$$W(\varphi, \chi) = W_0 \left[\frac{1}{2}m^2\chi^2 + \Lambda^4\left(1 - \cos\left(\frac{2\pi}{f}\varphi\right)\right)\right] . \tag{4.28}$$

W_0 again sets the energy scale of the potential, but is dimensionless here. In fact, replacing the collective potential with an effective two-field potential is well motivated, see for example [140], where they showed that the energy density of the universe is dominated by fields with comparable masses even if one starts with thousands of fields, including the post-inflationary reheating stage. As the field ranges are sub-Planckian in the original picture Eq. (4.27), reheating in models of N-flation proceeds preferentially via a perturbative decay route as opposed to via parametric resonance and preheating [140, 141].

Amplitude of the Power Spectrum, A_ζ

In the effective two-field description of the axion N-flation model, inflation happens when the effective field χ is of super-Planckian value. From here onwards we will refer to φ as the axion and χ as the inflaton in this model. By suitably choosing the axion/inflaton mass ratio in vacuum, various scenarios can be realised. For example, if the axion is sufficiently massive it may quickly decay to its minimum during inflation, where it becomes trapped without oscillating. In this case, the adiabatic limit is established long before reheating begins, and the perturbative decay of the inflaton into radiation does not affect the evolution of ζ.

It is also possible to realise dynamics where both fields minimise after inflation has ended, entering an oscillating phase such that perturbative reheating can be applied. For example, with $\Lambda^4 = m^2 f^2/4\pi^2$, $\varphi_* = (\frac{1}{2} - 0.001)f$, $\chi_* = 16 M_{\rm p}$ and $f = m = M_{\rm p}$, the inflaton minimises before the axion, but both fields minimise after inflation has ended. In this example both fields acquire the same mass in vacuum. Since both fields oscillate rapidly about their minima, both fields must be coupled to radiation in order to recover a standard Big Bang radiation-dominated Universe. If one field is instead left uncoupled, its energy density will scale as matter since the minimum is quadratic, and will eventually come to dominate over radiation which redshifts away more quickly.

Here we are interested in the latter case where isocurvature perturbations persist during reheating. Again it is useful to inspect the evolution of the δN coefficients first. Similar to the one minimum case, N_χ remains very much constant over the entire evolution as long as there is a hierachy between the kinetic energies of the fields at horizon-exit, regardless of the decay rates Γ_χ and Γ_φ. As shown in Fig. 4.13, we see $N_\chi M_{\rm p} \approx (1/\sqrt{2\epsilon_\chi})_* \approx \chi_*/2$. However, the second order δN coefficient $N_{\chi\chi}$ is no longer constant and it does depend on the decay rates Γ_χ and Γ_φ here. On the other hand, while remaining subdominant during inflation, N_φ and $N_{\varphi\varphi}$ evolve significantly after horizon-exit. Comparing the second order δN coefficients, we see there is also a large hierachy between the magnitudes of $N_{\varphi\varphi}$, $N_{\chi\chi}$ and $N_{\varphi\chi}$. These are shown in Fig. 4.14. However, unlike the one minimum case where the Universe is reheated from only a single field, the φ field has left slow roll by the time reheating starts. Hence, the non–linear dynamics during the oscillating phase is essential and we could not find any

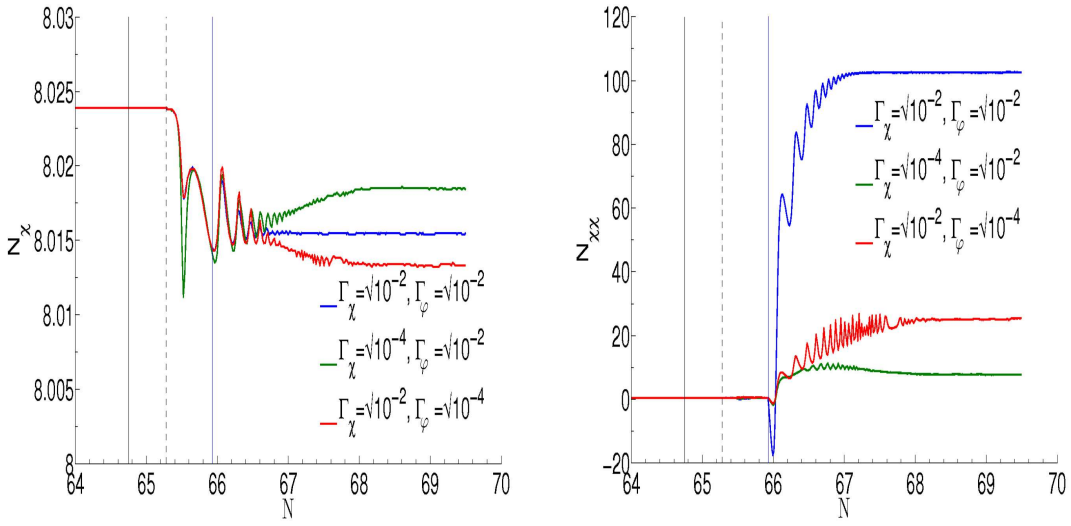

Figure 4.13: Potential: $W(\varphi,\chi) = W_0\left[\frac{1}{2}m^2\chi^2 + \Lambda^4\left(1-\cos\left(\frac{2\pi}{f}\varphi\right)\right)\right]$. Evolution of the δN coefficients N_χ (*left panel*) and $N_{\chi\chi}$ (*right panel*) in the effective 'two-field' N-flation model, both in Planckian units. All decay rates are given in unit of $\sqrt{W_0}M_{\rm p}$. The parameters used are: $\Lambda^4 = m^2f^2/4\pi^2$, $\varphi_* = (\frac{1}{2}-0.001)f$, $\chi_* = 16M_{\rm p}$, $f = m = M_{\rm p}$. The solid vertical (black) line denotes the end of inflation, $N_{\rm e}$, the dashed vertical (black) line denotes $N_{\varphi=0}$, and the solid vertical (blue) line denotes $N_{\chi=0}$. The background Hubble rates at the χ and φ reheating surfaces are $H_r^\chi \approx \sqrt{5\times10^{-2}W_0}M_{\rm p}$ and $H_r^\varphi \approx \sqrt{10^{-2}W_0}M_{\rm p}$ respectively.

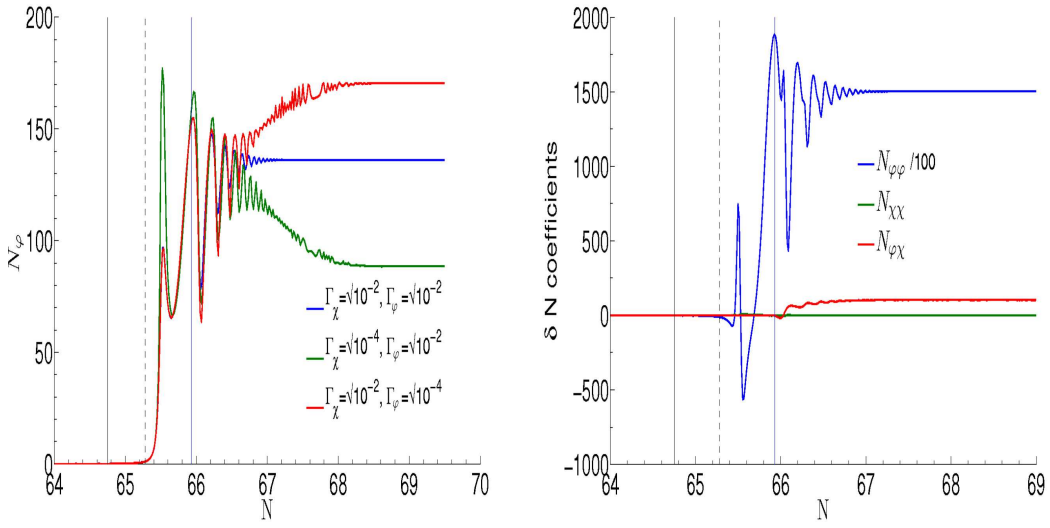

Figure 4.14: Potential: $W(\varphi,\chi) = W_0\left[\frac{1}{2}m^2\chi^2 + \Lambda^4\left(1-\cos\left(\frac{2\pi}{f}\varphi\right)\right)\right]$. *Left panel:* Evolution of the δN coefficients N_φ in the effective 'two-field' N-flation model. *Right panel:* Comparison of the second order δN coefficients in the effective 'two-field' N-flation model after inflation ends, with $\Gamma_\varphi = \Gamma_\chi = \sqrt{W_0/100}M_{\rm p}$. All decay rates are given in unit of $\sqrt{W_0}M_{\rm p}$. In both panels, the δN coefficients are given in unit of $M_{\rm p}$ and the parameters used are: $\Lambda^4 = m^2f^2/4\pi^2$, $\varphi_* = (\frac{1}{2}-0.001)f$, $\chi_* = 16M_{\rm p}$, $f = m = M_{\rm p}$. The solid vertical (black) line denotes the end of inflation, $N_{\rm e}$, the dashed vertical (black) line denotes $N_{\chi=0}$ and the solid vertical (blue) line denotes $N_{\varphi=0}$. The background Hubble rates at the χ and φ reheating surfaces are $H_r^\chi \approx \sqrt{5\times10^{-2}W_0}M_{\rm p}$ and $H_r^\varphi \approx \sqrt{10^{-2}W_0}M_{\rm p}$ respectively.

simple scaling relation between $N_{\varphi\varphi}$, $N_{\varphi\chi}$ and N_{φ}.

The evolution of the power spectrum amplitude A_ζ in this model is shown in Fig. 4.15. Again we see the amplitude A_ζ evolves after inflation ends, though it remains very much constant during slow-roll inflation. It oscillates and only becomes conserved after reheating is completed when the Universe becomes radiation dominated. The magnitude is always enhanced as compared to that at the end of inflation.

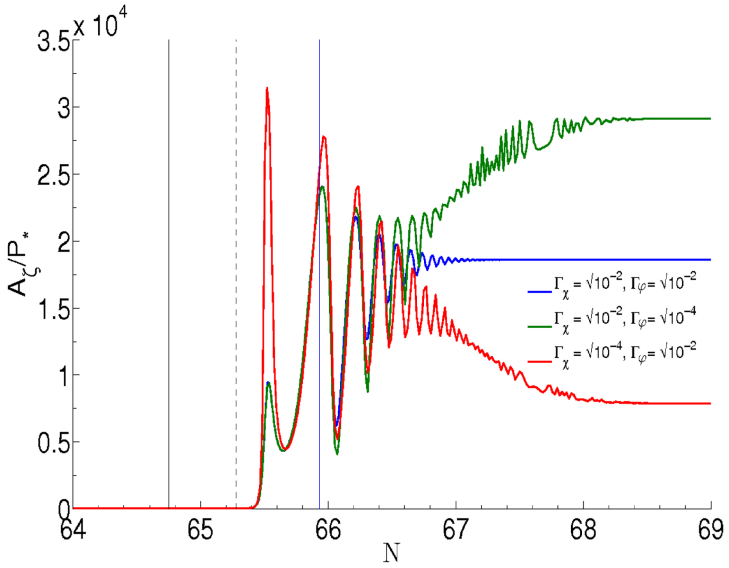

Figure 4.15: Potential: $W(\varphi,\chi) = W_0\left[\frac{1}{2}m^2\chi^2 + \Lambda^4\left(1-\cos\left(\frac{2\pi}{f}\varphi\right)\right)\right]$. Evolution of A_ζ/P_* in the effective 'two-field' N-flation model in unit of $M_{\rm p}$. The parameters used are: $\Lambda^4 = m^2f^2/4\pi^2$, $\varphi_* = (\frac{1}{2}-0.001)f$, $\chi_* = 16M_{\rm p}$, $f = m = M_{\rm p}$. All decay rates are given in unit of $\sqrt{W_0}M_{\rm p}$. The solid vertical (black) line denotes the end of inflation, $N_{\rm e}$, the dashed vertical (black) line denotes $N_{\chi=0}$ and the solid vertical (blue) line denotes $N_{\varphi=0}$. The background Hubble rates at the χ and φ reheating surfaces are $H_r^\chi \approx \sqrt{5\times10^{-2}W_0}M_{\rm p}$ and $H_r^\varphi \approx \sqrt{10^{-2}W_0}M_{\rm p}$ respectively.

Spectral Index $n_{\rm s}$ and Tensor-to-Scalar Ratio r

Similarly, the spectral index $n_{\rm s}$ and the tensor-to-scalar ratio r evolve during reheating, though they hardly evolve during inflation. Unlike the one minimum case where r remains very much negligible from the end of inflation until reheating completes for all decay rates, we see that r changes by three orders of magnitude during the post-inflationary evolution here as shown in Fig. 4.16. This can be understood from the evolution of N_φ. From Fig. 4.14, we see N_φ changes rapidly by a few orders of mag-

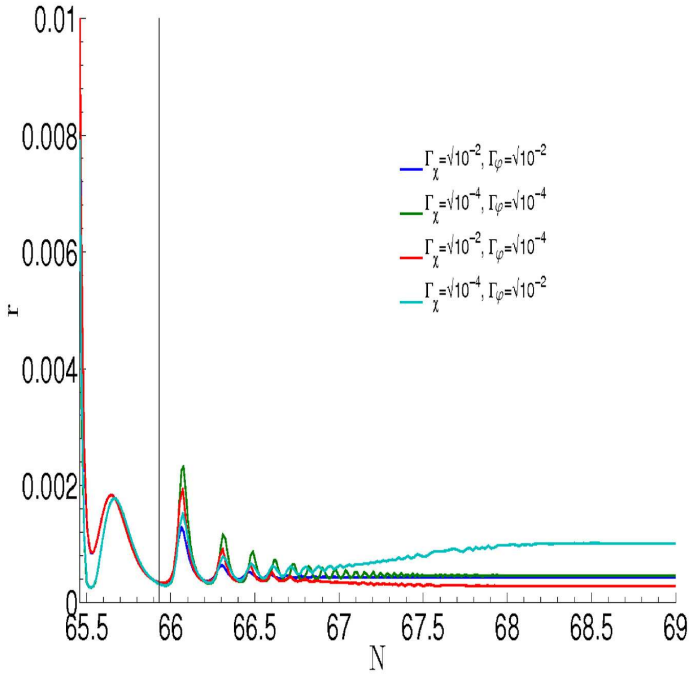

Figure 4.16: Potential: $W(\varphi,\chi) = W_0\left[\frac{1}{2}m^2\chi^2 + \Lambda^4\left(1-\cos\left(\frac{2\pi}{f}\varphi\right)\right)\right]$. Evolution of r in the effective 'two-field' N-flation model. The parameters used are: $\Lambda^4 = m^2f^2/4\pi^2$, $\varphi_* = (\frac{1}{2}-0.001)f$, $\chi_* = 16M_{\rm p}$, $f = m = M_{\rm p}$. All decay rates are given in unit of $\sqrt{W_0}M_{\rm p}$. Here the solid vertical (black) line denotes denotes the start of reheating, $N_{\varphi=0}$. The background Hubble rates at the χ and φ reheating surfaces are $H_r^\chi \approx \sqrt{5\times10^{-2}W_0}M_{\rm p}$ and $H_r^\varphi \approx \sqrt{10^{-2}W_0}M_{\rm p}$ respectively. Note r always decreases after inflation ends ($\epsilon_H = 1$).

nitude after inflation ends and dominates over N_χ. As a result, from Eq. (3.66), we can deduce that r is very suppressed after reheating ends as compared to that at the end of inflation.

On the other hand, compared to r, the spectral index $n_{\rm s}$, is very insensitive to reheating and its final value after reheating is close to that evaluated at inflation ends. This is shown in Table 4.2. We again use Eq. (3.78) to understand this. Since the potential W is sum-separable in this model, $\eta_{\varphi\chi}$ is exactly zero. Given χ dominates the potential W with $W \approx W_0m^2\chi^2/2$, the remaining η_{IJ} slow-roll parameters at horizon-exit are given by

$$(\eta_{\varphi\varphi})_* \approx M_{\rm p}^2\frac{\Lambda^4(4\pi^2)}{m^2f^2}\left[\frac{2\cos(2\pi\varphi_*/f)}{\chi_*^2}\right],\ (\eta_{\chi\chi})_* \approx M_{\rm p}^2\frac{2}{\chi_*^2}. \tag{4.29}$$

For initial conditions where φ starts off close to the ridge at horizon-exit, i.e. $\varphi_* \approx (f/2)$, we can see the two slow-roll parameters are approximately equal for the model

parameter $\Lambda^4(4\pi^2)/(m^2 f^2) = 1$. During the slow-roll regime, the subdominant axion φ is very much frozen and sits at the top of the ridge and we have $N_\chi \gg N_\varphi$. After inflation ends, φ starts rolling down the ridge and we have the opposite hierachy between the δN coefficients, $N_\varphi \gg N_\chi$. But since $(\eta_{\varphi\varphi})_* \approx -(\eta_{\chi\chi})_*$, in both limits the spectral index is approximated by

$$\begin{aligned} n_{\rm s} - 1 &\approx -2(\epsilon_H)_* - \frac{1}{M_{\rm p}^2}\frac{2}{N_\chi^2} + \frac{2N_\chi^2(\eta_{\chi\chi})_*}{N_\chi^2} = -\frac{8M_{\rm p}^2}{\chi_*^2} \quad \text{end of inflation, } N_\chi^2 \gg N_\varphi^2 \\ n_{\rm s} - 1 &\approx -2(\epsilon_H)_* - \frac{1}{M_{\rm p}^2}\frac{2}{N_\varphi^2} + \frac{2N_\varphi^2(\eta_{\varphi\varphi})_*}{N_\varphi^2} \approx -\frac{8M_{\rm p}^2}{\chi_*^2} \quad \text{end of reheating, } N_\varphi^2 \gg N_\chi^2 \end{aligned} \tag{4.30}$$

Here we have used the results $N_\chi^2 M_{\rm p}^2 \approx (1/\epsilon_\chi)_*$ and $(\epsilon_H)_* \approx (\epsilon_\chi)_*$. In the second line, the second term on the RHS can be dropped since it is very subdominant. As a result, we conclude that $n_{\rm s}$ hardly changes from inflation ends till reheating is completed for this choice of model parameters where $\Lambda^4(4\pi^2)/(m^2 f^2)$. For other parameter choices, it is possible that there is a stronger dependence on the reheating dynamics for $n_{\rm s}$.

4.3 Three-Point Statistics After Reheating, $f_{\rm NL}$

Next we consider the influence of reheating on the three-point statistics of ζ, particularly on the non-linear parameter $f_{\rm NL}$. Again we focus on the canonical two-field models discussed above, considering the one minimum and two minima case separately.

Model with One Minimum

Consider again the quadratic exponential model Eq. (4.17). Before moving on to discuss the influence of reheating on $f_{\rm NL}$, it is useful to revisit how $f_{\rm NL}$ evolves during inflation for the initial conditions we consider. For initial conditions close to the top of the ridge where $\varphi_* \sim 0$, during the slow-roll regime, the bundle of field trajectories always diverges as the fields roll away from the ridge, leading to negative values of $f_{\rm NL}$. An example of the slow-roll evolution of the non-linear parameter $f_{\rm NL}$ is given in

Fig. 4.17. In this model, as discussed in the last section, there is always a hierachy be-

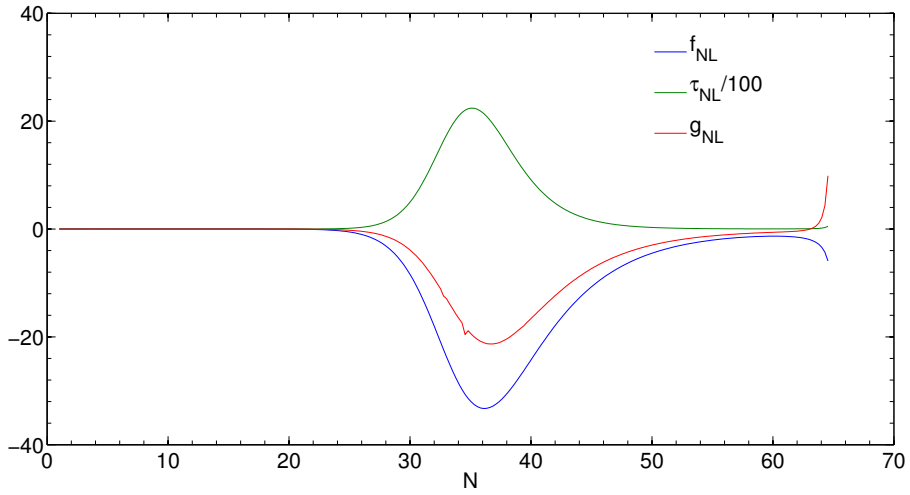

Figure 4.17: Potential: $W(\chi,\varphi) = W_0\chi^2 e^{-\lambda\varphi^2/M_{\rm P}^2}$, with $\lambda = 0.06$, $\varphi_* = 10^{-3}Mp$, $\chi_* = 16M_{\rm p}$. Evolution of the non-linear parameters $f_{\rm NL}$, $\tau_{\rm NL}$, $g_{\rm NL}$ during inflation, evaluated numerically, are shown here. Here we terminate when $\epsilon_H = 1$.

tween the magnitudes of the second order δN coefficients, i.e. $|N_{\varphi\varphi}| \gg |N_{\varphi\chi}|, |N_{\chi\chi}|$ for the model parameter space we consider. Therefore, the non-linear parameter $f_{\rm NL}$ can be well approximated by

$$f_{\rm NL} \approx \frac{5}{6}\frac{N_\varphi^2 N_{\varphi\varphi}}{(N_\varphi^2 + N_\chi^2)^2}\,, \tag{4.31}$$

This were shown in the slow-roll regime in [106]. We now move on to discuss the dependence of $f_{\rm NL}^{\rm final}$ on Γ_χ, keeping the same parameter choice $\lambda = \{0.05, 0.06\}$, $\varphi_* = 10^{-3}M_{\rm p}$ and $\chi_* = 16.0M_{\rm p}$. In the top panel of Fig. 4.18 we show the final stages in the evolution of $f_{\rm NL}$ as a function of N for various decay rate Γ_χ. Most importantly, we see that reheating does *not* damp out $f_{\rm NL}$ to zero. We interpret the finer details of the plot as follows: At the end of inflation ($N_{\rm e} = 64.56$) a large, negative $f_{\rm NL}$ is still present, and just before reheating begins ($N_{\chi=0} = 65.10$) $f_{\rm NL}$ is growing increasingly more negative. We see that as the decay rate Γ_χ is increased from zero, $|f_{\rm NL}^{\rm final}|$ freezes out to larger values. In another example $\lambda = 0.05$ where $f_{\rm NL}$ is decaying toward zero as reheating begins, the effect of increasing the decay rate from zero is to freeze out $|f_{\rm NL}^{\rm final}|$ to smaller values. This is shown in the bottom panel of Fig. 4.18.

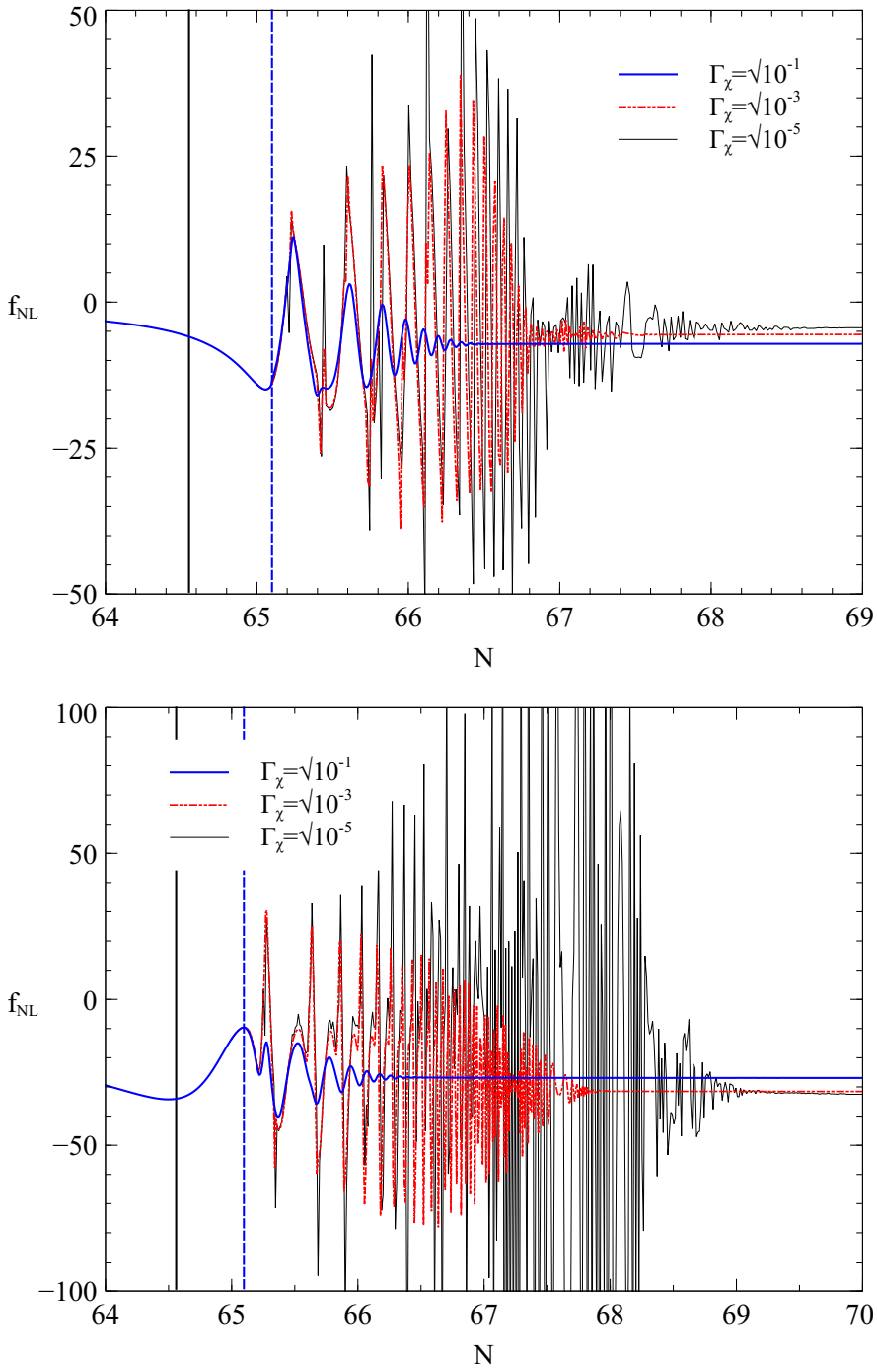

Figure 4.18: Potential: $W(\varphi, \chi) = W_0 \chi^2 e^{-\lambda\varphi^2}$. We show the evolution of $f_{\rm NL}$ during reheating for various decay rates Γ_χ, which are in units of $\sqrt{W_0}$. In both panels, the solid vertical (black) line denotes the end of inflation, $N_{\rm e}$, and the dashed vertical (blue) line denotes the start of reheating, $N_{\rm r}$. *Top Panel*: The parameters used are: $\lambda = 0.06$, $\varphi_* = 10^{-3} M_{\rm p}$ and $\chi_* = 16.0 M_{\rm p}$. The Hubble rate at the start of reheating is $H_r \approx \sqrt{7 \times 10^{-2} W_0}$. *Bottom Panel*: The parameters used are: $\lambda = 0.05$, $\varphi_* = 10^{-3} M_{\rm p}$ and $\chi_* = 16.0 M_{\rm p}$. The Hubble rate at the start of reheating is $H_r \approx \sqrt{6 \times 10^{-2} W_0}$.

This opposite dependence of $|f_{\rm NL}^{\rm final}|$ on Γ_χ for $\lambda = 0.05$ and $\lambda = 0.06$ is a consequence

of the non–trivial dependence of $f_{\rm NL}$ on N_φ. Let us begin by considering the splitting

$$N = \int_{H_*}^{H_c} \frac{H}{\dot{H}} \mathrm{d}H = \int_{H_*}^{H_r} \frac{H}{\dot{H}} \mathrm{d}H + \int_{H_r}^{H_c} \frac{H}{\dot{H}} \mathrm{d}H = N_0 + N_1 \,. \tag{4.32}$$

Here N_0 is the number of e–foldings from horizon crossing (t_*) up to the start of reheating ($T_{\rm R}$, when χ first passes the minimum $\chi = 0$) and N_1 is the number of e–foldings from the start of reheating up to radiation domination (t_c). Firstly, it is important to appreciate that N_0 contains contributions not only from the slow roll inflationary phase, but also from the non–negligible post–inflation/pre–reheating evolution, that must be accounted for. Unlike the slow-roll contributions, these post–inflation/pre–reheating contributions cannot be computed analytically. Secondly, N_0 does not contain any dependence on the reheating process. Since we are interested here in studying the effects of reheating on $f_{\rm NL}^{\rm final}$, we compute N_0 and its derivatives numerically and focus on trying to understand the correction N_1, which contains all the dependence on Γ_χ.

For the derivative of the correction N_1 with respect to φ_* we need only consider the term

$$N_{1,\varphi_*} = \int_{H_r}^{H_c} \frac{\partial}{\partial \varphi_*} \left(\frac{1}{\dot{H}} \right)_H H \mathrm{d}H \,, \tag{4.33}$$

since the derivative at the boundary at r cancels with the N_0 contribution and the derivative at the boundary c vanishes since c is defined as a surface of constant H. Since $\dot{H}$ is a function of $\dot{\chi}(t)$, $\dot{\varphi}(t)$ and $\rho_\gamma(t)$, all of which depend on φ_*, this integral cannot be performed analytically beyond slow roll. However, we can make progress by using our results in Section 4.2, $N_\chi M_{\rm p} \approx (2\epsilon_\chi)_*^{-1/2}$, $\{N_{\varphi\chi}\,,\, N_{\chi\chi}\} \ll N_{\varphi\varphi}$ and $N_{\varphi\varphi} \sim N_\varphi/\varphi_*$ which also hold during reheating. Then, using the observation that during reheating $N_{1,\chi_*} \approx 0$, and taking the time t_c to be deep in the radiation dominated era such that $N_{1,\varphi_*} = \mathrm{const}$, Eq. (4.31) becomes

$$f_{\rm NL}^{\rm final} \approx \frac{5}{6|\varphi_*|} \frac{(N_{0,\varphi_*} + N_{1,\varphi_*})^3}{[(N_{0,\varphi_*} + N_{1,\varphi_*})^2 + g_*^2]^2} \,. \tag{4.34}$$

Here again $g_* \equiv M_{\rm p}^{-1} N_\chi \approx (2\epsilon_\chi)_*^{-1/2}$. We plot this *algebraic* function, $f_{\rm NL}^{\rm final}$ against N_{1,φ_*}, in the top panel of Fig. 4.19 for three different choices of the potential parameter $\lambda = \{0.05\,, 0.06\,, 0.07\}$, with the same field values at horizon crossing $\varphi_* = 10^{-3} M_{\rm p}$

and $\chi_* = 16.0 M_{\rm p}$. Varying λ changes g_* and modifies the evolution of the bundle, and thus N_{0,φ_*}. In the bottom panel of Fig. 4.19 we show the evolution of N_φ for various decay rates with $\lambda = 0.05$. The final values of $N_{1,\varphi}(\text{final}) = N_\varphi(\text{final}) - N_{0,\varphi_*}$ are marked on the corresponding curve in the top panel of Fig. 4.19. Only the $N_{1,\varphi_*} \leq 0$ region of Eq. (4.34) is physical: we argue that diverging trajectories can only generate negative N_{1,φ_*}, which can be confirmed numerically. As can be seen from the top panel of Fig. 4.19, Eq. (4.34) has three stationary points at finite N_{1,φ_*}:

$$-N_{0,\varphi_*}\,, \quad -N_{0,\varphi_*} \pm \sqrt{3} g_*\,. \tag{4.35}$$

The $N_{1,\varphi_*} = -N_{0,\varphi_*}$ root is an inflection point where $f_{\rm NL}^{\rm final} = 0$. The $N_{1,\varphi_*} = -N_{0,\varphi_*} + \sqrt{3} g_*$ root is a local maximum where $f_{\rm NL}^{\rm final}$ would be always positive and so is not physical. The minimum at $N_{1,\varphi_*} = -N_{0,\varphi_*} - \sqrt{3} g_*$ however is physical and bounds the maximum value of $|f_{\rm NL}^{\rm final}|$ when Eq. (4.34) has a minimum at negative N_{1,φ_*}:

$$|f_{\rm NL}^{\rm final}|_{\rm max} \approx \frac{1}{|g_* \varphi_*|} \sqrt{\frac{75}{1024}}\,, \quad \text{for} \quad N_{0,\varphi_*} + \sqrt{3} g_* > 0\,. \tag{4.36}$$

For instance in the case $\lambda = 0.05$ as seen in the top panel of Fig. 4.19. If on the other hand, the minimum exists at positive N_{1,φ_*}, (i.e., $N_{0,\varphi_*} + \sqrt{3} g_* < 0$) then the maximum value of $|f_{\rm NL}^{\rm final}|$ is instead bounded by its value at the start of reheating:

$$|f_{\rm NL}^{\rm final}|_{\rm max} \approx |f_{\rm NL}(t_r)| \approx \frac{5}{6|\varphi_*|} \frac{N_{0,\varphi_*}^2}{[N_{0,\varphi_*}^2 + g_*^2]^2}\,, \quad \text{for} \quad N_{0,\varphi_*} + \sqrt{3} g_* < 0\,. \tag{4.37}$$

This is the case for the $\lambda = 0.06$ and $\lambda = 0.07$ models shown in the top panel of Fig. 4.19. These bounds are independent of the decay rate Γ_χ. Furthermore, the bound Eq. (4.36) is written solely in terms of quantities evaluated at horizon crossing, and hence may be computed without explicitly knowing the full non–linear evolution of the bundle during the reheating process. Whether this maximum value, $|f_{\rm NL}^{\rm final}|_{\rm max}$, is obtained at the end of reheating is of course dependent on Γ_χ.

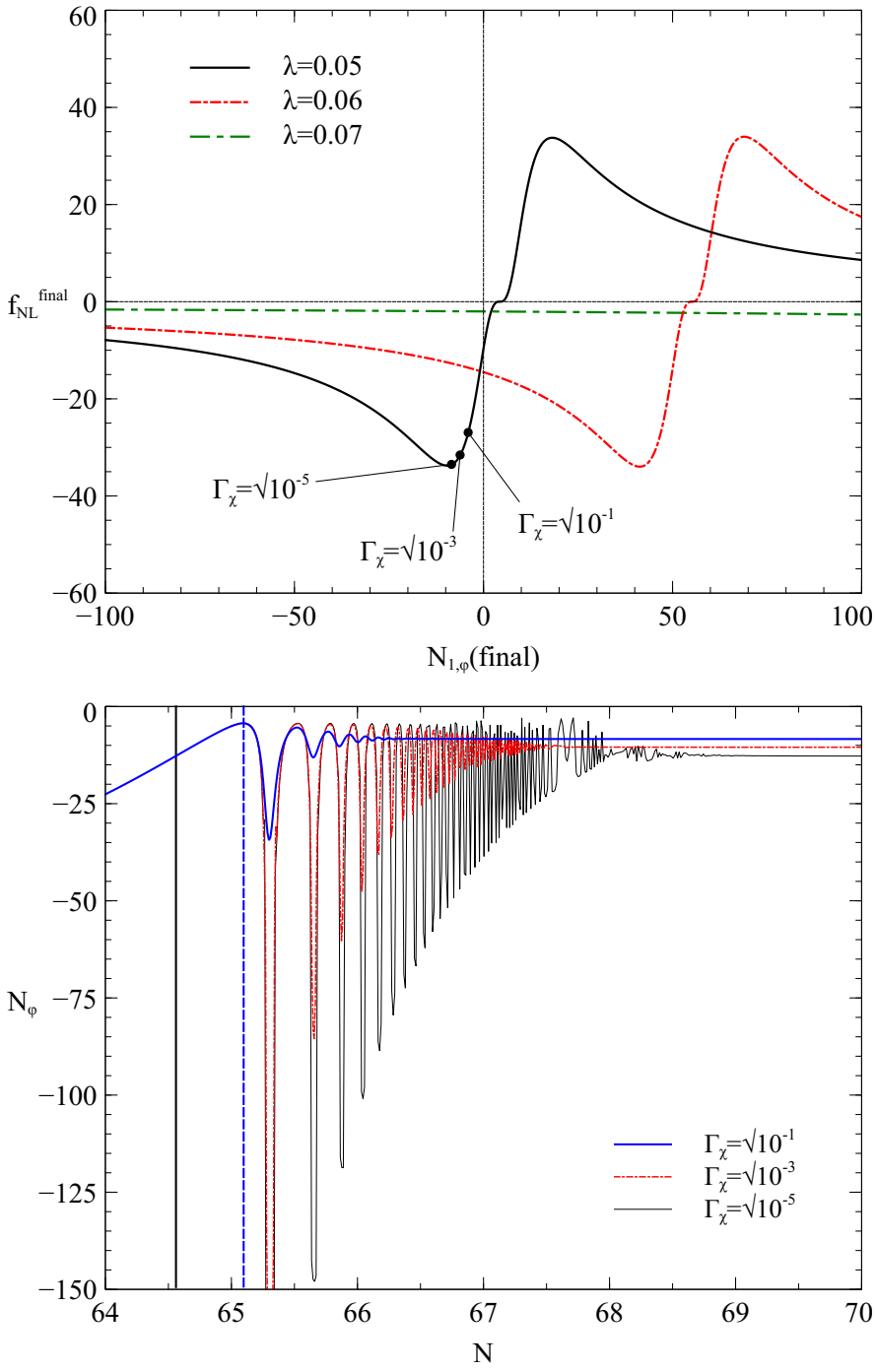

Figure 4.19: Potential: $W(\varphi,\chi) = W_0\chi^2 e^{-\lambda\varphi^2/M_{\rm p}^2}$. *Top Panel*: The algebraic function $f_{\rm NL}^{\rm final}$ as a function of the final value of the correction N_{1,φ_*}, Eq. (4.34). We label the positions along the $\lambda = 0.05$ curve which correspond to the decay rates given in the right panel. *Bottom Panel*: The evolution of the derivative $N_\varphi = N_{0,\varphi_*} + N_{1,\varphi_*}$ for the same decay rates as Fig. 4.18, for $\lambda = 0.05$. All decay rates are in units of $\sqrt{W_0}$. The solid vertical (black) line denotes the end of inflation, $N_{\rm e}$, and the dashed vertical (blue) line denotes the start of reheating, $N_{\chi=0}$. The Hubble rate at the start of reheating is $H_r \approx \sqrt{7\times 10^{-2} W_0}$.

The existence of a minimum of Eq. (4.34) at negative N_{1,φ_*} for $\lambda = 0.05$ explains

the seemingly opposite dependence of $f_{\rm NL}^{\rm final}$ on Γ_χ: for the $\lambda = 0.05$ model, as Γ_χ is increased further, φ freezes out sooner, driving N_{1,φ_*} toward zero. The minimum of Eq. (4.34) is encountered, past which point $|f_{\rm NL}^{\rm final}|$ is reduced. For $\lambda = 0.06$, increasing Γ_χ still drives N_{1,φ_*} toward zero, but this time $|f_{\rm NL}^{\rm final}|$ is increased as no extreme point exists for negative N_{1,φ_*}.

For $\lambda = 0.07$, the function Eq. (4.34) is almost completely flat for $N_{1,\varphi_*} < 0$, which indicates that no matter how slowly or rapidly the universe is reheated, the value of $f_{\rm NL}$ at the start of reheating will survive until completion. In the limit of instantaneous reheating, $\Gamma_\chi \to \infty$, $N_{1,\varphi_*} \approx 0$, and so $f_{\rm NL}^{\rm final} \approx f_{\rm NL}(T_{\rm R})$. This is only approximate since, as reheating does not begin on a hypersurface of constant density, there will be some small correction N_{1,φ_*}.

Another interesting observation is that $|f_{\rm NL}^{\rm final}|$ (or more accurately the derivative N_{1,φ_*}) is fairly insensitive to changing the decay rate by many orders of magnitude. For example, as can be seen from Table 4.1, $|f_{\rm NL}^{\rm final}|$ changes by less than $O(3)$ as the decay rate is increased from $\Gamma_\chi = \sqrt{10^{-5} W_0}$ to $\Gamma_\chi = \sqrt{10^{-1} W_0}$. We caution here that the decay rate could, in principle, be many orders of magnitude weaker than the weakest decay rate studied here and still be consistent with the bound derived from BBN constraints, $\Gamma_\chi \gtrsim 4 \times 10^{-40} M_{\rm p}$. These tiny (but non–zero) values of Γ_χ are beyond our numerical capabilities: to compute the statistics of ζ at the completion of reheating requires integrating the field equations up until the universe is radiation dominated, which for such weak rates, can take $\mathcal{O}(30)$ e–folds. Substantial errors are accumulated if the field equations are integrated over such long periods of time, which in turn induces large errors in the computation of the δN derivatives. For this reason, we only quote values of $f_{\rm NL}$, $n_{\rm s}$ and r for decay rates for which we are confident that we have control over all sources of numerical error. However we believe the physics describing here is valid in the other regimes as well.

The overall results for two and three-point statistics of ζ in this model are summarised in the following Table 4.1. We see model predictions evaluated at the end of inflation are in general different from that after reheating, verifying the importance of taking the subsequent post-inflationary evolution into account when comparing model predictions

to observations. [3]

$\lambda = 0.06$: $f_{\rm NL}(t_e) = -5.93$, $n_{\rm s}(t_e) = 0.763$, $r(t_e) = 2.8 \times 10^{-4}$

Γ_χ	$f_{\rm NL}^{\rm final}$	$n_s^{\rm final}$	$r^{\rm final}$
$\sqrt{10^{-5}}$	-4.35	0.761	2.4×10^{-4}
$\sqrt{10^{-3}}$	-5.54	0.762	3.9×10^{-4}
$\sqrt{10^{-1}}$	-7.14	0.762	6.3×10^{-4}

$\lambda = 0.05$: $f_{\rm NL}(t_e) = -34.10$, $n_s(t_e) = 0.836$, $r(t_e) = 0.035$

Γ_χ	$f_{\rm NL}^{\rm final}$	$n_s^{\rm final}$	$r^{\rm final}$
$\sqrt{10^{-5}}$	-33.4	0.837	3.5×10^{-2}
$\sqrt{10^{-3}}$	-31.5	0.853	4.6×10^{-2}
$\sqrt{10^{-1}}$	-26.9	0.873	6.0×10^{-2}

Table 4.1: Statistics of ζ for $W(\varphi, \chi) = W_0 \chi^2 e^{-\lambda\varphi^2/M_{\rm P}^2}$ for different decay rates. All decay rates are in units of $\sqrt{W_0}$. We give values computed at the end of inflation (t_e) and at the completion of reheating (final) where ζ is conserved. The model parameters are $\varphi_* = 10^{-3} M_{\rm P}$ and $\chi_* = 16.0 M_{\rm P}$. *Left Table*: $\lambda = 0.06$; *Right Table*: $\lambda = 0.05$.

For completeness, we also plot the final asymptotic values of the observables at the end of reheating as a function of the decay rate Γ_χ for different λ in Fig. 4.20. From the plots, we can see how sensitive the observables are to reheating depends also upon λ in this model.

Models with Two Minima

Next we consider the case where both fields are directly involved in reheating, again taking the effective two-field description of the N-flation model Eq. (4.28) as an example. During slow-roll inflation, it was found that $f_{\rm NL}$ is dominated by the following term in the case where adiabaticity is reached before inflation ends [106]:

$$f_{\rm NL} \approx \frac{5}{6} \frac{N_{\varphi\varphi}}{N_\varphi^2} \,. \tag{4.38}$$

Although there is no scaling relations between the δN coefficients in this model, we find that Eq. (4.38) remains a good approximation beyond slow-roll for the model parameter space considered where both fields minimise after inflation ends. As can be seen from the left panel of Fig. 4.21, $f_{\rm NL}^{\rm final}$ is almost completely insensitive to reheating when $\Gamma_\chi \sim \Gamma_\varphi$. However, as can be seen from the right panel, a mild hierarchy

[3] We stress here we only consider the model as a toy model since the model predictions are inconsistent with current observations.

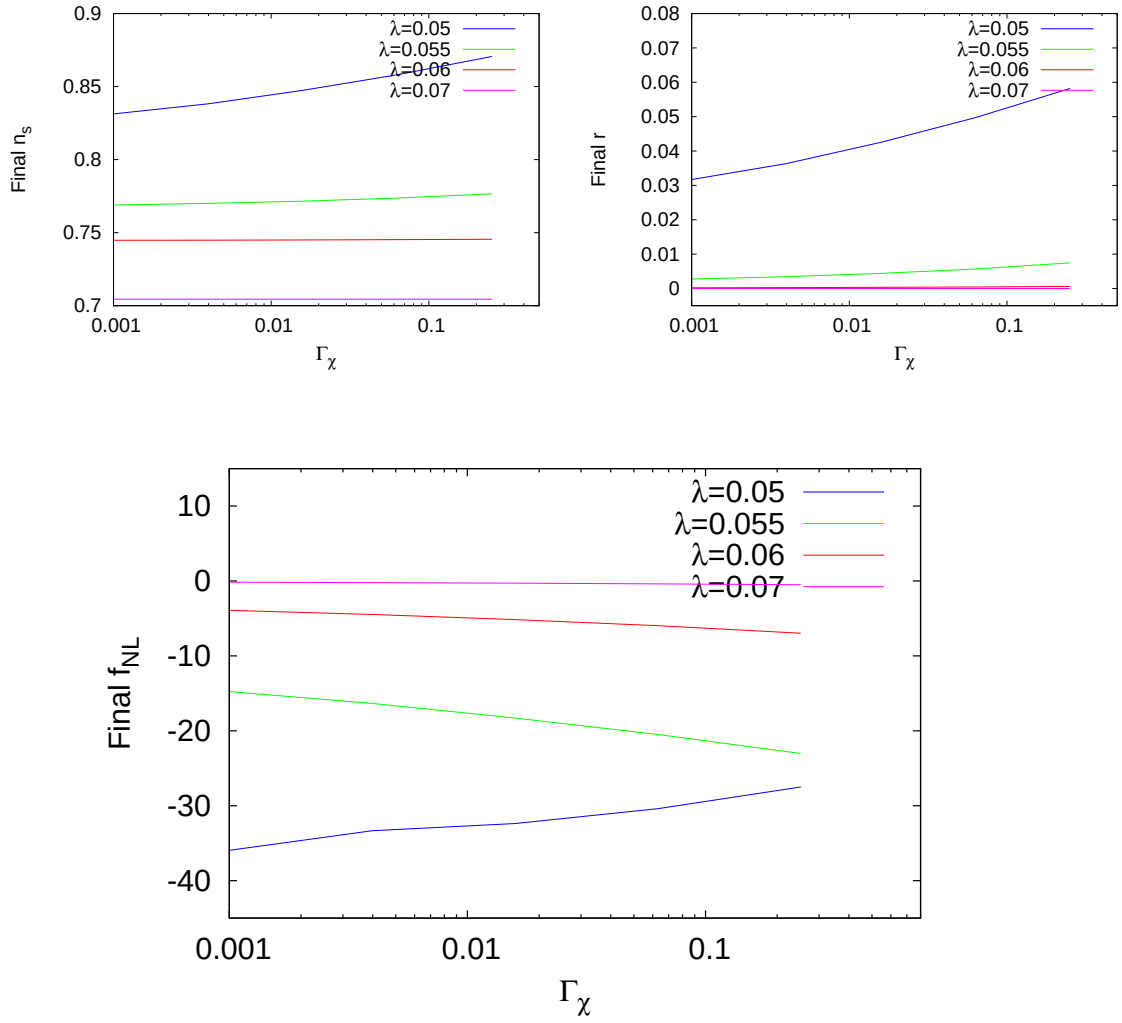

Figure 4.20: $W(\varphi,\chi) = W_0\chi^2 e^{-\lambda\varphi^2/M_{\rm p}^2}$. The final asymptotic values of $n_{\rm s}$ (*top left panel*), r (*top right panel*) and $f_{\rm NL}$ (*bottom panel*) at the end of reheating as a function of the decay rate Γ_χ for four different λ. The initial field values are $\varphi_* = 10^{-3}M_{\rm p}$ and $\chi_* = 16.0M_{\rm p}$.

between Γ_χ and Γ_φ generates significant corrections to to $f_{\rm NL}^{\rm final}$. This effect is *not* due to the axion reheating hypersurface being distinctly separated from the inflaton surface (the vertical dotted (red) and dashed (blue) lines of Fig. 4.21 respectively) and we have confirmed this numerically. What is important however, is the axion/inflation mass ratio in vacuum. The model parameters which realise the dynamics seen in Fig. 4.21 give $m_\varphi = m_\chi$ at the minimum. The differences induced in $f_{\rm NL}^{\rm final}$ when a mild hierarchy exists between Γ_χ and Γ_φ is greatest when the masses are equal. As the masses are separated, keeping the ratio $\Gamma_\chi/\Gamma_\varphi$ fixed, the sensitivity of $f_{\rm NL}^{\rm final}$ to reheating decreases. This can be understood as follows: first consider the situation where the two fields have different masses, for instance, $m_\chi > m_\varphi$. Assuming both fields reheat at roughly the same time, the more massive field χ will dominate the energy density and

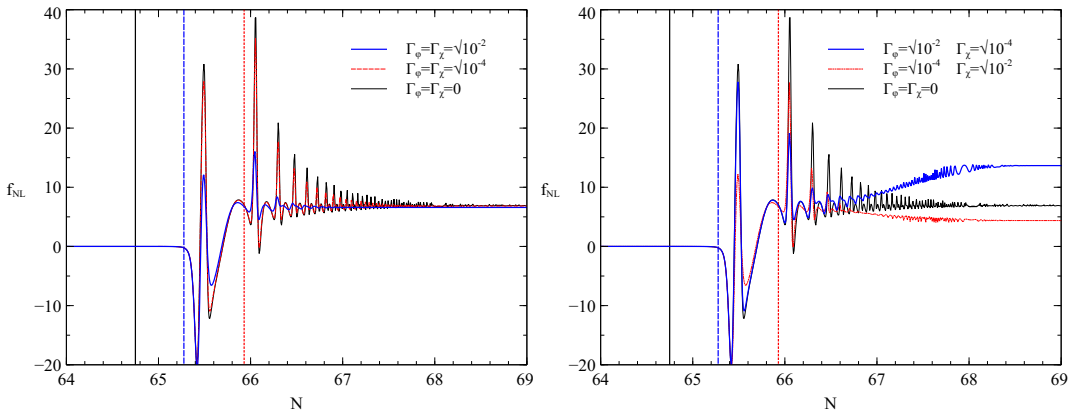

Figure 4.21: $W(\varphi,\chi) = W_0\left[\frac{1}{2}m^2\chi^2 + \Lambda^4\left(1-\cos\left(\frac{2\pi}{f}\varphi\right)\right)\right]$. The parameters used are: $\Lambda^4 = m^2f^2/4\pi^2$, $\varphi_* = (\frac{1}{2}-0.001)f$, $\chi_* = 16M_{\rm p}$, $f = m = M_{\rm p}$. Both panels show the evolution of $f_{\rm NL}$ during reheating. *Left Panel*: Equal decay rates, $\Gamma_\chi = \Gamma_\varphi \neq 0$. For comparison we also show the $\Gamma_\chi = \Gamma_\varphi = 0$ limit (thin black line). *Right Panel*: Unequal decay rates, $\Gamma_\chi \neq \Gamma_\varphi \neq 0$. For comparison we also show the $\Gamma_\chi = \Gamma_\varphi = 0$ limit (thin black line). All decay rates are given in unit of $\sqrt{W_0}M_{\rm p}$. In both panels, the solid vertical (black) line denotes the end of inflation, $N_{\rm e}$, the dashed vertical (blue) line denotes the start of χ reheating and the dotted vertical (red) line denotes the start of φ reheating. The background Hubble rates at the χ and φ reheating surfaces are $H_r^\chi \approx \sqrt{5\times10^{-2}W_0}M_{\rm p}$ and $H_r^\varphi \approx \sqrt{10^{-2}W_0}M_{\rm p}$ respectively.

thus the dynamics of the universe during reheating. Evaluating on constant energy hypersurfaces, the initial horizon crossing dependence of the χ field dynamics is smaller compared to the case $m_\chi = m_\varphi$, where the energy density of the universe is distributed evenly between the fields. As a result, we expect the number of e–folds of expansion N and $f_{\rm NL}^{\rm final}$ are less sensitive in the case $m_\chi \neq m_\varphi$.

In fact, having the two fields decay at different rates is a form of modulated reheating, although it is different from the standard scenario [142, 143, 144, 145, 146]. In the standard modulated reheating scenario, inflation is driven by a single field, whose decay rate is modulated by a second, subdominant field that remains light and plays a negligible role during inflation. The fluctuation of the subdominant field induces fluctuations in the inflaton decay rate and thus generates the curvature perturbation during reheating. In the two-minima case here, note that the initial horizon crossing values of the fields φ_*, χ_* determine how the energy density of the universe is distributed between the two scalar fields. Therefore, although the field decay rates are constant here, the rate of energy transfer from the scalar fields to the radiation fluid can be different for each inflationary trajectory in the bundle and thus can generate an extra contribution to the curvature perturbation, provided there is a mild hierarchy in the decay rates. Therefore it is not surprising that $f_{\rm NL}$ can acquire such a significant

correction during reheating when the two decay rates are different. The two-minima scenario is also similar in spirit to a model of two field inflation with equal masses followed by instant preheating, in which the two fields have very different couplings to the preheat field [147], for a related scenario see also [148]. Note however that all of these instant preheating models are very tightly constrained even at the level of linear perturbations [149].

Recently, by modelling the fields as two effective matter fluids and applying the sudden decay approximation, Tarrant and Meyers have derived analytical expressions for $f_{\rm NL}^{\rm local}$, $n_{\rm s}$ and r, verifying the qualitative behaviour in this model [134]. This fluid approximation approach was later generalised to arbitrary sum-separable potentials and other models like inhomogeneous end of inflation and generalised curvaton scenarios by Elliston et al. [135]. They have also demostrated that the behaviour can be explained by considering the relative redshifting of the two effective scalar field fluids.

Again we summarise the overall results in Table 4.2. Depending on the physics of reheating, we see that the final value of the non-linear parameter $f_{\rm NL}$ can be quite different for different decay rates Γ_χ and Γ_φ, whereas r and $n_{\rm s}$ are much less sensitive in this model compared to the 'runaway' type quadratic exponential model. Notice also the dramatic decrease in r after the end of inflation.

χ^2 minimum: $f_{\rm NL}(t_e) \approx 0$,
$n_s(t_e) = 0.969, r(t_e) = 0.124$

Γ_φ	Γ_χ	$f_{\rm NL}^{\rm final}$	$n_s^{\rm final}$	$r^{\rm final}$
0	0	6.88	0.935	4.6×10^{-4}
$\sqrt{10^{-2}}$	$\sqrt{10^{-2}}$	6.59	0.969	4.3×10^{-4}
$\sqrt{10^{-4}}$	$\sqrt{10^{-4}}$	6.83	0.969	4.6×10^{-4}
$\sqrt{10^{-2}}$	$\sqrt{10^{-4}}$	13.66	0.969	1.0×10^{-3}
$\sqrt{10^{-4}}$	$\sqrt{10^{-2}}$	4.37	0.969	2.7×10^{-4}

Table 4.2: Statistics of ζ for $W(\varphi,\chi) = W_0\left[\frac{1}{2}m^2\chi^2 + \Lambda^4\left(1-\cos\left(\frac{2\pi}{f}\varphi\right)\right)\right]$ for different decay rates. All decay rates are in units of $\sqrt{W_0}M_{\rm p}$. We give values computed at the end of inflation (t_e) and at the completion of reheating (final) where ζ is conserved. The model parameters are $\Lambda^4 = m^2f^2/4\pi^2$, $\varphi_* = (\frac{1}{2}-0.001)f$, $\chi_* = 16M_{\rm p}$, $f = m = M_{\rm p}$. Notice the very large decrease in the tensor–to–scalar ratio r from the end of inflation to its final value.

4.4 Quadratic vs Quartic Potentials

In the previous sections, we have illustrated the influence of reheating on two and three-point statistics of ζ in multifield models where the reheating fields oscillate about some quadratic potentials. Here we consider the case where the reheating fields now oscillate about a quartic potential instead. While the oscillatory dynamics of the fields are different, we will see similar qualitative behaviour as in the previous models with quadratic potentials, which again can be explained using the analytic approach as in [135].

Models with One Minimum

Again we take the runaway type model Eq. (4.17) as an example of the one minimum case, but now with a quartic minimum in the χ direction. The potential now reads as

$$W(\varphi, \chi) = W_0 \chi^4 e^{-\lambda\varphi^2/M_{\rm p}^2} \tag{4.39}$$

The background inflationary dynamics are similar to the $\chi^2 e^{-\lambda\varphi^2}$ model as can be seen from the slow-roll solutions to the Klein-Gordon field equations:

$$\chi^2 = \chi_*^2 - 8NM_{\rm p}^2\,, \qquad \varphi = \varphi_* e^{2\lambda N}\,. \tag{4.40}$$

The oscillatory dynamics about the minimum are somewhat different to that of the χ^2 case however, due to the potential being much shallower around $\chi = 0$. This is described by the solution Eq. (4.3).

Provided λ is not too large, the φ field remains slowly rolling throughout the entire reheating phase. In the left and right panels of Fig. 4.22 we show the final stages in the evolution of $f_{\rm NL}$ and N_φ respectively as a function of N for various decay rate Γ_χ. We see that the qualitative dependence of $f_{\rm NL}^{\rm final}$ on the decay rate is the same as for the χ^2 model, which can be explained by appealing to Eq. (4.34) with similar arguments. This implies that the shape of the minimum does not change the qualitative dependence of $f_{\rm NL}^{\rm final}$ on the reheating process. Of course, as reheating proceeds, the shape of the χ minimum does not remain exactly quartic (or quadratic in the case of the previous model) due to the coupling with the φ field.

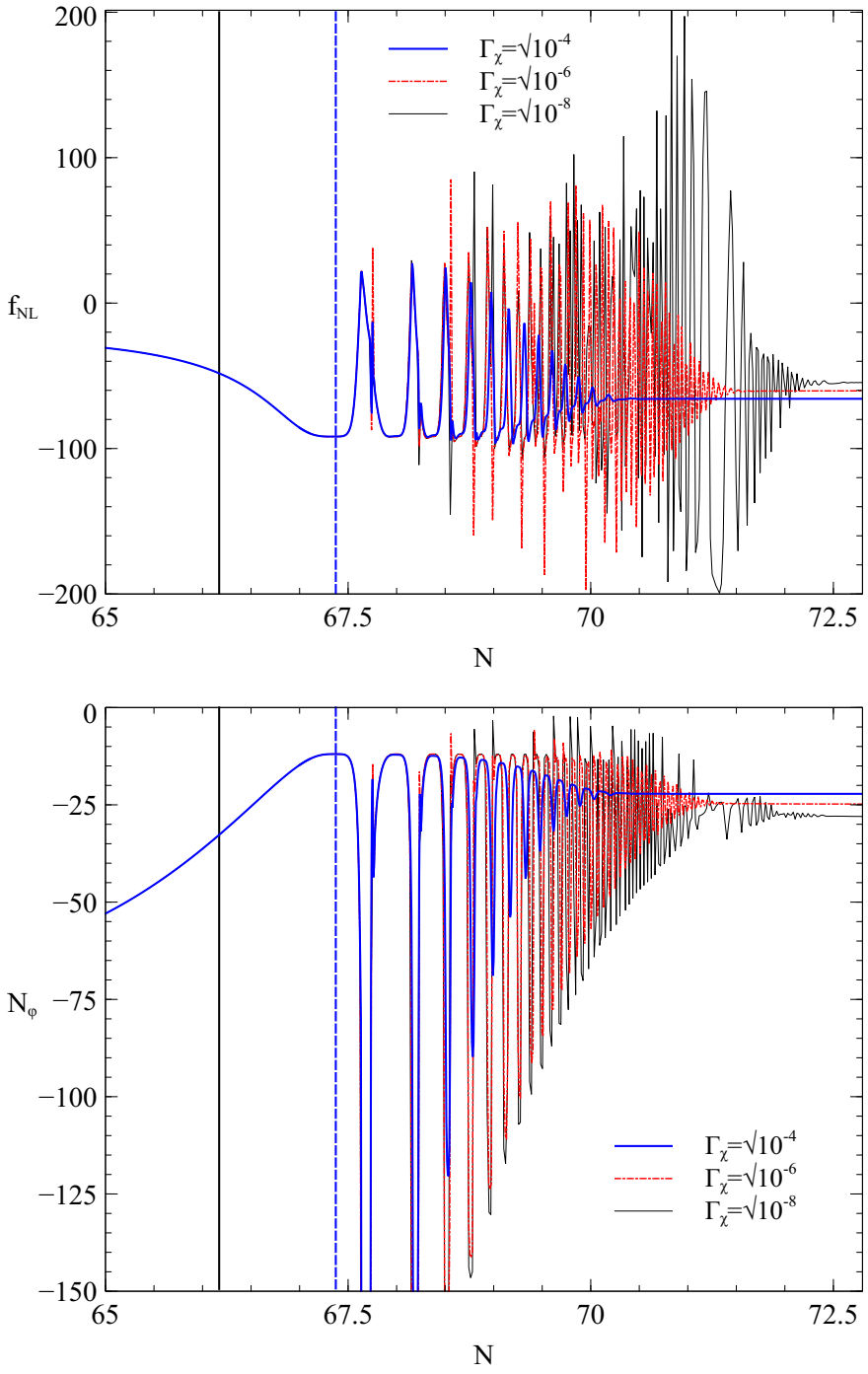

Figure 4.22: $W(\varphi,\chi) = W_0\chi^4 e^{-\lambda\varphi^2/M_{\rm p}^2}$. The parameters used are: $\lambda = 0.055$, $\varphi_* = 5\times 10^{-4}M_{\rm p}$ and $\chi_* = 23.0M_{\rm p}$. *Top Panel*: The evolution of $f_{\rm NL}$ during reheating for various decay rates Γ_χ. *Bottom Panel*: The evolution of the derivative N_φ during reheating for various decay rates Γ_χ. All decay rates are in units of $\sqrt{W_0}M_{\rm p}$. In both panels, the solid vertical (black) line denotes the end of inflation, $N_{\rm e}$, and the dashed vertical (blue) line denotes the start of reheating, $N_{\chi=0}$. The Hubble rate at the start of reheating is $H_r \approx \sqrt{10^{-1}W_0}M_{\rm p}$.

On the other hand, the spectral index $n_{\rm s}$ and the tensor-to-scalar ratio r are very less sensitive to reheating, with their final values after reheating finishes hardly varying for

different decay rates Γ_χ. The predictions for n_s and r evaluated at the end of inflation are close to the final asymptotic values after reheating as well. The overall results are summarised in Table 4.3.

$$\chi^4 \text{ minimum: } f_\mathrm{NL}(t_e) = -48.29,$$
$$n_s(t_e) = 0.770,\, r(t_e) = 7.2 \times 10^{-3}$$

Γ_χ	$f_\mathrm{NL}^\mathrm{final}$	n_s^final	r^final
$\sqrt{10^{-8}}$	-54.40	0.772	9.7×10^{-3}
$\sqrt{10^{-6}}$	-60.32	0.778	1.2×10^{-2}
$\sqrt{10^{-4}}$	-65.80	0.776	1.5×10^{-2}

Table 4.3: Statistics of ζ for $W(\varphi,\chi) = W_0\chi^4 e^{-\lambda\varphi^2/M_\mathrm{p}^2}$ for different decay rates. All decay rates are in units of $\sqrt{W_0}M_\mathrm{p}$. We give values computed at the end of inflation (t_e) and at the completion of reheating (final) where ζ is conserved. The model parameters are $\lambda = 0.055$, $\varphi_* = 5\times10^{-4}M_\mathrm{p}$ and $\chi_* = 23.0M_\mathrm{p}$.

Models with Two Minima

Similar to the one-minimum case, we use a modified N-flation model where the quadratic term χ^2 is replaced by a quartic term

$$W(\varphi,\chi) = W_0\left[\frac{\lambda}{4}\chi^4 + \Lambda^4\left(1-\cos\left(\frac{2\pi}{f}\varphi\right)\right)\right]. \tag{4.41}$$

This modification was studied in [133] and [107], in which the latter consider the model parameters such that ζ becomes conserved during slow-roll. Here we consider a different set of model parameters where isocurvature perturbations persist at the start of reheating, e.g. $\Lambda^4 = \lambda M_\mathrm{p}^2 f^2/8\pi^2$, $\varphi_* = (\frac{1}{2} - 0.001)f$, $\chi_* = 22M_\mathrm{p}$, $2f^2/M_\mathrm{p}^2 = \lambda$. The overall results comparing the values of the observables of ζ for this models at the end of inflation to that at the end of reheating are summarised in Table 4.4 below:

From Table 4.4, we can see a similar qualitative behaviour of $f_\mathrm{NL}^\mathrm{final}$ as in the quadratic case: the asymptotic values of f_NL are very insensitive to the decay rates of the scalar fields when they are equal, and slightly more sensitive if they are different. Compared to the quadratic minimum case, all observables are much less sensitive to decay rates here, including the non-linear parameter f_NL. Although n_s and r are pretty much

χ^4 minimum: $f_{\rm NL}(t_e) \approx 0$,
$n_s(t_e) = 0.951, r(t_e) = 0.263$

Γ_φ	Γ_χ	$f_{\rm NL}^{\rm final}$	$n_s^{\rm final}$	$r^{\rm final}$
0	0	5.04	0.966	2.9×10^{-4}
$\sqrt{10^{-5}}$	$\sqrt{10^{-5}}$	4.99	0.972	3.0×10^{-4}
$\sqrt{10^{-4}}$	$\sqrt{10^{-4}}$	5.06	0.966	3.0×10^{-4}
$\sqrt{10^{-1}}$	$\sqrt{10^{-5}}$	5.39	0.967	3.3×10^{-4}
$\sqrt{10^{-2}}$	$\sqrt{10^{-4}}$	5.28	0.967	3.2×10^{-4}

Table 4.4: Statistics of ζ for $W(\varphi,\chi) = W_0\left[\frac{\lambda}{4}\chi^4 + \Lambda^4\left(1-\cos\left(\frac{2\pi}{f}\varphi\right)\right)\right]$ for different decay rates. All decay rates are in units of $\sqrt{W_0}M_{\rm p}$. We give values computed at the end of inflation (t_e) and at the completion of reheating (final) where ζ is conserved. Here the model parameters are $\Lambda^4 = \lambda M_{\rm p}^2 f^2/8\pi^2$, $\varphi_* = (\frac{1}{2} - 0.001)f$, $\chi_* = 22M_{\rm p}$, $2f^2/M_{\rm p}^2 = \lambda$. Notice the very large decrease in the tensor–to–scalar ratio from the end of inflation to its final value.

insensitive to different combinations of the decay rates Γ_χ and Γ_φ, their final asymptotic values after reheating finishes are very different from that evaluated at the end of inflation.

4.5 Separable vs Non-Separable Potentials

In the previous sections, we have studied the evolution of $f_{\rm NL}$ and its asymptotic value at the end of reheating, $f_{\rm NL}^{\rm final}$, in examples where one or both fields reheat from a two–field *separable* potential. In this section, we will repeat the same analysis, but this time for a *non–separable* potential.

As an example, we consider a modified version of Eq. (4.39), by adding an extra quadratic mass term, first introduced in [133]

$$W(\chi,\varphi) = W_0(\chi^4 e^{-\lambda\varphi^2/M_{\rm p}^2} + \kappa^2\chi^2)\,. \tag{4.42}$$

Before discussing reheating, it is useful to discuss the inflationary regime. During inflation, the quadratic χ^2 mass term has a negligible effect on the field dynamics when the χ field is of $O(1)$ in Planckian units, unless $\kappa \gg O(M_{\rm p})$ or $\lambda\varphi^2 \gg O(M_{\rm p}^2)$. Here we consider the case $\kappa \sim O(M_{\rm p})$ and $\lambda\varphi^2 \ll O(M_{\rm p}^2)$, for which we can approximate the field dynamics and $f_{\rm NL}$ during inflation as the same as setting $\kappa^2 = 0$. Therefore,

in the region of parameter space where $\kappa \leq O(M_{\rm p})$, $f_{\rm NL}$ is expected to follow similar evolution as in the separable case studied in Section 4.4 during the slow-roll regime, with large deviations only coming in at late times towards the end of inflation. The mechanism for generating large $f_{\rm NL}$ is the same as discussed in [106], which is well illustrated from the fact that there exists a scaling relation for the subdominant field δN derivatives.

For model parameters $\kappa = M_{\rm p}$, $\varphi_* = 10^{-3} M_{\rm p}$ and $\chi_* = 22 M_{\rm p}$, a large negative $f_{\rm NL}$ is generated during inflation as the φ field rolls down the ridge and the bundle of trajectories diverge. The evolution is similar to the separable case where $\kappa = 0$, with $f_{\rm NL} \approx -44$ close to the end of slow-roll. Things are however a bit different after inflation even before reheating starts. For $\lambda = 0.06$, the additional quadratic term becomes comparable to the quartic term slightly earlier than in the case $\lambda = 0.05$. In this case, $f_{\rm NL}$ swaps sign shortly after the end of inflation. This unexpected behaviour, which we do not see in other cases, could be explained as follows: although the trajectories are still diverging in the φ direction, the fact that the quadratic term becomes dominant suggests that the local potential geometries around each trajectory converge to the same quadratic shape, independent of φ. This would have the same effect as the trajectories themselves converging in the separable case where H is converging, thus giving momentarily large positive $f_{\rm NL}$.

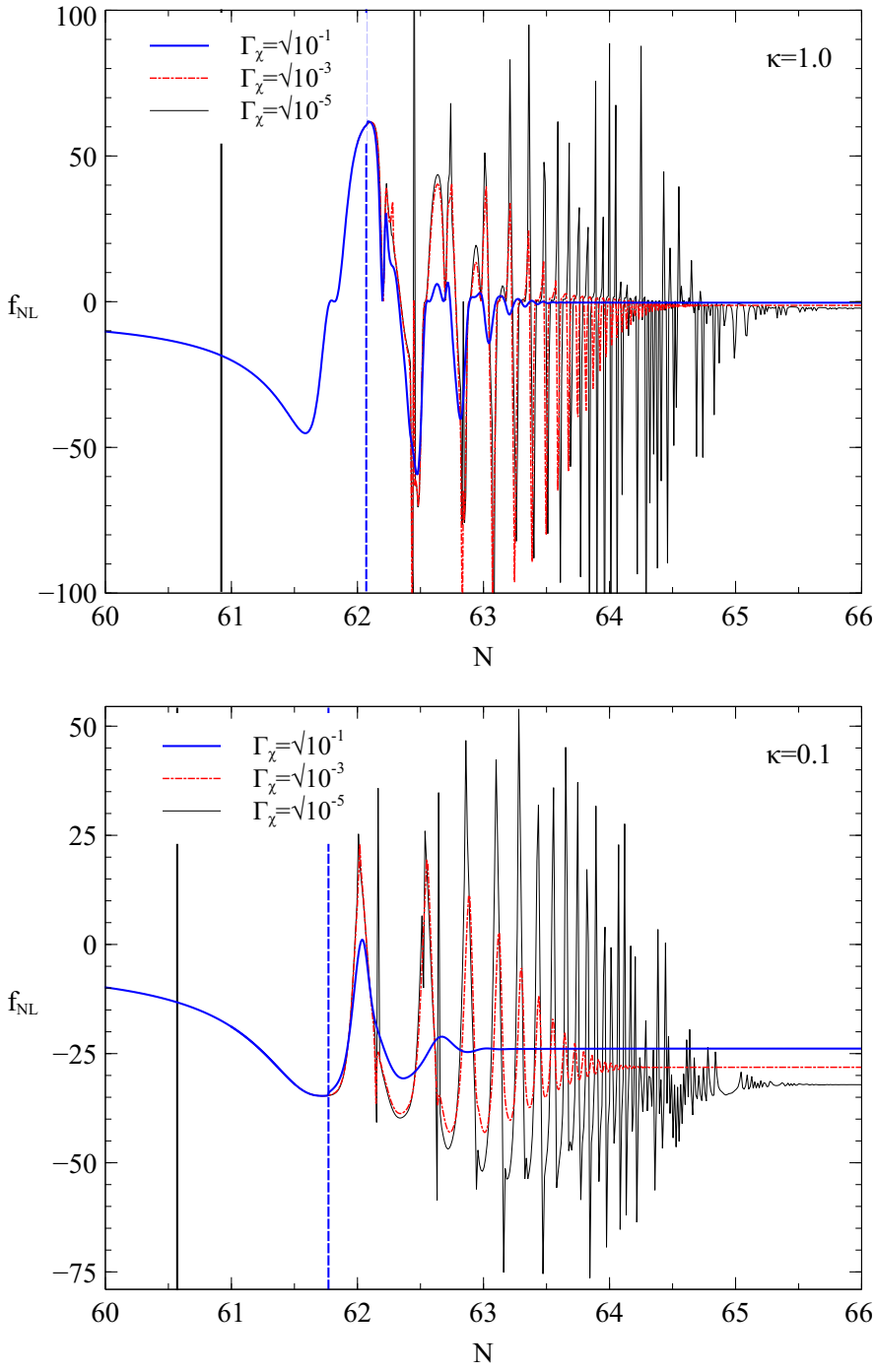

Figure 4.23: $W(\chi,\varphi) = W_0(\chi^4 e^{-\lambda\varphi^2/M_{\rm p}^2} + \kappa^2\chi^2)$. We show $f_{\rm NL}$ as a function of N during reheating. The parameters used are: $\varphi_* = 10^{-3}M_{\rm p}$, $\chi_* = 22M_{\rm p}$ and $\lambda = 0.06$. In both panels, the solid vertical (black) line denotes the end of inflation, $N_{\rm e}$, and the dashed vertical (blue) line denotes the start of reheating, $N_{\rm r}$. *Top Panel*: $\kappa^2 = M_{\rm p}^2$. The Hubble rate at the start of reheating is $H_r \approx \sqrt{2\times 10^{-1}W_0}M_{\rm p}$. *Bottom Panel*: $\kappa^2 = 0.1M_{\rm p}^2$. The Hubble rate at the start of reheating is $H_r \approx \sqrt{10^{-1}W_0}M_{\rm p}$.

Shortly after inflation ends, when the χ field reaches sub–Planckian values, the χ^2 term starts to dominate over the χ^4 term. Therefore, we expect the additional χ^2 term

modifies the field dynamics during the reheating phase and possibly $f_{\rm NL}$ as well. The additional χ^2 term makes the potential less shallow around the minimum. This saves the χ field from being frozen to non-zero values, leaving unwanted residual potential energy if Γ_χ is too large.

Similar to the separable case, as shown in Fig. 4.23, $f_{\rm NL}$ oscillates roughly in phase with χ^2 during the early reheating stage, with a larger amplitude for smaller Γ_χ. However, unlike the previous separable case in Section 4.4, the δN derivatives and $f_{\rm NL}$ are now much less sensitive to Γ_χ and thus the reheating timescale. The relative change of $f_{\rm NL}$ with respect to Γ_χ is much smaller for $\kappa = M_{\rm p}$ compared to that for $\kappa = 0.1M_{\rm p}$. This is summarised in Table 4.5. We conclude that the additional quadratic mass term reduces the sensitivity of $f_{\rm NL}$ to the reheating timescale. [4] This might be understood in terms of modulation on the mass of the χ field due to couplings with φ, which will be explained in the next section.

$\kappa^2 = M_{\rm p}^2$ $f_{\rm NL}(t_e) = -18.71$, $n_s(t_e) = 0.748$, $r(t_e) = 4.1 \times 10^{-3}$

Γ_χ	$f_{\rm NL}^{\rm final}$	$n_s^{\rm final}$	$r^{\rm final}$
$\sqrt{10^{-5}}$	-2.27	0.912	2.0×10^{-1}
$\sqrt{10^{-3}}$	-1.28	0.896	2.1×10^{-1}
$\sqrt{10^{-1}}$	-0.345	0.899	2.1×10^{-1}

$\kappa^2 = 0.1M_{\rm p}$ $f_{\rm NL}(t_e) = -13.23$, $n_s(t_e) = 0.746$, $r(t_e) = 2.0 \times 10^{-3}$

Γ_χ	$f_{\rm NL}^{\rm final}$	$n_s^{\rm final}$	$r^{\rm final}$
$\sqrt{10^{-5}}$	-32.1	0.747	1.5×10^{-2}
$\sqrt{10^{-3}}$	-28.1	0.752	1.1×10^{-2}
$\sqrt{10^{-1}}$	-23.9	0.751	7.8×10^{-3}

Table 4.5: Statistics of ζ for $W(\chi,\varphi) = W_0(\chi^4 e^{-\lambda\varphi^2/M_{\rm p}^2} + \kappa\chi^2)$ for different decay rates. All decay rates are in unit of $\sqrt{W_0}M_{\rm p}$. We give values computed at the end of inflation (t_e) and at the completion of reheating (final) where ζ is conserved. *Left Table*: $\kappa = M_{\rm p}$; *Right Table*: $\kappa = 0.1M_{\rm p}$.

4.6 Remarks and Summary

In this chapter, we have discussed the effects of perturbative reheating on the key inflationary observables $f_{\rm NL}$, $n_{\rm s}$ and r, for canonical two-field inflation models. In particular, we have considered two classes of potential: the 'runaway' type which has a minimum in only one direction; and potentials which have a minimum in both directions.

[4] Note that changing κ also slightly changes the times that inflation ends and reheating starts. This however has negligible effect on the dependence of the observables on Γ_χ in the parameter space of interest.

One important difference between the single-minimum models and the two-minima model is that in the former case, the fields are coupled via the potential, whilst in the latter they are coupled only via gravity. Thus, for the single-minimum models, the local geometries of the χ minima are functions of the subdominant field φ, and these geometries are different for different inflationary trajectories in the bundle. The shape of these 'reheating minima' evolves in time as reheating proceeds, and this affects the dynamics of the oscillating χ field. This can be seen as the effective mass of the oscillating field is modified by φ and thus the oscillating frequency being modulated. In two-minima models however, where the potential is sum-separable and the fields are coupled only through gravity, this modulation effect is absent.

This modulation effect depends on the strength of the coupling between the fields, as we have illustrated with the non-separable model Eq. (4.42). The larger κ is, the weaker is the the coupling between the φ and χ fields. This explains why we found the sensitivity of the δN derivatives to Γ_χ decreases as κ increases.

To summarise, we see that although the way the observables depend on the reheating dynamics is a model-dependent question even for the simplest case where the decay rates are constants, the model predictions evaluated at the end of inflation are generically different to the final asymptotic values after reheating, particularly the non-linear parameter $f_{\rm NL}$. If $|f_{\rm NL}|$ is large at the start of reheating, it typically remains large (i.e. $|f_{\rm NL}| > O(1)$) and is of the same sign after reheating for a wide range of decay rates. The same qualitative conclusion can be drawn regardless of the geometry of the reheating minima.

Chapter 5

The Influence of Reheating on the Trispectrum and Beyond

In Chapter 4, we have discussed how a phase of perturbative reheating changes the inflationary model predictions at the level of the power spectrum P_ζ and bispectrum B_ζ in various examples of canonical two-field models.

Here in this chapter we extend the discussion of reheating to the trispectrum and scale dependence of non-linear parameters, focussing particularly on the trispectrum non-linear parameters $\tau_{\rm NL}$ and $g_{\rm NL}$ and the spectral indices $n_{f_{\rm NL}}$ and $n_{\tau_{\rm NL}}$ in Section 5.1. As in the previous chapter, we consider the two broad classes of canonical two-field models where minimum exists in one or both field directions. In Section 5.2, we illustrate that while individually primordial observables could change significantly after reheating, consistency relations between different observables are much more robust and thus act as better probes to distinguish different multifield models. Finally we comment on the difficulties in realising $g_{\rm NL}$ as the dominating statistics of the trispectrum in multifield models in Section 5.3 and conclude in Section 5.4. Again we restrict ourselves to the parameter space where a large (temporary) non-Gaussianity is plausible.

5.1 Four-Point Statistics and Scale Dependence of Non-linear Parameters

In this section, we consider the influence of reheating on the four-point statistics of ζ, particularly on $\tau_{\rm NL}$, $g_{\rm NL}$ and the spectal index $n_{\tau_{\rm NL}}$. Again we apply the δN formalism and use the numerical recipe in Appendix B to evaluate the δN coefficients. As in the previous chapter, we study a simple repesentative of the class of multifield models, the canonical two-field models, where minima exist in either one field direction or both field directions. The results were first shown in [110].

Model with One Minimum

Again we consider the 'runaway' type quadratic exponential models with potential

$$W(\varphi,\chi) = W_0\chi^2 e^{-\lambda\varphi^2/M_{\rm P}^2} \tag{5.1}$$

as an example. Before studying how the trispectrum non-linear parameters $\tau_{\rm NL}$ and $g_{\rm NL}$ evolve during reheating, it is useful to revisit their evolution during the inflationary phase. Because the potential is of a product-separable form, analytic expressions exist for $\tau_{\rm NL}$ and $g_{\rm NL}$ during slow-roll as discussed in Appendix A. The expressions were first derived by Elliston et al. [107] and the slow-roll evolution of the trispectrum has been studied in the literature [107, 138]. To summarise, a large $\tau_{\rm NL}$ is produced in similar regions of parameter space as that of a large $f_{\rm NL}$, with $\tau_{\rm NL}$ peaks slightly earlier than $f_{\rm NL}$. $g_{\rm NL}$ remains subdominant though, unless there are significant terms beyond quadratic order in the potential. For instance, see Fig. 4.17 in Chapter 4.

Evolution of Third-order δN Coefficients

Before we begin discussing the trispectrum, it is useful to discuss the evolution of the third-order δN coefficients first. Similar to the second order terms, while all of them evolve after inflation ends, there is a hierachy in magnitude between different third-order δN coefficients, with $|N_{\varphi\varphi\varphi}| > |N_{\chi\chi\chi}|, |N_{\varphi\varphi\chi}|, |N_{\varphi\chi\chi}|$ regardless of the decay

rates. In Fig. 5.1, we illustrate this by showing the fractional differences between $|N_{\varphi\varphi\varphi}|$ and magnitudes of the other third order δN coefficients, defined as

$$\Delta_{\chi\chi\chi} \equiv \frac{|N_{\varphi\varphi\varphi}| - |N_{\chi\chi\chi}|}{|N_{\varphi\varphi\varphi}|}\,, \quad \Delta_{\varphi\chi\chi} \equiv \frac{|N_{\varphi\varphi\varphi}| - |N_{\varphi\chi\chi}|}{|N_{\varphi\varphi\varphi}|}\,, \quad \Delta_{\varphi\varphi\chi} \equiv \frac{|N_{\varphi\varphi\varphi}| - |N_{\varphi\varphi\chi}|}{|N_{\varphi\varphi\varphi}|}\,, \tag{5.2}$$

for a particular model parameter choice. We see that $|N_{\varphi\varphi\varphi}|$ is always orders of magnitude larger than $|N_{\chi\chi\chi}|$ and $|N_{\varphi\chi\chi}|$, whereas the final asymptotic value of $|N_{\varphi\varphi\varphi}|$ after reheating ends is of the same order as $|N_{\varphi\varphi\chi}|$.

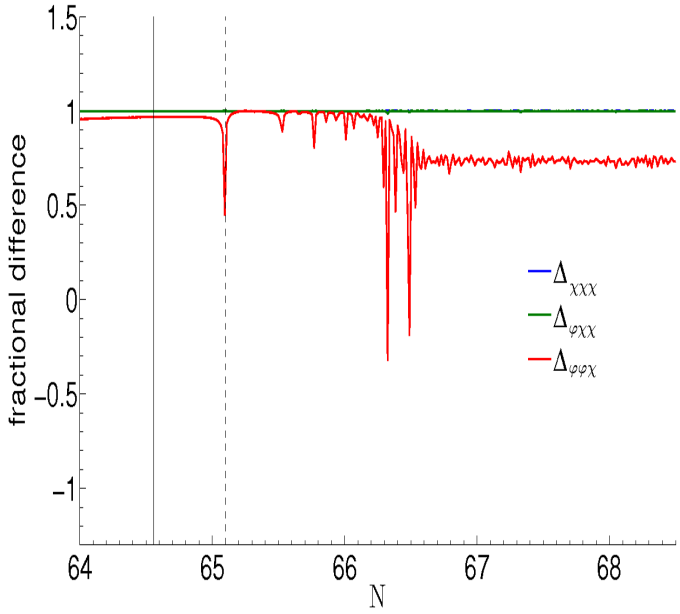

Figure 5.1: Potential: $W(\varphi,\chi) = W_0\chi^2 e^{-\lambda\varphi^2/M_{\rm P}^2}$. Fractional differences Δ between $|N_{\varphi\varphi\varphi}|$ and magnitudes of the other third order δN coefficients, defined as in Eq. (5.2). The model parameters are $\lambda = 0.05$, $\varphi_* = 10^{-3}M_{\rm p}$, $\chi_* = 16.0M_{\rm p}$ and $\Gamma_\chi = \sqrt{W_0/10}$. Here the solid (black) vertical line denotes the end of inflation, $N_{\rm e}$, and the dashed (black) line denotes the start of reheating, $N_{\chi=0}$.

Trispectrum After Reheating, $\tau_{\rm NL}$

Now we consider the post-inflationary evolution during reheating. Starting with $\tau_{\rm NL}$, the evolution of $\tau_{\rm NL}$ during reheating with two different decay rates Γ_χ, for two slightly different slopes of the ridge in the potential which are set by λ is shown in Fig. 5.2. The model parameters are $\lambda = \{0.05,\, 0.06\}$, $\varphi_* = 10^{-3}M_{\rm p}$ and $\chi_* = 16M_{\rm p}$. Similar to

$f_{\rm NL}$, $\tau_{\rm NL}$ oscillates during reheating when χ oscillates about its minimum. No generic trend independent of λ can be seen as the decay rate increases, $\tau_{\rm NL}$ can either grow or decay.

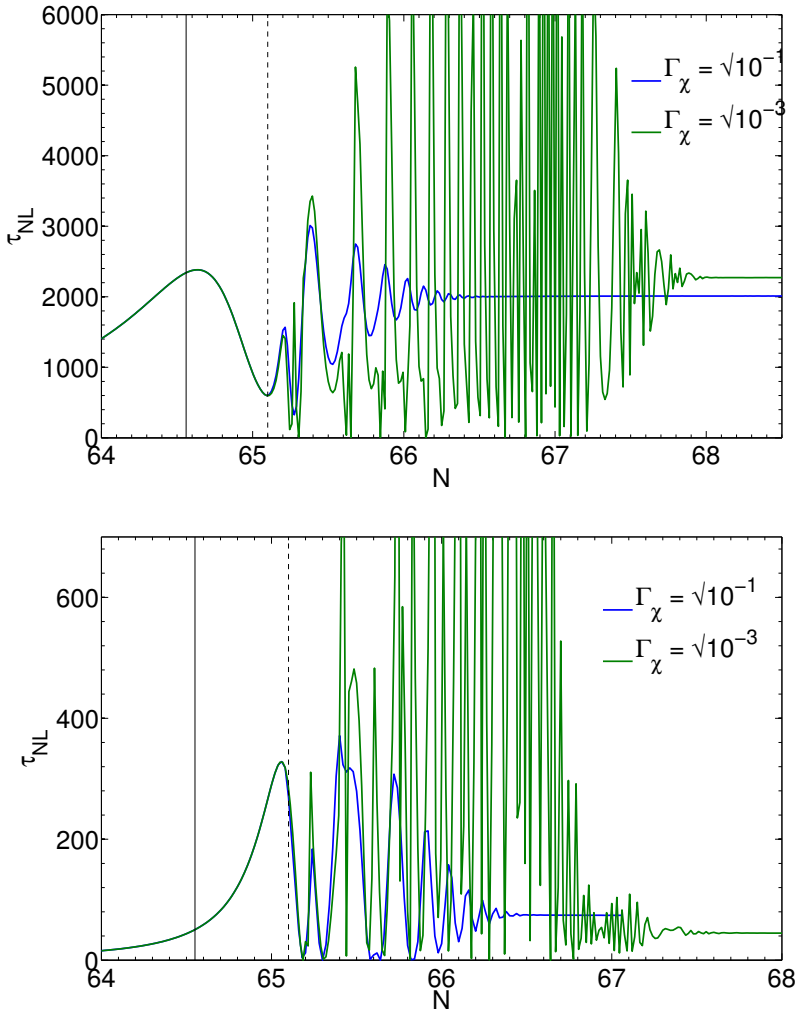

Figure 5.2: Potential: $W(\varphi,\chi) = W_0\chi^2 e^{-\lambda\varphi^2/M_{\rm p}^2}$. *Top panel*: The evolution of τ_{NL} during post–inflationary period, with $\lambda = 0.05$, $\varphi_* = 10^{-3}M_{\rm p}$ and $\chi_* = 16.0M_{\rm p}$. *Bottom panel*: Same initial conditions with $\lambda = 0.06$. All decay rates are given in unit of $\sqrt{W_0}$ here. In both panels, the solid vertical line denotes the end of inflation, $N_{\rm e}$, and the dashed line denotes the start of reheating, $N_{\chi=0}$.

This quantitative behaviour can be understood by taking certain approximations in a similar fashion as in the case of $f_{\rm NL}$. As demonstrated in Section 4.2, $N_{\chi\chi}$ and $N_{\varphi\chi}$ are negligible compared to $N_{\varphi\varphi}$ and there exists a scaling relation between $N_{\varphi\varphi}$ and N_φ, where $N_{\varphi\varphi} \approx N_\varphi/\varphi_*$. Applying these results, $\tau_{\rm NL}$ may be written as

$$\tau_{\rm NL} = \frac{(N_\varphi^4)}{(N_\varphi^2 + g_*^2)^3}\left(\frac{1}{\varphi_*^2}\right) . \tag{5.3}$$

Again here $g_* \equiv N_\chi = M_{\rm p}^{-1}(2\epsilon_\chi)_*^{-1/2}$. The result that $N_\chi \approx g_* = const$ comes from the fact that the χ field dominates the energy density over the whole evolution. This

algebraic function has three stationary points at certain values of N_φ,

$$N_\varphi = 0, \pm\sqrt{2}g_* \,. \tag{5.4}$$

The $N_\varphi = 0$ root is an infection point where $\tau_{\rm NL} = 0$, while the $N_\varphi = \sqrt{2}g_*$ corresponds to a local maximum. Both $N_\varphi = 0$ and $N_\varphi = \sqrt{2}g_*$ roots are unphysical here because N_φ is always negative with diverging trajectories. The other root, $N_\varphi = -\sqrt{2}g_*$, however is physical and bounds the maximum value of $\tau_{\rm NL}$, given by

$$(\tau_{\rm NL})_{\rm max} = \frac{4}{27 g_*^2}\left(\frac{1}{\varphi_*^2}\right) \,. \tag{5.5}$$

This bound depends entirely on the initial conditions at horizon crossing, not on superhorizon evolution including reheating. The exact final value of $\tau_{\rm NL}$ at the end of reheating of course depends upon Γ_χ though. But since a bound exists, even if the details of reheating such as Γ_χ are unknown, it is still possible to constrain the range where $\tau_{\rm NL}$ could lie in this model. The algebraic function Eq. (5.3) also explains the difference in the qualitative behaviour in the evolution of $\tau_{\rm NL}$ for different λ, particularly why we see the asymptotic value of $\tau_{\rm NL}$ evolves in opposite ways for two slightly different λ. This is shown in Fig 5.3. For $\lambda = 0.05$, N_φ is much smaller and the algebraic function Eq. (5.3) is close to its maximum value; whereas for $\lambda = 0.06$, N_φ is much larger and the algebraic function Eq. (5.3) is almost flat as a function of N_φ.

Trispectrum After Reheating, $g_{\rm NL}$

Next we consider the non-linear parameter $g_{\rm NL}$. The evolution of $g_{\rm NL}$ during reheating for two different Γ_χ, with the same model parameters as in $\tau_{\rm NL}$, is shown in Fig. 5.4. Similarly, $g_{\rm NL}$ oscillates during reheating, with the final asymptotic value after reheating different from that evaluated at the end of slow-roll. Unlike $\tau_{\rm NL}$, the final value of $g_{\rm NL}$ is less sensitive to Γ_χ and the reheating dynamics. Generically, compared to $\tau_{\rm NL}$, it remains very much subdominant and smaller than the current observational limit in ongoing CMB experiments, i.e. $g_{\rm NL} \ll O(1000)$.

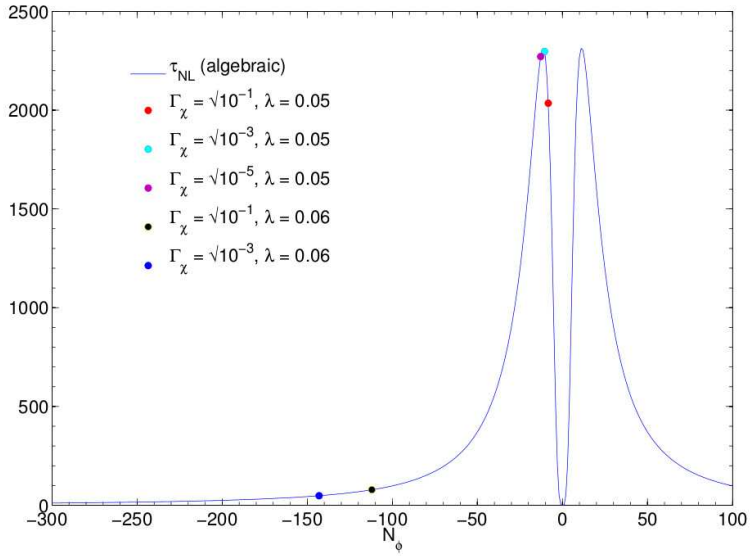

Figure 5.3: Potential: $W(\varphi,\chi) = W_0\chi^2 e^{-\lambda\varphi^2/M_{\rm P}^2}$. The algebraic function $\tau_{\rm NL}$ as a function of N_φ (in unit of $M_{\rm p}$), Eq. (5.3). We give the final asymptotic value of N_φ after reheating for $\lambda = \{0.5, 0.6\}$ with different decay rate Γ_χ. All decay rates are in units of $\sqrt{W_0}$.

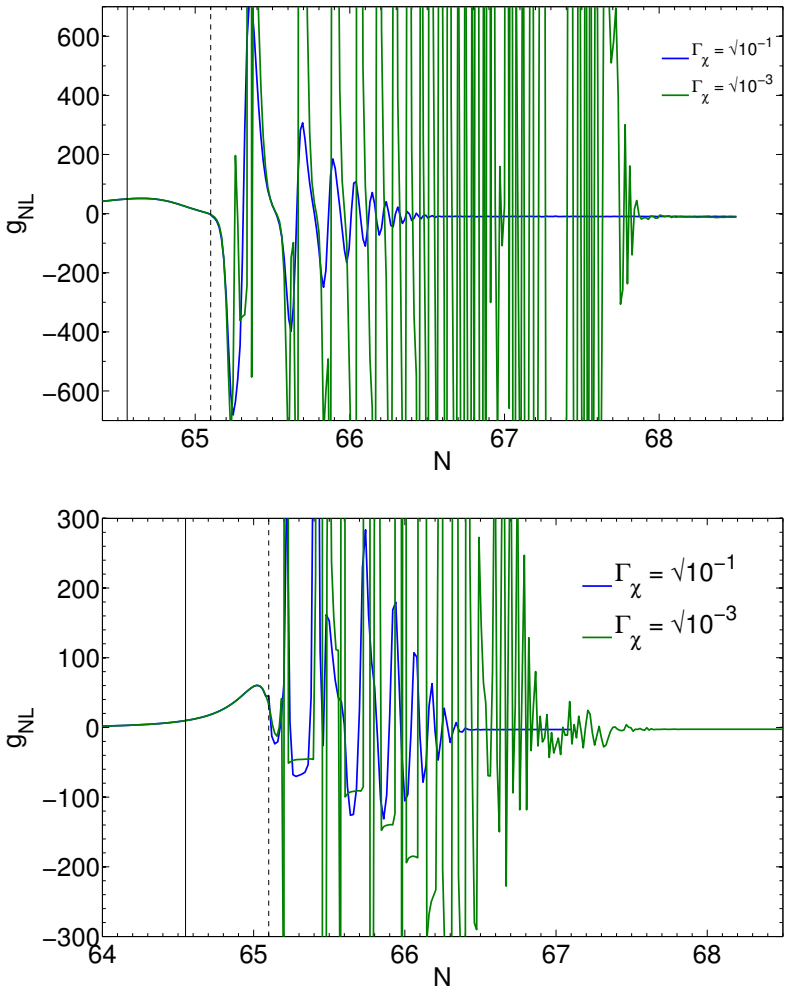

Figure 5.4: Potential: $W(\varphi,\chi) = W_0\chi^2 e^{-\lambda\varphi^2/M_{\rm P}^2}$. The post–inflationary evolution of $g_{\rm NL}$ for three different decay rate Γ_χ. The model parameters are $\lambda = 0.06$, $\varphi_* = 10^{-3}M_{\rm P}$ and $\chi_* = 16.0M_{\rm P}$. *Top Panel*: $\lambda = 0.05$, *Bottom Panel*: $\lambda = 0.06$. All decay rates are given in unit of $\sqrt{W_0}$ here. In both panels, the solid vertical line denotes the end of inflation, $N_{\rm e}$, and the dashed line denotes the start of reheating, $N_{\chi=0}$.

Given hierachies between the first and third order δN coefficients as mentioned, $g_{\rm NL}$ is dominated by a single term in the δN expression

$$g_{\rm NL} \approx \frac{25}{54}\frac{N_{\varphi\varphi\varphi}N_\varphi^3}{(N_\varphi^2+N_\chi^2)^3}\,. \tag{5.6}$$

However, without any scaling relations between $N_{\varphi\varphi\varphi}$ and N_φ, explicit dependence on the reheating dynamics cannot be explained in a similar fashion as in the case of $f_{\rm NL}$ and $\tau_{\rm NL}$.

Scale Dependence of Non–linear parameters, $n_{f_{\rm NL}}$ and $n_{\tau_{\rm NL}}$

As discussed earlier, it is natural that ζ is scale dependent. Apart from the amplitude of bi- and trispectra in different shapes, one may also study their scale dependence. Indeed it has been shown that while $f_{\rm NL}$ is insensitive to preheating in canonical single field models (as well as being too small to be observed), it is strongly scale dependent [150].

Here we focus on the spectral indices of $f_{\rm NL}$ and $\tau_{\rm NL}$, denoted by $n_{f_{\rm NL}}$ and $n_{\tau_{\rm NL}}$ respectively. We ignore the scale dependence of $g_{\rm NL}$ here as $g_{\rm NL}$ is small and currently irrelevant in observations. In Fig. 5.5 we give the evolution of $n_{f_{\rm NL}}$ and $n_{\tau_{\rm NL}}$ from around 30 e-folds of inflation after horizon-exit up until the completion of reheating. For a particular choice of λ, i.e. $\lambda = 0.05$, $n_{f_{\rm NL}}$ and $n_{\tau_{\rm NL}}$ can be of order $O(0.1)$ and be potentially observed in CMB experiments if the fiducial values are large enough.

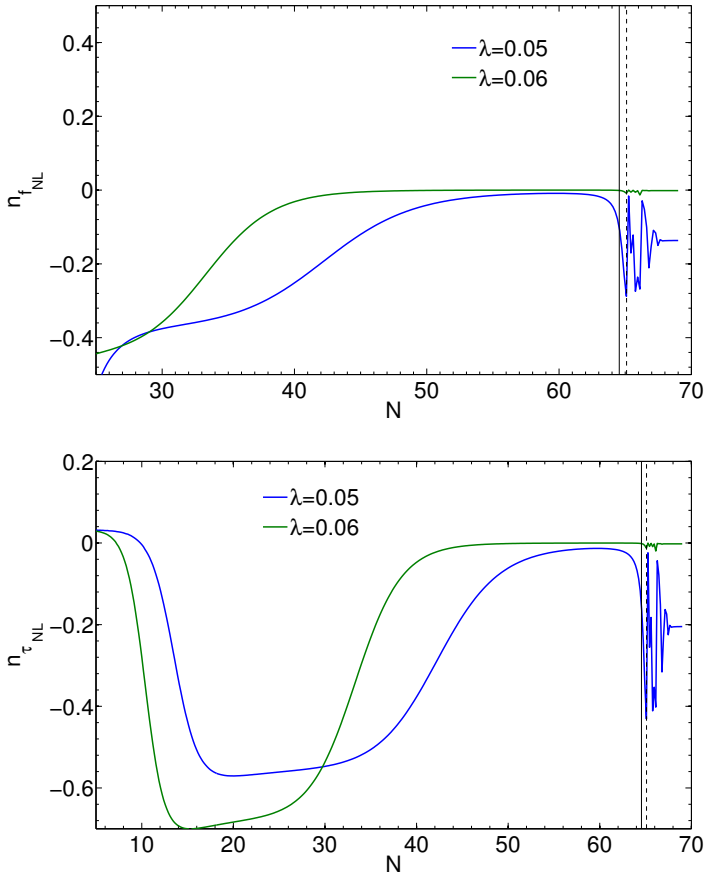

Figure 5.5: Potential: $W(\varphi,\chi) = W_0\chi^2 e^{-\lambda\varphi^2/M_{\rm p}^2}$. *Top panel*: The evolution of $n_{f_{\rm NL}}$. *Bottom panel*: The evolution of $n_{\tau_{\rm NL}}$. The model parameters are $\lambda = \{0.05,\, 0.06\}$, $\varphi_* = 10^{-3}M_{\rm p}$ and $\chi_* = 16.0M_{\rm p}$, with the decay rate $\Gamma_\chi = \sqrt{10^{-3}W_0}$. For $\lambda = 0.05$, $n_{f_{\rm NL}}$ and $n_{\tau_{\rm NL}}$ may be large enough to be observationally relevant, while for $\lambda = 0.06$ the non–linear parameters are almost scale–independent. In both panels, the solid vertical line denotes the end of inflation, $N_{\rm e}$, and the dashed line denotes the start of reheating, $N_{\chi=0}$.

To understand why $n_{f_{\rm NL}}$ and $n_{\tau_{\rm NL}}$ are much larger for $\lambda = 0.05$, we first rewrite Eqs. (3.80)-(3.81) as

$$\begin{aligned} n_{f_{\rm NL}} = \quad & -2\left[n_{\rm s} - 1 + 2(\epsilon_H)_*\right] - \frac{5}{192}\frac{r^2}{f_{\rm NL}} \\ & + \frac{5}{6f_{\rm NL}}\sum_{IJK}\left[\frac{4\eta_{IK*}N_{IJ}N_JN_K + \eta_{IJ*}N_IN_J + (W_{IJK}/W)_*N_IN_JN_K}{(\sum_L N_L^2)^2}\right], \end{aligned} \tag{5.7}$$

$$\begin{aligned} n_{\tau_{\rm NL}} = \quad & -3\left[n_{\rm s} - 1 + 2(\epsilon_H)_*\right] - \frac{1}{256}\frac{r^3}{\tau_{\rm NL}} \\ & + \frac{2}{\tau_{\rm NL}}\sum_{IJKL}\left[\frac{2\eta_{JL*}N_{IJ}N_{IK}N_LN_K + \eta_{IJ*}N_IN_J + \eta_{IJ*}N_{JL}N_{IK}N_LN_K}{(\sum_M N_M^2)^3}\right. \\ & \left. + \frac{(W_{IJL}/W)_*N_{IK}N_JN_KN_L}{(\sum_M N_M^2)^3}\right], \end{aligned} \tag{5.8}$$

using Eq. (3.66) where r is the tensor–to–scalar ratio. From this, it is not difficult to see that the second terms in the first line of both equations are small in general as r is smaller than $O(0.1)$ in most cases. Making use of the approximate formulae for $f_{\rm NL}$ and $\tau_{\rm NL}$, the dominating terms in Eqs. (5.7)-(5.8) are

$$n_{\tau_{\rm NL}} \simeq \frac{3}{2} n_{f_{\rm NL}} \simeq -3[n_{\rm s} - 1 + 2(\epsilon_H)_*] + 6(\eta_{\varphi\varphi})_* \simeq 6(\eta_{\varphi\varphi})_* \left(\frac{N_\chi^2}{N_\varphi^2 + N_\chi^2} \right) , \quad (5.9)$$

where we assumed slow-roll at horizon–crossing such that $(W_{IJK}/W)_* \ll O(1)$ and used $n_{\rm s} - 1 + 2(\epsilon_H)_* \approx 2(\eta_{\varphi\varphi})_* \left(\frac{N_\varphi^2}{N_\varphi^2 + N_\chi^2} \right)$. We have also assumed that the numerators in the square brackets in Eqs. (5.7)-(5.8) are dominated by the N_φ and $N_{\varphi\varphi}$ terms. In Fig. 5.6, we show the comparison between the exact Eqs. (5.7)-(5.8) and the approximate formula Eq. (5.9). From this, we see the approximate formula agrees very well with the full expressions after about 30 e-folds of inflation, even during the reheating phase.

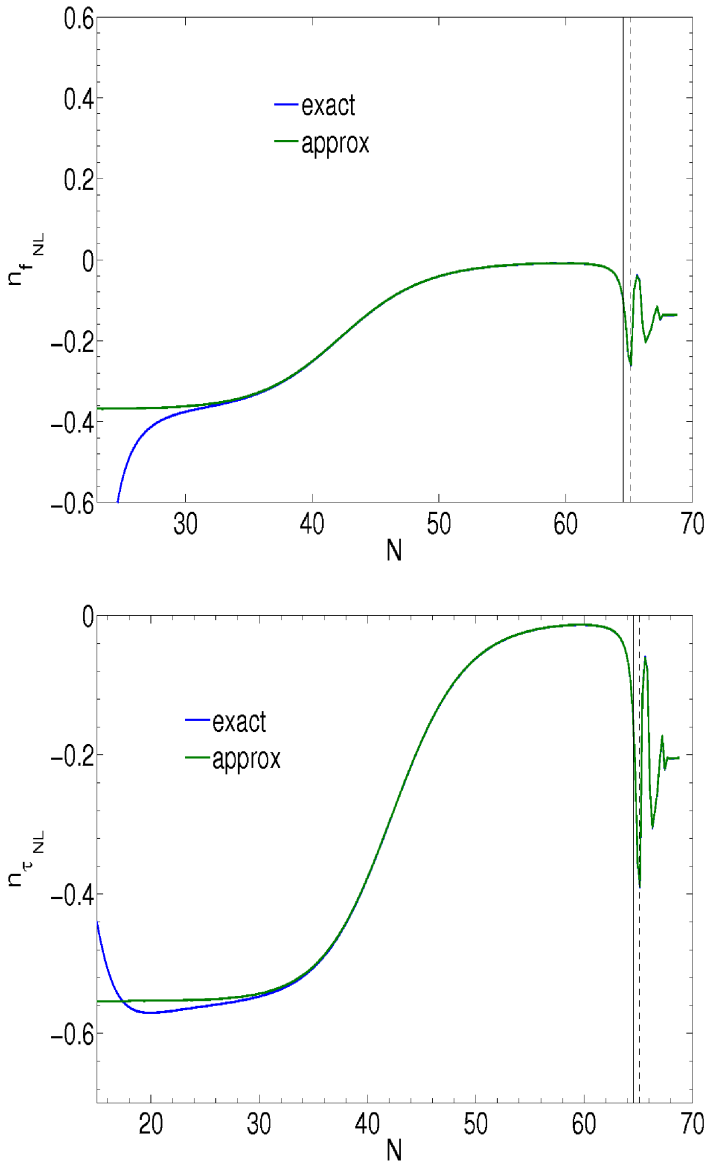

Figure 5.6: Potential: $W(\varphi,\chi) = W_0\chi^2 e^{-\lambda\varphi^2/M_{\rm p}^2}$. Comparison of the exact Eqs. (5.7)-(5.8) and approximate formula Eq. (5.9). *Top panel*: The evolution of $n_{f_{\rm NL}}$. *Bottom panel*: The evolution of $n_{\tau_{\rm NL}}$. The model parameters are $\lambda = 0.05$, $\varphi_* = 10^{-3}M_{\rm p}$ and $\chi_* = 16.0M_{\rm p}$, for the decay rate $\Gamma_\chi = \sqrt{10^{-3}W_0}$. The equations agree to a good approximation after about 30 e–folds of inflation.

From Eq. (5.9), one may see that the spectral indices are relatively large when $N_\varphi \sim N_\chi$, which is the case when $\lambda = 0.05$, but very small when $|N_\varphi| \gg |N_\chi|$, which is the case when $\lambda = 0.06$. Notice that if $|N_\varphi| \gg |N_\chi|$, both spectral indices are driven to zero and hence become independent of the decay rate.

In Table 5.1 we summarise the results, showing the comparison between the primordial observables evaluated at the end of inflation (slow-roll stage) and at the end of reheat-

ing. Notice the different qualitative behaviour for the non–linear parameters in the models for different λ, where the magnitudes of $f_{\rm NL}$ and $\tau_{\rm NL}$ decrease with larger Γ_χ for $\lambda = 0.05$, but increase for $\lambda = 0.06$. In general, the final values of the non–linear parameters at the completion of reheating are different from the end of inflation values, whilst $g_{\rm NL}$ remains small $\ll O(100)$ in this model which is unlikely be observable in future experiments. The spectral indices $n_{f_{\rm NL}}$ and $n_{\tau_{\rm NL}}$ are large in the case $\lambda = 0.05$ and are redder for larger Γ_χ.

End of Inflation, $\lambda = 0.05$

$-$	$f_{\rm NL}$	$\tau_{\rm NL}$	$g_{\rm NL}$	$n_{f_{\rm NL}}$	$n_{\tau_{\rm NL}}$
$-$	-34.1	2.34×10^3	-49.6	-0.105	-0.158

End of Reheating, $\lambda = 0.05$

Γ_χ	$f_{\rm NL}$	$\tau_{\rm NL}$	$g_{\rm NL}$	$n_{f_{\rm NL}}$	$n_{\tau_{\rm NL}}$
$\sqrt{10^{-5}}$	-33.4	2.25×10^3	-13	-0.105	-0.157
$\sqrt{10^{-3}}$	-31.5	2.27×10^3	-11.6	-0.137	-0.205
$\sqrt{10^{-1}}$	-26.9	2.01×10^3	-9.96	-0.177	-0.266

End of Inflation, $\lambda = 0.06$

$-$	$f_{\rm NL}$	$\tau_{\rm NL}$	$g_{\rm NL}$	$n_{f_{\rm NL}}$	$n_{\tau_{\rm NL}}$
$-$	-5.93	50.7	9.86	-1.0×10^{-3}	-1.5×10^{-3}

End of Reheating, $\lambda = 0.06$

Γ_χ	$f_{\rm NL}$	$\tau_{\rm NL}$	$g_{\rm NL}$	$n_{f_{\rm NL}}$	$n_{\tau_{\rm NL}}$
$\sqrt{10^{-5}}$	-4.35	28.1	-2.41	-9.1×10^{-4}	-1.3×10^{-3}
$\sqrt{10^{-3}}$	-5.54	44.5	-2.62	-1.4×10^{-3}	-2.1×10^{-3}
$\sqrt{10^{-1}}$	-7.14	73.9	-2.96	-2.3×10^{-3}	-3.4×10^{-3}

Table 5.1: Statistics of ζ for $W(\varphi, \chi) = W_0 \chi^2 e^{-\lambda\varphi^2/M_{\rm p}^2}$ for different decay rates. All decay rates are in unit of $\sqrt{W_0}$. We give values computed at the end of inflation (t_e) and at the completion of reheating (final) where ζ is conserved. The model parameters are $\lambda = 0.05$ *(Top panel)* and 0.06 *(Bottom panel)*, $\varphi_* = 10^{-3} M_{\rm p}$ and $\chi_* = 16.0 M_{\rm p}$.

Model with Two Minima

Next we repeat the analysis for the two-minima models. Again the example considered is the effective two–field description of axion N–flation introduced earlier in Chapter 4, where the potential is again given by

$$W(\varphi, \chi) = W_0 \left[\frac{1}{2} m^2 \chi^2 + \Lambda^4 \left(1 - \cos\left(\frac{2\pi}{f} \varphi \right) \right) \right] . \tag{5.10}$$

Recall that in this model, the axion φ, is described by its decay constant f and its potential energy scale Λ. To generate a large non–gaussianity, we must have φ close to the "hilltop" at horizon-crossing [106]. In this configuration, the second field χ, drives inflation.

Evolution of Third-order δN Coefficients

Before we begin discussing the trispectrum, it is useful to discuss the evolution of the third-order δN coefficients first. Similar to the second order terms, the φ coefficients only become large after the end of inflation and there is a large hierachy between the magnitudes of different third order δN coefficients, with $|N_{\varphi\varphi\varphi}| \gg |N_{\chi\chi\chi}|, |N_{\varphi\varphi\chi}|, |N_{\varphi\chi\chi}|$. This can be seen in terms of the fractional differences between the magnitudes of third order δN coefficients defined in Eq. (5.2) as shown in Fig. 5.7.

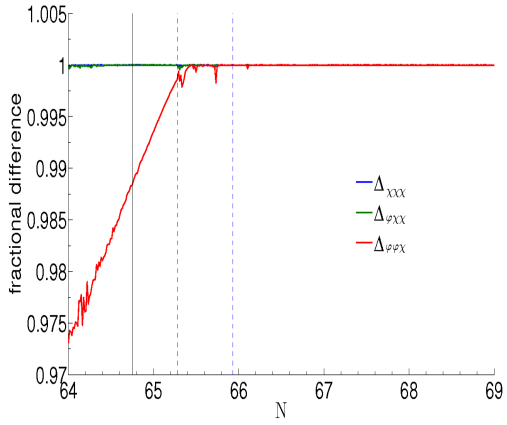

Figure 5.7: Potential: $W(\varphi,\chi) = W_0\left[\frac{1}{2}m^2\chi^2 + \Lambda^4\left(1-\cos\left(\frac{2\pi}{f}\varphi\right)\right)\right]$. Fractional difference Δ between $|N_{\varphi\varphi\varphi}|$ and magnitudes of the other third order δN coefficients, defined as in Eq. (5.2). The model parameters are $\Lambda^4 = m^2f^2/4\pi^2$, $\varphi_* = (\frac{1}{2}-0.001)f$, $\chi_* = 16M_{\rm p}$, $f = m = M_{\rm p}$, with $\Gamma_\chi = \Gamma_\varphi = \sqrt{W_0/100}M_{\rm p}$. The solid vertical line denotes the end of inflation, $N_{\rm e}$, and the dashed lines denote the start of reheating, $N_{\varphi=0}$ (blue) and $N_{\chi=0}$ (black), respectively.

Trispectrum After Reheating

The model parameters we consider are $\Lambda^4 = m^2f^2/4\pi^2$, $\varphi_* = (\frac{1}{2}-0.001)f$, $\chi_* = 16M_{\rm p}$ and $f = m = M_{\rm p}$. All $f_{\rm NL}$, $\tau_{\rm NL}$ and $g_{\rm NL}$ are negligible during inflation as the axion φ is sufficiently light that it remains almost frozen near the top of the ridge. In

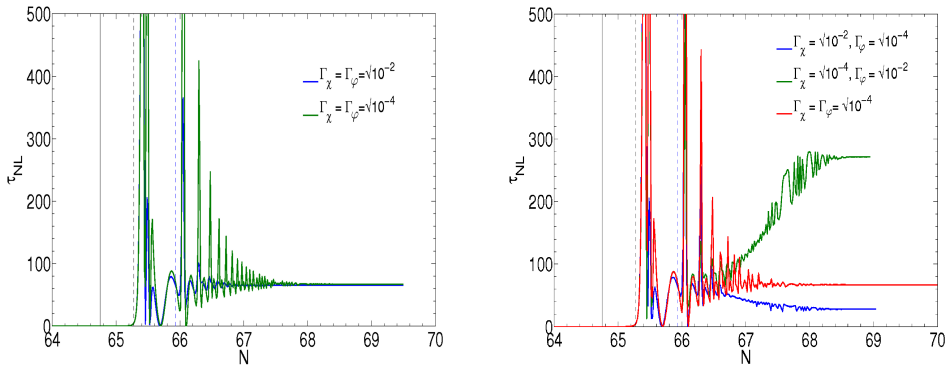

Figure 5.8: Potential: $W(\varphi,\chi) = W_0[\frac{1}{2}m^2\chi^2 + \Lambda^4(1-\cos(\frac{2\pi}{f}\varphi))]$. The evolution of $\tau_{\rm NL}$ during the post–inflationary period. The model parameters are $\Lambda^4 = m^2 f^2/4\pi^2$, $f = m = M_{\rm p}$, $\varphi_* = (\frac{1}{2} - 0.001)f$ and $\chi_* = 16.0M_{\rm p}$. For these model parameters, the χ field minimises before the φ field. *Left panel*: Equal decay rates, $\Gamma_\chi = \Gamma_\varphi$. *Right panel*: Unequal decay rates, $\Gamma_\chi \neq \Gamma_\varphi$. The solid vertical line denotes the end of inflation, $N_{\rm e}$, and the dashed lines denote the start of reheating, $N_{\varphi=0}$ (blue) and $N_{\chi=0}$ (black), respectively. All decay rates are given in unit of $\sqrt{W_0}M_{\rm p}$ here. Notice that $\tau_{\rm NL}$ changes by a few orders of magnitude during reheating. Also, $\tau_{\rm NL}$ is sensitive to Γ_χ and Γ_φ if there is a hierarchy between the two decay rates.

this sense, this scenario is similar to the curvaton model. Things are different after inflation ends however.

When inflation ends, the axion φ starts rolling down the ridge, producing a negative spike in $f_{\rm NL}$. $f_{\rm NL}$ then evolves to positive value when the φ field converges to its minimum as shown in the last Chapter. It is similar for $\tau_{\rm NL}$, except $\tau_{\rm NL}$ is always positive. In Fig. 5.8 we give the evolution of $\tau_{\rm NL}$ during reheating for various combinations of Γ_χ and Γ_φ. Similar to $f_{\rm NL}$, although the final value of $\tau_{\rm NL}$ is different from that at the end of inflation, it is almost completely insensitive to the decay rates if $\Gamma_\chi = \Gamma_\varphi$. Things are different however if there is a mild hierachy between Γ_χ and Γ_φ. When $\Gamma_\chi \neq \Gamma_\varphi$, the final value of $\tau_{\rm NL}$ does depend on the reheating timescale. Compared to the value where $\Gamma_\chi = \Gamma_\varphi$, it grows for $\Gamma_\varphi > \Gamma_\chi$ and decays for $\Gamma_\chi > \Gamma_\varphi$.

As mentioned earlier, unlike the one-minimum case, there is no scaling relation between $N_{\varphi\varphi}$ and N_φ. Yet by the observations that N_φ and $N_{\varphi\varphi}$ dominate over the first and second-order δN coefficients respectively, $\tau_{\rm NL}$ is approximately given by

$$\tau_{\rm NL} \approx \frac{N_{\varphi\varphi}^2}{N_\varphi^4}\,. \tag{5.11}$$

For $g_{\rm NL}$, things are similar to $f_{\rm NL}$ and $\tau_{\rm NL}$. In Fig. 5.9 we give the evolution of $g_{\rm NL}$ for different combinations of Γ_χ and Γ_φ, with the same model parameters. While the final

values of $g_{\rm NL}$ at the end of reheating is different from that at the end of inflation, they are almost completely insensitive to Γ_χ and Γ_φ unless there is a mild hierachy between the decay rates. Because of a hierachy between the third-order δN coefficients, $g_{\rm NL}$

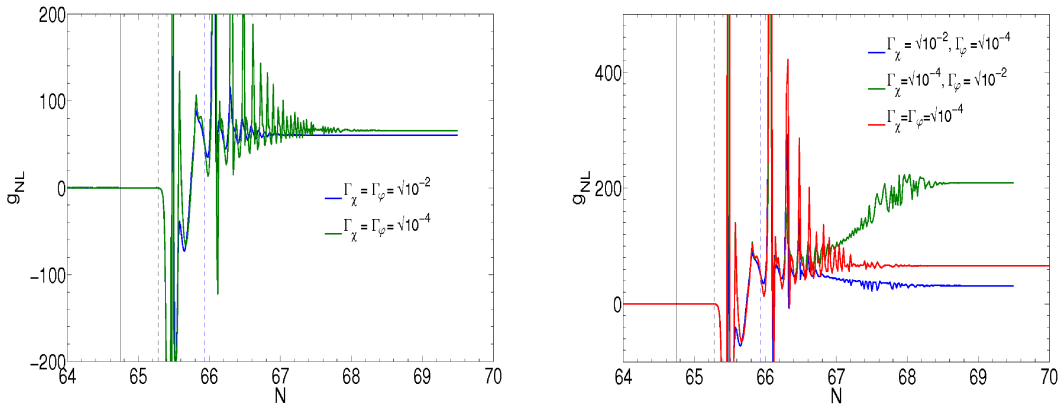

Figure 5.9: Potential: $W(\chi,\varphi) = W_0\left\{\frac{1}{2}m^2\chi^2 + \Lambda^4\left[1-\cos(\frac{2\pi}{f}\varphi)\right]\right\}$. The model parameters are $\Lambda^4 = m^2f^2/4\pi^2$, $\varphi_* = (\frac{1}{2}-0.001)f$, $\chi_* = 16M_{\rm p}$, $f = m = M_{\rm p}$. *Left panel*: Equal decay rates, $\Gamma_\chi = \Gamma_\varphi$; *Right panel*: Unequal decay rates, $\Gamma_\chi \neq \Gamma_\varphi$. Similar to $\tau_{\rm NL}$, $g_{\rm NL}$ changes by a few orders of magnitude during reheating and is more sensitive to the decay rates whenever there is a hierarchy between them. All decay rates are given in unit of $\sqrt{W_0}M_{\rm p}$ here. The solid vertical line denotes the end of inflation, $N_{\rm e}$, and the dashed lines denote the start of reheating, $N_{\varphi=0}$ (blue) and $N_{\chi=0}$ (black), respectively.

can be well approximated by

$$g_{\rm NL} \approx \frac{25}{54}\frac{N_{\varphi\varphi\varphi}}{N_\varphi^3}\,. \tag{5.12}$$

Although $g_{\rm NL}$ is again much smaller than the current CMB observational limit, unlike the one minimum model, $g_{\rm NL}$ is of the same order as $\tau_{\rm NL}$ in this model. This is a characteristic of the non-vacuum dominated sum-separable models. We will discuss this in further detail in Section 5.2.1.

Scale Dependence of non–linear parameters, $n_{f_{\rm NL}}$ and $n_{\tau_{\rm NL}}$

We now turn our attention to the spectral indices $n_{f_{\rm NL}}$ and $n_{\tau_{\rm NL}}$ in this model. Similar results are found as in the one-minimum case where $\lambda = 0.06$ where both spectral indices are negligible regardless of the decay rates and reheating timescale, with $n_{f_{\rm NL}}, n_{\tau_{\rm NL}} \ll O(0.1)$.

In Table 5.2 we summarise the two-minima model results, showing the comparison

between the primordial observables evaluated at the end of inflation (slow-roll stage) and at the end of reheating. The table clearly shows the non–linear parameters in multifield models strongly depend on the reheating timescale in general. Notice the large differences between the statistics evaluated at the end of inflation, compared to the end of reheating. This is because the axion field only begins to roll after inflation has ended and so until this point, the observables do not evolve appreciably.

End of Inflation						
$-$	$-$	$f_{\rm NL}$	$\tau_{\rm NL}$	$g_{\rm NL}$	$n_{f_{\rm NL}}$	$n_{\tau_{\rm NL}}$
$-$	$-$	0.006	1.3×10^{-3}	-3.1×10^{-5}	1.7×10^{-2}	4.9×10^{-4}
End of Reheating						
Γ_χ	Γ_φ	$f_{\rm NL}$	$\tau_{\rm NL}$	$g_{\rm NL}$	$n_{f_{\rm NL}}$	$n_{\tau_{\rm NL}}$
0	0	6.88	0.69×10^{2}	0.63×10^{2}	-1.2×10^{-6}	-1.8×10^{-6}
$\sqrt{10^{-2}}$	$\sqrt{10^{-2}}$	6.59	0.76×10^{2}	0.55×10^{2}	-9.3×10^{-7}	-1.6×10^{-6}
$\sqrt{10^{-2}}$	$\sqrt{10^{-4}}$	4.37	0.29×10^{2}	0.29×10^{2}	-7.2×10^{-7}	-1.2×10^{-6}
$\sqrt{10^{-4}}$	$\sqrt{10^{-2}}$	13.66	2.75×10^{2}	1.91×10^{2}	-2.5×10^{-6}	-3.7×10^{-6}
$\sqrt{10^{-4}}$	$\sqrt{10^{-4}}$	6.83	0.68×10^{2}	0.59×10^{2}	-1.1×10^{-6}	-1.7×10^{-6}

Table 5.2: Statistics of ζ for $W(\varphi,\chi)=W_0\left[\frac{1}{2}m^2\chi^2+\Lambda^4\left(1-\cos\left(\frac{2\pi}{f}\varphi\right)\right)\right]$ for different decay rates. All decay rates are in units of $\sqrt{W_0}M_{\rm p}$. We give values computed at the end of inflation (t_e) and at the completion of reheating (final) where ζ is conserved. The model parameters are $\Lambda^4=m^2f^2/4\pi^2$, $\varphi_*=(\frac{1}{2}-0.001)f$, $\chi_*=16M_{\rm p}$, $f=m=M_{\rm p}$. Note that the values in the second row where $\Gamma_\chi=\Gamma_\varphi=0$ do not correspond to end of reheating since the decay rates are zero. However an adiabatic limit is still reached as both φ and χ behave as matter fluids when oscillating about their minima.

5.2 Consistency Relations Between Observables

So far we have only considered each primordial observable individually. However, in general observables are not completely independent of one another. For some classes of models, there exists consistency relations between different observables. A simple example is the single-field slow-roll consistency relation. From Eq. (3.43) in Chapter 3, we can see that in canonical single field models the tensor-to-scalar ratio r and the spectral tilt of the tensor power spectrum $n_{\rm T}$ are always related by

$$r=-8n_{\rm T}\,. \tag{5.13}$$

This consistency relation has also been shown to hold for all potential-driven slow-roll inflation in the generalised G-inflation setup by Kobayashi et al. [151].

Similar to single field models, there also exists consistency relations in multifield models. While perturbative reheating in general leads to significant changes in individual primordial observables, particularly the non-linear parameters, as compared to the slow-roll predictions, consistency relations between the observables predicted under slow-roll, representing certain classes of models, seem to be more robust to reheating and therefore serve as a better discriminator to different models of inflation. We will see this in the following for some classes of canonical multifield models.

5.2.1 Relation Between $\tau_{\rm NL}$ and $g_{\rm NL}$

The first class of canonical multifield models we consider is models with non–vacuum dominated sum–separable potentials. For this class of models, by making use of the slow-roll analytic expressions for the δN coefficients, Elliston et al. [107] have shown that $g_{\rm NL}$ and $\tau_{\rm NL}$ are of the same order during slow-roll inflation

$$\frac{27}{25} g_{\rm NL} \approx \tau_{\rm NL} \,, \tag{5.14}$$

in the absence of significant terms beyond quadratic order in the potential. The effective two-field description of N–flation model Eq. (5.10) discussed previously is an example of this class.

Following the evolution of the third-order non-linear parameters $\tau_{\rm NL}$ and $g_{\rm NL}$ beyond slow-roll inflation, we see that this consistancy relation Eq. (5.14) survives through reheating, even though individually $\tau_{\rm NL}$ and $g_{\rm NL}$ do evolve. The relation holds beyond the slow-roll regime and during reheating for a wide range of mass ratios between the axion and inflaton where they both minimise after the end of inflation, only mildly violated when $\Gamma_\chi \gg \Gamma_\varphi$. This is illustrated in Fig. 5.10. A violation of this consistency relation could therefore rule out this class of models if reheating proceeds perturbatively.

The reason that $g_{\rm NL} \sim \tau_{\rm NL}$ regardless of subsequent evolution beyond slow-roll may be understood if we split the contributions to the non–linear parameters into instrinsic

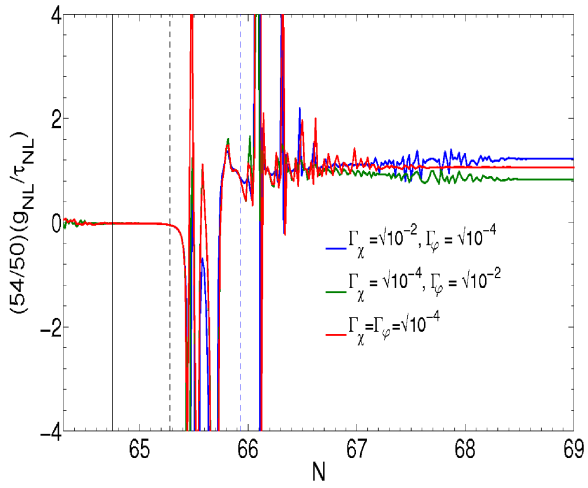

Figure 5.10: Potential: $W(\chi,\varphi) = W_0\left\{\frac{1}{2}m^2\chi^2 + \Lambda^4\left[1-\cos(\frac{2\pi}{f}\varphi)\right]\right\}$. The evolution of the ratio $(27/25)(g_{\rm NL}/\tau_{\rm NL})$ during reheating for different combinations of decay rates. The model parameters are $\Lambda^4 = m^2f^2/4\pi^2$, $\varphi_* = (\frac{1}{2}-0.001)f$, $\chi_* = 16M_{\rm p}$, $f = m = M_{\rm p}$. Notice that the relation Eq. (5.14) are satisfied after reheating in most cases, and only mildly violated when $\Gamma_\chi \gg \Gamma_\varphi$. All decay rates are given in unit of $\sqrt{W_0}M_{\rm p}$.

terms which depend on the instrinsic non–gaussianity of $\delta\varphi^I$ at late times and gauge terms which do not. This is more transparent in the moment transport technique developed by Mulryne et al. [152], where ζ is evaluated by evolving the field correlation functions from horizon–crossing to the time of interest, then gauge–transforming to ζ on an uniform energy hypersurface.

5.2.2 The Suyama-Yamaguchi (SY) Inequality

In general, $\tau_{\rm NL}(k_1,k_2,k_3,k_4)$ and $f_{\rm NL}(k_1,k_2,k_3)$ are functions of external momenta which cannot be compared directly. Yet in canonical models, when the non–Gaussianity is large, it is dominated by the shape independent parts. It is thus reasonable to compare the non–linear parameters directly in such models.

The Suyama-Yamaguchi inequality, for instance, relates $f_{\rm NL}$ in the squeezed limit $(k_1 \to 0)$ to $\tau_{\rm NL}$ in the collapsed limit $(k_1+k_2 \to 0)$ [144]

$$\tau_{\rm NL} \geq \left(\frac{6}{5}f_{\rm NL}\right)^2 . \tag{5.15}$$

This inequality follows simply from the Cauchy-Schwarz inequality and has been studied and verified extensively in the literature, see e.g. [153, 154, 155, 156, 157, 158,

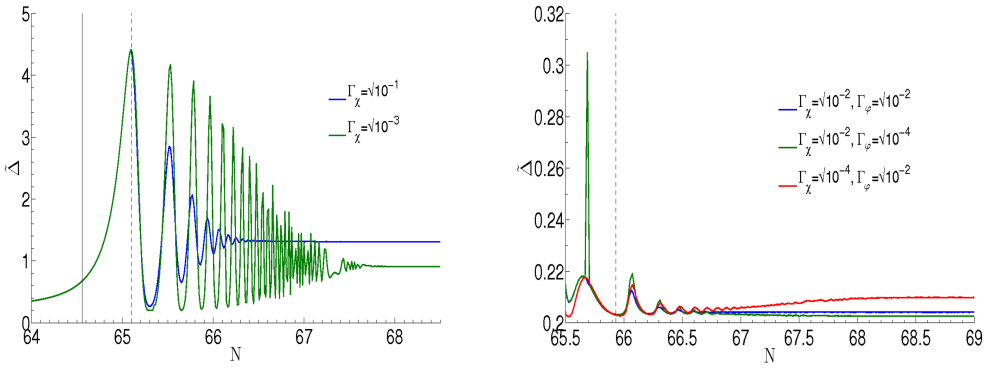

Figure 5.11: Fractional difference between $25\tau_{\rm NL}/36$ and $f^2_{\rm NL}$ after inflation ends. *Left panel*: Potential: $W(\varphi,\chi) = W_0\chi^2 e^{-\lambda\varphi^2/M_{\rm p}^2}$. The model parameters are $\lambda = 0.05$, $\varphi_* = 10^{-3}M_{\rm p}$ and $\chi_* = 16.0M_{\rm p}$. *Right panel*: Potential: $W(\chi,\varphi) = W_0\left\{\frac{1}{2}m^2\chi^2 + \Lambda^4\left[1-\cos(\frac{2\pi}{f}\varphi)\right]\right\}$. The model parameters are $\Lambda^4 = m^2f^2/4\pi^2$, $\varphi_* = (\frac{1}{2}-0.001)f$, $\chi_* = 16M_{\rm p}$, $f = m = M_{\rm p}$. All decay rates are given in units of $\sqrt{W_0}$ or $\sqrt{W_0}M_{\rm p}$. Here the solid vertical line denotes the end of inflation, $N_{\rm e}$, and the dashed line denotes the start of reheating, $N_{\chi=0}$.

159]. Here the equality in Eq. (5.15) holds for single–source models [153]. For a recent review about the inequality, see [160].

While the inequality suggests $\tau_{\rm NL}$ can be very much larger than $f^2_{\rm NL}$, recently Peterson et al.[105] have shown that this is not the case in two–field canonical models in general by applying both the slow-roll and slow-turn approximations without excessive fine-tuning. This was also shown by Elliston et al. [107] for separable potentials in the slow-roll limit. Here we are interested to see if this remains true beyond the slow-roll limit, particularly after a period of perturbative reheating.

In Fig. 5.11, we plot the fractional difference between $\tau_{\rm NL}$ and $f^2_{\rm NL}$ in the two models discussed in this Chapter, defined as

$$\tilde{\Delta} \equiv \frac{(25\tau_{\rm NL}/36) - f^2_{\rm NL}}{f^2_{\rm NL}}\,. \tag{5.16}$$

Equality here corresponds to $\tilde{\Delta} = 0$, whereas $\tilde{\Delta} \gg 1$ if $\tau_{\rm NL}$ is very much larger than $f^2_{\rm NL}$. From the plots, we see that while reheating may enlarge the difference between $\tau_{\rm NL}$ and $f^2_{\rm NL}$, $\tilde{\Delta}$ never becomes much larger than unity and $\tau_{\rm NL}$ remains not much larger than $f^2_{\rm NL}$ for a wide range of decay rates that vary by a few orders of magnitude. We may conclude that an observation $\tau_{\rm NL} \gg f^2_{\rm NL}$ could put canonical two-field models under tension if reheating takes place perturbatively.

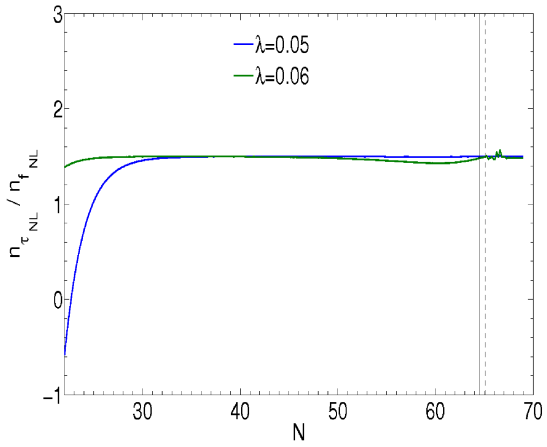

Figure 5.12: Potential: $W(\chi,\varphi) = W_0\chi^2 e^{-\lambda\varphi^2/M_{\rm p}^2}$. The evolution of the ratio $n_{\tau_{\rm NL}}/n_{f_{\rm NL}}$ until the completion of reheating. The model parameters are $\lambda = \{0.05,\, 0.06\}$, $\varphi_* = 10^{-3}Mp$, $\chi_* = 16M_{\rm p}$ and $\Gamma_\chi = \sqrt{0.3W_0}$. The ratio settles to $3/2$ quickly after about 30 e–folds of inflation after horizon-exit, showing the consistency relation Eq. (5.17) is satisfied.

5.2.3 Relation Between the Scale Dependence of Bi- and Trispectra

Next we investigate any possible relations between the spectral indices $n_{f_{\rm NL}}$ and $n_{\tau_{\rm NL}}$. We found that whether $n_{f_{\rm NL}}$ and $n_{\tau_{\rm NL}}$ are of a detectable level or not after reheating, for both the one-minimum and two-minima models discussed, they always satisfy the following consistency relation

$$n_{\tau_{\rm NL}} = \frac{3}{2} n_{f_{\rm NL}}\,, \tag{5.17}$$

regardless of the reheating timescale. For instance, see Figs. 5.12 and 5.13 for the quadratic exponential Eq. (5.1) and effective N-axion models Eq. (5.10) respectively.

This relation Eq. (5.17) was first found by Byrnes et al. [60] in the class of two–field local type models with ζ of the form

$$\zeta(k) = \zeta_k^{G,\varphi} + \zeta_k^{G,\chi} + f_\varphi(\zeta^{G,\varphi} \star \zeta^{G,\varphi})_k + g_\varphi(\zeta^{G,\varphi} \star \zeta^{G,\varphi} \star \zeta^{G,\varphi})_k\,, \tag{5.18}$$

when f_φ and g_φ are some scale independent functions and $\zeta^{G,\varphi}$, $\zeta^{G,\chi}$ are Gaussian variables. Again $\star$ denotes convolution in momentum space. For all models considered only one of the fields acquires significant deviation from a Gaussian statistic after horizon-exit, so they fit into this ansatz. The question is whether f_φ and g_φ are scale independent, for the models we study. They are if the field which generates non-

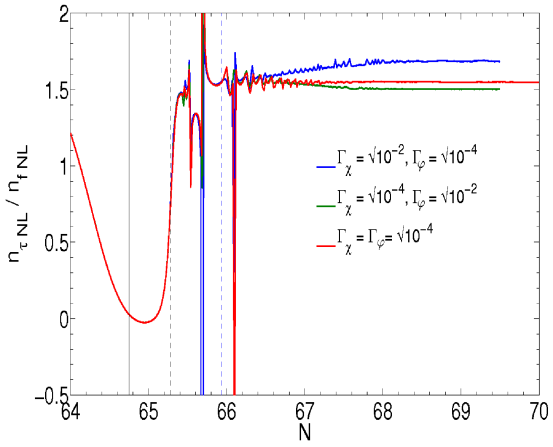

Figure 5.13: Potential: $W(\varphi,\chi) = W_0\left\{\frac{1}{2}m^2\chi^2 + \Lambda^4\left[1 - cos(\frac{2\pi}{f}\varphi)\right]\right\}$. The evolution of the ratio $n_{\tau_{\rm NL}}/n_{f_{\rm NL}}$ during post–inflationary period. The model parameters are $\Lambda^4 = m^2f^2/4\pi^2$, $f = m = M_{\rm p}$, $\varphi_* = 0.499Mp$, $\chi_* = 16M_{\rm p}$. Here the decay rates Γ_φ and Γ_χ are given in unit of $\sqrt{W_0}M_p$. The solid vertical line denotes the end of inflation, $N_{\rm e}$, and the dashed lines denote the start of reheating times, $N_{\chi=0}$ (blue) and $N_{\varphi=0}$ (black), respectively. Here axion φ reheats first.

Gaussianity is strongly subdominant, has negligible interactions with the inflaton field and a quadratic potential. Many of the models we study are approximately of this type, and hence we often observe $3n_{f_{\rm NL}} \simeq 2n_{\tau_{\rm NL}}$.

On the other hand, for single source models there is a different consistency relation, which trivially follows from $\tau_{\rm NL} = 36f_{\rm NL}^2/25$,

$$n_{\tau_{\rm NL}} = 2n_{f_{\rm NL}}\,. \tag{5.19}$$

In the limit that $\zeta_k^{G,\varphi} \ll \zeta_k^{G,\chi}$, which corresponds to $N_\chi^2 \gg \max\left\{N_\varphi^2, 1\right\}$, the model becomes effectively single source. If the assumptions discussed earlier remain valid, the non-linearity parameters then have to be scale independent.

5.3 Additional Comments on $g_{\rm NL}$

So far for all two–field models considered in the literature, $g_{\rm NL}$ is at most of the same order of magnitude as $\tau_{\rm NL}$ and is much less than the current observational limit in CMB experiments and large scale surveys which is about $O(10^5)$. Using slow-roll analytic expressions and heatmap analysis, Elliston et al. have shown that it is hard to engineer a model where $g_{\rm NL}$ can be as large as $O(10^5)$ during inflation and dominates

the statistics in the trispectrum for canonical separable potentials, even if one goes beyond quadratic order in the potential [107].

This however only applies to slow-roll inflation regime. It remains to be seen beyond the slow-roll regime. In particular, $g_{\rm NL}$ could be dramatically enhanced such that it is above the observational limit after reheating. Yet we found the same conclusion in the simple setup of perturbative reheating in all models considered. For the effective N-flation model, $g_{\rm NL}$ does increase dramatically from 0 to $O(100)$ for some of the combinations of decay rates, for instance see Fig. 5.8. One may expect that a larger hierarchy between the decay rates may thus produce a large observable $g_{\rm NL}$. However we argue that this could require $\Gamma_\varphi^2/\Gamma_\chi^2 \gg O(10^3)$ and is beyond the numerical capabilities of our code.

5.4 Conclusion

In this Chapter, we have extended the discussion on the influence of reheating to the trispectrum of ζ and possible consistency relations between observables. Similar to the bispectrum, the trispectrum continues to evolve after inflation ends with the presence of isocurvature perturbations and so do the corresponding non-linear parameters $\tau_{\rm NL}$ and $g_{\rm NL}$ in general. Moreover, the trispectrum in general is sensitive to the decay rates during reheating, although in some cases in which both fields oscillate during inflation, the sensitivity to the decay rates can be very small provided that they are equal for both fields. The evolution during reheating is significant enough that a comparison between observables and their values at the end of inflation would typically lead to the wrong conclusions, since the change in observables may be larger than the expected error bars of the observables. While the evolution to an adiabatic attractor during inflation often (but by no means always) results in negligible non-Gaussianity [107, 131, 161, 162], this is not the case during reheating, typically a model which is non-Gaussian at the end of inflation will remain non-Gaussian, and in most cases which we studied, the sign of the non-linearity parameters will also remain the same. The reverse is not always true, we have seen how in the axion model the perturbations are Gaussian at the end of inflation but not at the end of reheating.

Despite ζ-related observables typically evolving during reheating, it could still be possible to test models of multifield inflation against the new observational data without specifying the reheating dynamics. For instance, we could look for consistency relations between the non-linear parameters. First of all, it is very hard to engineer a two-field canonical model where $\tau_{\rm NL} \gg f_{\rm NL}^2$, regardless of the reheating dynamics. Interestingly, we have also seen that the consistency relation in non-vacuum sum-separable models $g_{\rm NL} \simeq \tau_{\rm NL}$ typically remains true during reheating. Given the observational bounds on $\tau_{\rm NL}$, it will be hard to observe $g_{\rm NL}$ in such models. Finally we have also discussed the relation between $n_{f_{\rm NL}}$ and $n_{\tau_{\rm NL}}$, showing that in many cases $3n_{f_{\rm NL}} \simeq 2n_{\tau_{\rm NL}}$ both during and after inflation. These relations between observables allow the underlying inflation models to be tested even when one cannot predict the actual values of some model parameters, particularly the reheating parameters.

Chapter 6

Conformal Inflation

In this chapter, we introduce a new class of two-field inflation models which are locally scale invariant (or Weyl invariant). This is known as conformal inflation, first introduced by Kallosh and Linde [3]. Although this is a two-field model, because of the local scale invariance symmetry, only one scalar degree of freedom is physical. Thus this model is in fact equivalent to the case of single-field inflation and perturbations are purely adiabatic. Unlike the class of two-field inflation models discussed previously, ζ and therefore the corresponding model predictions are conserved after horizon-exit. Subsequent (p)reheating does not change the model predictions as long as perturbations remain purely adiabatic. Motivated by the original model, we are interested in studying how universality classes arise in conformal inflation in general, beyond the original paradigm.

In Section 6.1, we first introduce Kallosh and Linde's original conformal inflation model and discuss its universal behaviour. In Section 6.2 and 6.3, we discuss how one would go beyond the original paradigm and construct the most general bi-scalar conformal inflation model with global $SO(1,1)$ symmetry. We then move on to discuss whether the universal behaviour of the original model is extended to the generalised model, particularly focussing on the class of K-inflation models. Finally motivated by BICEP2, we discuss the possibility of realising a different universality class with a large r in the context of conformal inflation in Section 6.6.

6.1 The Original Model

Consider the following bi-scalar theory with canonical kinetic terms (up to a negative sign for the π field) and the scalar fields non-minimally coupled to the scalar curvature $R(g)$

$$S = \int \mathrm{d}^4x\sqrt{-g}\left[\frac{1}{2}\partial_\mu\pi\partial^\mu\pi - \frac{1}{2}\partial_\mu\chi\partial^\mu\chi + \frac{\pi^2-\chi^2}{12}R(g) - \frac{1}{36}F\left(\frac{\chi}{\pi}\right)\left(\chi^2-\pi^2\right)^2\right], \tag{6.1}$$

where F is an arbitrary function of χ/π. This theory is locally scale invariant, i.e. invariant under the following transformations

$$g_{\mu\nu} \to e^{-2\sigma(x)}g_{\mu\nu}\,,\ \pi \to e^{\sigma(x)}\pi\,,\ \chi \to e^{\sigma(x)}\chi\,, \tag{6.2}$$

for any $\sigma(x)$. In the case F is a constant function, i.e. $F = \mathrm{const}$, there is also a global $SO(1,1)$ symmetry between the π and χ field. Here the π field is often referred to as a conformal compensator or conformon field. Its kinetic term comes with the wrong sign. Yet it is not a ghost field, since with the scale-invariance symmetry, only one scalar degree of freedom is in fact physical. [1] The unphysical degree of freedom can be removed from the theory by gauge fixing π.

Motivated from the superconformal formulation of supergravity, this model was first introduced by Kallosh and Linde [3], where π and χ are moduli fields. Gauge fixing was interpreted as a spontaneous symmetry breaking due to existence of a classical field. The global $SO(1,1)$ symmetry between the π and χ field is restored near the boundary of the moduli space where $\pi, \chi \to \infty$, and is originated from $SU(1,1)$ symmetry of the embedding Kahler manifold. This is the enhanced symmetry point where critical phenomenon happens, as we will see later. The model was later extended to the multifield paradigm [163].

To study this model, we need to first fix the gauge. An example would be the gauge

[1] This is true classically. Quantum corrections in general lead to conformal anomalies which break the local scale-invariance symmetry.

$\pi = \sqrt{6}M_{\rm p}$. The full Lagrangian then becomes

$$\mathcal{L} = \sqrt{-g}\left[\frac{M_{\rm p}^2 R}{2}\left(1 - \frac{\chi^2}{6M_{\rm p}^2}\right) - \frac{1}{2}\partial_\mu\chi\partial^\mu\chi - F(\chi/\sqrt{6}M_{\rm p})\left(\frac{\chi^2}{6M_{\rm p}^2} - 1\right)^2\right], \quad (6.3)$$

which is in the Jordan frame. To work out the model predictions, one could perform a conformal transformation on the metric $g_{\mu\nu}$ and write the theory in the Einstein frame. Alternatively, because of the global $SO(1,1)$ symmetry, it is convenient to choose the following gauge

$$\pi^2 - \chi^2 = 6M_{\rm p}^2\,. \quad (6.4)$$

Upon fixing this gauge, the action Eq. (6.1) is automatically in the Einstein frame, and reduces to

$$S = \int \mathrm{d}^4x\sqrt{-g}\left[\frac{M_{\rm p}^2 R}{2} - \frac{1}{2}(\partial\varphi)^2 - F[\tanh(\varphi/\sqrt{6}M_{\rm p})]\right], \quad (6.5)$$

where φ is the canonically-normalised field, defined by $\pi = \sqrt{6}M_{\rm p}\cosh(\varphi/\sqrt{6}M_{\rm p})$ and $\chi = \sqrt{6}M_{\rm p}\sinh(\varphi/\sqrt{6}M_{\rm p})$. This gauge is referred to as the rapidity gauge by Kallosh and Linde because of the similarity between φ and rapidity in special relativity. From Eq. (6.5), we can see the gauge-fixed theory is equivalent to chaotic single field models. In general the function F is arbitrary and can take any form. However, arguing from the original bi-scalar action Eq. (6.1), we expect the function F to be some analytic function of the gauge-invariant variable

$$\tilde{\varphi} \equiv \chi/\pi \quad (6.6)$$

as in the standard approach to chaotic inflation. This restricts the form of the function F and we shall see this leads to a universal class of inflation models in some appropriate limit.

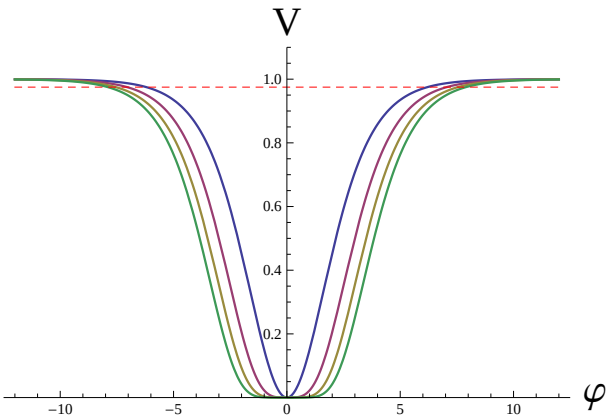

Figure 6.1: The T-model motivated from conformal inflation where the potential is given by $V = \tanh^{2n}(\varphi/\sqrt{6}M_{\rm p})$ for $n = 1$(blue), 2(red), 3(brown), 4(green), in units of $M_{\rm p}$. Credit Kallosh and Linde [3].

Universal Predictions from Conformal Inflation

Recall that the arbitrary function F deforms the global $SO(1,1)$ symmetry between the two fields. Now consider model Eq. (6.5) in the large φ limit, where $\tanh(\varphi/\sqrt{6}M_{\rm p}) \to 1$ and $F \to \text{const}$ asymptotically and the $SO(1,1)$ symmetry is restored. This is also the region where slow-roll inflation naturally occurs, since $V(\varphi) = F(\varphi) \approx \text{const}$ and thus dominate over the gradient term.

For a simple set of functions $F(\tilde{\varphi}) = \lambda\tilde{\varphi}^{2n}$, in terms of the canonically normalised field φ, one finds

$$V(\varphi) = F[\tanh(\varphi/\sqrt{6}M_{\rm p})] = \lambda_n \tanh^{2n}(\varphi/\sqrt{6}M_{\rm p})\,. \tag{6.7}$$

for some constants λ_n which is of mass dimension 4. This is a basis representative of the universality class of models depending on $\tanh(\varphi/\sqrt{6}M_{\rm p})$ and is called the T-model by Kallosh and Linde [3]. In Fig. 6.1, we plot how the potential looks like as function of the canonically-normalised field φ.

Near the boundary of moduli space, or the large φ limit, to leading order, the potential Eq. (6.7) is approximately given by

$$V(\varphi) = \lambda_n[1 - 4ne^{-\sqrt{2/3}(\varphi/M_{\rm p})}]\,. \tag{6.8}$$

λ_n sets the energy scale of inflation and again can be fixed by the CMB normalisation.

This universal form of the potential around the critical point leads to universal predictions in this model. To see this, we first write the slow-roll field equation for φ in terms of the number of e-folds N

$$\frac{\mathrm{d}\varphi}{\mathrm{d}N} \approx -M_{\mathrm{p}}^2 \frac{V_\varphi}{V} \approx -4nM_{\mathrm{p}}\sqrt{\frac{2}{3}}e^{-\sqrt{2/3}(\varphi/M_{\mathrm{p}})}\,. \tag{6.9}$$

Integrating this, we get

$$e^{-(\sqrt{2/3})\Delta\varphi/M_{\mathrm{p}}} = \frac{3}{8nN}\,, \tag{6.10}$$

where $\Delta\varphi$ denotes the field range of φ over the course of N e-folds of expansion. In the large N limit, where the initial field value φ_* is large, this reduces to

$$e^{-\sqrt{2/3}(\varphi_*/M_{\mathrm{p}})} = \frac{3}{8nN}\,. \tag{6.11}$$

Using these, we can write the slow-roll parameters at horizon-exit t_* as

$$(\epsilon_V)_* \equiv \frac{M_{\mathrm{p}}^2}{2}\left(\frac{V_\varphi}{V}\right)_*^2 \approx \frac{3}{4N^2}\,,\;\; (\eta_V)_* \equiv M_{\mathrm{p}}^2\left(\frac{V_{\varphi\varphi}}{V}\right)_* \approx \frac{1}{N}\,. \tag{6.12}$$

Recalling that in the single-field canonical models, the spectral index n_{s} and tensor-to-scalar ratio r can be expressed purely in terms of the slow-roll parameters at horizon-exit, we therefore have

$$n_{\mathrm{s}} - 1 = -2/N\,,\;\; r = 12/N^2\,. \tag{6.13}$$

This is the universal prediction of the model. Given the number of e-folds of inflation after the observed CMB pivot scale leaves the horizon, we have universal predictions for n_{s} and r regardless of the form of the potential V. For instance, $n_{\mathrm{s}} \approx 0.967$ and $r \approx 0.0032$ for $N \approx 60$, which are in perfect agreement with the recent Planck results [44]. [2]

This universal behaviour is a critical phenomenon near the point of enhanced symmetry where the global $SO(1,1)$ symmetry is restored. In fact, the $SO(1,1)$ symmetry

[2] But not with BICEP2

manifests itself as a shift symmetry in φ in the single-field description after gauge fixing, see [164] for relevant discussion.

Besides universal predictions, it was argued that conformal inflation also sets the initial conditions for inflation under the Damour-Polyakov mechanism if the model is coupled to non-relativistic matter [165]. Similar model setups have also been discussed in the context of the cyclic Higgs model [166].

6.2 Beyond the Original Model, Generalised Conformal Inflation

While Kallosh and Linde's original model is simple, it is possible to generalise their models to non-canonical case that involves higher-order derivatives. In fact, the most general scale invariant bi-scalar theory with at most second-order field equations was first found by Padilla et al. by performing the following field redefinitions on the Horndeski action $S_{\rm Horn}[\tilde{g}_{\mu\nu},\tilde{\varphi}]$ [167]

$$\tilde{\varphi}\to\chi/\pi\,,\quad \tilde{g}_{\mu\nu}\to\pi^2 g_{\mu\nu}\,, \tag{6.14}$$

where $S_{\rm Horn}[\tilde{g}_{\mu\nu},\tilde{\varphi}]$ is given by [168]

$$\begin{aligned} S_{\rm Horn}[\tilde{\varphi},\tilde{g}_{\mu\nu}] = \int d^4x\sqrt{-\tilde{g}}\Big[&K(\tilde{\varphi},\tilde{X})-G_3(\tilde{\varphi},\tilde{X})\tilde{\mathcal{E}}_1+G_4(\tilde{\varphi},\tilde{X})\tilde{R}+G_{4,\tilde{X}}\tilde{\mathcal{E}}_2\\ &+G_5(\tilde{\varphi},\tilde{X})\tilde{G}_{\mu\nu}\tilde{\nabla}^\mu\tilde{\nabla}^\nu\tilde{\varphi}-G_{5,\tilde{X}}\tilde{\mathcal{E}}_3/6\Big]\,. \end{aligned} \tag{6.15}$$

Here $\tilde{X}\equiv-\frac{1}{2}(\nabla\tilde{\varphi})^2$, $\tilde{\mathcal{E}}_n = n!\nabla_{[\mu_1}\nabla^{\mu_1}\tilde{\varphi}...\nabla_{\mu_n]}\nabla^{\mu_n}\tilde{\varphi}$ where the anti-symmetriser acts only on the lower indices. $G_{\mu\nu}$ is the Einstein tensor, $\tilde{R}$ is the Ricci scalar, both built from the metric $\tilde{g}_{\mu\nu}$, and K, G_3, G_4 and G_5 are arbitrary functions of $\tilde{X}$ and $\tilde{\varphi}$. Subscripts $\tilde{\varphi}$ and $\tilde{X}$ denote partial differentiations with respect to $\tilde{\varphi}$ and $\tilde{X}$ respectively.

The resulting action $S_{\rm local}[\chi,\pi,g_{\mu\nu}]$ can be expressed in the form as Eq. (6.15), with

the relevant terms in terms of π and χ fields given by

$$\sqrt{-\tilde{g}} = \sqrt{-g}\pi^4\,,\;\; \tilde{R} = \pi^{-2}R - 6\pi^{-3}\Box\pi\,,\;\; \tilde{X} = \frac{X_{\chi\chi}}{\pi^4} - \frac{2\chi X_{\chi\pi}}{\pi^5} + \frac{\chi^2 X_{\pi\pi}}{\pi^6}$$
$$\tilde{G}^{\mu\nu} = \pi^{-4}G^{\mu\nu} + 4\pi^{-6}\nabla^\mu\pi\nabla^\nu\pi - \pi^{-6}g^{\mu\nu}\nabla^\kappa\pi\nabla_\kappa\pi - 2\pi^{-5}\nabla^\mu\nabla^\nu\pi + 2g^{\mu\nu}\pi^{-5}\Box\pi$$
$$\tilde{\nabla}_\mu\tilde{\nabla}_\nu\tilde{\varphi} = \pi^{-1}\nabla_\mu\nabla_\nu\chi - \chi\,\pi^{-2}\nabla_\mu\nabla_\nu\pi - 4\pi^{-2}\nabla_{(\mu}\chi\nabla_{\nu)}\pi + \pi^{-2}g_{\mu\nu}\nabla^\alpha\pi\nabla_\alpha\chi$$
$$+4\chi\,\pi^{-3}\nabla_\mu\pi\nabla_\nu\pi - \chi\,\pi^{-3}g_{\mu\nu}\nabla^\alpha\pi\nabla_\alpha\pi \tag{6.16}$$

and

$$\tilde{\mathcal{E}}_1 = \tilde{\Box}\tilde{\varphi} = \pi^{-3}\Box\chi - \chi\,\pi^{-4}\Box\pi$$
$$\tilde{\mathcal{E}}_2 = 2\delta^{\mu_1}_{[\mu_2}\delta^{\mu_3}_{\mu_4]}\big(\pi^{-3}\nabla_{\mu_1}\nabla^{\mu_2}\chi - \chi\pi^{-4}\nabla_{\mu_1}\nabla^{\mu_2}\pi - 2\pi^{-4}\nabla_{\mu_1}\chi\nabla^{\mu_2}\pi - 2\pi^{-4}\nabla^{\mu_2}\chi\nabla_{\mu_1}\pi$$
$$+\pi^{-4}\delta^{\mu_2}_{\mu_1}\nabla^\alpha\pi\nabla_\alpha\chi + 4\chi\,\pi^{-5}\nabla_{\mu_1}\pi\nabla^{\mu_2}\pi - \chi\,\pi^{-5}\delta^{\mu_2}_{\mu_1}\nabla^\alpha\pi\nabla_\alpha\pi\big)\big(\pi^{-3}\nabla_{\mu_3}\nabla^{\mu_4}\chi$$
$$-\chi\,\pi^{-4}\nabla_{\mu_3}\nabla^{\mu_4}\pi - 2\pi^{-4}\nabla_{\mu_3}\chi\nabla^{\mu_4}\pi - 2\pi^{-4}\nabla^{\mu_4}\chi\nabla_{\mu_3}\pi + \pi^{-4}\delta^{\mu_4}_{\mu_3}\nabla^\alpha\pi\nabla_\alpha\chi$$
$$+4\chi\,\pi^{-5}\nabla_{\mu_3}\pi\nabla^{\mu_4}\pi - \chi\,\pi^{-5}\delta^{\mu_4}_{\mu_3}\nabla^\alpha\pi\nabla_\alpha\pi\big)$$
$$\tilde{\mathcal{E}}_3 = 6\delta^{\mu_1}_{[\mu_2}\delta^{\mu_3}_{\mu_4}\delta^{\mu_5}_{\mu_6]}\big(\pi^{-3}\nabla_{\mu_1}\nabla^{\mu_2}\chi - \chi\,\pi^{-4}\nabla_{\mu_1}\nabla^{\mu_2}\pi - 2\pi^{-4}\nabla_{\mu_1}\chi\nabla^{\mu_2}\pi$$
$$-2\pi^{-4}\nabla^{\mu_2}\chi\nabla_{\mu_1}\pi + \pi^{-4}\delta^{\mu_2}_{\mu_1}\nabla^\alpha\pi\nabla_\alpha\chi + 4\chi\,\pi^{-5}\nabla_{\mu_1}\pi\nabla^{\mu_2}\pi - \chi\,\pi^{-5}\delta^{\mu_2}_{\mu_1}\nabla^\alpha\pi\nabla_\alpha\pi\big)$$
$$\big(\pi^{-3}\nabla_{\mu_3}\nabla^{\mu_4}\chi - \chi\,\pi^{-4}\nabla_{\mu_3}\nabla^{\mu_4}\pi - 2\pi^{-4}\nabla_{\mu_3}\chi\nabla^{\mu_4}\pi - 2\pi^{-4}\nabla^{\mu_4}\chi\nabla_{\mu_3}\pi$$
$$+\pi^{-4}\delta^{\mu_4}_{\mu_3}\nabla^\alpha\pi\nabla_\alpha\chi + 4\chi\,\pi^{-5}\nabla_{\mu_3}\pi\nabla^{\mu_4}\pi - \chi\,\pi^{-5}\delta^{\mu_4}_{\mu_3}\nabla^\alpha\pi\nabla_\alpha\pi\big)\big(\pi^{-3}\nabla_{\mu_5}\nabla^{\mu_6}\chi$$
$$-\chi\,\pi^{-4}\nabla_{\mu_5}\nabla^{\mu_6}\pi - 2\pi^{-4}\nabla_{\mu_5}\chi\nabla^{\mu_6}\pi - 2\pi^{-4}\nabla^{\mu_6}\chi\nabla_{\mu_5}\pi + \pi^{-4}\delta^{\mu_6}_{\mu_5}\nabla^\alpha\pi\nabla_\alpha\chi$$
$$+4\chi\,\pi^{-5}\nabla_{\mu_5}\pi\nabla^{\mu_6}\pi - \chi\,\pi^{-5}\delta^{\mu_6}_{\mu_5}\nabla^\alpha\pi\nabla_\alpha\pi\big) \tag{6.17}$$

Here $X_{\chi\pi} \equiv -\frac{1}{2}g^{\mu\nu}\nabla_\mu\chi\nabla_\nu\pi$ and similarly for $X_{\pi\pi}$, $X_{\chi\chi}$. Note that this action is invariant under the interchange of π and χ. The most general conformal bi-scalar inflation model can be constructed by imposing slow-roll conditions to the action $S_{\rm local}[\chi,\pi,g_{\mu\nu}]$. As discussed previously, because of local scale invariance, one scalar degree of freedom can be gauged away and the gauge-fixed model is equivalent to the most general scalar-tensor Horndeski theory.

Here in this thesis, we are interested in the $SO(1,1)$ (or shift symmetric) subset of the whole bi-scalar conformal inflation models. In particular, we are going to study the possible critical phenomenon for generalised bi-scalar conformal inflation models that admit an enhanced $SO(1,1)$ symmetry point, to see if the same universal behaviour

emerges as in the original conformal inflation model.

6.3 Constructing the Most General Bi-scalar Local Scale Invariant Model with $SO(1,1)$ Symmetry

To start with, we discuss how one could construct the most general bi-scalar local scale invariant theory with $SO(1,1)$ symmetry between the two fields. For any bi-scalar models that possess global $SO(1,1)$ symmetry between the scalar fields φ^I, the action must be invariant under the Lorentz transformation $\varphi^I \to \Lambda^I_J \varphi^I$

$$S[\varphi^I, g_{\mu\nu}] \to S'[\Lambda^I_J \varphi^I, g_{\mu\nu}] = S[\varphi^I, g_{\mu\nu}] = \int \mathrm{d}^4x\sqrt{-g}\mathcal{L}[\varphi^I, g_{\mu\nu}]\,, \tag{6.18}$$

or in other words, the Lagrangian $\mathcal{L}$ transforms up to some total derivatives. Here I, J run from 1 to 2 and the transformation matrix is given by

$$\Lambda^I_J = \begin{pmatrix} \cosh\vartheta & -\sinh\vartheta \\ -\sinh\vartheta & \cosh\vartheta \end{pmatrix}\,, \tag{6.19}$$

where ϑ is some dimensionless constant. Take $\varphi^I = (\chi, \pi)$ and consider an infinitesimal Lorentz transformation, $\chi \to \chi - \vartheta\pi$ and $\pi \to \pi - \vartheta\chi$. The change in the Lagrangian $\mathcal{L}$ is given by

$$\begin{aligned}\Delta\mathcal{L} &= \vartheta\nabla_\mu\left[\frac{\partial\mathcal{L}}{\partial(\nabla_\mu)\chi}\pi + \frac{\partial\mathcal{L}}{\partial(\nabla_\mu)\pi}\chi\right] \\ &+\vartheta\left\{\left[\frac{\partial\mathcal{L}}{\partial\chi} - \nabla_\mu\left(\frac{\partial\mathcal{L}}{\partial(\nabla_\mu\chi)}\right)\right]\pi + \left[\frac{\partial\mathcal{L}}{\partial\pi} - \nabla_\mu\left(\frac{\partial\mathcal{L}}{\partial(\nabla_\mu\pi)}\right)\right]\chi\right\}\,.\end{aligned} \tag{6.20}$$

The first term is a total derivative, which corresponds to the conserved current, whereas the second term is proportional to the EOM, which is guaranteed to vanish on-shell. This is Noether's theorem. However, because we are interested in the case where the $SO(1,1)$ symmetry is a global off-shell symmetry, i.e. the symmetry holds for any field configurations π, χ and metric $g_{\mu\nu}$, the second term in Eq. (6.20) must vanish up

to some total derivatives. This gives a constraint on the form of $\mathcal{L}$

$$\left[\frac{\partial\mathcal{L}}{\partial\chi}-\nabla_\mu\left(\frac{\partial\mathcal{L}}{\partial(\nabla_\mu\chi)}\right)\right]\pi+\left[\frac{\partial\mathcal{L}}{\partial\pi}-\nabla_\mu\left(\frac{\partial\mathcal{L}}{\partial(\nabla_\mu\pi)}\right)\right]\chi$$
$$=\text{sum of total derivatives}. \quad (6.21)$$

To find the subset of the bi-scalar local scale-invariant models that respect $SO(1,1)$ symmetry as well, we apply the constraint Eq. (6.21) to the most general bi-scalar local scale invariant theory $\mathcal{L}_{\rm local}[\chi,\pi,g_{\mu\nu}]$.

As an example, we consider the K-essence case, where the Lagrangian is given by

$$\mathcal{L}=\sqrt{-\tilde{g}}\left[K(\tilde{\varphi},\tilde{X})+G_4(\tilde{\varphi})\tilde{R}\right], \quad (6.22)$$

or in terms of χ, π and $g_{\mu\nu}$

$$\mathcal{L}=\sqrt{-g}\left\{\pi^4K+G_4\pi^2R+6(\nabla\pi)^2G_4+6G_{4,\tilde{\varphi}}(\nabla\pi)\cdot\left[(\nabla\chi)-\frac{\chi}{\pi}(\nabla\pi)\right]\right\}. \quad (6.23)$$

Here we have suppressed the arguments in K and G_4. Varying this Lagrangian $\mathcal{L}$ with respect to χ, π, $\nabla\chi$ and $\nabla\pi$, we have

$$\begin{aligned}
\frac{\partial\mathcal{L}}{\partial\chi}&=\sqrt{-g}\left\{\pi^3K_{\tilde{\chi}}+\pi RG_{4,\tilde{\varphi}}+(K_{\tilde{X}}+6G_{4,\tilde{\varphi}\tilde{\varphi}})\left[\frac{(\nabla\pi)\cdot(\nabla\chi)}{\pi}-\frac{\chi}{\pi^2}(\nabla\pi)^2\right]\right\},\\
\frac{\partial\mathcal{L}}{\partial\pi}&=\sqrt{-g}\left\{4\pi^3K-\pi^2\chi K_{\tilde{\varphi}}+(2G_4\pi-\chi G_{4,\tilde{\varphi}})R+2K_{\tilde{X}}\frac{(\nabla\chi)^2}{\pi}\right.\\
&\quad\left.-\frac{\chi}{\pi^2}(\nabla\pi)\cdot(\nabla\chi)\left[5K_{\tilde{X}}+6G_{4,\tilde{\varphi}\tilde{\varphi}}\right]+\frac{\chi^2}{\pi^3}(\nabla\pi)^2(3K_{\tilde{X}}+6G_{4,\tilde{\varphi}\tilde{\varphi}})\right\},\\
\frac{\partial\mathcal{L}}{\partial(\nabla\chi)}&=\sqrt{-g}\left\{\left[6G_{4,\tilde{\varphi}}+K_{\tilde{X}}\left(\frac{\chi}{\pi}\right)\right](\nabla\pi)-K_{\tilde{X}}(\nabla\chi)\right\},\\
\frac{\partial\mathcal{L}}{\partial(\nabla\pi)}&=\sqrt{-g}\left\{\left[6G_{4,\tilde{\varphi}}+K_{\tilde{X}}\left(\frac{\chi}{\pi}\right)\right](\nabla\chi)\right.\\
&\quad\left.+\left[12G_4-12G_{4,\tilde{\varphi}}\left(\frac{\chi}{\pi}\right)-K_{\tilde{X}}\left(\frac{\chi}{\pi}\right)^2\right](\nabla\chi)\right\}. \quad (6.24)
\end{aligned}$$

Substituting Eq. (6.24) into the constraint Eq. (6.21) and collecting terms with Ricci

scalar R, we can deduce

$$(\pi^2 - \chi^2)G_{4,\tilde{\varphi}} + 2\chi\pi G_4 = 0\,, \tag{6.25}$$

since Eq. (6.21) must hold for any metric $g_{\mu\nu}$ and thus R. Here for simplicity, we have considered the constraint Eq. (6.21) identically vanishes instead of up to some total derivatives. [3] Solving Eq. (6.25) then gives

$$G_4 = A(1 - \tilde{\varphi}^2) \tag{6.26}$$

for some constant A. This fixes G_4. To satisfy the constraint Eq. (6.21), we also need the remaining terms to vanish, which gives

$$\begin{aligned}
&\pi^4 K_{\tilde{\varphi}} + 4\pi^3\chi K - \pi^2\chi^2 K_{\tilde{\varphi}} + (\nabla\pi)^2\left[6G_{4,\tilde{\varphi}} - 6G_{4,\tilde{\varphi}\tilde{\varphi}}\left(\frac{\chi}{\pi}\right)\right.\\
&\left.+(3K_{\tilde{X}} + 6G_{4,\tilde{\varphi}\tilde{\varphi}})\left(\frac{\chi}{\pi}\right)^3\right] + (\nabla\pi)\cdot(\nabla\chi)\left[12G_4 + 6G_{4,\tilde{\varphi}\tilde{\varphi}} - 12G_{4,\tilde{\varphi}}\left(\frac{\chi}{\pi}\right)\right.\\
&\left.-(6K_{\tilde{X}} + 6G_{4,\tilde{\varphi}\tilde{\varphi}})\left(\frac{\chi}{\pi}\right)^2\right] + (\nabla\chi)^2\left[6G_{4,\tilde{\varphi}} + 3K_{\tilde{X}}\left(\frac{\chi}{\pi}\right)\right] = 0\,,
\end{aligned} \tag{6.27}$$

with G_4 given in Eq. (6.26). In general, Eq. (6.27) is difficult to solve. For simplicity, we consider the sum-separable case where $K(\tilde{X}, \tilde{\varphi}) = g(\tilde{X}) + h(\tilde{\varphi})$. In this case, Eq. (6.27) can be solved exactly, where the solution is

$$\begin{aligned}
g(\tilde{X}) &= \tilde{X} + c\tilde{X}^{2/3}\,,\\
h(\tilde{\varphi}) &= \lambda(1 - \tilde{\varphi}^2)^2\,,
\end{aligned} \tag{6.28}$$

for $A = 1/12$ and $\lambda = \text{const}$. For this example, written in terms of $\tilde{X}$ and $\tilde{\varphi}$, the full bi-scalar action is therefore given by

$$\mathcal{L} = \sqrt{-g}\pi^4\left[\left(1 - \tilde{\varphi}^2\right)\frac{\tilde{R}}{12} + \tilde{X} + c\tilde{X}^{2/3} + \lambda(1 - \tilde{\varphi}^2)^2\right]\,. \tag{6.29}$$

The original Kallosh and Linde model Eq. (6.1) at the critical enhanced $SO(1,1)$ symmetry point where $F = \text{const}$ corresponds to the case $c = 0$.

[3] We will consider the total derivatives case later.

This general approach works for any theory of arbitrary number of fields with any continuous symmetries. For the global $SO(1,1)$ symmetry we consider, instead of parametrising φ^I as (χ, π), it is more convenient to consider an alternative parametrisation as we will see later.

Alternative Parametrisation

In fact, to construct terms that are $SO(1,1)$ and locally scale invariant, it is better to reparametrise the fields as

$$\pi = \tilde{\rho}\cosh(\theta) \ , \ \ \chi = \tilde{\rho}\sinh(\theta)\,, \tag{6.30}$$

where θ is a dimensionless field and $\tilde{\rho}$ is of mass dimension 1. In this field parametrisation, the global $SO(1,1)$ transformation of the fields corresponds a constant shift in θ, i.e. $\theta \to \theta + \vartheta$, ϑ is again some dimensionless constant, whereas the local scaling transformation becomes $\tilde{\rho} \to \tilde{\rho}/\sigma$ and $g_{\mu\nu} \to \sigma^2 g_{\mu\nu}$. A similar parametrisation can be applied to models that respect $SO(2)$ between the two fields instead of $SO(1,1)$, with the field redefinition

$$\pi = \tilde{\rho}\cos(\theta) \ , \ \ \chi = \tilde{\rho}\sin(\theta)\,, \tag{6.31}$$

The locally scale-invariant bi-scalar action $S_{\rm local}$ expressed in terms of $\tilde{\rho}$ and θ can be found simply by performing the following field redefinitions on the Horndeski action Eq. (6.15)

$$\tilde{\varphi} \to \theta\,, \ \ \tilde{g}_{\mu\nu} \to \tilde{\rho}^2 g_{\mu\nu}\,. \tag{6.32}$$

Using Noether's theorem as previously discussed, in this parametrisation $(\tilde{\rho}, \theta)$, it is easy to see for an infinitesimal global $SO(1,1)$ transformation $\theta \to \theta + \vartheta$, the Lagrangian $\mathcal{L}[\tilde{\rho}, \theta, g_{\mu\nu}]$ changes as

$$\Delta\mathcal{L} = \vartheta\frac{\partial\mathcal{L}}{\partial\theta} \tag{6.33}$$

for an infinitesimally small constant ϑ. Global $SO(1,1)$ invariance simply means the Lagrangian cannot have explicit θ dependence except up to some total derivatives, i.e.

$$\frac{\partial \mathcal{L}}{\partial \theta} = \text{sum of total derivatives}\,. \tag{6.34}$$

for any fields $\tilde{\rho}$, θ and $g_{\mu\nu}$.

The Most General SO$(1,1)$ and Local Weyl Invariant K-inflation Model

Consider the case of K-essence Eq. (6.22) as an example, which in terms of $\tilde{\rho}$ and θ is given by

$$\mathcal{L} = \sqrt{-g}\left[G_4(\theta)(\tilde{\rho}^2 R - 6\tilde{\rho}\Box\tilde{\rho}) + \tilde{\rho}^4 K(\theta, \tilde{X}_{\theta\theta})\right] \tag{6.35}$$

where $\tilde{X}_{\theta\theta} = -\frac{1}{2}\tilde{\rho}^{-2} g^{\mu\nu}\nabla_\mu\theta\nabla_\nu\theta$. In this parametrisation, the constraint Eq. (6.34) reads as

$$\sqrt{-g}\left[\tilde{\rho}^4 K_\theta + G_{4,\theta}(\tilde{\rho}^2 R - 6\tilde{\rho}\Box\tilde{\rho})\right] = \text{sum of total derivatives}\,. \tag{6.36}$$

Since Eq. (6.36) must holds for $g_{\mu\nu}$, the term with the Ricci scalar R on its own must vanish up to some total derivatives. This implies G_4 is a constant function since G_4 is independent of $\tilde{\rho}$ and does not contain any derivative terms. The only remaining term left is $\sqrt{-g}\tilde{\rho}^4 K_\theta$. For generic function K, the constraint then implies K cannot depend explictly on θ, i.e. $K_\theta = 0$.

As a result, we finally arrive at the full bi-scalar $SO(1,1)$ K-essence action

$$S = \int \mathrm{d}^4x\sqrt{-g}\left[c_1\tilde{\rho}^2 R - 6c_1\tilde{\rho}\Box\tilde{\rho} + \tilde{\rho}^4 K(\tilde{X}_{\theta\theta})\right]\,. \tag{6.37}$$

Written in terms of χ and π and pulling out the terms in the Kallosh and Linde original

model Eq. (6.1) at the critical point where $F = \lambda_n = \text{const}$, this becomes

$$S = \int \mathrm{d}^4x\sqrt{-g}\left\{\frac{\pi^2-\chi^2}{12}R + \frac{1}{2}(\partial\pi)^2 - \frac{1}{2}(\partial\chi)^2 - \frac{\lambda_n}{36}(\pi^2-\chi^2)^2 \right.$$
$$\left. +(\pi^2-\chi^2)^2 f(Z)\right\}\,, \tag{6.38}$$

where $Z \equiv \frac{1}{2}(\pi^2-\chi^2)^{-3}[\pi^2 X_{\chi\chi} - 2\chi\pi X_{\pi\chi} + \chi^2 X_{\pi\pi}]$. Here we have chosen $c_1 = 1/12$. This is the most general action with SO$(1,1)$ and local Weyl symmetry in the class of K-essence. Here the second line are all the possible extra terms beyond the original Kallosh and Linde model in the class of K-essence.

With Soft Shift Symmetry Breaking Prefactors

The model Eq. (6.37) does not provide a natural mechanism to end slow-roll inflation. This can be seen by gauge fixing $\tilde{\rho} = M_\mathrm{p}$. However, recall that in the original model Eq. (6.1), the function $F(\varphi/\pi)$ breaks the $SO(1,1)$ symmetry. The symmetry is only restored near the critical point, i.e the boundary of moduli space or in the large φ limit. Here since we are interested in the model behaviour in the vicinity of the critical point, we consider the same for the general action Eq. (6.37). That is, we promote the dimensionless coefficients such as c_1 to functions of the scale-invariant variables that break the $SO(1,1)$ symmetry in general but not at the critical point.

In terms of the redefined fields Eq. (6.30), the resulting action is

$$S = \int \mathrm{d}^4x\sqrt{-g}\left[c_1(\theta)\frac{\tilde{\rho}^2 R}{2} - 3c_1(\theta)\tilde{\rho}\Box\tilde{\rho} + \tilde{\rho}^4 K(\tilde{X}_{\theta\theta},\theta)\right]\,. \tag{6.39}$$

Here $\theta \to \infty$ is the natural critical point where the $SO(1,1)$ symmetry is restored, as θ becomes shift symmetric at ∞. Upon fixing the gauge $\tilde{\rho} = M_\mathrm{p}$ and performing a conformal transformation on the metric $g_{\mu\nu} \to g_E = c_1^{-1} g_{\mu\nu}$ back into the Einstein frame, the action Eq. (6.39) becomes

$$S_E = \int \mathrm{d}^4x\sqrt{-g_E}\left[\frac{M_\mathrm{p}^2 R_E}{2} - \frac{3M_\mathrm{p}^2}{4}\frac{c_{1,\theta}^2}{c_1^2}(\partial\theta)^2 + \frac{M_\mathrm{p}^4 K(\tilde{X},\theta)}{c_1^2}\right] \tag{6.40}$$

where $c_{1,\theta} \equiv \partial c_1/\partial\theta$ and now $\tilde{X}$ reads as $\tilde{X} = -\frac{c_1}{2}M_{\rm p}^{-2}(\partial\theta)^2$. We have suppressed the argument of c_1 here. We call this model **generalised conformal K-inflation**. If we demand $c_1(\theta)$ and $K(\tilde{X},\theta)$ to be analytic functions near the critical point $\theta \to \infty$, then $c_1(\theta)$ must also asymptote to a dimensionless constant and $K(\tilde{X},\theta) \to K(\tilde{X})$.

6.4 Conditions for Realising Universal Model Predictions

Before we discuss the model predictions of the generalised conformal K-inflation model Eq. (6.39) near the enhanced $SO(1,1)$ symmetry point and check if any universal behaviour emerges, it is useful to first study the sufficient conditions for realising universal model predictions. For instance, in the case of chaotic inflation, the asymptotic scaling relations $(\epsilon_V)_* \propto 1/N^p$ and $(\eta_V)_* \propto 1/N^q$ for some p and q in the large N limit, where $p, q > 0$, lead to universal model predictions. This was first noted by Roest [169]. The results were later extended to some other scaling relations by Garcia-Bellido and Roest [170]. In the following, we use the same approach and study the corresponding scaling relations in the case of K-inflation.

6.4.1 Slow-roll K-inflation

We begin by introducing the K-inflation model and briefly discussing its background dynamics and model predictions. The Lagrangian of K-inflation is given by

$$\mathcal{L} = \sqrt{-g}\left[K(X,\varphi) + M_{\rm p}^2 R/2\right] . \tag{6.41}$$

It was first introduced by Armendariz-Picon, Damour and Mukhanov [171]. An example of K-inflation is the Dirac-Born-Infeld (DBI) inflation [90]. For K-inflation, the background Einstein equations in a FRW universe are

$$\begin{aligned} 3H^2 &= M_{\rm p}^{-2}(2XK_X - K) \\ \dot{H} &= M_{\rm p}^{-2}(-XK_X) . \end{aligned} \tag{6.42}$$

Demanding the Hamiltonian is bounded from below and the equations of motion remain hyperbolic, the function K must satisfy the conditions [172]

$$K_X > 0\,,\ 2XK_{XX} + K_X > 0\,. \tag{6.43}$$

It is useful to introduce a new quantity c_s defined by

$$c_s^2 = \frac{K_X}{2XK_{XX} + K_X}\,. \tag{6.44}$$

This quantity c_s corresponds to the 'sound speed' of the density fluctuations and takes values between 0 to 1 for physical models. In general c_s is time dependent, where its dynamics can be described by the following sound flow functions

$$s_{n+1} \equiv \frac{\mathrm{d}\ln|s_n|}{\mathrm{d}N}\,,\ \ s_1 \equiv \frac{\dot{c_s}}{Hc_s}\,. \tag{6.45}$$

Slow-roll inflation happens where the following slow-roll parameters are small

$$\begin{aligned}\epsilon_H &\equiv -\frac{\dot{H}}{H^2} = \frac{3XK_X}{2XK_X - K} \ll O(1)\,,\\ \eta_H &\equiv -\frac{1}{2}\frac{\dot{\epsilon_H}}{H\epsilon_H} = -\epsilon_H - \frac{1}{2}\frac{\ddot{H}}{H\dot{H}} \ll O(1)\,.\end{aligned} \tag{6.46}$$

It was also shown that consistent slow-roll inflation models require the sound speed does not change abruptly, or $s_n \ll O(1)$ [173, 174]. Demanding $\epsilon_H \ll O(1)$ is equivalent to the condition $-K \gg XK_X$. As a result, the Friedmann equation in the slow-roll limit becomes

$$3M_{\mathrm{p}}^2H^2 = 2XK_X - K \approx -K\,. \tag{6.47}$$

Since $\epsilon_H \ll O(1)$, to have $\eta_H \ll O(1)$ we also need $\ddot{H}/(H\dot{H}) \ll O(1)$. Using the background equations Eq. (6.42), we can work out $\ddot{H}$ in terms of K and its partial derivatives

$$M_{\mathrm{p}}^2\ddot{H} = -\dot{X}K_X - K_{XX}X\dot{X} - K_{X\varphi}X\dot{\varphi}\,. \tag{6.48}$$

Rewritten in terms of c_s and $\delta \equiv -\ddot{\varphi}/(H\dot{\varphi})$, η_H then reads as

$$\eta_H = -\epsilon_H + \frac{1}{2}(1+1/c_s^2)\delta - \frac{1}{2}\frac{K_{X\varphi}}{K_X}\frac{d\varphi}{dN}\,. \tag{6.49}$$

To realise inflation, we only need the sum of the last two terms in Eq. (6.49) to be small but not individually. Here for simplicity, we restrict ourselves to models where φ is slowly rolling such that $\delta \ll O(1)$ and all terms on the RHS of Eq. (6.49) are small.

Now consider the full φ equation of motion in K-inflation from varying the action Eq. (6.41)

$$3HK_X\dot{\varphi} + K_X\ddot{\varphi} + K_{X\varphi}\dot{\varphi}^2 + K_{XX}\dot{\varphi}\dot{X} = K_\varphi \tag{6.50}$$

at background level. Dividing this by $HK_X\dot{\varphi}$ and expressing in terms of the physical slow-roll parameters ϵ_H and η_H, this becomes

$$3 - 2\epsilon_H - 2\eta_H + \delta = \frac{K_\varphi}{HK_X}\frac{1}{\dot{\varphi}}\,. \tag{6.51}$$

In the slow-roll limit where ϵ_H, η_H, $\delta \ll O(1)$, we therefore obtain the slow-roll equation for X

$$X \approx -\frac{1}{6}\left(\frac{K_\varphi}{K_X}\right)^2\left(\frac{1}{K}\right)\,. \tag{6.52}$$

Now we consider perturbations about the homogeneous background. Applying perturbation theory as in the case of canonical single field models, where we perturb the field φ and the metric to linear order as in Chapter 3, one can find the corresponding scalar and tensor perturbations in the spatially flat gauge satisfy a modified Mukhanov-Sasaki equation in Fourier space [175]

$$\begin{aligned} v_k'' + \left(c_s^2k^2 - \frac{z''}{z}\right)v_k = 0\,,\\ \tilde{h}_k^{s\prime\prime} + \left(k^2 - \frac{a''}{a}\right)\tilde{h}_k^s = 0\,, \end{aligned} \tag{6.53}$$

where again $v_k \equiv a\delta\varphi_k$ and $\tilde{h}_k^s$ defined as in Chapter 3. The scalar and tensor power spectra can be worked out by solving the modified Mukhanov-Sasaki equations and

the corresponding model predictions are given by [175]

$$\begin{aligned} n_{\rm s} - 1 &\approx -2(\epsilon_H)_* + 2(\eta_H)_* - (s_1)_* \,, \\ n_T &\approx -2(\epsilon_H)_* \,, \\ r &= 16(\epsilon_H)_* c_s \,. \end{aligned} \tag{6.54}$$

to leading order. These results were later extended to second-order in slow-roll by Martin et al. [176]. For generalised G-inflation with the full Horndeski action, this was first done by Kobayashi et al. [151] at the level of the power spectrum, and later to the bispectrum by Tsujikawa et al. [177]. Current observational constraints on K-inflation models are given in [44] for DBI inflation and recently in [178] for some other models where the sound speed c_s is constant.

In the following we will restrict our attention to models where the sound speed c_s is effectively constant such that $(s_1)_* \ll (\epsilon_H)_*, (\eta_H)_*$. For these models, universal behaviour can be realised when $(\epsilon_H)_*$ scales as $1/N^p$ in the large N limit for some p, where N is the number of e-folds of expansion from horizon exit t_* to the end of inflation t_e. [4] We will consider what constraints this asymptotic scaling relation implies on H and the form of K.

Scaling Relation, $(\epsilon_H)_* \propto 1/N$

The first example we consider is the case where $p = 1$

$$(\epsilon_H)_* = \frac{a_1}{N} \,. \tag{6.55}$$

Here a_1 is some arbitrary constant, which is fixed for a particular model and can be constrained by comparing with observations. This corresponds to the universality class where

$$r \propto 1/N \,, \quad n_{\rm s} - 1 \propto 1/N \,. \tag{6.56}$$

[4] Note by definition, it follows automatically $(\eta_H)_*$ scales as $1/N$

Note that universality requires the scaling relation to be satisfied for all the relevant scales k_* under consideration. In general to check if the scaling relation is satisfied, one can solve for N, which depends on $H(t_e)$, and check how $(\epsilon_H)_*$ scales with it in a particular model. However, in single-field models, since $H(t_e)$ is always fixed, we can simply just check how H scales with t instead.

Using the definition of ϵ_H and differentiating Eq. (6.55) with respect to t_*, we get

$$(2a_1 - 1)\left(\frac{\dot{H}}{H}\right)_* = a_1\left(\frac{\ddot{H}}{\dot{H}}\right)_* , \tag{6.57}$$

assuming $\dot{H}_* \neq 0$. Integrating Eq.(6.57) with respect to t_*, we arrive at a scaling relation between H and $\dot{H}$

$$H^{2a_1-1} = \Sigma\left(-\dot{H}\right)^{a_1} \text{ or } \frac{1}{H} = \Sigma\epsilon_H^{a_1} , \tag{6.58}$$

where Σ is some integration constant which sets the energy scale of H. This is the condition on H in order to satisfy the scaling relation Eq. (6.55), which holds for all t. In the case of K-inflation, by using the background equations Eqs. (6.42), this can be translated to a condition on K to leading order in slow-roll

$$\Sigma(-3XK_X)^{a_1} = \sqrt{3}(-K)^{a_1-1/2} , \tag{6.59}$$

Substituting the slow-roll equation Eq. (6.52), this becomes

$$\Sigma\left[\frac{1}{2}\frac{(K_\varphi)^2}{K_X}\left(\frac{1}{K}\right)\right]^{a_1} = \sqrt{3}(-K)^{a_1-1/2} , \tag{6.60}$$

For canonical single field models where $K(X,\varphi) = X - V(\varphi)$, Eq. (6.60) reduces to the Roest result [169]

$$(\epsilon_V)^{2a_1} = \frac{\tilde{\lambda}}{V} , \tag{6.61}$$

where $\tilde{\lambda} = \sqrt{3}/\Sigma$, by taking the slow-roll approximation $V \gg X$. It is not difficult to show Eq. (6.61) is satisfied for chaotic inflation with a monomial scalar potential $V = \lambda_n\varphi^n$ where λ_n is constant. In general Eq. (6.60) cannot be solved without

assuming the functional form of K.

Scaling Relation, $(\epsilon_H)_* \propto 1/N^p$

Next we consider the general case where $p \neq 1$

$$(\epsilon_H)_* \approx \frac{a_p}{N^p}\,, \tag{6.62}$$

We can follow a similar analysis as $p = 1$ to work out the corresponding condition on H. Starting with Eq. (6.62), differentiating both sides with respect to t_*, this becomes

$$-H_* = \frac{(-a_p)^{1/p}}{p}\left(\frac{H^2}{\dot{H}}\right)_*^{1/p-1}\left[2H - \frac{H^2\ddot{H}}{\dot{H}^2}\right]_*\,, \tag{6.63}$$

Multiplying each side by $(\dot{H}^2/H^4)_*$ and integrating with respect to t_*, we have

$$\Sigma H = \exp\left[\frac{(-a_p)^{1/p}}{p-1}\left(-\epsilon_H\right)^{1-1/p}\right]\,, \tag{6.64}$$

where Σ is again some integration constant. Note that during slow-roll $\epsilon_H < O(1)$, therefore for $p > 1$, as long as a_p is not too large, one can Taylor expand the exponential in Eq. (6.64) to leading order

$$\Sigma H = 1 + (-1)^{2/p-1}\left(\frac{a_p^{1/p}}{p-1}\right)\epsilon_H^{1-1/p}\,. \tag{6.65}$$

This is the general scaling relation between H and ϵ_H for the asymptotic behaviour Eq. (6.62). The constant a_p and p remains arbitrary as long as the scalar-tensor theory is not specified. For slow-roll inflation where $\dot{H}$ is always negative, a_p must be positive. In the case of K-inflation, using the background equations, this becomes

$$\Sigma\left(\frac{-K}{3}\right)^{1/2} = 1 + (-1)^{2/p-1}\left(\frac{a_p^{1/p}}{p-1}\right)\left(\frac{3XK_X}{-K}\right)^{1-1/p}\,, \tag{6.66}$$

to leading order in slow-roll. The original conformal inflation model Eq. (6.1) belongs to the universal class where $p = 2$. The scaling relation Eq. (6.66) for $p = 2$ is indeed satisfied by the model, as we now confirm:

Consider the T-model where $K = X - V$ and the potential V can be approximated by

$$V = V_*[1 - 4ne^{-\sqrt{2/3}\varphi} + O(n^2 e^{-\sqrt{8/3}\varphi})]\,, \tag{6.67}$$

in the large φ limit, where V_* is some constant. Taking the slow-roll limit for the Klein-Gordon equation where $\dot{\varphi} \approx -V_\varphi/3H$, the kinetic term X is well approximated by

$$X \approx \frac{V}{6}\left(\frac{V_\varphi}{V}\right)^2 \approx V_* \frac{8n^2}{3}\left(\frac{2}{3}\right) e^{-\sqrt{8/3}\varphi}\,, \tag{6.68}$$

in the large φ limit. Subsituting Eq. (6.68) for X into Eq. (6.66), we have

$$\begin{aligned} LHS &= \Sigma\sqrt{\frac{V_*}{3}}\left[1 - 2ne^{-\sqrt{2/3}\varphi} + O(n^2 e^{-\sqrt{8/3}\varphi})\right] \\ RHS &= 1 - a_2^{1/2}\frac{4}{\sqrt{3}} ne^{-\sqrt{2/3}\varphi} + O(n^2 e^{-\sqrt{8/3}\varphi})\,. \end{aligned} \tag{6.69}$$

Therefore they are equal provided $a_2 = 3/4$ and $\Sigma = \sqrt{3}V_*^{-1/2}$, corresponding to $\epsilon_H \approx \epsilon_\varphi = 3/4N^2$.

6.5 Universal Behaviour of Generalised Conformal K-Inflation

In this section, we discuss the universal behaviour of the generalised conformal K-inflation model introduced in Section 6.3. Generically, we expect K is of polynomial form in $\tilde{X}$ such that $K(\tilde{X}) = \sum_n b_n \tilde{X}^n - \lambda$, where b_n are some dimensionless constants with $b_{n+1} < b_n$. For potential-driven slow-roll inflation, to leading order we typically have $K \approx b_1(\theta)\tilde{X} - \lambda(\theta)$ and the effective sound speed $c_s^2 \approx 1$. As a result, we can assume c_s to be constant and the sound flow functions s_n contribution to the model predictions in Eq. (6.54) can be neglected.

The action Eq. (6.40) now reads as

$$S_E = \int \mathrm{d}^4x\sqrt{-g_E}\left[\frac{M_\mathrm{p}^2 R_E}{2} - \frac{M_\mathrm{p}^2}{2c_1(\theta)}\left(b_1(\theta) + \frac{3}{2}\frac{c_{1,\theta}^2(\theta)}{c_1(\theta)}\right)(\partial\theta)^2 - \frac{\lambda(\theta)M_\mathrm{p}^4}{c_1^2(\theta)}\right] \tag{6.70}$$

Recall that we demand the soft breaking functions and their derivatives are analytic at the critical point $\theta \to \infty$. In the vicinity of large θ, in simple generic cases, these functions can be represented by the following expansions

$$b_1(\theta) = \tilde{b}[1 - be^{-\theta} + O(e^{-2\theta})] \text{ or } b_1(\theta) = \tilde{b}[1 - \frac{b}{\theta} + O(\frac{1}{\theta^2})]\,, \tag{6.71}$$

and similarly for λ and c_1 in general. Here $\tilde{b}$ and b are some dimensionless constants. As a result, for large θ, the second term in the coefficient of the kinetic piece $(\partial\theta)^2$ in Eq. (6.70) is negligible compared to the first term and the resulting action is

$$S_E = \int \mathrm{d}^4x\sqrt{-g_E}\left\{\frac{M_\mathrm{p}^2 R_E}{2} - \frac{M_\mathrm{p}^2}{2}\left[\frac{\tilde{b}}{\tilde{c}} + O(e^{-2\theta}, \frac{1}{\theta})\right](\partial\theta)^2 \right. \\ \left. - \frac{\tilde{\lambda}M_\mathrm{p}^4}{\tilde{c}^2}\left[1 - O(e^{-\theta}, \frac{1}{\theta})\right]\right\}\,, \tag{6.72}$$

to leading order. Unless $\tilde{b}$ or $\tilde{c}$ vanishes, we can rewrite the action in terms of the canonically-normalised field $\varphi = M_\mathrm{p}(\tilde{b}/\tilde{c})^{1/2}\theta$,

$$S_E = \int \mathrm{d}^4x\sqrt{-g_E}\left\{\frac{M_\mathrm{p}^2 R_E}{2} - \frac{1}{2}(\partial\varphi)^2 - V_*\left[1 - O(e^{-\tilde{n}\varphi/M_\mathrm{p}}, \frac{M_\mathrm{p}}{\varphi})\right]\right\}\,, \tag{6.73}$$

where $V_* \equiv \tilde{\lambda}M_\mathrm{p}^4/\tilde{c}^2$ and $\tilde{n} = (\tilde{b}/\tilde{c})^{-1/2}$. If the next to leading order term in the potential is $O(e^{-\tilde{n}\varphi/M_\mathrm{p}})$, then the model is similar to Kallosh and Linde's original model in the large φ limit

$$S_E = \int \mathrm{d}^4x\sqrt{-g_E}\left[\frac{M_\mathrm{p}^2 R_E}{2} - \frac{1}{2}(\partial\varphi)^2 - V_*(1 - \Theta e^{-n\varphi/M_\mathrm{p}})\right]\,. \tag{6.74}$$

Here Θ is a dimensionless constant and must be positive if inflation is to end naturally. By computing the number of e-folds N and the slow-roll parameters ϵ_V and η_V in the slow-roll and large N limit as in the original model, it is not difficult to show that the model has the same universal behaviour as the original model where $r \propto 1/N^2$ and $n_\mathrm{s} - 1 \propto -1/N$.

On the other hand, if the next to leading order term for the effective potential in Eq. (6.72) is $O(\frac{M_\mathrm{p}}{\varphi})$, then a different universalily class where $r \propto N^{-4/3}$ and $n_\mathrm{s} - 1 \propto$

$-1/N$ is realised. This can be seen as the slow-roll parameters $(\epsilon_V)_*$ and $(\eta_V)_*$ are related to the number of e-folds N as

$$(\epsilon_V)_* \propto \frac{1}{N^{4/3}}\,, \quad (\eta_V)_* \propto \frac{1}{N} \tag{6.75}$$

in the large N limit.

We argue the same universal behaviour holds for other classes of $SO(1,1)$ bi-scalar conformal inflation models as well in general. For the generalised bi-scalar conformal inflation which is potential-driven such that

$$\begin{aligned} K(\theta, \tilde{X}) &= -V(\theta) + b_i(\theta)\tilde{X} + \dots\,, \\ G_i(\theta, \tilde{X}) &= g_i(\theta) + h_i(\theta)\tilde{X} + \dots \end{aligned} \tag{6.76}$$

and θ is slowly rolling, terms involving higher order derivatives are suppressed in general. To leading order, only the canonical kinetic term $\tilde{X}$ survives and the action reduces to Eq. (6.70) assuming the functions b_i, g_i and h_i are of similar order. The same universal behaviour as conformal K-inflation is thus expected. For the pivot CMB scale $k_* = 0.002\mathrm{Mpc}^{-1}$ where the amount of observable inflation is $N \sim 60$, we therefore conclude that $SO(1,1)$ bi-scalar conformal inflation universally predicts negligible level of tensor perturbations with $r < O(0.01)$.

6.6 Universality Class with Large r?

In the light of the recent BICEP2 results which suggest tensor-to-scalar ratio $r \sim O(0.1)$, we will also discuss the possibility of realising a universality class where r can be large in generalised bi-scalar conformal $SO(1,1)$ models.

6.6.1 K-inflation

In the last section, we have seen that conformal K-inflation models give small r if $K(\tilde{X})$ is a power series in $\tilde{X}$. In the following we drop this assumption and keep $K(\tilde{X})$ as arbitrary.

Sum-Separable Case: $K(\tilde{X},\theta) = G(\tilde{X}) - F(\theta)$

Consider a sum-separable case where $K(\tilde{X},\theta) = G(\tilde{X}) - F(\theta)$ for arbitrary functions G and F. The gauge-fixed action Eq. (6.40) then reads as

$$S_E = \int \mathrm{d}^4x\sqrt{-g_E}\left\{\frac{M_\mathrm{p}^2 R_E}{2} - \frac{3}{4}\left(\frac{c_{1,\theta}}{c_1}\right)^2(\partial\varphi)^2 + \frac{M_\mathrm{p}^4}{c_1^2}\left[G(\tilde{X}) + F(\varphi/M_\mathrm{p})\right]\right\}, \tag{6.77}$$

in terms of a dimensionful field $\varphi \equiv \theta M_\mathrm{p}$. Again c_1 and F are functions of θ which have the asymptotic form as in Eq. (6.71) near the critical point $\varphi \to \infty$, and $\tilde{X} \equiv -\frac{1}{2}c_1(\varphi/M_\mathrm{p})(\partial\varphi)^2$. For slow-roll potential-driven inflation, the term $F(\varphi)$ dominates and we have $3M_\mathrm{p}^2H^2 \approx M_\mathrm{p}^4F/c_1^2$. The partial derivatives of K with respect to X and φ are then

$$\begin{aligned} K_\varphi &\approx \frac{F_\varphi}{c_1^2} - \frac{2Fc_{1,\varphi}}{c^3}, \\ K_X &= -\frac{3}{2}\left(\frac{c_{1,\varphi}}{c_1}\right)^2 + \frac{K_{\tilde{X}}}{c_1}. \end{aligned} \tag{6.78}$$

Now we check if K can satisfy the scaling relation $(\epsilon_H)_* \propto 1/N$ for slow-roll potential-driven inflation in this case. Substituting Eq. (6.78) into the universality condition Eq. (6.60), we have

$$\begin{aligned} RHS &= \sqrt{3}(F/c_1^2)^{a_1-1/2} \approx \sqrt{3}(\tilde{F}/\tilde{c}_1^2)^{a_1-1/2} + O(e^{-\varphi/M_\mathrm{p}}, \frac{1}{\varphi}), \\ LHS &= \Sigma\left\{\frac{1}{2}\frac{c_1^2}{F}\left(\frac{F_\varphi}{c_1^2} - \frac{2Fc_{1,\varphi}}{c_1^3}\right)^2\left[\frac{K_{\tilde{X}}}{c_1} - \frac{3}{2}\left(\frac{c_{1,\varphi}}{c_1}\right)^2\right]^{-1}\right\}, \end{aligned} \tag{6.79}$$

to leading order in large φ limit. $\tilde{F}$ and $\tilde{c}_1$ are dimensionless constants where F and c_1 asymptote to. To satisfy the universality condition, we need the leading term in the LHS to be a constant. This is only possible if $M_\mathrm{p}^4\frac{K_{\tilde{X}}}{c_1} \gg -\frac{3}{2}\left(\frac{c_{1,\varphi}}{c_1}\right)^2$, since for our choice of c_1 and F, their derivatives $c_{1,\varphi}$ and F_φ are always of the order of

$O(e^{-\varphi/M_{\rm P}}, \frac{1}{\varphi})$. In that case,

$$LHS \approx \Sigma \left[\frac{1}{2}\frac{c_1^3}{F}\left(\frac{K_\varphi^2}{K_{\tilde{X}}}\right)\right] = \Sigma \left[\frac{1}{2Fc_1}\left(F_\varphi - \frac{2Fc_{1,\varphi}}{c_1}\right)^2 \frac{1}{K_{\tilde{X}}}\right], \tag{6.80}$$

which asymptotes to a constant in the large φ limit only if $K_\varphi^2/K_{\tilde{X}} \to \text{const}$. This is the necessary condition for the universality condition Eq. (6.60).

However, assuming φ is slowly rolling, from the slow-roll solution Eq. (6.52) for X in K-inflation, we also have

$$\tilde{X} = c_1 X \approx -\frac{c_1^3}{6}\left(\frac{K_\varphi}{K_{\tilde{X}}}\right)^2 \frac{1}{K} = -\frac{1}{6}\left(\frac{c_1^3}{K_{\tilde{X}}}\right)\frac{1}{K} \propto \frac{1}{G_{\tilde{X}}}\,. \tag{6.81}$$

to leading order. Therefore we find a solution for $G(\tilde{X})$

$$G(\tilde{X}) = \ln \tilde{X}\,. \tag{6.82}$$

Nevertheless, the solution $G(\tilde{X}) \propto \ln \tilde{X}$ violates the second condition in Eq. (6.43) and gives imaginary sound speed c_s in general. As a result, we conclude the universality condition $\epsilon_H \sim a/N$ cannot be satisfied for slow-roll power-driven conformal K-inflation and therefore the model predicts $r \ll O(0.1)$ in general. There is a caveat that a different scaling relation with $p < 1$ may still be plausible though.

6.7 Summary

Conformal inflation is a new class of inflation models and is natural in the superconformal formulation of supergravity. In addition, universal behaviour emerges as a critical phenomenon near the point of enhanced $SO(1,1)$ or shift symmetry, which is naturally taken to be the boundary of the moduli space $(\chi, \pi) \to \infty$. For generic Lagrangians where inflation happens near the enhanced symmetry point (including the relevant observed scales), this therefore leads to the same universal model-independent predictions, with the attractor points

$$n_{\rm s} - 1 \propto -\frac{1}{N}\,, \quad r \propto \left\{\frac{1}{N^2}, \frac{1}{N^{4/3}}\right\}\,. \tag{6.83}$$

This universal behaviour also extends to generalised bi-scalar conformal models beyond canonical kinetic terms for slow-roll potential-driven inflation. This can be understood as all models reduce to the same asymptotic forms near the enhanced symmetry point. Whether the local scale invariance symmetry plays any significant role in realising universality classes remains to be seen.

For the pivot CMB scale $k_* = 0.002\mathrm{Mpc}^{-1}$ where the amount of observable inflation is $N \sim 60$, we therefore conclude that $SO(1,1)$ (or shift symmetric) bi-scalar conformal inflation universally predicts negligible level of tensor perturbations with $r \ll O(0.1)$. [5]

[5]Recently there have been work on building a conformal inflation models with large r that are consistent with the recent BICEP2 results, for instance see [179] and [180]. These models however either do not have an enhanced symmetry point or have singular behaviour near the enhanced symmetry point.

Chapter 7

Conclusion

Since the early work by Guth [20], inflation has become the dominant paradigm of the Early Universe prior to the standard Hot Big Bang. According to the original paradigm, our Universe underwent an early period of superluminal expansion, driven by a canonical scalar field slowly rolling down a flat potential. This early accelerated period of expansion does not only solve the classical problems in Hot Big Bang Cosmology, but offers an explanation to the generation of primordial fluctuations that seeded structure formation and the Cosmic Microwave Background (CMB) anisotropies. During inflation, quantum fluctuations of the inflaton field were stretched beyond the horizon and became classical. Over time they were gravitationally amplified, and eventually re-entered the horizon laying the foundations of all cosmic structure that we observe in the universe today. In Chapter 1, we briefly reviewed the cosmology of the Hot Big Bang, its shortcomings and the standard original paradigm of inflation.

Density perturbations are usually quantified in terms of the gauge-invariant curvature perturbation ζ, defined as the spatial curvature on uniform-density slices. In Chapter 2 we reviewed cosmological perturbation theory, the gauge-invariant defintion of ζ and its statistical properties. An important property of ζ is the fact that it is conserved on superhorizon scales in the absence of isocurvature perturbations. We demonstrated this in Section 2.5.1. We also reviewed the separate universe approximation and the δN formalism, which were used extensively in this thesis.

The original inflation paradigm also has universal predictions. In particular, the primor-

dial fluctuations produced are almost Gaussian and nearly scale-invariant. Primordial gravitational waves are also generated and could be strong enough to be observed depending on the shape of the potential. We reviewed this in Chapter 3, showing how the model predictions are computed. We also discussed how the predictions are compared to current observations. We then discussed a simple extension to the original paradigm, multifield inflation, in which inflation is driven by multiple scalar fields.

Unlike in single-field models, isocurvature perturbations exist in multifield models and could source the curvature perturbation ζ. For models where isocurvature perturbtions persist after the end of slow-roll, we showed in Chapters 4 and 5 that the subsequent post-inflationary evolution, particularly reheating, do significantly change the model predictions and therefore should be accounted for, even in the simple perturbative reheating setup. The model predictions evaluated at the end of the slow-roll regime are different to those after reheating in general, with the change being model-dependent. Compared to the spectral index $n_{\rm s}$, the non-linear parameters $f_{\rm NL}$, $\tau_{\rm NL}$ and $g_{\rm NL}$ are more sensitive to the physics of reheating. Although individual observables evolve during reheating, consistency relations between observables are more robust to the details of reheating. Examples are $g_{\rm NL} \approx \tau_{\rm NL}$ in non-vacuum dominated sum-separable potential models and $3n_{f_{\rm NL}} = 2n_{\tau_{\rm NL}}$ in two-field local type models. This suggests consistency relations act as a better tool to distinguish between different multifield models.

Another class of model we have considered is conformal inflation. The original model involves two canonical (up to a sign) scalar fields non-minimally coupled to gravity with an additional local scale invariance symmetry. This model is natural in the superconformal formulation of supergravity. Because of scale invariance, only one scalar degree of freedom is physical and perturbation is purely adiabatic. For that reason, ζ is conserved after horizon-exit as long as perturbations remain adiabatic and the model is more predictive. Universal model predictions emerge as a critical phenomenon near the enhanced SO$(1,1)$ or (shift) symmetry point. In Chapter 6, we showed that this universal behaviour also extends to generalised slow-roll potential-driven models.

While the single-field paradigm has been well studied and constrained today, an equivalent picture is lacking for the multifield paradigm. For instance, despite some recent

work [181, 182] which focuses on canonical models with a sum-separable quadratic potential, there is still work to be done in understanding how to constrain multi-field models in general, for instance how to take (p)reheating into account. Being more natural from particle physics point of view, a better understanding in the multi-field paradigm such as the field dynamics and model predictions would help us make progress in embedding inflation in unified theories like string theories.

On the other hand, despite being an important part of inflationary model building, (p)reheating remains much less understood compared to the slow-roll regime. In order to constrain theoretical models with observations, we however need a better understanding in the non-equilibrium physics of reheating, as we have seen in canonical models reheating does significantly change slow-roll model predictions in the presence of isocurvature perturbations, perhaps except consistency relations between observables. It remains to be seen if this also holds in a more generic (p)reheating setup, going beyond the simple perturbative reheating picture. The highly non-equilibrium nature of (p)reheating may also open up new observational windows to inflation and shed some light on the underlying inflation models in play in the Early Universe.

Motivated by Planck results and theoretical models such as conformal inflation, there have also been interests in universality classes of inflation models recently. A better understanding of different universality classes would help explore new classes of inflation models that are compatible with observations and their common features may give hints of the underlying fundamental theories in play during the early universe. As we now enter the era of precision cosmology, with more precise data coming, it is important to address these issues in the future.

Appendix A

Analytic Expressions for δN Coefficients

In Chapter 3, we stated that analytic expressions for the δN coefficients for potentials of separable form exist under slow-roll approximation. Here in this appendix, we briefly illustrate how they are derived. We will set $M_{\rm p} = 1$ here unless stated otherwise.

Consider the multifield canonical case, the slow-roll field equations give the following relation

$$\frac{\mathrm{d}\varphi^I}{W_I} = \frac{\mathrm{d}\varphi^J}{W_J}\,, \tag{A.1}$$

assuming the fields φ^I and φ^J are slowly rolling and evolve monotonically. Here again W_I denotes partial derivative of the potential W with respect to the field φ^I. We shall use Eq. (A.1) to construct a constant of motion along each classical slow-roll trajectory and work out the δN coefficients.

Let us consider a two field product-separable potential where W is of the form

$$W(\varphi, \chi) = U(\varphi)V(\chi)\,, \tag{A.2}$$

for some functions U and V. The number of e-folds N from some initial time t_* to

final time t_e can be written in terms of integrals of the fields

$$N = \int_e^* \frac{U}{U_\varphi} \mathrm{d}\varphi = \int_e^* \frac{V}{V_\chi} \mathrm{d}\chi \,. \tag{A.3}$$

Here $\int_e^* d\varphi^I$ denotes an integral of φ^I from the value φ_e^I at final time t_e to initial value φ_*^I at t_*. In what follows, subscripts $_*$ and e correspond to quantities evaluated at initial time t_* and final time t_e. Infinitesimal change in the number of e-folds N with respect to changes in φ_* and χ_* is then given by

$$\begin{aligned} \mathrm{d}N &= \left[\left(\frac{U}{U_\varphi}\right)_* + \frac{\partial\varphi_e}{\partial\varphi_*}\left(\frac{U}{U_\varphi}\right)_e\right]\mathrm{d}\varphi_* + \left[\frac{\partial\varphi_e}{\partial\chi_*}\left(\frac{U}{U_\varphi}\right)_e\right]\mathrm{d}\chi_* \\ &= \left[\left(\frac{V}{V_\chi}\right)_* + \frac{\partial\chi_e}{\partial\chi_*}\left(\frac{V}{V_\chi}\right)_e\right]\mathrm{d}\chi_* + \left[\frac{\partial\chi_e}{\partial\varphi_*}\left(\frac{V}{V_\chi}\right)_e\right]\mathrm{d}\varphi_* \,. \end{aligned} \tag{A.4}$$

The δN coefficients in the δN formalism can then be worked out once we know how the final field values $\{\varphi_e, \chi_e\}$ depend on their initial values $\{\varphi_*, \chi_*\}$, subject to the constraint $\{\varphi_e, \chi_e\}$ are such that the final hypersurface at t_e is of uniform energy density.

Using Eq. (A.1), we can construct a constant of motion along each classical trajectory as

$$C = -\int \frac{\mathrm{d}\chi}{V_\chi} + \int \frac{\mathrm{d}\varphi}{U_\varphi} \,. \tag{A.5}$$

Since C is conserved along each trajectory, the final field values $\{\varphi_e, \chi_e\}$ are unique functions of C. One can then use C to work out the infinitesimal change in $\{\varphi_e, \chi_e\}$ with respect to changes in φ_* and χ_*

$$\begin{aligned} d\varphi_e &= \frac{\mathrm{d}\varphi_e}{\mathrm{d}C}\left(\frac{\partial C}{\partial\varphi_*}\mathrm{d}\varphi_* + \frac{\partial C}{\partial\chi_*}\mathrm{d}\chi_*\right) \\ d\chi_e &= \frac{\mathrm{d}\chi_e}{\mathrm{d}C}\left(\frac{\partial C}{\partial\varphi_*}\mathrm{d}\varphi_* + \frac{\partial C}{\partial\chi_*}\mathrm{d}\chi_*\right) \,. \end{aligned} \tag{A.6}$$

From the definition of C Eq. (A.5), we can easily see

$$\frac{\partial C}{\partial\varphi_*} = \left(\frac{1}{U_\varphi}\right)_* , \quad \frac{\partial C}{\partial\chi_*} = -\left(\frac{1}{V_\chi}\right)_* . \tag{A.7}$$

To compute the partial derivatives of the final field values with respect to their initial values $\partial\varphi_e^I/\partial\varphi_*^I$, we also need to know $d\varphi_e^I/dC$. Recall that in δN formalism, the final hypersurface at t_e is that of uniform density, which in the slow-roll limit corresponds to

$$W(t_e) = U(\varphi_e)V(\chi_e) = \text{const}\,. \tag{A.8}$$

Differentiating this with respect to C and use the identity $dC/dC = 1$, we finally arrive at

$$\begin{aligned}
\frac{\partial\chi_e}{\partial\chi_*} &= \left(\frac{U_\varphi}{U}\right)_e^2 \left(\frac{V}{V_\chi}\right)_e \left(\frac{\epsilon_\chi}{\epsilon}\right)_e \left(\frac{V}{V_\chi}\right)_*\,, \quad \frac{\partial\chi_e}{\partial\varphi_*} = -\left(\frac{U_\varphi}{U}\right)_e^2 \left(\frac{V}{V_\chi}\right)_e \left(\frac{\epsilon_\chi}{\epsilon}\right)_e \left(\frac{U}{U_\varphi}\right)_*\,, \\
\frac{\partial\varphi_e}{\partial\chi_*} &= -\left(\frac{U_\varphi}{U}\right)_e \left(\frac{\epsilon_\chi}{\epsilon}\right)_e \left(\frac{V}{V_\chi}\right)_*\,, \quad \frac{\partial\varphi_e}{\partial\varphi_*} = \left(\frac{U_\varphi}{U}\right)_e \left(\frac{\epsilon_\chi}{\epsilon}\right)_e \left(\frac{U}{U_\varphi}\right)_*\,,
\end{aligned} \tag{A.9}$$

where ϵ_χ, ϵ_φ and ϵ are defined in Eq. (3.83) in Chapter 3. Substituting these back into Eq. (A.4), we can then work out analytic expressions for the δN coefficients. For instance, the first order δN coefficients are

$$\frac{\partial N}{\partial\varphi_*} = \left(\frac{1}{\sqrt{2\epsilon_\varphi}}\right)_* \text{sign}[(U_\varphi)_*] \left(\frac{\epsilon_\varphi}{\epsilon}\right)_e\,, \frac{\partial N}{\partial\chi_*} = \left(\frac{1}{\sqrt{2\epsilon_\chi}}\right)_* \text{sign}[(V_\chi)_*] \left(\frac{\epsilon_\chi}{\epsilon}\right)_e\,. \tag{A.10}$$

One then differentiate Eq. (A.10) again to find the second order δN coefficients. Using these expressions, we can then work out expressions for the primordial observables, for instance n_s and $f_\text{NL}^{(4)}$

$$n_\text{s} - 1 = \quad -4\left[\frac{u^2}{(\epsilon_\varphi)_*} + \frac{v^2}{(\epsilon_\chi)_*}\right]^{-1} \left[1 - 2uv - \frac{u^2(\eta_{\varphi\varphi})_*}{2(\epsilon_\varphi)_*} - \frac{v^2(\eta_{\chi\chi})_*}{2(\epsilon_\chi)_*}\right] - 2(\epsilon_H)_*\,, \tag{A.11}$$

$$\begin{aligned}
f_\text{NL}^{(4)} = \quad & \frac{5}{6}\left[\frac{u^2}{(\epsilon_\varphi)_*} + \frac{v^2}{(\epsilon_\chi)_*}\right]^{-2} \left\{2\left[\frac{u^3}{(\epsilon_\varphi)_*} + \frac{v^3}{(\epsilon_\chi)_*}\right] - \frac{u^3(\eta_{\varphi\varphi})_*}{(\epsilon_\varphi)_*^2} - \frac{v^3(\eta_{\chi\chi})_*}{(\epsilon_\chi)_*^2}\right. \\
& \left. +2\left[\frac{u}{(\epsilon_\varphi)_*} - \frac{v}{(\epsilon_\chi)_*}\right]^2 \mathcal{A}_P\right\}
\end{aligned} \tag{A.12}$$

where $u \equiv (\epsilon_\varphi/\epsilon)_e$, $v \equiv (\epsilon_\chi/\epsilon)_e$ and

$$\eta_{ss} \equiv \frac{\epsilon_\chi \eta_{\varphi\varphi} + \epsilon_\varphi \eta_{\chi\chi} - 4\epsilon_\varphi \epsilon_\chi}{\epsilon}\,,$$
$$\mathcal{A}_p \equiv uv(\eta_{ss})_e\,. \tag{A.13}$$

Here $\eta_{\varphi\varphi}$ and $\eta_{\chi\chi}$ are defined in Eq. (3.83) in Chapter 3. These are first computed by Choi et al. [104] and later by Elliston et al. for third order δN coefficients and non-linear parameters of trispectrum $\tau_{\rm NL}$ and $g_{\rm NL}$ [107].

Other Solvable Models

We have previously showed how analytic expressions for δN coefficients and primordial observables can be derived for canonical models with a product-separable potential. Following similar approach, we can also derive analytic expressions of δN coefficients and model predictions for sum-separable potentials. This was first done by Vernizzi and Wands [103] for second order δN coefficients and the power spectrum, and later extended to third order δN coefficients and the trispectrum by Elliston et al. [107]. These results are later generalised to models with potentials that are arbitrary functions of these separable ansatz [183]. In fact, we can also apply the same expressions Eqs. (A.11) and (A.12) to sum-separable potential models by considering the following transformations

$$U \to \ln U\,,\;\; V \to \ln V\,,\;\; W \to \ln W\,. \tag{A.14}$$

Besides, analytic expressions also exist for models where the Hubble parameter H satisfies a product or sum-separable ansatz

$$H = H_1(\varphi) + H_2(\chi)\,,\;\; \text{or}\;\; H = H_1(\varphi)H_2(\chi)\,, \tag{A.15}$$

for some functions H_1 and H_2, by using the Hamilton-Jacobi field equations, i.e. $\dot\varphi = -2\partial H_1/\partial\varphi$ and $\dot\chi = -2\partial H_2/\partial\chi$. The expressions were first derived by Byrnes.et al. for the sum-separable ansatz for two fields [184] and were later generalised to trispectrum and arbitrary number of fields by Battefeld et al. [185]. These expressions

are valid beyond slow-roll. However, the fact that we can express the Hubble parameter H as in Eq. (A.15) relies on the fields evolving monotonically. This assumption usually breaks down shortly after inflation ends as the fields approach their respective minima and start oscillating.

All the analytic expressions discussed above rely on certain approximations and specific forms of the potential or Hubble parameter such that we can solve the field equations analytically. For multifield models with arbitrary potentials and/or beyond slow-roll regime, we can at best express the δN coefficients in terms of some integrals which cannot be solved analytically, for instance see [186].

Appendix B

Numerical Recipe for Computing δN Coefficients

In this appendix, we discuss the numerical recipe used in this thesis for computing δN coefficients. As discussed, the δN formalism is based on the assumption that (smoothed) spatially separated patches of the universe will evolve on superhorizon scales like independent, unperturbed universes up to small corrections. An ensemble of smoothed regions picks out a collection of trajectories in phase space which is often referred to as a 'bundle' [106, 187]. In essence, the δN formalism requires that such a bundle, centred on a fiducial trajectory, is evolved. Our choice of gauge demands that each trajectory in the bundle is evolved from an initially flat hypersurface up to a hypersurface of constant energy density. Hence, each trajectory will experience a slightly different expansion history in order to bring them to a common energy density. The adiabatic mode is generated by fluctuations along the fiducial trajectory, whilst fluctuations between neighbouring trajectories generate the isocurvature modes.

Acknowledging this simple picture, we implement the δN formalism numerically as follows: First, the fiducial trajectory emanating from $\{\varphi_*, \chi_*\}$ is constructed by solving the full, non–linear system of second order field equations Eq. (4.16) using the Verner's 5th and 6th order pair Runge-Kutta Method. Ths is done in Fortran using the public domain Fortran 77 subroutine **DVERK** written by Hull, Enright and Jackson [188].

The epoch of horizon-crossing is set by $N = 0$, where the initial field velocitites $\{\dot{\varphi}_*, \dot{\chi}_*\}$ are set by imposing the slow-roll attractor solution $3H\dot{\varphi}^I = -W_I$. As long as the onset of inflation happens slightly before the pivot scale under consideration exits the horizon, we expect this to be a very good approximation. To illustrate this, in Fig. B.1, we show the slow-roll evolution of the fields in the quadratic times exponential model, one with $\{\dot{\varphi}_*, \dot{\chi}_*\}$ set by the slow-roll attractor solution and one with slightly different $\{\dot{\varphi}_*, \dot{\chi}_*\}$.

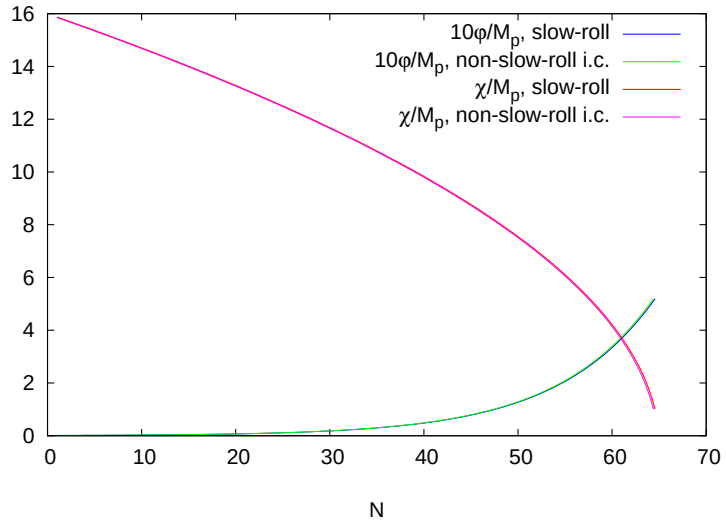

Figure B.1: Potential: $W(\varphi, \chi) = W_0 \chi^2 e^{-\lambda\varphi^2/M_{\rm p}^2}$. The slow-roll evolution of the background fields (in Planck units), one with $\{\dot{\varphi}_*, \dot{\chi}_*\}$ set by the slow-roll attractor solution and one with slightly different initial field velocities. The model parameters $\lambda = 0.05$, $\varphi_* = 10^{-3} M_{\rm p}$ and $\chi_* = 16.0 M_{\rm p}$.

The bundle of trajectories is then formed by evolving neighbouring trajectories with slightly perturbed initial conditions, $\varphi_* \to \varphi_* + \delta\varphi_*$ and $\chi_* \to \chi_* + \delta\chi_*$. To evaluate the δN derivatives and primordial observables at N, each trajectory in the bundle is then brought to a common energy hypersurface with respect to the central fiducial trajectory emanating from $\{\varphi_*, \chi_*\}$ where $N(\varphi_*, \chi_*)$ is evaluated. This is done by calculating $\rho(N)$ for the central fiducial trajectory and using binary search algorithm to find the corresponding the number of e-folds N for neighbouring trajectories with slightly different initial horizon-exit field values with the same energy density.

The partial derivatives of $N(t_c, t_*)$ with respect to the field values at horizon crossing $\{\varphi_*, \chi_*\}$ are then calculated using a seven–point (or nine–point) 'stencil' finite difference method [189]. Finally, convergence check with respect to the step sizes

$\{\delta\varphi_*, \delta\chi_*\}$ used are done to ensure the numerical result are robust against numerical noises.

In the following, we plot the δN derivatives and the primordial observables evaluated using this numerical scheme as a function of the step sizes $\{\delta\varphi_*, \delta\chi_*\}$ for some of the models considered in this thesis, demonstrating there exists regions where the numerical results converge and become independent of the step sizes used. For instance, Figs. B.2 to B.6 for the quadratic times exponential model and Figs. B.7 to B.11 for the effective N-flation model. In all the plots, we can see there exists regions where the numerical results converge with respect to step sizes used.

Quadratic Exponential Model

First Order δN coefficients

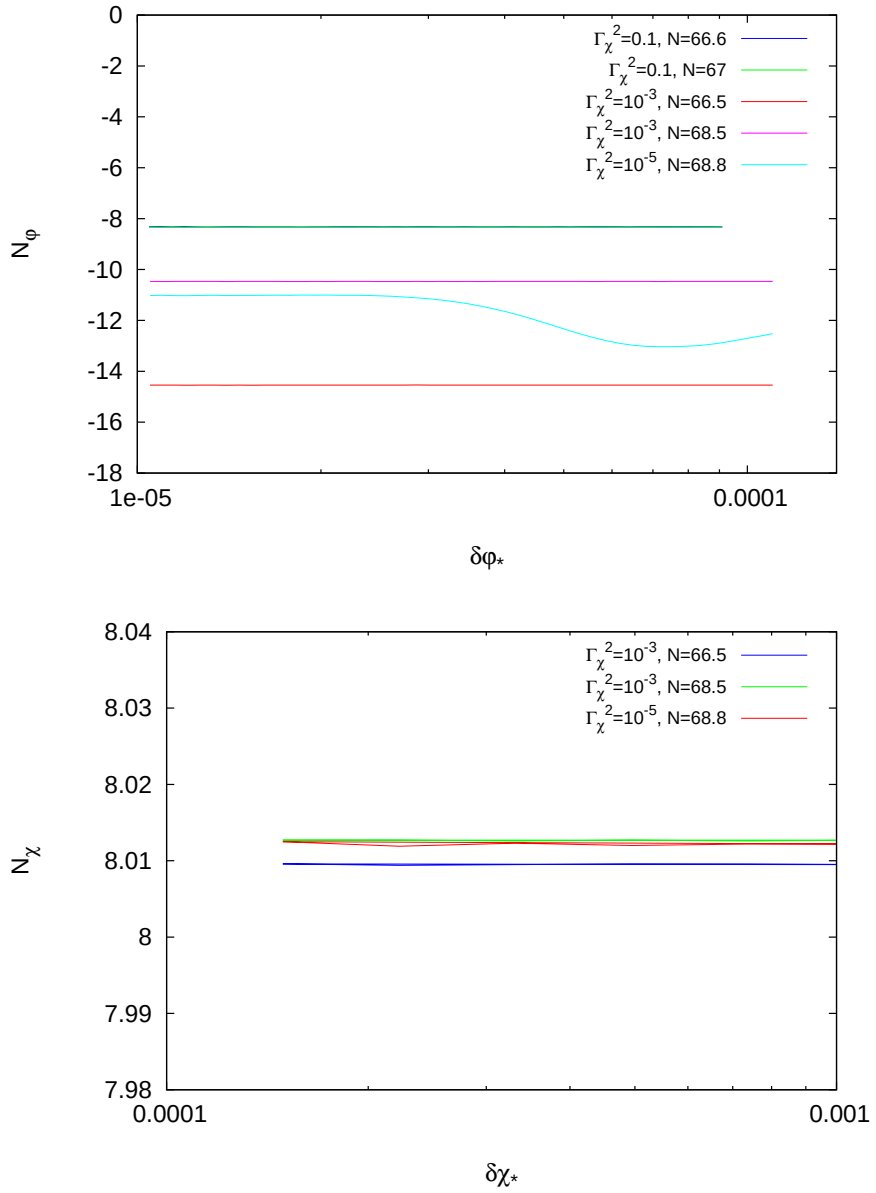

Figure B.2: Potential: $W(\varphi, \chi) = W_0 \chi^2 e^{-\lambda \varphi^2/M_{\rm p}^2}$. The model parameters $\lambda = 0.05$, $\varphi_* = 10^{-3} M_{\rm p}$ and $\chi_* = 16.0 M_{\rm p}$. First order δN coefficients evaluated using the numerical recipe discussed as a function of the step sizes: N_φ (*top panel*) and N_χ (*bottom panel*).

Second Order δN coefficients

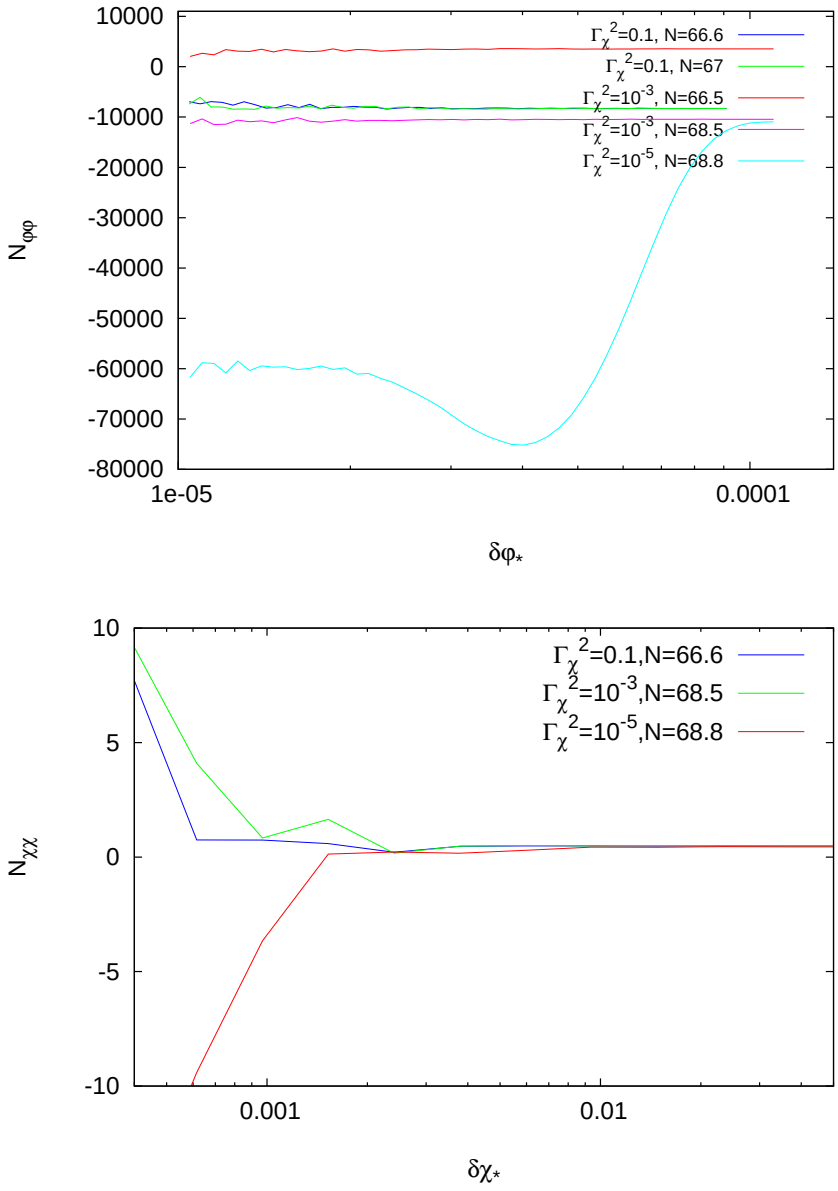

Figure B.3: Potential: $W(\varphi, \chi) = W_0 \chi^2 e^{-\lambda\varphi^2/M_{\rm P}^2}$. The model parameters $\lambda = 0.05$, $\varphi_* = 10^{-3} M_{\rm P}$ and $\chi_* = 16.0 M_{\rm P}$. Second order δN coefficients evaluated using the numerical recipe discussed as a function of the step sizes: $N_{\varphi\varphi}$ (*top panel*) and $N_{\chi\chi}$ (*bottom panel*).

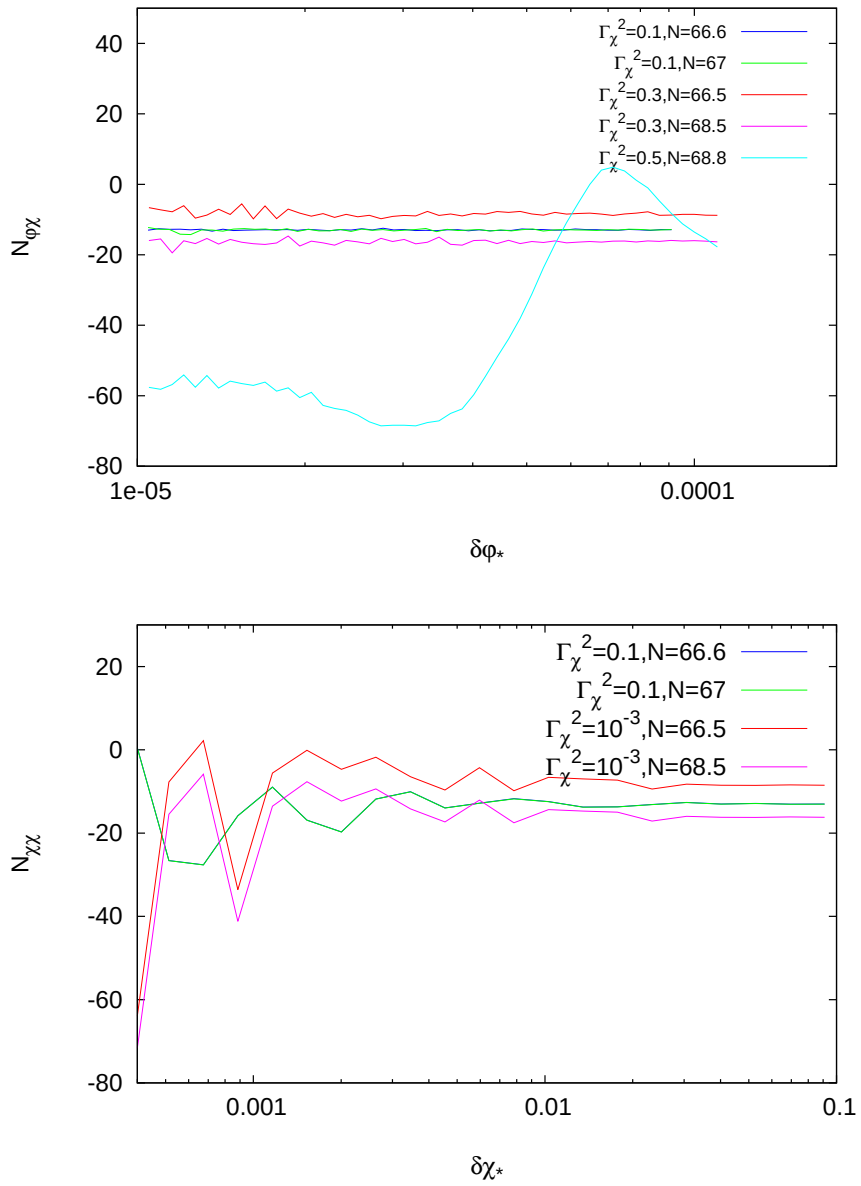

Figure B.4: Potential: $W(\varphi,\chi) = W_0\chi^2 e^{-\lambda\varphi^2/M_{\rm p}^2}$. The model parameters $\lambda = 0.05$, $\varphi_* = 10^{-3}M_{\rm p}$ and $\chi_* = 16.0M_{\rm p}$. Second order δN coefficient $N_{\varphi\chi}$ evaluated using the numerical recipe discussed as a function of the step sizes: $\delta\varphi_*$, with fixed $\delta\chi_* \sim O(10^{-2})$ (*top panel*) and $\delta\chi_*$ with fixed $\delta\varphi_* = 2.1\times10^{-5}$ (*bottom panel*).

Primordial Observables

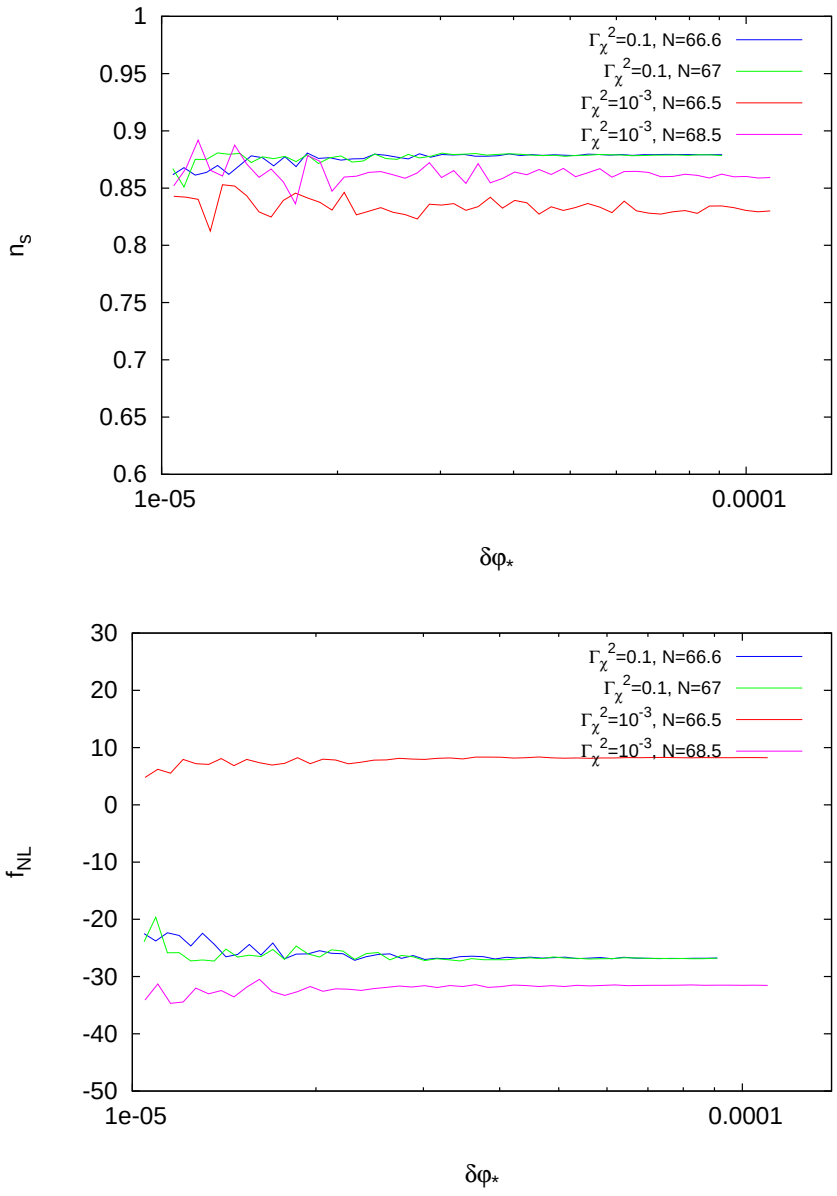

Figure B.5: Potential: $W(\varphi, \chi) = W_0 \chi^2 e^{-\lambda\varphi^2/M_{\rm P}^2}$. The model parameters $\lambda = 0.05$, $\varphi_* = 10^{-3} M_{\rm P}$ and $\chi_* = 16.0 M_{\rm P}$. First order δN coefficients evaluated using the numerical recipe discussed as a function of the step size $\delta\varphi_*$, with fixed $\delta\chi_* \sim O(10^{-2})$: $n_{\rm s}$ (*top panel*) and $f_{\rm NL}$ (*bottom panel*).

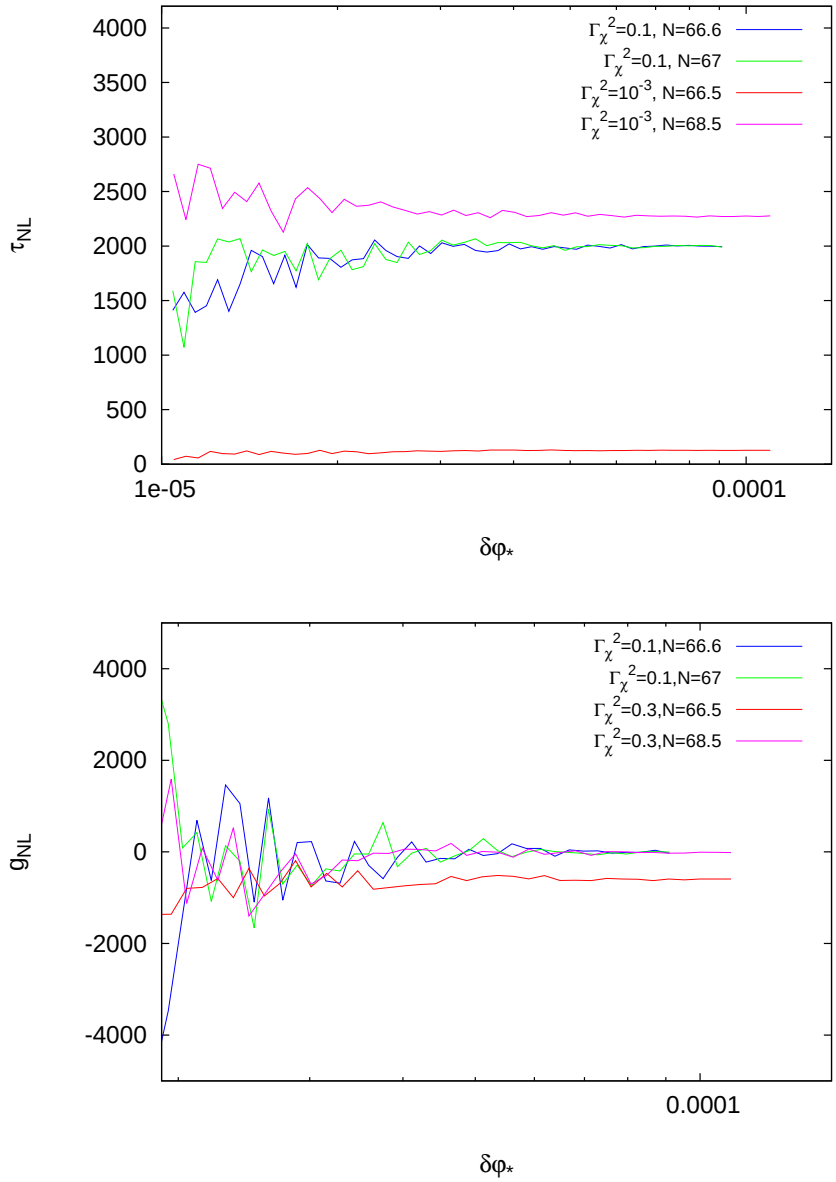

Figure B.6: Potential: $W(\varphi, \chi) = W_0 \chi^2 e^{-\lambda\varphi^2/M_{\rm p}^2}$. The model parameters $\lambda = 0.05$, $\varphi_* = 10^{-3} M_{\rm p}$ and $\chi_* = 16.0 M_{\rm p}$. First order δN coefficients evaluated using the numerical recipe discussed as a function of the step size $\delta\varphi_*$, with fixed $\delta\chi_* \sim O(10^{-2})$: $\tau_{\rm NL}$ (*top panel*) and $g_{\rm NL}$ (*bottom panel*).

Effective N-flation Model

First Order δN coefficients

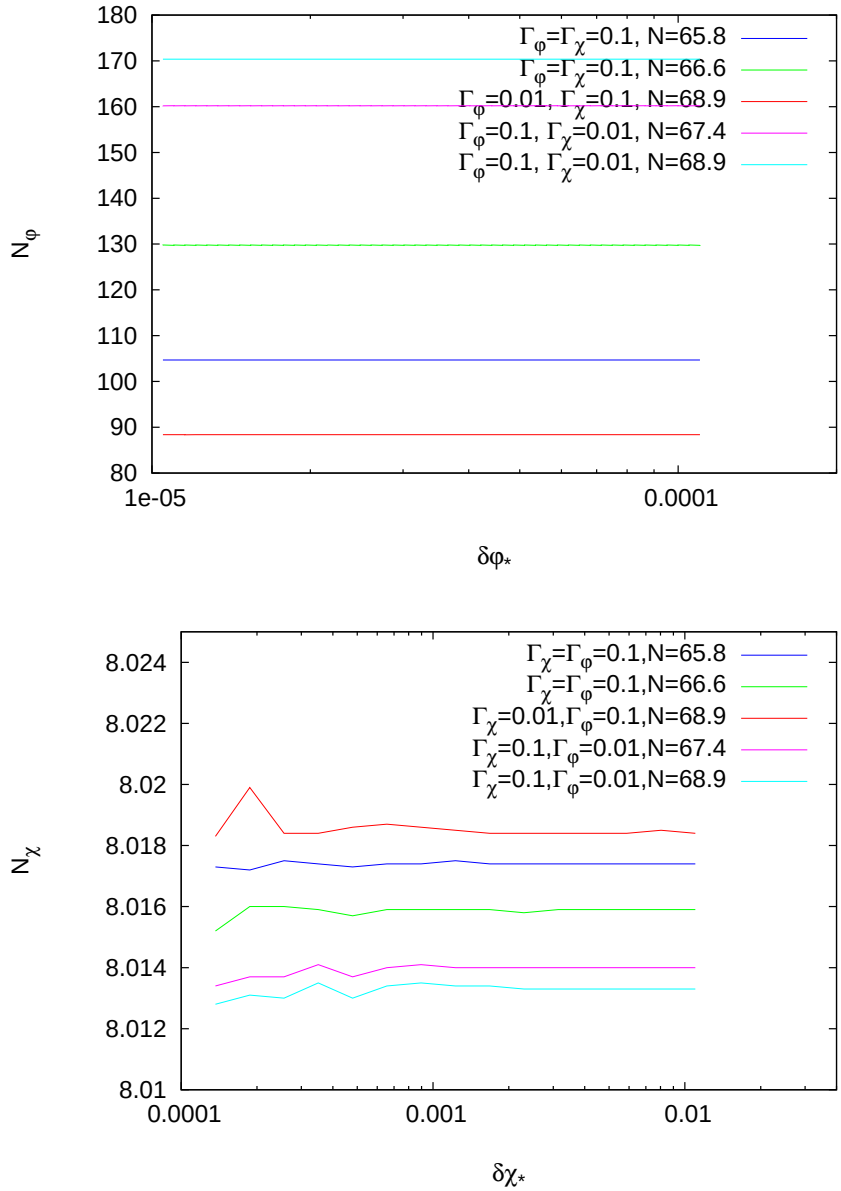

Figure B.7: $W(\varphi,\chi) = W_0\left[\frac{1}{2}m^2\chi^2 + \Lambda^4\left(1-\cos\left(\frac{2\pi}{f}\varphi\right)\right)\right]$. The parameters used are: $\Lambda^4 = m^2f^2/4\pi^2$, $\varphi_* = (\frac{1}{2}-0.001)f$, $\chi_* = 16M_{\rm p}$, $f = m = M_{\rm p}$. First order δN coefficients evaluated using the numerical recipe discussed as a function of the step sizes used, for different combinations of decay rates and : N_φ (*top panel*) and N_χ (*bottom panel*).

Second Order δN coefficients

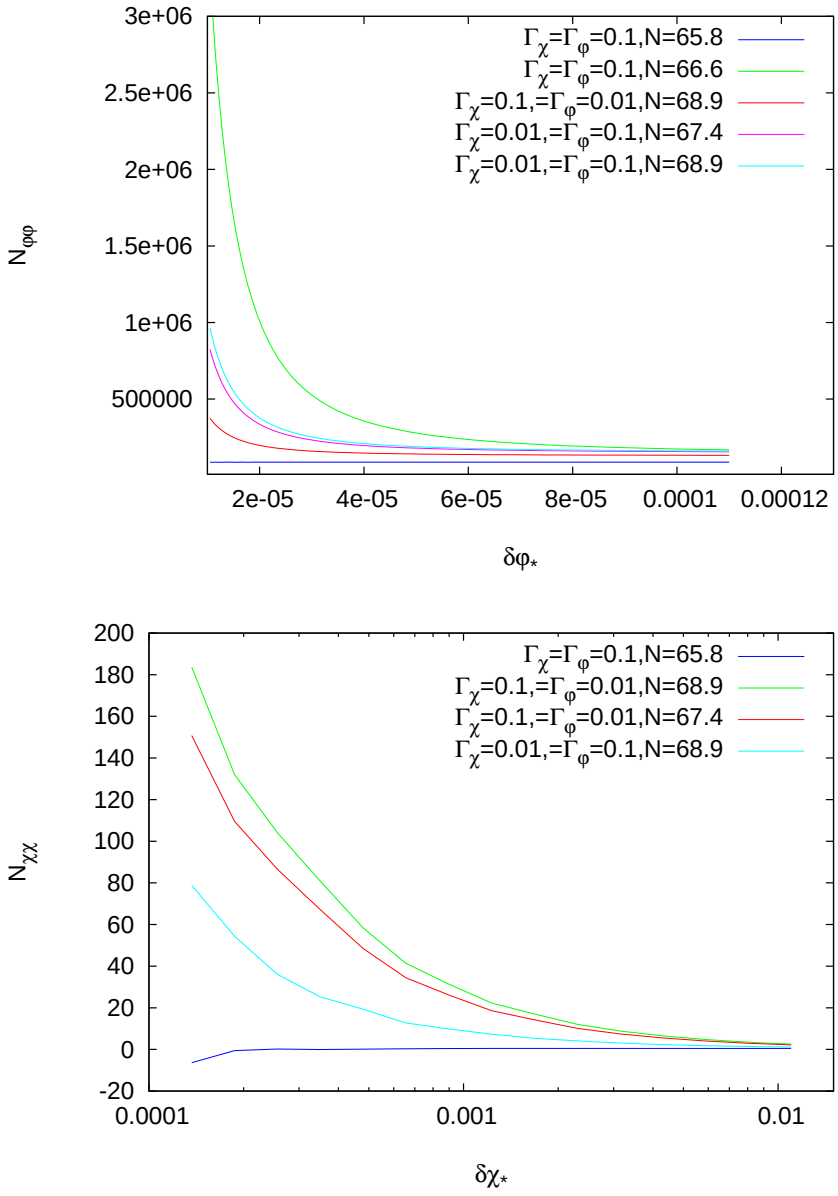

Figure B.8: $W(\varphi,\chi) = W_0\left[\frac{1}{2}m^2\chi^2 + \Lambda^4\left(1-\cos\left(\frac{2\pi}{f}\varphi\right)\right)\right]$. The parameters used are: $\Lambda^4 = m^2f^2/4\pi^2$, $\varphi_* = (\frac{1}{2}-0.001)f$, $\chi_* = 16M_{\rm p}$, $f = m = M_{\rm p}$. Second order δN coefficients evaluated using the numerical recipe discussed as a function of the step sizes used: $N_{\varphi\varphi}$ (*top panel*) and $N_{\chi\chi}$ (*bottom panel*).

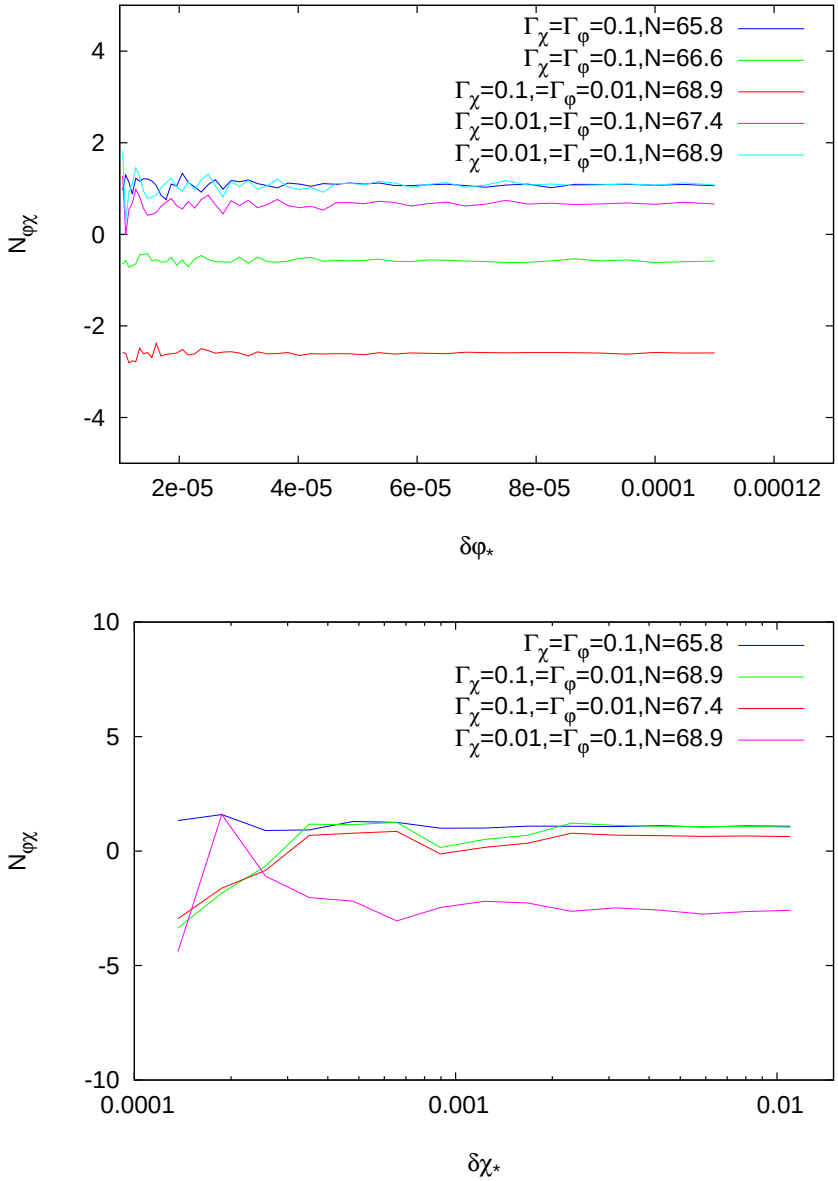

Figure B.9: $W(\varphi,\chi) = W_0\left[\frac{1}{2}m^2\chi^2 + \Lambda^4\left(1-\cos\left(\frac{2\pi}{f}\varphi\right)\right)\right]$. The parameters used are: $\Lambda^4 = m^2f^2/4\pi^2$, $\varphi_* = (\frac{1}{2}-0.001)f$, $\chi_* = 16M_{\rm p}$, $f = m = M_{\rm p}$. Second order δN coefficient $N_{\varphi\chi}$ evaluated using the numerical recipe discussed as a function of the step sizes used: $\delta\varphi_*$, with fixed $\delta\chi_* = 1.1\times10^{-2}$ (*top panel*) and $\delta\chi_*$, with fixed $\delta\varphi_* = 1.1\times10^{-4}$(*bottom panel*).

Primordial Observables

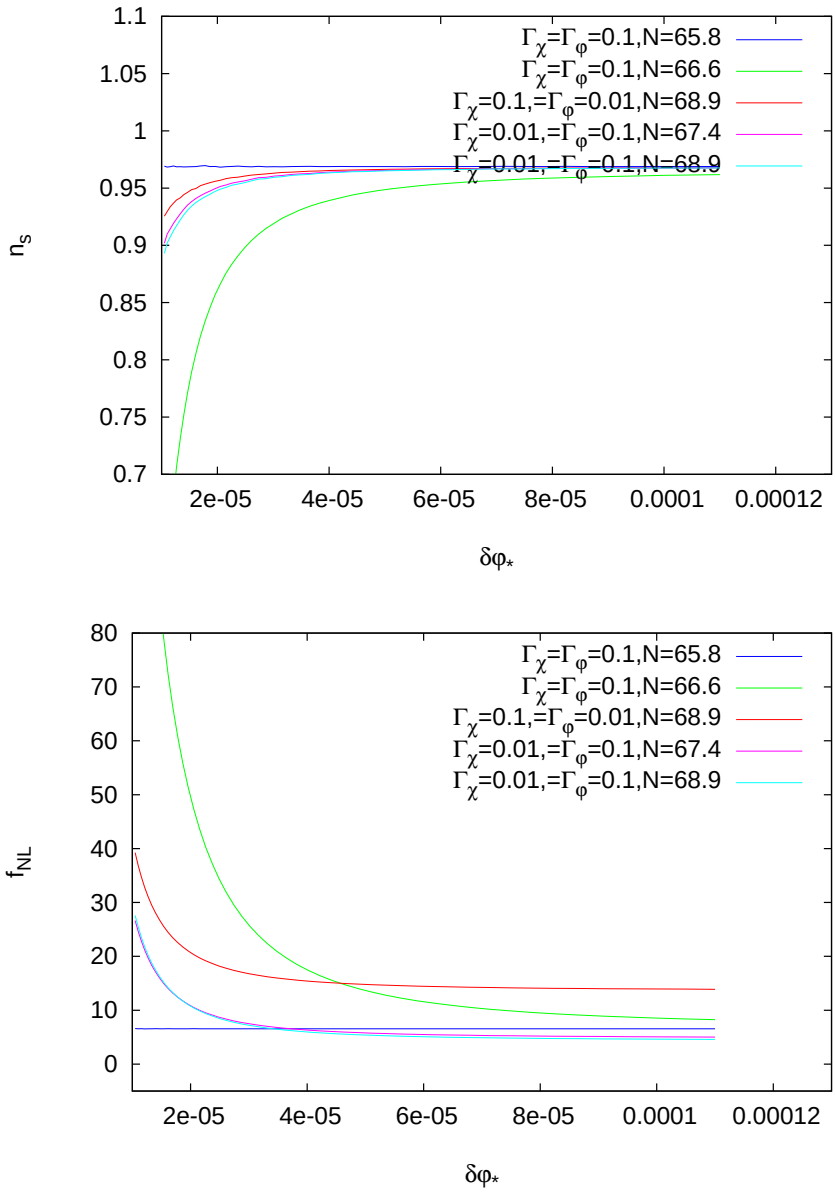

Figure B.10: $W(\varphi,\chi) = W_0\left[\frac{1}{2}m^2\chi^2 + \Lambda^4\left(1-\cos\left(\frac{2\pi}{f}\varphi\right)\right)\right]$. The parameters used are: $\Lambda^4 = m^2f^2/4\pi^2$, $\varphi_* = (\frac{1}{2}-0.001)f$, $\chi_* = 16M_{\rm p}$, $f = m = M_{\rm p}$. Observables evaluated using the numerical recipe discussed as a function of the step size $\delta\varphi_*$ used, with fixed $\delta\chi_* \sim O(10^{-2})$: $n_{\rm s}$ (*top panel*) and $f_{\rm NL}$ (*bottom panel*).

This numerical recipe provides a fast, efficient method for computing the δN coefficients for an arbitrary two–field model, valid beyond slow–roll and through a phase of reheating. Numerical codes based on the moment transport equations have also been developed [152] and have been extended to study sub-horizon evolution [190].

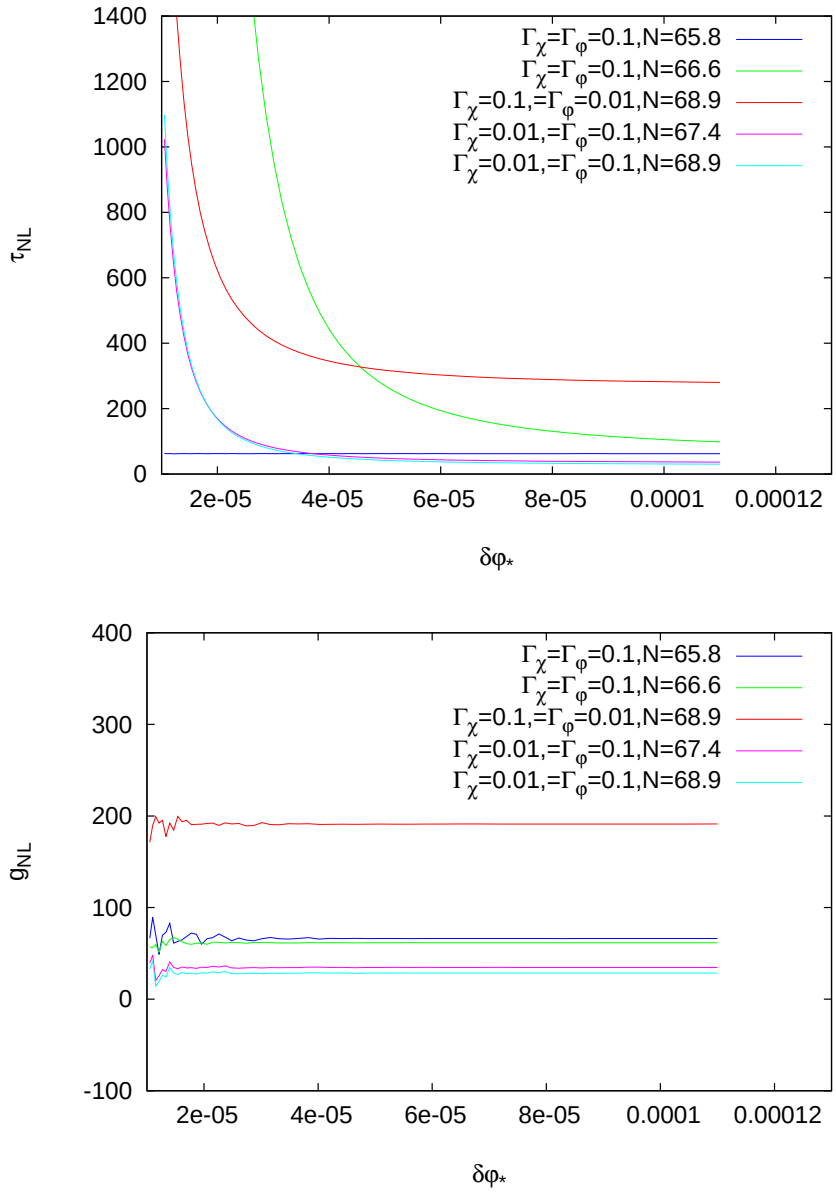

Figure B.11: $W(\varphi,\chi) = W_0\left[\frac{1}{2}m^2\chi^2 + \Lambda^4\left(1-\cos\left(\frac{2\pi}{f}\varphi\right)\right)\right]$. The parameters used are: $\Lambda^4 = m^2f^2/4\pi^2$, $\varphi_* = (\frac{1}{2}-0.001)f$, $\chi_* = 16M_{\rm p}$, $f = m = M_{\rm p}$. Observables evaluated using the numerical recipe discussed as a function of the step size $\delta\varphi_*$ used, with fixed $\delta\chi_* \sim O(10^{-2})$: $\tau_{\rm NL}$ (*top panel*) and $g_{\rm NL}$ (*bottom panel*).

B.1 Discussion on the Definition of Reheating Hypersurfaces

As discussed in Section 4.1, the reheating parameters Γ_φ and Γ_χ are set to zero during inflation. It is only when each individual trajectory in the bundle passes through its minimum $\{\chi_0,\varphi_0\}$ for the first time that Γ_φ and Γ_χ are introduced to the field equa-

tions, sourcing the radiation fluid. In general, for any given trajectory, φ will not reach the minimum of its potential at the same time as χ, and so Γ_φ and Γ_χ are 'switched on' at different times along the same trajectory. Furthermore, for each of the two directions of the potential, the foliation of the entire bundle of trajectories as determined by each trajectory reaching χ_0 (and likewise φ_0) does not in general occur at a surface of constant time or a surface of constant energy, but rather at a surface of constant χ_0 (and φ_0)[1]. We refer to these surfaces as the *reheating hypersurfaces*. For potentials which have minima in both directions there are two such hypersurfaces. If the potential does not have a minimum in the χ (or φ) direction, then $\Gamma_\chi = 0$ (or $\Gamma_\varphi = 0$) always. Furthermore, we also ensure that when the potential has a minimum in, say, the χ direction, the conditions $m_\chi \gg \Gamma_\chi$ and $m_\chi \gg H$ are satisfied. This definition of the reheating hypersurface is more refined than that of [106], where reheating was initiated at a surface of constant density. It is also different to that of [191], where the decay terms were present throughout inflation.

The main qualitative results are however independent of the definition of the reheating hypersurface. We demonstrate this by using the quadratic time exponential model as an example. Using a different definition of the reheating hypersurface where Γ is switched on when $H = \Gamma$, we plot the final asymptotic value of the observables after reheating in the model in Fig. B.12. In brief, we see the observables are sensitive to reheating in the case where $\lambda = 0.05$ and $N_\varphi \sim N_\chi$. Comparing with the results with Fig. 4.20 in Section 4.3, we again see the final asmyptotic value of $f_{\rm NL}$ can be sensitive to the decay rate Γ_χ, particularly for $\lambda = 0.05$. $n_{\rm s}$ and r however are much less sensitive to Γ_χ in this choice of the reheating hypersurface.

[1]This is true for global minima. If the oscillations of one field, χ say, occurred in a local minimum, which is a function of the other field, $\chi_0(\varphi)$, this statement will not hold true. We do not consider such models in this thesis.

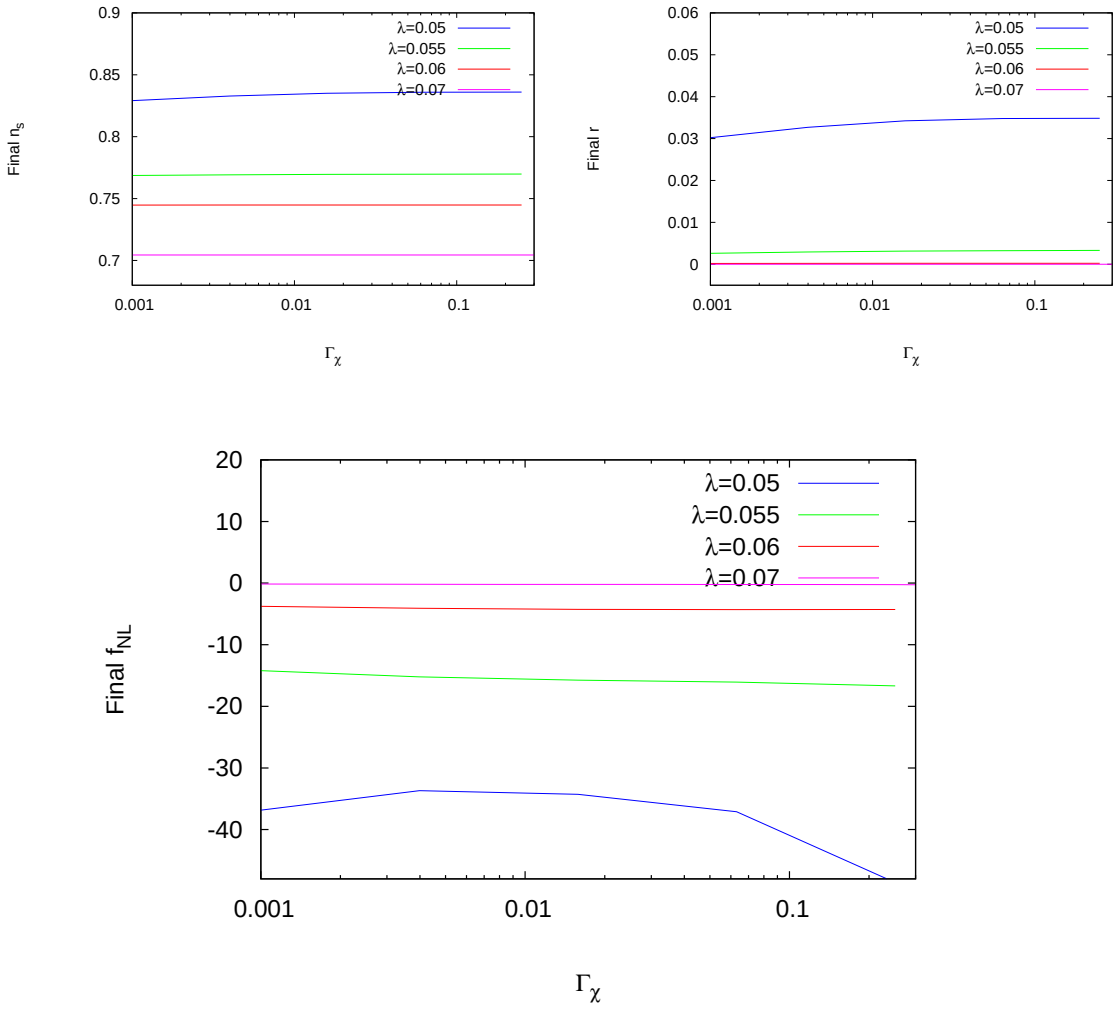

Figure B.12: $W(\varphi,\chi) = W_0\chi^2 e^{-\lambda\varphi^2/M_{\rm p}^2}$. The final asymptotic values of $n_{\rm s}$ (*top left panel*), r (*top right panel*) and $f_{\rm NL}$ (*bottom panel*) at the end of reheating as a function of the decay rate Γ_χ for four different λ. The initial field values are $\varphi_* = 10^{-3}M_{\rm p}$ and $\chi_* = 16.0M_{\rm p}$.

Bibliography

[1] Smoot G.F., Bennett C., Kogut A., Wright E., Aymon J., *et al.*, "Structure in the COBE differential microwave radiometer first year maps," *Astrophys.J.* **396** (1992) L1–L5.

[2] WMAP Collaboration, Spergel D. *et al.*, "First year Wilkinson Microwave Anisotropy Probe (WMAP) observations: Determination of cosmological parameters," *Astrophys.J.Suppl.* **148** (2003) 175–194, arXiv:astro-ph/0302209 [astro-ph].

[3] Kallosh R. and Linde A., "Universality Class in Conformal Inflation," *JCAP* **1307** (2013) 002, arXiv:1306.5220 [hep-th].

[4] Clifton T., Clarkson C., and Bull P., "The isotropic blackbody CMB as evidence for a homogeneous universe," *Phys.Rev.Lett.* **109** (2012) 051303, arXiv:1111.3794 [gr-qc].

[5] Planck Collaboration Collaboration, Ade P. *et al.*, "Planck 2013 results. XXIII. Isotropy and statistics of the CMB," *Astron.Astrophys.* **571** (2014) A23, arXiv:1303.5083 [astro-ph.CO].

[6] Scrimgeour M., Davis T., Blake C., James J.B., Poole G., *et al.*, "The WiggleZ Dark Energy Survey: the transition to large-scale cosmic homogeneity," *Mon.Not.Roy.Astron.Soc.* **425** (2012) 116–134, arXiv:1205.6812 [astro-ph.CO].

[7] Clowes R.G., Harris K.A., Raghunathan S., Campusano L.E., Soechting I.K., *et al.*, "A structure in the early universe at z $\sim$ 1.3 that exceeds the homogeneity scale of the R-W concordance cosmology," *Mon.Not.Roy.Astron.Soc.* **429** (2013) 2910–2916, arXiv:1211.6256 [astro-ph.CO].

[8] Planck Collaboration Collaboration, Ade P. *et al.*, "Planck 2013 results. I. Overview of products and scientific results," *Astron.Astrophys.* **571** (2014) A1, arXiv:1303.5062 [astro-ph.CO].

[9] Weinberg S., *Cosmology*. Oxford University Press, USA, Apr., 2008.

[10] Paal G., Horvath I., and Lukacs B., "Inflation and compactification from galaxy redshifts?," *Astrophysics and Space Science* **191** (1992) 107–124.

[11] Weinberg S., "The Cosmological Constant Problem," *Rev.Mod.Phys.* **61** (1989) 1–23.

[12] Carroll S.M., "The Cosmological constant," *Living Rev.Rel.* **4** (2001) 1, arXiv:astro-ph/0004075 [astro-ph].

[13] Carroll S.M., "In What Sense Is the Early Universe Fine-Tuned?," arXiv:1406.3057 [astro-ph.CO].

[14] Dicke R. and Peebles P., "The big bang cosmology: Enigmas and nostrums," *in* General relativity: an Einstein centenary survey **1** (1979) 504–517.

[15] Planck Collaboration Collaboration, Ade P. *et al.*, "Planck 2013 results. XVI. Cosmological parameters," *Astron.Astrophys.* **571** (2014) A16, arXiv:1303.5076 [astro-ph.CO].

[16] Liddle A.R. and Cortês M., "Cosmic microwave background anomalies in an open universe," *Phys.Rev.Lett.* **111** (2013) no. 11, 111302, arXiv:1306.5698 [astro-ph.CO].

[17] Carroll S.M. and Tam H., "Unitary Evolution and Cosmological Fine-Tuning," CALT-68-2797, arXiv:1007.1417 [hep-th].

[18] Misner C.W., "Mixmaster universe," *Phys.Rev.Lett.* **22** (1969) 1071–1074.

[19] Hooft G., "Magnetic monopoles in unified gauge theories," *Nuclear Physics B* **79** (1974) no. 2, 276 – 284.

[20] Guth A.H., "Inflationary universe: A possible solution to the horizon and flatness problems," *Phys.Rev.D* **23** (1981) 347–356.

[21] Starobinsky A., "A new type of isotropic cosmological models without singularity," *Physics Letters B* **91** (1980) no. 1, 99 – 102.

[22] Penrose R., "Difficulties with inflationary cosmology," *Annals N.Y.Acad.Sci.* **571** (1989) 249–264.

[23] Linde A., "A new inflationary universe scenario: A possible solution of the horizon, flatness, homogeneity, isotropy and primordial monopole problems," *Physics Letters B* **108** (1982) no. 6, 389 – 393.

[24] Liddle A.R. and Lyth D.H., "COBE, gravitational waves, inflation and extended inflation," *Phys.Lett.* **B291** (1992) 391–398, arXiv:astro-ph/9208007 [astro-ph].

[25] Liddle A.R. and Lyth D.H., "The Cold dark matter density perturbation," *Phys.Rept.* **231** (1993) 1–105, arXiv:astro-ph/9303019 [astro-ph].

[26] Liddle A.R. and Leach S.M., "How long before the end of inflation were observable perturbations produced?," *Phys.Rev.* **D68** (2003) 103503, arXiv:astro-ph/0305263 [astro-ph].

[27] Bardeen J.M., "Gauge Invariant Cosmological Perturbations," *Phys.Rev.* **D22** (1980) 1882–1905.

[28] Kodama H. and Sasaki M., "Cosmological Perturbation Theory," *Prog.Theor.Phys.Suppl.* **78** (1984) 1–166.

[29] Mukhanov V.F., Feldman H.A., and Brandenberger R.H., "Theory of cosmological perturbations," *Phys.Rep* **215** (1992) 203–333.

[30] Sasaki M. and Tanaka T., "Superhorizon scale dynamics of multiscalar inflation," *Prog.Theor.Phys.* **99** (1998) 763–782, arXiv:gr-qc/9801017 [gr-qc].

[31] Wands D., Malik K.A., Lyth D.H., and Liddle A.R., "A New approach to the evolution of cosmological perturbations on large scales," *Phys.Rev.* **D62** (2000) 043527, arXiv:astro-ph/0003278 [astro-ph].

[32] Lyth D.H. and Wands D., "Conserved cosmological perturbations," *Phys.Rev.* **D68** (2003) 103515, arXiv:astro-ph/0306498 [astro-ph].

[33] Sasaki M. and Stewart E.D., "A General analytic formula for the spectral index of the density perturbations produced during inflation," *Prog.Theor.Phys.* **95** (1996) 71–78, arXiv:astro-ph/9507001 [astro-ph].

[34] Starobinsky A.A., "Multicomponent de Sitter (Inflationary) Stages and the Generation of Perturbations," *JETP Lett.* **42** (1985) 152–155.

[35] Christopherson A.J., Malik K.A., and Matravers D.R., "Vorticity generation at second order in cosmological perturbation theory," *Phys.Rev.* **D79** (2009) 123523, arXiv:0904.0940 [astro-ph.CO].

[36] Lukash V., "Production of phonons in an isotropic universe," *Sov.Phys.JETP* **52** (1980) 807–814.

[37] Lyth D., "Large Scale Energy Density Perturbations and Inflation," *Phys.Rev.* **D31** (1985) 1792–1798.

[38] Bardeen J.M., Steinhardt P.J., and Turner M.S., "Spontaneous Creation of Almost Scale - Free Density Perturbations in an Inflationary Universe," *Phys.Rev.* **D28** (1983) 679.

[39] Martin J. and Schwarz D.J., "The Influence of cosmological transitions on the evolution of density perturbations," *Phys.Rev.* **D57** (1998) 3302–3316, arXiv:gr-qc/9704049 [gr-qc].

[40] White J., Minamitsuji M., and Sasaki M., "Curvature perturbation in multi-field inflation with non-minimal coupling," *JCAP* **1207** (2012) 039, arXiv:1205.0656 [astro-ph.CO].

[41] White J., Minamitsuji M., and Sasaki M., "Non-linear curvature perturbation in multi-field inflation models with non-minimal coupling," *JCAP* **1309** (2013) 015, arXiv:1306.6186 [astro-ph.CO].

[42] Postma M. and Volponi M., "Equivalence of the Einstein and Jordan frames," arXiv:1407.6874 [astro-ph.CO].

[43] Cortês M., Liddle A.R., and Mukherjee P., "On what scale should inflationary observables be constrained?," *Phys.Rev.* **D75** (2007) 083520, arXiv:astro-ph/0702170 [astro-ph].

[44] Planck Collaboration Collaboration, Ade P. *et al.*, "Planck 2013 results. XXII. Constraints on inflation," *Astron.Astrophys.* **571** (2014) A22, arXiv:1303.5082 [astro-ph.CO].

[45] BICEP2 Collaboration, Ade P. *et al.*, "Detection of B-Mode Polarization at Degree Angular Scales by BICEP2," *Phys.Rev.Lett.* **112** (2014) 241101, arXiv:1403.3985 [astro-ph.CO].

[46] Flauger R., Hill J.C., and Spergel D.N., "Toward an Understanding of Foreground Emission in the BICEP2 Region," arXiv:1405.7351 [astro-ph.CO].

[47] Komatsu E. and Spergel D.N., "Acoustic signatures in the primary microwave background bispectrum," *Phys.Rev.* **D63** (2001) 063002, arXiv:astro-ph/0005036 [astro-ph].

[48] Byrnes C.T., Sasaki M., and Wands D., "The primordial trispectrum from inflation," *Phys.Rev.* **D74** (2006) 123519, arXiv:astro-ph/0611075 [astro-ph].

[49] Seery D. and Lidsey J.E., "Non-Gaussianity from the inflationary trispectrum," *JCAP* **0701** (2007) 008, arXiv:astro-ph/0611034 [astro-ph].

[50] Chen X., "Primordial Non-Gaussianities from Inflation Models," *Adv.Astron.* **2010** (2010) 638979, arXiv:1002.1416 [astro-ph.CO].

[51] Planck Collaboration Collaboration, Ade P. *et al.*, "Planck 2013 Results. XXIV. Constraints on primordial non-Gaussianity," *Astron.Astrophys.* **571** (2014) A24, arXiv:1303.5084 [astro-ph.CO].

[52] Giannantonio T., Ross A.J., Percival W.J., Crittenden R., Bacher D., *et al.*, "Improved Primordial Non-Gaussianity Constraints from Measurements of Galaxy Clustering and the Integrated Sachs-Wolfe Effect," *Phys.Rev.* **D89** (2014) 023511, arXiv:1303.1349 [astro-ph.CO].

[53] Leistedt B., Peiris H.V., and Roth N., "Constraints on primordial non-Gaussianity from 800,000 photometric quasars," arXiv:1405.4315 [astro-ph.CO].

[54] Karagiannis D., Shanks T., and Ross N.P., "Search for primordial non-Gaussianity in the quasars of SDSS-III BOSS DR9," *Mon.Not.Roy.Astron.Soc.* **441** (2014) 486–502, arXiv:1310.6716 [astro-ph.CO].

[55] Byrnes C.T., Nurmi S., Tasinato G., and Wands D., "Implications of the Planck bispectrum constraints for the primordial trispectrum," *Europhys.Lett.* **103** (2013) 19001, arXiv:1306.2370 [astro-ph.CO].

[56] Sekiguchi T. and Sugiyama N., "Optimal constraint on g_{NL} from CMB," *JCAP* **1309** (2013) 002, arXiv:1303.4626 [astro-ph.CO].

[57] Regan D., Gosenca M., and Seery D., "Constraining the WMAP9 bispectrum and trispectrum with needlets," arXiv:1310.8617 [astro-ph.CO].

[58] Chen X., "Running non-Gaussianities in DBI inflation," *Phys.Rev.* **D72** (2005) 123518, arXiv:astro-ph/0507053 [astro-ph].

[59] Byrnes C.T., Choi K.Y., and Hall L.M., "Large non-Gaussianity from two-component hybrid inflation," *JCAP* **0902** (2009) 017, arXiv:0812.0807 [astro-ph].

[60] Byrnes C.T., Gerstenlauer M., Nurmi S., Tasinato G., and Wands D., "Scale-dependent non-Gaussianity probes inflationary physics," *JCAP* **1010** (2010) 004, arXiv:1007.4277 [astro-ph.CO].

[61] Shandera S., Dalal N., and Huterer D., "A generalized local ansatz and its effect on halo bias," *JCAP* **1103** (2011) 017, arXiv:1010.3722 [astro-ph.CO].

[62] Byrnes C.T., Enqvist K., Nurmi S., and Takahashi T., "Strongly scale-dependent polyspectra from curvaton self-interactions," *JCAP* **1111** (2011) 011, arXiv:1108.2708 [astro-ph.CO].

[63] Kobayashi T. and Takahashi T., "Runnings in the Curvaton," *JCAP* **1206** (2012) 004, arXiv:1203.3011 [astro-ph.CO].

[64] Byrnes C.T., Cortês M., and Liddle A.R., "Comprehensive analysis of the simplest curvaton model," *Phys.Rev.* **D90** (2014) 023523, arXiv:1403.4591 [astro-ph.CO].

[65] Sefusatti E., Liguori M., Yadav A.P., Jackson M.G., and Pajer E., "Constraining Running Non-Gaussianity," *JCAP* **0912** (2009) 022, arXiv:0906.0232 [astro-ph.CO].

[66] Biagetti M., Perrier H., Riotto A., and Desjacques V., "Testing the running of non-Gaussianity through the CMB μ-distortion and the halo bias," *Phys.Rev.* **D87** (2013) no. 6, 063521, arXiv:1301.2771 [astro-ph.CO].

[67] Lyth D.H., Malik K.A., and Sasaki M., "A General proof of the conservation of the curvature perturbation," *JCAP* **0505** (2005) 004, arXiv:astro-ph/0411220 [astro-ph].

[68] Salopek D.S. and Bond J.R., "Nonlinear evolution of long-wavelength metric fluctuations in inflationary models," *Phys. Rev. D* **42** (1990) 3936–3962.

[69] Lyth D.H. and Rodriguez Y., "The Inflationary prediction for primordial non-Gaussianity," *Phys.Rev.Lett.* **95** (2005) 121302, arXiv:astro-ph/0504045 [astro-ph].

[70] Arnowitt R.L., Deser S., and Misner C.W., "Dynamical Structure and Definition of Energy in General Relativity," *Phys.Rev.* **116** (1959) 1322–1330.

[71] Rigopoulos G. and Shellard E., "The separate universe approach and the evolution of nonlinear superhorizon cosmological perturbations," *Phys.Rev.* **D68** (2003) 123518, arXiv:astro-ph/0306620 [astro-ph].

[72] Christopherson A.J. and Malik K.A., "The non-adiabatic pressure in general scalar field systems," *Phys.Lett.* **B675** (2009) 159–163, arXiv:0809.3518 [astro-ph].

[73] Naruko A. and Sasaki M., "Conservation of the nonlinear curvature perturbation in generic single-field inflation," *Class.Quant.Grav.* **28** (2011) 072001, arXiv:1101.3180 [astro-ph.CO].

[74] Gao X., "Conserved cosmological perturbation in Galileon models," *JCAP* **1110** (2011) 021, arXiv:1106.0292 [astro-ph.CO].

[75] Maldacena J.M., "Non-Gaussian features of primordial fluctuations in single field inflationary models," *JHEP* **0305** (2003) 013, arXiv:astro-ph/0210603 [astro-ph].

[76] Weinberg S., "Quantum contributions to cosmological correlations," *Phys.Rev.* **D72** (2005) 043514 UTTG-01-05, arXiv:hep-th/0506236 [hep-th].

[77] Adshead P., Easther R., and Lim E.A., "The 'in-in' Formalism and Cosmological Perturbations," *Phys.Rev.* **D80** (2009) 083521, arXiv:0904.4207 [hep-th].

[78] Saffin P.M., "The covariance of multi-field perturbations, pseudo-susy and f_{NL}," *JCAP* **1209** (2012) 002, arXiv:1203.0397 [hep-th].

[79] Elliston J., Seery D., and Tavakol R., "The inflationary bispectrum with curved field-space," *JCAP* **1211** (2012) 060, arXiv:1208.6011 [astro-ph.CO].

[80] Gong J.O. and Tanaka T., "A covariant approach to general field space metric in multi-field inflation," *JCAP* **1103** (2011) 015, arXiv:1101.4809 [astro-ph.CO].

[81] Mukhanov V.F., "Gravitational Instability of the Universe Filled with a Scalar Field," *JETP Lett.* **41** (1985) 493–496.

[82] Sasaki M., "Large Scale Quantum Fluctuations in the Inflationary Universe," *Prog.Theor.Phys.* **76** (1986) 1036.

[83] Stewart E.D. and Lyth D.H., "A More accurate analytic calculation of the spectrum of cosmological perturbations produced during inflation," *Phys.Lett.* **B302** (1993) 171–175, arXiv:gr-qc/9302019 [gr-qc].

[84] Lidsey J.E., Liddle A.R., Kolb E.W., Copeland E.J., Barreiro T., *et al.*, "Reconstructing the inflation potential : An overview," *Rev.Mod.Phys.* **69** (1997) 373–410, arXiv:astro-ph/9508078 [astro-ph].

[85] Hwang J.C. and Noh H., "Cosmological perturbations in generalized gravity theories," *Phys.Rev.* **D54** (1996) 1460–1473.

[86] Bunch T.S. and Davies P.C.W., "Quantum field theory in de Sitter space - Renormalization by point-splitting," *Royal Society of London Proceedings Series A* **360** (1978) 117–134.

[87] Nalson E., Christopherson A.J., Huston I., and Malik K.A., "Quantifying the behaviour of curvature perturbations during inflation," *Class.Quant.Grav.* **30** (2013) 065008, arXiv:1111.6940 [astro-ph.CO].

[88] Seery D. and Lidsey J.E., "Primordial non-Gaussianities in single field inflation," *JCAP* **0506** (2005) 003, arXiv:astro-ph/0503692 [astro-ph].

[89] Bartolo N., Matarrese S., and Riotto A., "Non-Gaussianity and the Cosmic Microwave Background Anisotropies," *Advances in Astronomy* **2010** (2010) , arXiv:1001.3957 [astro-ph.CO].

[90] Alishahiha M., Silverstein E., and Tong D., "DBI in the sky," *Phys.Rev.* **D70** (2004) 123505, arXiv:hep-th/0404084 [hep-th].

[91] Bean R., Chen X., Hailu G., Tye S.H.H., and Xu J., "Duality Cascade in Brane Inflation," *JCAP* **0803** (2008) 026, arXiv:0802.0491 [hep-th].

[92] Battefeld D., Battefeld T., Giblin John T. J., and Pease E.K., "Observable Signatures of Inflaton Decays," *JCAP* **1102** (2011) 024, arXiv:1012.1372 [astro-ph.CO].

[93] Barnaby N. and Huang Z., "Particle Production During Inflation: Observational Constraints and Signatures," *Phys.Rev.* **D80** (2009) 126018, arXiv:0909.0751 [astro-ph.CO].

[94] Ashoorioon A., Krause A., and Turzynski K., "Energy Transfer in Multi Field Inflation and Cosmological Perturbations," *JCAP* **0902** (2009) 014, arXiv:0810.4660 [hep-th].

[95] Romano A.E. and Sasaki M., "Effects of particle production during inflation," *Phys.Rev.* **D78** (2008) 103522, arXiv:0809.5142 [gr-qc].

[96] Lyth D.H. and Riotto A., "Particle physics models of inflation and the cosmological density perturbation," *Phys.Rept.* **314** (1999) 1–146, arXiv:hep-ph/9807278 [hep-ph].

[97] Linde A.D., "Inflation and string cosmology," *Prog.Theor.Phys.Suppl.* **163** (2006) 295–322, arXiv:hep-th/0503195 [hep-th].

[98] Liddle A.R., Mazumdar A., and Schunck F.E., "Assisted inflation," *Phys.Rev.* **D58** (1998) 061301, arXiv:astro-ph/9804177 [astro-ph].

[99] Dimopoulos S., Kachru S., McGreevy J., and Wacker J.G., "N-flation," *JCAP* **0808** (2008) 003, arXiv:hep-th/0507205 [hep-th].

[100] Gordon C., Wands D., Bassett B.A., and Maartens R., "Adiabatic and entropy perturbations from inflation," *Phys.Rev.* **D63** (2001) 023506, arXiv:astro-ph/0009131 [astro-ph].

[101] Seery D. and Lidsey J.E., "Primordial non-Gaussianities from multiple-field inflation," *JCAP* **0509** (2005) 011, arXiv:astro-ph/0506056 [astro-ph].

[102] Byrnes C.T., Choi K.Y., and Hall L.M., "Conditions for large non-Gaussianity in two-field slow-roll inflation," *JCAP* **0810** (2008) 008, arXiv:0807.1101 [astro-ph].

[103] Vernizzi F. and Wands D., "Non-gaussianities in two-field inflation," *JCAP* **0605** (2006) 019, arXiv:astro-ph/0603799 [astro-ph].

[104] Choi K.Y., Hall L.M., and van de Bruck C., "Spectral Running and Non-Gaussianity from Slow-Roll Inflation in Generalised Two-Field Models," *JCAP* **0702** (2007) 029, arXiv:astro-ph/0701247 [astro-ph].

[105] Peterson C.M. and Tegmark M., "Non-Gaussianity in Two-Field Inflation," *Phys.Rev.* **D84** (2011) 023520, arXiv:1011.6675 [astro-ph.CO].

[106] Elliston J., Mulryne D.J., Seery D., and Tavakol R., "Evolution of fNL to the adiabatic limit," *JCAP* **1111** (2011) 005, arXiv:1106.2153 [astro-ph.CO].

[107] Elliston J., Alabidi L., Huston I., Mulryne D., and Tavakol R., "Large trispectrum in two-field slow-roll inflation," *JCAP* **1209** (2012) 001, arXiv:1203.6844 [astro-ph.CO].

[108] Byrnes C.T., Nurmi S., Tasinato G., and Wands D., "Scale dependence of local f_{NL}," *JCAP* **1002** (2010) 034, arXiv:0911.2780 [astro-ph.CO].

[109] Nakamura T.T. and Stewart E.D., "The Spectrum of cosmological perturbations produced by a multicomponent inflaton to second order in the slow roll approximation," *Phys.Lett.* **B381** (1996) 413–419, arXiv:astro-ph/9604103 [astro-ph].

[110] Leung G., Tarrant E.R., Byrnes C.T., and Copeland E.J., "Influence of Reheating on the Trispectrum and its Scale Dependence," *JCAP* **1308** (2013) 006, arXiv:1303.4678 [astro-ph.CO].

[111] Gao X., Li T., and Shukla P., "Cosmological observables in multi-field inflation with a non-flat field space," arXiv:1403.0654 [hep-th].

[112] Yang I.S., "The Strong Multifield Slowroll Condition and Spiral Inflation," *Phys.Rev.* **D85** (2012) 123532, arXiv:1202.3388 [hep-th].

[113] Berera A., "Warm inflation," *Phys.Rev.Lett.* **75** (1995) 3218–3221, arXiv:astro-ph/9509049 [astro-ph].

[114] Bassett B.A., Tsujikawa S., and Wands D., "Inflation dynamics and reheating," *Rev.Mod.Phys.* **78** (2006) 537–589, arXiv:astro-ph/0507632 [astro-ph].

[115] Allahverdi R., Brandenberger R., Cyr-Racine F.Y., and Mazumdar A., "Reheating in Inflationary Cosmology: Theory and Applications," *Ann.Rev.Nucl.Part.Sci.* **60** (2010) 27–51, arXiv:1001.2600 [hep-th].

[116] Dolgov A. and Linde A.D., "Baryon Asymmetry in Inflationary Universe," *Phys.Lett.* **B116** (1982) 329.

[117] Abbott L., Farhi E., and Wise M.B., "Particle Production in the New Inflationary Cosmology," *Phys.Lett.* **B117** (1982) 29.

[118] Kofman L., Linde A.D., and Starobinsky A.A., "Towards the theory of reheating after inflation," *Phys.Rev.* **D56** (1997) 3258–3295, arXiv:hep-ph/9704452 [hep-ph].

[119] Shtanov Y., Traschen J.H., and Brandenberger R.H., "Universe reheating after inflation," *Phys.Rev.* **D51** (1995) 5438–5455, arXiv:hep-ph/9407247 [hep-ph].

[120] Kofman L.A., "The Origin of matter in the universe: Reheating after inflation," arXiv:astro-ph/9605155 [astro-ph].

[121] Linde A.D., "Particle physics and inflationary cosmology," *Contemp.Concepts Phys.* **5** (1990) 1–362, arXiv:hep-th/0503203 [hep-th].

[122] Peskin M.E. and Schroeder D.V., *An Introduction To Quantum Field Theory (Frontiers in Physics)*. Westview Press, Oct., 1995.

[123] Kolb E.W. and Turner M.S., *The early universe*. Addison-Wesley, Jan., 1990.

[124] Kawasaki M., Kohri K., and Sugiyama N., "Cosmological constraints on late time entropy production," *Phys.Rev.Lett.* **82** (1999) 4168, arXiv:astro-ph/9811437 [astro-ph].

[125] Ichikawa K., Kawasaki M., and Takahashi F., "The Oscillation effects on thermalization of the neutrinos in the Universe with low reheating temperature," *Phys.Rev.* **D72** (2005) 043522, arXiv:astro-ph/0505395 [astro-ph].

[126] Khlopov M.Y. and Linde A.D., "Is It Easy to Save the Gravitino?," *Phys.Lett.* **B138** (1984) 265–268.

[127] Kohri K., Moroi T., and Yotsuyanagi A., "Big-bang nucleosynthesis with unstable gravitino and upper bound on the reheating temperature," *Phys.Rev.* **D73** (2006) 123511, arXiv:hep-ph/0507245 [hep-ph].

[128] Steffen F.D., "Probing the Reheating Temperature at Colliders and with Primordial Nucleosynthesis," *Phys.Lett.* **B669** (2008) 74–80, arXiv:0806.3266 [hep-ph].

[129] Bassett B.A., Tsujikawa S., and Wands D., "Inflation dynamics and reheating," *Rev.Mod.Phys.* **78** (2006) 537–589, arXiv:astro-ph/0507632 [astro-ph].

[130] Kim S.A., Liddle A.R., and Seery D., "Non-gaussianity in axion Nflation models," *Phys.Rev.Lett.* **105** (2010) 181302, arXiv:1005.4410 [astro-ph.CO].

[131] Meyers J. and Sivanandam N., "Adiabaticity and the Fate of Non-Gaussianities: The Trispectrum and Beyond," *Phys.Rev.* **D84** (2011) 063522, arXiv:1104.5238 [astro-ph.CO].

[132] Watanabe Y., "δN versus covariant perturbative approach to non-Gaussianity outside the horizon in multifield inflation," *Phys.Rev.* **D85** (2012) 103505, arXiv:1110.2462 [astro-ph.CO].

[133] Leung G., Tarrant E.R., Byrnes C.T., and Copeland E.J., "Reheating, Multifield Inflation and the Fate of the Primordial Observables," *JCAP* **1209** (2012) 008, arXiv:1206.5196 [astro-ph.CO].

[134] Meyers J. and Tarrant E.R.M., "Perturbative Reheating After Multiple-Field Inflation: The Impact on Primordial Observables," *Phys.Rev.* **D89** (2014) 063535, arXiv:1311.3972 [astro-ph.CO].

[135] Elliston J., Orani S., and Mulryne D.J., "General analytic predictions of two-field inflation and perturbative reheating," *Phys.Rev.* **D89** (2014) 103532, arXiv:1402.4800 [astro-ph.CO].

[136] Dias M. and Seery D., "Transport equations for the inflationary spectral index," *Phys.Rev.* **D85** (2012) no. 4, , arXiv:1111.6544.

[137] Huston I. and Christopherson A., "Calculating nonadiabatic pressure perturbations during multifield inflation," *Phys.Rev.* **D85** (2012) no. 6, , arXiv:1111.6919.

[138] Anderson G.J., Mulryne D.J., and Seery D., "Transport equations for the inflationary trispectrum," *JCAP* **1210** (2012) 019, arXiv:1205.0024 [astro-ph.CO].

[139] Adams F.C., Bond J.R., Freese K., Frieman J.A., and Olinto A.V., "Natural inflation: Particle physics models, power law spectra for large scale structure, and constraints from COBE," *Phys.Rev.* **D47** (1993) 426–455, arXiv:hep-ph/9207245 [hep-ph].

[140] Battefeld D. and Kawai S., "Preheating after N-flation," *Phys.Rev.* **D77** (2008) 123507, arXiv:0803.0321 [astro-ph].

[141] Battefeld D., Battefeld T., and Giblin J.T., "On the Suppression of Parametric Resonance and the Viability of Tachyonic Preheating after Multi-Field Inflation," *Phys.Rev.* **D79** (2009) 123510, arXiv:0904.2778 [astro-ph.CO].

[142] Kofman L., "Probing string theory with modulated cosmological fluctuations," CITA-03-12, arXiv:astro-ph/0303614 [astro-ph].

[143] Dvali G., Gruzinov A., and Zaldarriaga M., "A new mechanism for generating density perturbations from inflation," *Phys.Rev.* **D69** (2004) 023505, arXiv:astro-ph/0303591 [astro-ph].

[144] Suyama T. and Yamaguchi M., "Non-Gaussianity in the modulated reheating scenario," *Phys.Rev.* **D77** (2008) 023505, arXiv:0709.2545 [astro-ph].

[145] Zaldarriaga M., "Non-Gaussianities in models with a varying inflaton decay rate," *Phys.Rev.* **D69** (2004) 043508, arXiv:astro-ph/0306006 [astro-ph].

[146] Bernardeau F., Kofman L., and Uzan J.P., "Modulated fluctuations from hybrid inflation," *Phys.Rev.* **D70** (2004) 083004, arXiv:astro-ph/0403315 [astro-ph].

[147] Byrnes C.T. and Wands D., "Scale-invariant perturbations from chaotic inflation," *Phys.Rev.* **D73** (2006) 063509, arXiv:astro-ph/0512195 [astro-ph].

[148] Kolb E.W., Riotto A., and Vallinotto A., "Curvature perturbations from broken symmetries," *Phys.Rev.* **D71** (2005) 043513, arXiv:astro-ph/0410546 [astro-ph].

[149] Byrnes C.T., "Constraints on generating the primordial curvature perturbation and non-Gaussianity from instant preheating," *JCAP* **0901** (2009) 011, arXiv:0810.3913 [astro-ph].

[150] Hazra D.K., Martin J., and Sriramkumar L., "The scalar bi-spectrum during preheating in single field inflationary models," *Phys.Rev.* **D86** (2012) 063523, arXiv:1206.0442 [astro-ph.CO].

[151] Kobayashi T., Yamaguchi M., and Yokoyama J., "Generalized G-inflation: Inflation with the most general second-order field equations," *Prog.Theor.Phys.* **126** (2011) 511–529, arXiv:1105.5723 [hep-th].

[152] Mulryne D.J., Seery D., and Wesley D., "Moment transport equations for the primordial curvature perturbation," *JCAP* **1104** (2011) 030, arXiv:1008.3159 [astro-ph.CO].

[153] Suyama T., Takahashi T., Yamaguchi M., and Yokoyama S., "On Classification of Models of Large Local-Type Non-Gaussianity," *JCAP* **1012** (2010) 030, arXiv:1009.1979 [astro-ph.CO].

[154] Lewis A., "The real shape of non-Gaussianities," *JCAP* **1110** (2011) 026, arXiv:1107.5431 [astro-ph.CO].

[155] Smith K.M., LoVerde M., and Zaldarriaga M., "A universal bound on N-point correlations from inflation," *Phys.Rev.Lett.* **107** (2011) 191301, arXiv:1108.1805 [astro-ph.CO].

[156] Sugiyama N.S., "Consistency Relation for multifield inflation scenario with all loop contributions," *JCAP* **1205** (2012) 032, arXiv:1201.4048 [gr-qc].

[157] Assassi V., Baumann D., and Green D., "On Soft Limits of Inflationary Correlation Functions," *JCAP* **1211** (2012) 047, arXiv:1204.4207 [hep-th].

[158] Kehagias A. and Riotto A., "Operator Product Expansion of Inflationary Correlators and Conformal Symmetry of de Sitter," *Nuclear Physics* **B864** (2012) 492–529, arXiv:1205.1523 [hep-th].

[159] Tasinato G., Byrnes C.T., Nurmi S., and Wands D., "Loop corrections and a new test of inflation," *Phys.Rev.* **D87** (2013) no. 4, 043512, arXiv:1207.1772 [hep-th].

[160] Rodriguez Y., Beltran Almeida J.P., and Valenzuela-Toledo C.A., "The different varieties of the Suyama-Yamaguchi consistency relation and its violation as a signal of statistical inhomogeneity," *JCAP* **1304** (2013) 039, arXiv:1301.5843 [astro-ph.CO].

[161] Kim S., Liddle A., and Seery D., "Non-Gaussianity in axion N-flation models: Detailed predictions and mass spectra," *Phys.Rev.* **D85** (2012) no. 2, , arXiv:1108.2944.

[162] Meyers J. and Sivanandam N., "Non-Gaussianities in Multifield Inflation: Superhorizon Evolution, Adiabaticity, and the Fate of fnl," *Phys.Rev.* **D83** (2011) 103517, arXiv:1011.4934 [astro-ph.CO].

[163] Kallosh R. and Linde A., "Multi-field Conformal Cosmological Attractors," *JCAP* **1312** (2013) 006, arXiv:1309.2015 [hep-th].

[164] Hertzberg M.P., "Inflation, Symmetry, and B-Modes," arXiv:1403.5253 [hep-th].

[165] Brax P. and Davis A., "Conformal Inflation Coupled to Matter," *JCAP* **1405** (2014) 019, arXiv:1401.7281 [astro-ph.CO].

[166] Bars I., Steinhardt P.J., and Turok N., "Cyclic Cosmology, Conformal Symmetry and the Metastability of the Higgs," *Phys.Lett.* **B726** (2013) 50–55, arXiv:1307.8106.

[167] Padilla A., Stefanyszyn D., and Tsoukalas M., "Generalised Scale Invariant Theories," *Phys.Rev.* **D89** (2014) 065009, arXiv:1312.0975 [hep-th].

[168] Horndeski G.W., "Second-order scalar-tensor field equations in a four-dimensional space," *Int.J.Theor.Phys.* **10** (1974) 363–384.

[169] Roest D., "Universality classes of inflation," *JCAP* **01** (2014) 007, arXiv:1309.1285 [hep-th].

[170] Garcia-Bellido J. and Roest D., "Large-N running of the spectral index of inflation," *Phys.Rev.* **D89** (2014) 103527, arXiv:1402.2059.

[171] Armendariz-Picon C., Damour T., and Mukhanov V.F., "k - inflation," *Phys.Lett.* **B458** (1999) 209–218, arXiv:hep-th/9904075 [hep-th].

[172] Bruneton J.P., "On causality and superluminal behavior in classical field theories: Applications to k-essence theories and MOND-like theories of gravity," *Phys.Rev.* **D75** (2007) 085013, arXiv:gr-qc/0607055 [gr-qc].

[173] Lorenz L., Martin J., and Ringeval C., "K-inflationary Power Spectra in the Uniform Approximation," *Phys.Rev.* **D78** (2008) 083513, arXiv:0807.3037 [astro-ph].

[174] Kinney W.H. and Tzirakis K., "Quantum modes in DBI inflation: exact solutions and constraints from vacuum selection," *Phys.Rev.* **D77** (2008) 103517, arXiv:0712.2043 [astro-ph].

[175] Garriga J. and Mukhanov V.F., "Perturbations in k-inflation," *Phys.Lett.* **B458** (1999) 219–225, arXiv:hep-th/9904176 [hep-th].

[176] Martin J., Ringeval C., and Vennin V., "K-inflationary Power Spectra at Second Order," *JCAP* **1306** (2013) 021, arXiv:1303.2120 [astro-ph.CO].

[177] De Felice A. and Tsujikawa S., "Shapes of primordial non-Gaussianities in the Horndeski's most general scalar-tensor theories," *JCAP* **1303** (2013) 030, arXiv:1301.5721 [hep-th].

[178] Tsujikawa S., Ohashi J., Kuroyanagi S., and De Felice A., "Planck constraints on single-field inflation," *Phys.Rev.* **D88** (2013) 023529, arXiv:1305.3044 [astro-ph.CO].

[179] Cai Y.F., Gong J.O., and Pi S., "Conformal description of inflation and primordial B-modes," arXiv:1404.2560 [hep-th].

[180] Costa R. and Nastase H., "Conformal inflation from the Higgs," *JHEP* **1406** (2014) 145, arXiv:1403.7157 [hep-th].

[181] Frazer J., "Predictions in multifield models of inflation," *JCAP* **1** (2014) 28, arXiv:1303.3611 [astro-ph.CO].

[182] Easther R., Frazer J., Peiris H.V., and Price L.C., "Simple predictions from multifield inflationary models," *Phys.Rev.Lett.* **112** (2014) 161302, arXiv:1312.4035 [astro-ph.CO].

[183] Wang T., "Note on Non-Gaussianities in Two-field Inflation," *Phys.Rev.* **D82** (2010) 123515, arXiv:1008.3198 [astro-ph.CO].

[184] Byrnes C.T. and Tasinato G., "Non-Gaussianity beyond slow roll in multi-field inflation," *JCAP* **0908** (2009) 016, arXiv:0906.0767 [astro-ph.CO].

[185] Battefeld D. and Battefeld T., "On Non-Gaussianities in Multi-Field Inflation (N fields): Bi and Tri-spectra beyond Slow-Roll," *JCAP* **0911** (2009) 010, arXiv:0908.4269 [hep-th].

[186] Mazumdar A. and Wang L.F., "Separable and non-separable multi-field inflation and large non-Gaussianity," *JCAP* **1209** (2012) 005, arXiv:1203.3558 [astro-ph.CO].

[187] Seery D., Mulryne D.J., Frazer J., and Ribeiro R.H., "Inflationary perturbation theory is geometrical optics in phase space," *JCAP* **1209** (2012) 010, arXiv:1203.2635 [astro-ph.CO].

[188] http://www.netlib.org/ode/dverk.f.

[189] Abramowitz M., *Handbook of Mathematical Functions, With Formulas, Graphs, and Mathematical Tables,*. Dover Publications, Incorporated, 1974.

[190] Mulryne D.J., "Transporting non-Gaussianity from sub to super-horizon scales," *JCAP* **1309** (2013) 010, arXiv:1302.3842 [astro-ph.CO].

[191] Mulryne D., Orani S., and Rajantie A., "Non-Gaussianity from the hybrid potential," *Phys.Rev.* **D84** (2011) 123527, arXiv:1107.4739 [hep-th].